EXAMINATION OF THE ROLE OF HIV-1 CAPSID SEQUENCE ON VIRUS INFECTIVITY, HOST PROTEIN INTERACTIONS, AND CAPSID UNCOATING

by

Douglas Kite Fischer

Bachelor of Arts, Bridgewater College, 1995

Master of Science, James Madison University, 2001

Submitted to the Graduate Faculty of

the School of Medicine in partial fulfillment

of the requirements for the degree of

Doctor of Philosophy

University of Pittsburgh

2019

UNIVERSITY OF PITTSBURGH

SCHOOL OF MEDICINE

This dissertation was presented

by

Douglas Kite Fischer

It was defended on

April 23, 2019

and approved by

Jennifer M. Bomberger, Associate Professor, Department of Microbiology and Molecular Genetics

Fred L. Homa, Professor, Department of Microbiology and Molecular Genetics

Nicolas P. Sluis-Cremer, Professor, Department of Medicine (Infectious Diseases)

Simon C. Watkins, Distinguished Professor and Vice Chair, Department of Cell Biology

Dissertation Director: Zandrea A. Ambrose, Associate Professor, Department of Microbiology and Molecular Genetics

Examination of the Role of HIV-1 Capsid Sequence on Virus Infectivity, Host Protein Interactions, and Capsid Uncoating

Douglas Kite Fischer, PhD

University of Pittsburgh, 2019

Human immunodeficiency virus type 1 (HIV-1) infection persists for life, requiring the regular administration of antiretroviral therapy (ART) to suppress viral replication. Poorly tolerated side effects and the continued emergence of drug resistance mutations to current pharmaceuticals prompts the development of new therapies against novel targets. The HIV-1 capsid plays a critical role in every post-entry early virus life cycle step and its impairment is highly detrimental to successful infection. Combined with a high degree of mutational fragility and a lack of host cell analogs to either the monomeric capsid protein (CA) or the assembled capsid, these characteristics make capsid a viable target for therapeutic intervention. In this dissertation, we examined the influence of capsid from different virus strains on early virus life cycle steps in different cell types. We characterized differences in the infectivity defect of the cell cycle dependent CA mutation N57A when incorporated into the closely related lab-adapted virus strains HIV-1_{NL4-3} and HIV-1_{LAI}. We extended these lab-adapted strain studies to include clinical isolates and demonstrated that a single CA amino acid polymorphism in the transmitted/founder strain HIV-1_{CH040} enhances capsid stability compared with HIV-1_{LAI}. Examination of an HIV-1 sequence database revealed strong conservation of CA sequence and the potential for broader applicability of our findings in lab-adapted strains. Capsid interacts with numerous host proteins that facilitate virus infectivity. We examined the effects of inhibiting capsid interaction with three of these proteins, cleavage and polyadenylation specificity factor 6 (CPSF6), cyclophilin A (CypA), and nucleoporin 153

(Nup153), on virus infectivity. We also explored the manner in which a mislocalized, truncated form of CPSF6 (CPSF6-358) restricts virus infectivity. The capsid must become dissociated, or uncoat, within the host cell for early virus life cycle steps to proceed and lead to successful infection. We designed and performed initial testing of a new, live cell capable capsid permeabilization assay that will permit further insight into the initial steps of uncoating. Together, these studies serve to advance our understanding of how capsid functions to promote infection and how capsid mutations and differences in virus strains and cell types can alter virus infectivity.

Table of Contents

List of Tables

List of Figures

List of Abbreviations

3'PPT	3' polypurine tract
3D	three-dimensional
3TC	lamivudine
ABC	abacavir
AIDS	acquired immunodeficiency syndrome
APOBEC3G	apolipoprotein B mRNA-editing enzyme-catalytic polypeptide-like 3G
ART	antiretroviral therapy
ARV	AIDS-associated retrovirus
ASM	American Society for Microbiology
ATV	atazanavir
AZT	azidothymidine, or zidovudine
B	bursa-derived
BICD2	bicaudal D2
bp	base pair
BSA	bovine serum albumin
CA	capsid
CA^{CTD}	capsid C-terminal domain
CA^{NTD}	capsid N-terminal domain
cART	combination antiretroviral therapy
CCR5	C-C chemokine receptor type 5

CD4	cluster of differentiation 4
CD8	cluster of differentiation 8
CDC	Centers for Disease Control
CFI_m	cleavage factor I_m
cGAS	cyclic guanosine monophosphate-adenosine monophosphate synthase
CLEM	correlative light electron microscopy
CMV	cytomegalovirus
CNS	central nervous system
cPPT	central polypurine tract
CPSF6	cleavage and polyadenylation specificity factor 6
CRF	circulating recombinant form
cryo-ET	cryo-electron tomography
CsA	cyclosporine A
CTD	C-terminal domain
CTL	cytotoxic T lymphocyte
CXCL10	C-X-C motif chemokine ligand 10
CXCR4	C-X-C chemokine receptor type 4
CYP3A	cytochrome P450 3A
CypA	cyclophilin A
DCAF1	DDB1 and CUL4-associated factor 1
DEAE	diethylaminoethyl
Dia	diaphanous
DIC	differential interference contrast

DMEM	Dulbecco's Modified Eagle Medium
DNA	deoxyribonucleic acid
DNase I	deoxyribonuclease I
dNTP	deoxynucleoside triphosphate
DOR	doravirine
dpi	days post-infection
DRF	Diaphanous-related formin
DRV	darunavir
DTG	dolutegravir
EDTA	ethylenediaminetetraacetic acid
EFV	efavirenz
ELISA	enzyme-linked immunosorbent assay
EM	electron microscopy
EMCCD	electron multiplying charge-coupled device
Env	envelope
ER	endoplasmic reticulum
ESCRT	endosomal sorting complex required for transport
ETR	etravirine
EU	5-ethynyl uridine
FAM	6-carboxyfluorescein
FAP	fluorogen activating protein
FBS	Fetal Bovine Serum
FDA	Federal Drug Administration

FEZ1	fasiculation and elongation factor zeta 1
FG	phenylalanine-glycine
FLAP	fluorescent light-up aptamer
FPV	fosamprenavir
FSC	forward scatter
FTC	emtricitabine
G	guanine
Gag	group-specific antigen
GALT	gut-associated lymphoid tissue
GAPDH	glyceraldehyde-3-phosphate dehydrogenase
GFP	green fluorescent protein
GM-CSF	granulocyte-macrophage colony-stimulating factor
H-REMD	Hamiltonian replica exchange molecular dynamics
HIV-1	human immunodeficiency virus type 1
HIV-2	human immunodeficiency virus type 2
HSV-TK	herpes simplex virus thymidine kinase
HTLV-III	human T lymphotropic virus type III
IBA	ibalizumab
IFI16	interferon gamma-inducible factor 16
IFN	interferon
IFN-α	interferon alpha
IgG	immunoglobulin G
IL-15	interleukin-15

IL-2	interleukin-2
IN	integrase
INmNG	INmNeonGreen
INSTI	integrase strand transfer inhibitor
IP-10	interferon gamma-induced protein 10
IP_6	inositol hexakisphosphate
IRF3	interferon regulatory factor 3
ISG	interferon stimulated gene
ISRE	interferon stimulated response element
IU	infectious units
kb	kilobase
KD	knockdown
K_d	dissociation constant
LANL	Los Alamos National Laboratory
LAV	lymphadenopathy-associated virus
LEDGF/p75	lens epithelium-derived growth factor / transcriptional coactivator p75
LTR	long terminal repeat
M-CSF	macrophage colony-stimulating factor
MA	matrix
MAP1	microtubule-associated protein 1
MDM	monocyte-derived macrophage
MG	malachite green
MOI	multiplicity of infection

mRNA	messenger RNA
MSM	men who have sex with men
MVC	maraviroc
MxB	myxovirus resistance protein B
NA	numerical aperture
NC	nucleocapsid
Nef	negative regulatory factor
NIH	National Institutes of Health
NK	natural killer
NLS	nuclear localization signal
NNRTI	non-nucleoside reverse transcriptase inhibitor
NPC	nuclear pore complex
NRTI	nucleoside/nucleotide reverse transcriptase inhibitor
NSI	nonsyncytium-inducing
NTD	N-terminal domain
Nup	nucleoporin
Nup153	nucleoporin 153
Nup358	nucleoporin 358
Nup358Cyp	Nup358 cyclophilin homology domain
NVP	nevirapine
P/S	penicillin/streptomycin
PAMP	pathogen-associated molecular pattern
PBMC	peripheral blood mononuclear cell

PBS	primer binding site
PBS	phosphate buffered saline
PCR	polymerase chain reaction
PEG	polyethylene glycol
PEI	polyethylenimine
PES	polyethersulfone
PF74	compound PF3450074
PFA	paraformaldehyde
PHA	phytohaemagglutinin
PI	protease inhibitor
$PI(4,5)P_2$	phosphatidylinositol-4,5-bisphosphate
PIC	preintegration complex
PMSF	phenylmethylsulfonyl fluoride
Pol	polymerase
PPT	polypurine tract
PQBP1	polyglutamine binding protein 1
PR	protease
PRR	pattern recognition receptor
PVDF	polyvinylidene difluoride
qPCR	quantitative polymerase chain reaction
qRT-PCR	quantitative reverse transcription polymerase chain reaction
R5	CCR5, C-C chemokine receptor type 5
RAL	raltegravir

RanBP2	Ran binding protein 2
Rev	regulator of virion
rhTRIM5α	rhesus tripartite motif containing protein 5α
RIG-I	retinoic acid-inducible gene I
RNA	ribonucleic acid
RNase H	ribonuclease H
RPMI	Roswell Park Memorial Institute
RPV	rilpivirine
RRE	Rev-response element
RT	reverse transcriptase
RT-PCR	reverse transcription polymerase chain reaction
RTC	reverse transcription complex
SAMHD1	sterile alpha motif and histidine/aspartic acid domain-containing protein 1
sCMOS	scientific complementary metal-oxide-semiconductor
SEM	standard error of the mean
SG-PERT	SYBR Green I-based product enhanced reverse transcription
shRNA	short hairpin RNA
SI	syncytium-inducing
siRNA	small interfering RNA
SIV	simian immunodeficiency virus
SP1	spacer peptide 1
SP2	spacer peptide 2
SQV	saquinavir

SR	serine-arginine
SSC	side scatter
SSNMR	solid state nuclear magnetic resonance
STED	stimulated emission depletion
STING	stimulator of interferon genes
SUN1	Sad1 and UNC84 domain containing protein 1
SUN2	Sad1 and UNC84 domain containing protein 2
T	thymus-derived
T-20	enfuvirtide
T/F	transmitted/founder
TAMRA	6-carboxytetramethylrhodamine
Tat	trans-activator of transcription
TBK-1	TANK-binding kinase 1
TDF	tenofovir
TIRF	total internal reflection fluorescence
TNPO3	transportin3
TO	thiazole orange
TPV	tipranavir
TREX1	three prime repair exonuclease 1
TRIM5α	tripartite motif containing protein 5α
TRN-SR2	transportin-SR2
$tRNA^{Lys3}$	lysine transfer RNA isoacceptor 3
U	units

UK	United Kingdom
UNAIDS	Joint United Nations Program on HIV/AIDS
Vif	virion infectivity factor
Vpr	virus protein R
Vpu	virus protein U
Vpx	virus protein X
VSV-G	vesicular stomatitis virus glycoprotein
WHO	World Health Organization
X4	CXCR4, C-X-C chemokine receptor type 4

Preface

No great event in life is experienced in a vacuum or without the involvement of numerous individuals. This PhD dissertation is no exception. There are many people to whom I owe a debt of gratitude and without whose support I could not have reached this point. Dr. Zandrea Ambrose, you have served as my mentor and advisor throughout my dissertation and have taught me how to navigate the waters of scientific research. I thank you for your unfailing support and your continued assistance and guidance. To all the current and former members of the Ambrose lab, your collegial friendship, support, and assistance are much appreciated. To my dissertation committee, you offered sound advice when I needed some direction, pushed me when I needed a nudge, and drove me to reach farther than I thought I could, and for that I thank you. Dr. Penelope Morel and Dr. Jennifer Bomberger, you took a chance on a physical and computer scientist unexperienced in biomedical research and offered me the opportunity to enter a new field. Thank you for your leap of faith.

To all my family and friends who offered warm encouragement, a sympathetic ear, sound advice, and sometimes a much-needed distraction from research, you helped me more than you may ever realize, and I am truly thankful for your love and support. My father, Douglas C. Fischer, was the first scientist I ever knew. He instilled in me a life-long love of science and taught me what it means to be a scientist. Although he did not survive long enough to see me enter the graduate program and complete my PhD, his influence permeates who I am, and I am forever grateful. Finally, to my wife, Dr. Molly Stitt-Fischer, without your undying love and support I could never have accomplished this. You have been there for me every step of the way, through

the frustrations and setbacks as well as the victories. We saw each other through our graduate programs as promised and together we make each other better. You are right, we do make a great team.

This dissertation is dedicated to all those individuals who are now or will in the future be infected with the HIV-1 virus, their families and friends, and those who have lost their lives to HIV/AIDS. You provide inspiration to researchers worldwide to advance our knowledge of the HIV-1 virus, to develop new therapies and, eventually, to find a cure for this disease.

1.0 Introduction

1.1 AIDS History and Public Health

Nobody could have predicted that a minor epidemiological report from southern California would have represented the opening salvo of one of the largest worldwide epidemics in human history.

Acquired immunodeficiency syndrome (AIDS) was first recognized as a distinct disease in 1981 with the identification of five previously healthy young homosexual men from Los Angeles, CA diagnosed with *Pneumocystis* pneumonia (1), an infection almost exclusively observed in severely immunocompromised individuals (2). This initial report by the United States Centers for Disease Control (CDC) was quickly followed one month later by the report of an additional 26 homosexual men in New York and California diagnosed with *Pneumocystis* pneumonia and Kaposi's Sarcoma (3), a rare disease that, prior to these reports, was most commonly found in elderly men of Jewish or Mediterranean ancestry (4). Later that year, these and other reports culminated in a set of articles in the *New England Journal of Medicine* associating the development of *Pneumocystis* pneumonia, Kaposi's sarcoma, mucosal candidiasis, and other opportunistic infections in otherwise healthy homosexual men and drug users with an acquired cellular immunodeficiency (5-7), or what came to be known as AIDS (8).

This new disease, transmitted by bodily fluids, in particular blood, breast milk, and sexual fluids (9, 10), was characterized by a systemic and chronic depletion of CD4+ helper T cells, preventing a robust cellular immune response to opportunistic infections, leading to chronic patient

morbidity and, in almost 100% of cases, death (11). The most vulnerable populations identified were those engaging in high-risk behaviors, particularly homosexual and bisexual men who have sex with men (MSM) and male and female intravenous drug users (9). Other at-risk populations were found to include female sex workers, individuals with hemophilia and other transfusion recipients, transgender women, and infants of infected women (10, 12). At a time when the western world was attempting to come to terms with a more prominent homosexual community and experiencing widespread drug abuse problems that led to the American "War on Drugs", coupled with a general fear and misunderstanding of the underlying disease (13), this emerging AIDS epidemic led to profound stigma against these vulnerable populations in general and AIDS patients in particular (14-16). The battle to prevent the spread of AIDS disease and misinformation, reduce the ostracization of at-risk communities, and effectively treat infected individuals became defining characteristics of 1980s American culture (13).

In time the magnitude of the AIDS epidemic and its devastating potential came to be appreciated. Similar patterns of disease were soon observed in other Western countries in North America and Europe, while in the Caribbean and sub-Saharan Africa more widespread disease was observed with no readily discernable epidemiological pattern (17). By 1985, at least one case of AIDS was reported in each region of the world (18) – a trend that rapidly exceeded all expectations of severity and scale of impact (19). On a positive note, this worldwide impact of AIDS helped to develop and promote the globalization of public health, research, and science and to define the model for emerging infectious disease response (10).

In 1983, two years after the initial epidemiological reports, a new retrovirus, human immunodeficiency virus type 1 (HIV-1), was discovered (20) and shown to be the causative agent of AIDS (21-24). This discovery led, in time, to the development of antiretroviral therapy (ART) to specifically treat HIV-1 infection and reduce transmission to others (25, 26), which has transitioned HIV-1 infection from a near-certain death sentence to a managed, chronic disease, albeit one with considerable complications and morbidities (27). While our best efforts have not yet yielded a cure for HIV-1 infection, a wide range of strategies are being examined that offer the hope of eliminating the virus, or at least its disease-inducing potential, from infected individuals (28-30).

Such advances notwithstanding, HIV/AIDS has continued to be a major global public health concern. Today, nearly 40 years after the start of the HIV/AIDS epidemic, the Joint United Nations Program on HIV/AIDS (UNAIDS) reported almost 37 million people worldwide living with HIV-1 in 2018, almost 40% of whom do not currently have access to ART (31). While the annual mortality rate of HIV/AIDS has fallen from its peak in 2004 and was estimated in 2017 to be below 1 million deaths for the first time since the late 1990s (31, 32), the World Health Organization (WHO) estimates that HIV/AIDS has overall been responsible for more than 35 million deaths (12) out of over 77 million individuals infected worldwide (32). Social, economic, and political challenges that mirror those prevalent in the early 1980s have led to increased HIV-1 infection among some populations (33-35). As such, continued research and global public health campaigns are needed to drive the development of better, universally available treatments, and perhaps an eventual cure, for HIV/AIDS.

1.2 HIV-1 Transmission and Pathogenesis

1.2.1 HIV-1 Transmission

The vast majority (75-85%) of HIV-1 transmission occurs through sexual contact (31, 36). While penile-vaginal intercourse is responsible for most cases of transmission worldwide, anal sex has a considerably higher probability of transmission (37). The overall probability of transmission may be relatively low for a single exposure event (1 to 2,000-3,000 for heterosexual intercourse) (37), but high-risk behavior of copulating with multiple partners greatly increases the likelihood of successful transmission (38, 39). HIV-1 virus or infected cells can be detected in both male (40) and female (41) sexual fluids, from where it comes into contact with and penetrates the sexual partner's mucosal epithelium via transcytosis or a gap between epithelial cells (37).

Two additional routes of transmission account for most of the remaining 15-25% of HIV-1 infections. Vertical transmission (mother to child) may occur during gestation (intrauterine) by exposure to maternal blood, during birth (intrapartum) by oral exposure to maternal blood and genital secretions, or after birth (postpartum) by oral consumption of breast milk (42). Transmission may also occur via direct viral access to the bloodstream from intravenous drug use, blood transfusions, transplants, or injury (36, 43, 44). Oral exposure requires viral penetration of the oral mucosal epithelium similar to sexual transmission, whereas direct transmission into the blood bypasses the need to navigate the epithelium.

1.2.2 HIV-1 Target Cells

Once the epithelial barrier has been breached, HIV-1 targets populations of hematopoietic leukocytes and myeloid cells expressing the cluster of differentiation 4 (CD4) receptor (45) and the C-C chemokine receptor type 5 (CCR5) co-receptor (46). While some HIV-1 strains will target cells expressing the C-X-C chemokine receptor type 4 (CXCR4) co-receptor instead of CCR5 (47), these viral strains are generally not found among transmitted viruses and develop later in the host infection (48-50). The targeted cell populations consist of thymus-derived (T) helper lymphocytes (CD4+ T cells) and macrophages (51, 52), which are found resident in lymphoid tissues and in various organs and tissues throughout the body. Importantly, both types of cells are present in the submucosa underlying the epithelia penetrated by HIV-1 during transmission (53).

T cells are broadly classified by their expression of one of two cell surface receptors (or both): cluster of differentiation 4 (CD4) and cluster of differentiation 8 (CD8) (54). Upon stimulation and activation, naïve CD4+ T cells differentiate into one of several effector phenotypes, characterized by the release of a specific set of cytokines that help tailor the immune response to the particular source of stimulation (55). These cytokines in turn assist in the activation of bursa-derived (B) lymphocytes (B cells), which provide a humoral immune response (56) and CD8+ cytotoxic T lymphocytes (CTLs), which provide a cellular immune response (54).

CD4+ T cells are the primary cellular target of HIV-1 infection (57, 58). Indeed, it is the depletion of CD4+ T cells and the concomitant immunodeficiency that develops that is the hallmark of HIV-1 infection (11). This depletion is accomplished by multiple mechanisms. Once the adaptive immune response has been activated, infected cells are targeted by CD8+ CTLs (59).

However, considerable CD4+ T cell death occurs prior to (60) and in the absence of (61) an immune response. This corresponds to the observation that HIV-1 infection is highly cytopathic to CD4+ T cells and productive viral infection generally results in cell death (11). While HIV-1-induced cell death of productively infected cells is associated with caspase-3-induced apoptosis (62, 63), the majority of CD4+ T cells depleted during HIV-1 infection are not productively infected but instead represent a bystander population (64, 65). Death of these bystander CD4+ T cells has been shown to be associated with abortive infection and intracellular innate immune activation (66), leading to inflammation and caspase-1-induced pyroptosis (63, 67). Even in the absence of cell death, infected CD4+ T cells often display profound dysfunction (68), preventing appropriate immune response.

Macrophages are terminally-differentiated, nondividing immune cells derived from monocytes or embryonic precursors (69, 70). They can be found resident in almost all tissues of the body, where they perform homeostasis and immune surveillance roles (71), including the phagocytosis of infected or senescent cells, extracellular debris, and pathogens (72), peptides from which are presented to CD4+ T cells, CD8+ CTLs, and B cells for adaptive immune system activation (56, 73, 74). HIV-1 virus can be isolated from macrophages from various biological organs and tissues of infected individuals (75, 76), particularly in the brain and other central nervous system (CNS) tissues (77-79), where HIV-1 infection can cause acute and chronic neurological dysfunction (80). These cells are capable of supporting low-level but sustained virus production (81, 82) and, unlike CD4+ T cells, do not exhibit appreciable cytopathic effects caused by HIV-1 infection (82, 83).

As such, macrophages serving as a potential viral reservoir was suggested from an early time point in HIV-1 research (11). However, despite clear evidence that macrophages are capable of supporting HIV-1 infection and replication, there is ongoing debate as to the clinical significance of macrophage HIV-1 infection (84). While the role of macrophages in the central nervous system of HIV-1-infected patients is well established and there is general consensus that CNS macrophages (microglia) represent the primary target of HIV-1 in the CNS (79), some studies have suggested macrophages are not a target of HIV-1 infection during transmission. These studies cite the inability of host HIV-1 viruses recovered from infected patients, particularly transmitted/founder viruses (85-87), to infect macrophages, even with the correct co-receptor tropism (88), owing in part to the paucity of CD4 expression on macrophages (89), low deoxynucleoside triphosphate (dNTP) levels (90), and the expression of the restriction factor sterile alpha motif and histidine/aspartic acid domain-containing protein 1 (SAMHD1) (91, 92). Other studies have noted high permissiveness of submucosal macrophages to CCR5-tropic HIV-1 infection and a much larger initial population of macrophages than CD4+ T cells in submucosal spaces and have suggested that tissue-resident macrophages represent the initial target of HIV-1 infection (83, 93, 94). However, a recent study posited that macrophages may acquire viral deoxyribonucleic acid (DNA) from engulfment of infected CD4+ T cells and, as such, might not represent a significant viral reservoir *in vivo* (87). Additional research is needed to establish the role(s) of macrophages in HIV-1 infection.

1.2.3 HIV-1 Pathogenesis

Clinical progression of HIV-1 infection typically follows a well-characterized sequential pattern of virologic and immunologic events (95, 96) (**Figure 1**). After the initial establishment of viral

infection in the submucosa, there is a 7- to 21-day eclipse phase without outward symptoms of infection (36), during which the virus propagates in tissue-resident CD4+ cells, which migrate to draining lymph nodes and spread virus into draining and systemic lymphatic tissues (97). A period of exponential viral growth follows with concomitant detection of virus in the blood (36, 98). Clinical symptoms of this acute phase of HIV-1 infection are generally non-specific, self-limited, and mononucleosis-like (fever, headache, sore throat, myalgia, lethargy, anorexia, rash, and lymphadenopathy) (99, 100) and while they may be severe enough to elicit medical attention, absent a clear risk factor for HIV-1 infection they rarely result in specific testing for the virus (101).

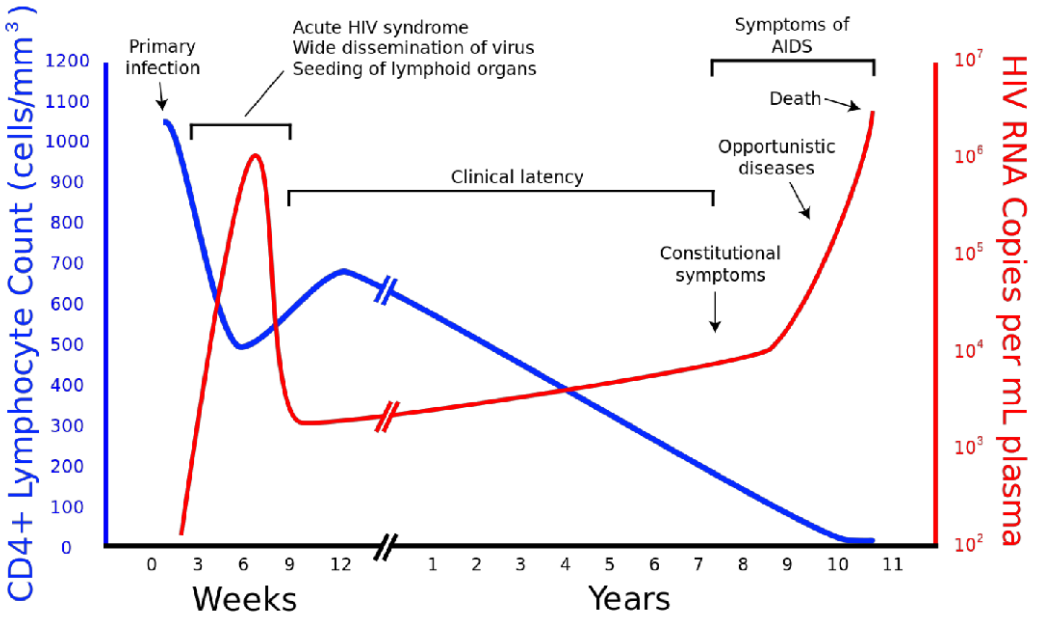

Figure 1. Schematic representation of typical clinical progression of untreated HIV-1 infection. Timeline of changes in peripheral CD4+ T cell counts (blue) and plasma HIV-1 viremia (red) as HIV-1 infection progresses from acute infection through clinical latency to the development of AIDS and death. Public domain image courtesy of Wikipedia, based upon an original from (Pantaleo et al., 1993) **(95)**.

Direct inoculation into the bloodstream foreshortens the eclipse phase and accelerates the development of acute clinical disease, with viremia detectable as soon as 2-3 days after intravenous infection (101).

CD4+ T cells will be significantly depleted (lymphopenia) during acute infection (99). This reduction is particularly prominent in the gut-associated lymphoid tissue (GALT) of the gastrointestinal tract, which comprises the largest collection of CD4+ T cells in the body (102-104). The depletion of these gastrointestinal CD4+ T cells can facilitate mucosal barrier permeabilization and bacterial invasion into submucosal spaces, lymphatic tissues, and the bloodstream, heightening overall immune activation, promoting greater HIV-1 replication, and worsening disease symptoms (105, 106).

The symptomatic, acute phase of HIV-1 clinical illness typically lasts 1-2 weeks (99). During acute infection, 6-15 days after onset of symptoms, high titers of cytopathic virus are detectable in plasma (as high as 10^7 copies of viral ribonucleic acid (RNA) per ml of blood (107)). The rise of plasma viremia coincides with an inflammatory cytokine cascade led by interferon alpha (IFN-α) and interleukin-15 (IL-15) (108). This innate immune response is punctuated by a rapid expansion and activation of natural killer (NK) effector cells (109, 110), but is unable by itself to control the acute viral infection. It is not until the adaptive immune response is activated 2-4 weeks after transmission (105) that the host can begin to effectively address the acute infection.

Both cellular and humoral adaptive immune responses are detectable during the acute phase of HIV-1 infection (111). The principal cellular response is via HIV-1-specific CD8+ CTLs

(112, 113), which increase dramatically in number (114, 115) and can be detected as early as 5 days after infection (116). CD8+ CTLs can exert an antiviral response by either directly killing infected cells through lysis or induction of apoptosis (59) or through the release of antiviral cytokines and chemokines (117).

The earliest humoral response is detected around 8 days after plasma viremia in the form of antibody-virus immune complexes with the first immunoglobulin G (IgG) plasma antibodies not observed until 5 days later (118, 119). This initial antibody response is non-neutralizing, with neutralizing antibodies not detected until three months or more after infection (105), 1-2 months after seroconversion (120). This delayed antibody response offers little, if any, assistance in addressing the acute-phase viremia. It is instead the cellular, CD8+ CTL response to primary infection that corresponds to clearance of acute viremia (112, 113, 121), with levels of virus in plasma falling at least 100-fold by day 27 and corresponding with a partial recovery of CD4+ T cell levels and resolution of clinical symptoms (122, 123).

The acute phase of HIV-1 infection is followed by a period of clinical latency characterized by a lack of clinical disease symptoms but with continued, persistent viral replication and progressive decline in CD4+ T cell levels (60, 116). The viral plasma level, while significantly reduced from acute, peak viremia, is maintained through latency at a “set point” that can vary among patients by more than 4 orders of magnitude (1-100,000 copies/ml) and can serve as an indicator of the rate of disease progression (124). This continued, low level of virus replication represents an inability of the host immune response to eradicate the remaining viral reservoir and clear the infection. Viral mutation results in escape from antibody neutralization (120) and killing

of infected host cells by CD8+ T cells (125) and NK cells (126, 127). This escape leads to a back and forth arms race between the host and virus, with the host attempting to neutralize succeeding generations of mutated virus and for these new generations of virus to further elude the host immune response (128).

If untreated, most HIV-1-infected individuals will continue to experience a slow depletion of CD4+ T lymphocytes over the course of clinical latency (116). Given the critical role played by CD4+ T cells in activating, directly or indirectly, multiple branches of the immune system, the depletion and disfunction of CD4+ T cells as a result of HIV-1 infection profoundly reduces the ability of the patient's immune system to respond to infection in general (11). This state of immunodeficiency permits the establishment of opportunistic infections that, in a healthy patient, would be readily eradicated. Typically, as the circulating CD4+ T cell count falls below 500 cells per μl of blood, the patient begins to experience the onset of clinical disease symptoms (111). When this count drops to 200 cells/μl the severity and frequency of symptoms increase and result in a diagnosis of AIDS (44, 101). With such a suppressed immune system, these individuals are highly susceptible to a wide range of opportunistic infections and malignancies (129), which are generally the proximal cause of mortality in AIDS patients (44).

The clinically latent phase of HIV-1 infection lasts for 10-11 years on average (130) and most (70-80%) infected individuals will experience this typical progression of disease if untreated (116), though two notable groups of patients have been identified with markedly different rates of progression. Rapid progressors account for 10-15% of infected individuals and advance to the state of AIDS within only 2-3 years of primary infection (116). On the opposite end of the spectrum,

long-term nonprogressors (< 5% of patients) will maintain normal levels of CD4+ T cells and competent immune function for an extended period of time (116). Once a diagnosis of AIDS has been reached, decline is rapid, with a median survival time of only about one year and a 5-year survival rate of 3.4% (131), though a small population of long-term survivors has been observed (116).

1.3 HIV-1 Retrovirology

1.3.1 Retroviruses

The central dogma of molecular biology describes a unidirectional flow of genetic information from a long-term repository based on DNA to an RNA intermediate via transcription, then to its final functional form in amino acid-based proteins via translation (132). While it was hypothesized that the initial transcription step might be made to flow in reverse (132), it was not until the discovery of an RNA-dependent DNA polymerase, or reverse transcriptase (RT), enzyme in two RNA tumor viruses (Rous sarcoma virus and Rauscher mouse leukemia virus) (133, 134) that the biological implications of such an enzyme were recognized. For these viruses it was observed that RT permits the viral genome, which exists in virus particles as RNA, to be converted to and exist as DNA within host cells (135, 136). This DNA genome (137) is integrated into the host genome as a provirus (138-140), where it persists within the host cell and is genetically transmitted to its progeny (141). Viruses with this dualistic, backwards, and persistent lifestyle were dubbed retroviruses.

Retroviruses belong to the *Retroviridae* family of viruses (retro- from the Latin for "backwards"), which are collectively able to infect a wide range of animal hosts, though individual viruses tend to have a narrowly defined host tropism (142). Members share the common characteristics of packaging a diploid, single-stranded RNA genome and an RT enzyme in their virions and using a DNA replication intermediate within infected host cells (143). The family is divided into two subfamilies, the non-pathogenic *Spumaretrovirinae* and the pathogenic *Orthoretrovirinae*, which is itself subdivided into 6 genera, 5 of which contain oncogenic viruses, and the genus *Lentivirus* (144). It is within this last genus that HIV-1 is classified.

Lentiviral infection (lenti- from the Latin for "slow") is characterized by a slowly progressing disease syndrome with a prolonged subclinical phase punctuated by a terminal phase of cachexia, multiple organ system failure, and death (145). Infection is directly transmitted between hosts, without the mediation of a vector, via exposure to infected bodily fluids (145, 146). Unlike other genera of *Retroviridae*, which require cell division for productive infection, lentiviruses possess the ability to infect nondividing cells (145, 147, 148), such as terminally-differentiated macrophages.

1.3.2 HIV-1 Origin

HIV-1 virus was initially isolated from AIDS patients in 1983 (20). During early investigations, the virus was alternatively known as human T lymphotropic virus type III (HTLV-III) (22), lymphadenopathy-associated virus (LAV) (20), and AIDS-associated retrovirus (ARV) (149). The current name, human immunodeficiency virus type 1, was coined in 1986 by the International Committee on Virus Nomenclature and Taxonomy (150). While identified during the emergence

of the AIDS pandemic, investigations into the origins of the HIV-1 virus would reveal that it had been present in humans for much longer.

The immediate precursor to HIV-1 is simian immunodeficiency virus (SIV), which has been circulating in nonhuman primates for at least 32,000 years (151). Originally identified in captive rhesus macaque monkeys (*Macaca mulatta*) in 1985 (152), SIV naturally infects Old World primate species native to sub-Saharan Africa, among which confirmed SIV infection can be found in at least 36 different species (153). SIV viruses are highly diverse and generally species-specific, with viruses classified according to the species of origin (153). Phylogenic analysis has demonstrated that SIV was transmitted into humans on four separate occasions over the past century to give rise to HIV-1 (146), most likely via exposure to infected primate blood from the bushmeat trade (154, 155).

1.3.3 HIV-1 Genetic Classification

HIV-1 virus strains are categorized hierarchically based upon genetic similarity or diversity into groups, subtypes, and, within some subtypes, into sub-subtypes (**Figure 2**) (156). Each lower level of division represents greater genetic similarity among members. HIV-1 groups M, N, O, and P represent the four separate zoonotic transmissions of SIV into humans in the West African country of Cameroon (146, 157). Groups M and N were transmitted from SIVcpz (158), which infects the common chimpanzee (*Pan troglodytes troglodytes*), around 1908 (159) and 1963 (160), respectively. Groups O and P were transmitted from SIVgor (161), which infects the Western gorilla (*Gorilla gorilla*), around 1920 for group O and at a yet-undetermined time for group P (146). A separate series of 8 transmission events of SIVsmm to humans from sooty mangabey

monkeys (*Cercocebus atys*) in the 1940s (162) gave rise to the related virus human immunodeficiency virus type 2 (HIV-2) (163), which is much less prevalent than HIV-1 (164) and will not be addressed here.

Group M (originally designated Main) is the only HIV-1 group that has spread globally and is responsible for the vast majority of infections worldwide (155). Group O (originally designated Outlier) has been identified in less than 1% of total infections and is mostly confined to sub-Saharan Africa, in particular Cameroon and surrounding countries, west Africa, and Zambia (165, 166). Group N (originally designated Non-Main Non-Outlier) has only 14 cases confirmed,

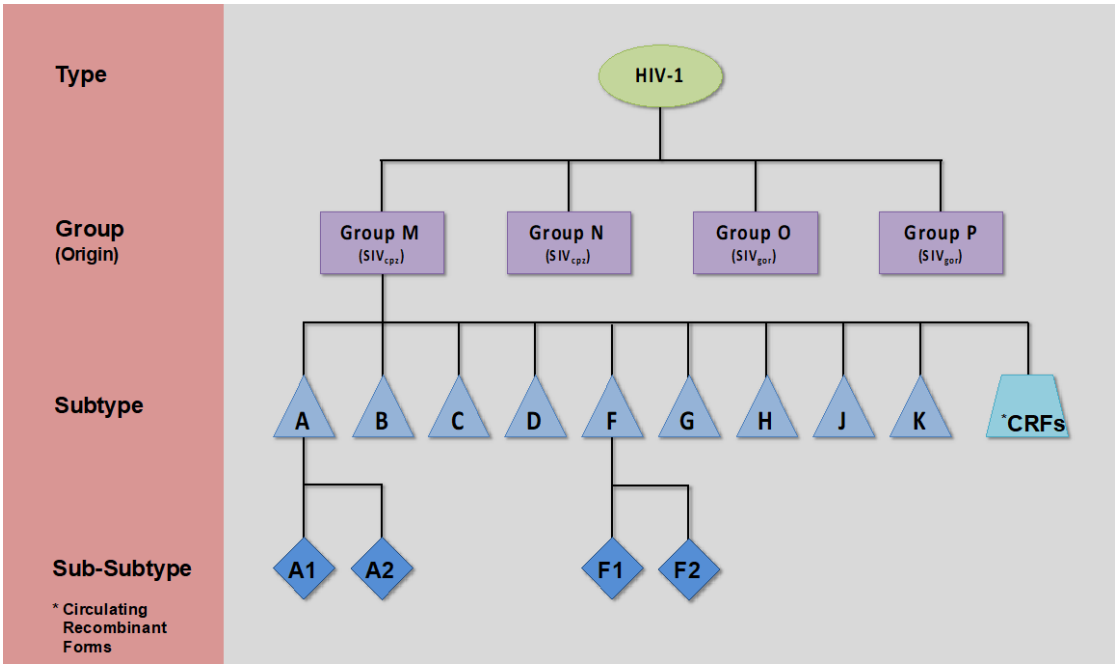

Figure 2. HIV-1 groups and subtypes. Hierarchical relationship of HIV-1 groups, subtypes, and sub-subtypes. Groups represent unique zoonotic transmission events. Group M is subdivided into 9 subtypes based upon sequence similarity, two of which, (A and F) are further subdivided into sub-subtypes. CRFs represent virus strains that originated from the recombination of strains from two or more subtypes.

all but one in Cameroon (167). Only two cases of infection with HIV-1 group P are known, both in Cameroon (167).

The pandemic HIV-1 group M is divided into subtypes – phylogenetically linked virus strains that are approximately the same genetic distance from one another (168) and represent diversification in the HIV-1 viral genome sequence within the human population after the original zoonotic transmission event (169). Much of this diversification can be traced to the area around Kinshasa, Democratic Republic of the Congo, where all subtypes can be found in circulation and where the pandemic spread of HIV-1 infection is believed to have originated (170). The nine recognized HIV-1 group M subtypes are designated by letters A through K except for E and I, with A and F further subdivided into sub-subtypes (168).

In addition to the hierarchical divisions, an array of 96 circulating recombinant forms (CRFs) of group M subtypes have been identified (171), which represent the genetic mixing of HIV-1 virus strains from different subtypes. These CRFs arise in part due to individuals with dual infections from multiple HIV-1 subtypes, which is a relatively common occurrence in Cameroon (172, 173), where all subtypes of group M except B are in circulation (173).

HIV-1 group M subtypes are responsible for a widely varying number of worldwide infections. A 2004 global survey showed that subtype C has caused about 50% of infections, subtypes A and B about 10% each, subtypes D and G about 3-5% each, and subtypes F, H, J, and K combined about 1%, with CRFs accounting for the remaining 20% (174, 175). These subtypes also exhibit considerable differences in geographic distribution (**Figure 3**). Of particular interest

in this work, HIV-1 infections in the developed Western world are almost exclusively subtype B. This stands in contrast to sub-Saharan Africa, where over 50% of infections are subtype C, but where also as a whole the greatest amount of diversity of subtypes and CRFs is observed, with all subtypes being represented, though there is considerable subregional difference in the distribution and prevalence of subtypes across the continent (168, 174, 175).

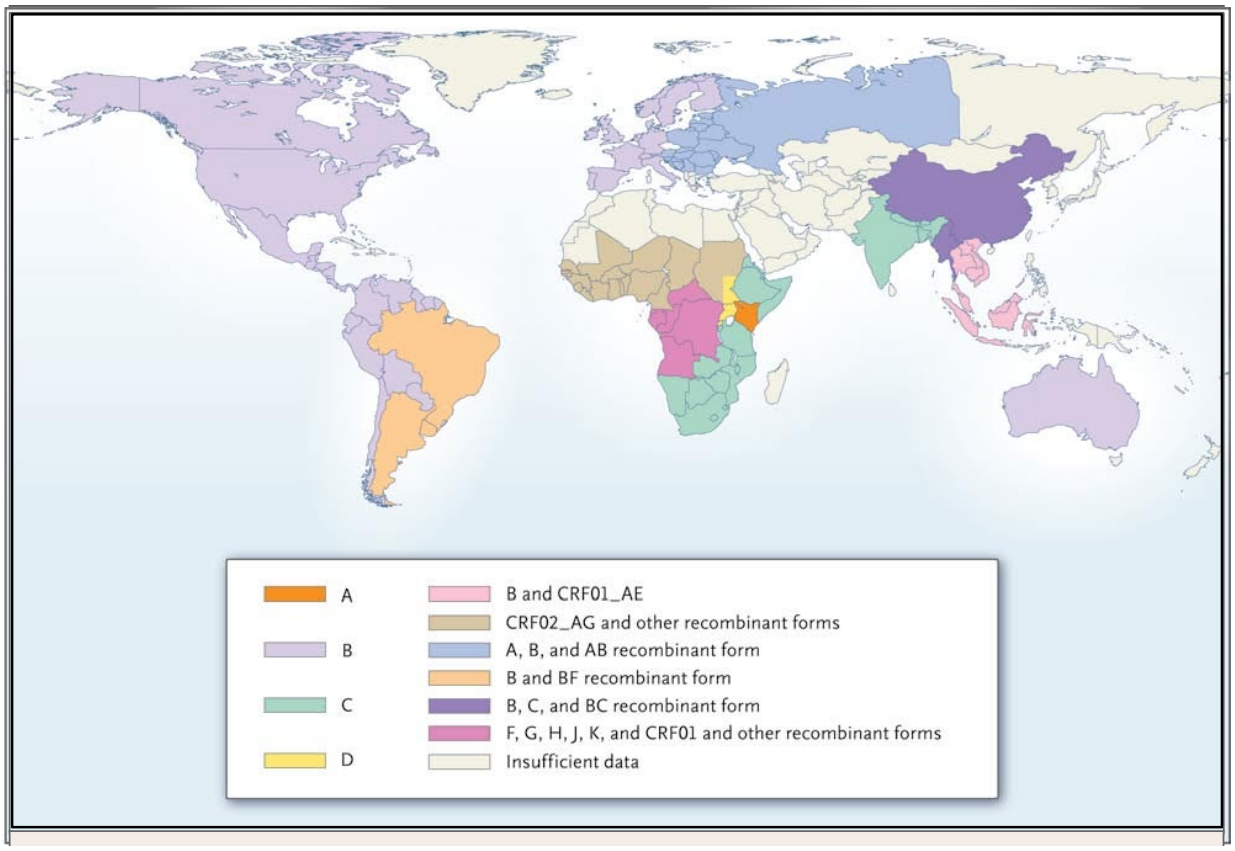

Figure 3. Global distribution of HIV-1 group M subtypes and CRFs. HIV-1 isolates from different countries and regions are generally representative of one or a few HIV-1 subtypes and/or CRFs, though all subtypes and CRFs are present in sub-Saharan Africa. Reproduced with permission from (Taylor et al., 2008) **(168)**, Copyright © 2008 Massachusetts Medical Society**.**

1.3.4 HIV-1 Phenotypic Classification

In addition to genetic categorization, HIV-1 strains can be classified according to infectious phenotype (e.g. cell tropism, cytopathic effect, transmissibility, or laboratory adaptation). Formerly, HIV-1 strains were broadly categorized by host cell tropism as T cell (T)-tropic or macrophage (M)-tropic and by cytopathic effect as syncytium-inducing (SI) or nonsyncytium-inducing (NSI) (61). With the development of a greater appreciation for the role of co-receptor usage in these infectivity phenotypes, HIV-1 strains are now instead categorized based upon target cell co-receptor usage as CCR5 (R5)-tropic, CXCR4 (X4)-tropic, or R5X4- or dual-tropic if either co-receptor can be used (176).

Only a small subset of HIV-1 strains are readily able to be transmitted and serve as a founder virus in a newly infected host. These transmitted/founder (T/F) virus strains almost exclusively are R5-tropic (177) and exhibit particular distinguishing genetic and phenotypic signatures (36). The specific study of these T/F virus strains will help provide a better understanding of the HIV-1 "transmission bottleneck" and a discovery of novel ways in which transmission might be prevented (36).

Primary isolates are derived from patient samples and represent virus that is circulating in the population. Comprehensive study of HIV-1 frequently requires large amounts of virus and extended observation of infected cells, which are challenging when working with precious patient samples and rational ethical constraints. As such, cell line culture of virus is necessary to overcome these limitations. However, despite the advantages gained by culturing virus *in vitro*, it has become

clear that propagation of virus under different conditions results in selection for particular traits (178), a process referred to as laboratory adaptation, or lab-adaptation.

Lab-adaptation, either through the serial passaging of virus in cell lines (179) or through the construction of unique virus strains cloned from primary isolates (180), allows for easier study of virus (180), including studying the phenotypes of particular mutations in a consistent background and the ability to grow virus to high titers (181). However, lab-adaptation can also cause phenotypic changes that are no longer consistent with primary HIV-1 isolates (182), such as altering interaction with CD4 receptors on host cells (183) or attenuating resistance to antibody neutralization, which is typically high in primary isolates (184). Additional research is required to examine phenotypic consistency between different, closely related lab-adapted strains and to determine how well lab-adapted strains represent primary isolates in terms of genetics and i*n vivo* infection phenotypes observed in patients.

1.3.5 HIV-1 Genome

The HIV-1 virus is encoded in a single-stranded, polyadenylated, positive sense RNA genome (**Figure 4**), about 9.7 kilobases (kb) in length (145), though the exact size varies by several hundred kb depending upon the reference genome (146). This genome contains a single transcriptional unit for producing 13 proteins from 9 opening reading frames (185). The group-specific antigen (*gag*) and envelope (*env*) structural genes and the polymerase (*pol*) enzymatic gene are common to all retroviruses (185) and encode polypeptides that are cleaved into their functional protein units during the virion production process (186). The Env glycoprotein is cleaved into non-covalently linked gp120 surface and gp41 transmembrane subunits; Gag is cleaved into matrix (MA), capsid

(CA), nucleocapsid (NC) and p6; and Pol (translated as part of the larger Gag-Pol polyprotein) is cleaved into protease (PR), reverse transcriptase (RT), and integrase (IN). In addition to the structural and enzymatic proteins, HIV-1 encodes for regulatory proteins trans-activator of transcription (Tat) and regulator of virion (Rev), which regulate the transcription and nuclear export of viral RNAs, respectively (145), and accessory proteins virion infectivity factor (Vif), virus protein R (Vpr), virus protein U (Vpu), and the misnamed negative regulatory factor (Nef) (186), which are required for optimal virus fitness and pathogenesis in the host (187). The gene-coding region of the genome is flanked by long terminal repeat (LTR) sequences that contain *cis*-acting regulatory elements necessary for the viral replication process (11), with other *cis*-acting elements encoded at various locations across the genome critical for different phases of the virus life cycle (discussed below) (185).

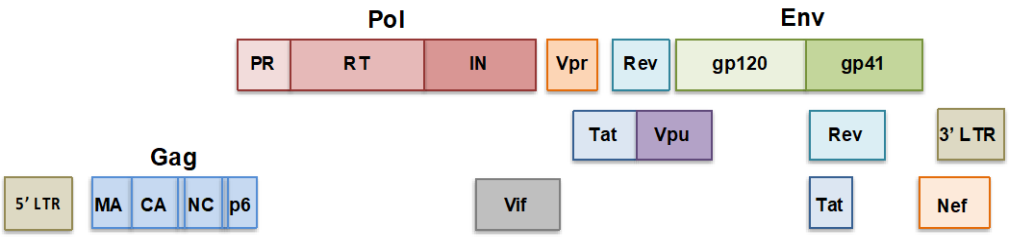

Figure 4. HIV-1 genome organization. The HIV-1 RNA genome is encoded in all three forward reading frames and contains three polyproteins that are cleaved post-translationally into individual functional units: *gag* encodes structural proteins matrix (MA), capsid (CA), nucleocapsid (NC), and p6; *pol* encodes enzymes protease (PR), reverse transcriptase (RT), and integrase (IN); and *env* encodes glycoprotein surface (gp120) and transmembrane (gp41) subunits. Regulatory proteins Tat and Rev regulate transcription and nuclear export of viral mRNAs and the full-length viral RNA genome. Accessory proteins Vif, Vpr, Vpu, and Nef modulate the host cell environment for efficient replication.

1.3.6 HIV-1 Virion

The mature HIV-1 virion (**Figure 5**) is roughly spherical and 100-120 nm in diameter (117). It is enclosed by a lipid bilayer membrane envelope derived from the host cell from which the virus particle was originally released (188), to which are bound a matrix of MA proteins on the inside surface (189) and trimers of the Env glycoprotein gp120/gp41 heterodimer on the outside surface (190). Packaged within the envelope is a distinctive conical capsid, consisting of about 1,500 copies of CA protein arranged in a hexameric lattice (191). The capsid contains two non-complementary copies of the single-stranded RNA genome in complex with NC protein, the PR, RT, and IN viral enzymes, and some viral accessory proteins and host cell factors (117).

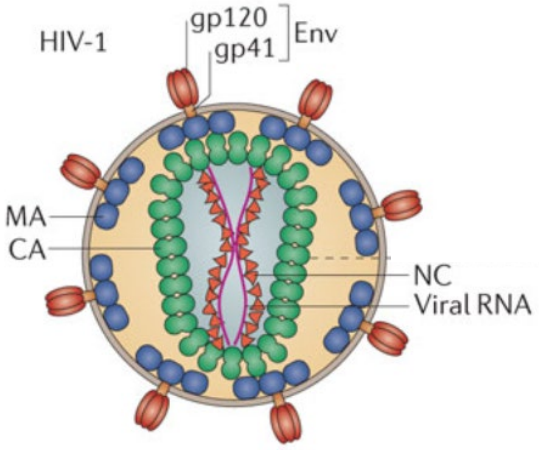

Figure 5. The HIV-1 virion. The mature HIV-1 virus particle is enclosed in a bilayer lipid membrane derived from the host cell and expresses trimers of the Env glycoprotein on the outer surface for target cell attachment. MA proteins are embedded in the inner membrane surface. Contained within the virion is a condensed conical capsid composed of CA that shields two copies of the RNA genome, which is enrobed by NC. Adapted by permission from Springer Nature Customer Service Center GmbH: Nature Reviews Microbiology (Campbell et al., 2015) **(192)**, Copyright © 2015.

Confusingly, the term ‘capsid’ has been used historically within HIV-1 research to indicate the capsid shell – both with and without its contents – or the CA monomer of which it is composed. More recently, a semi-concerted effort has been made to avoid ambiguity and distinguish these three entities by referring to them using three distinct terms – a convention which will be followed here. The individual monomer will be referred to as CA, the intact shell will be called the capsid, and core will be used to describe the capsid shell plus its contents.

1.3.7 HIV-1 Virus Life Cycle

The HIV-1 virus life cycle (**Figure 6**) is readily divisible into two phases, early and late. The early life cycle comprises those steps required for a virion to infect a target host cell: attachment, fusion, entry, trafficking to the nucleus, reverse transcription, capsid uncoating, nuclear entry, and integration. The late life cycle consists of those actions necessary for an infected host cell to produce progeny virions for subsequent rounds of infection – transcription, translation, packaging, assembly, budding, release, and maturation (117). The vast majority of HIV-1 virus particles will not ultimately be infectious (193, 194), due to virion defects that cause failure in one or more of the virus life cycle steps, to target cell resistance to infection, or to a failure to successfully enter a target cell and begin the infection process (195, 196).

As an obligate intracellular parasite, the HIV-1 virus relies almost exclusively on host cell factors to perform its various life cycle functions, packaging only those viral factors necessary to supplement – or counter – host cell functionality (197). Each stage of the virus life cycle involves interactions with dependency factors (host factors that promote viral infectivity) (198-201) and restriction factors (host factors that inhibit viral infectivity) (202-205), many with uncharacterized

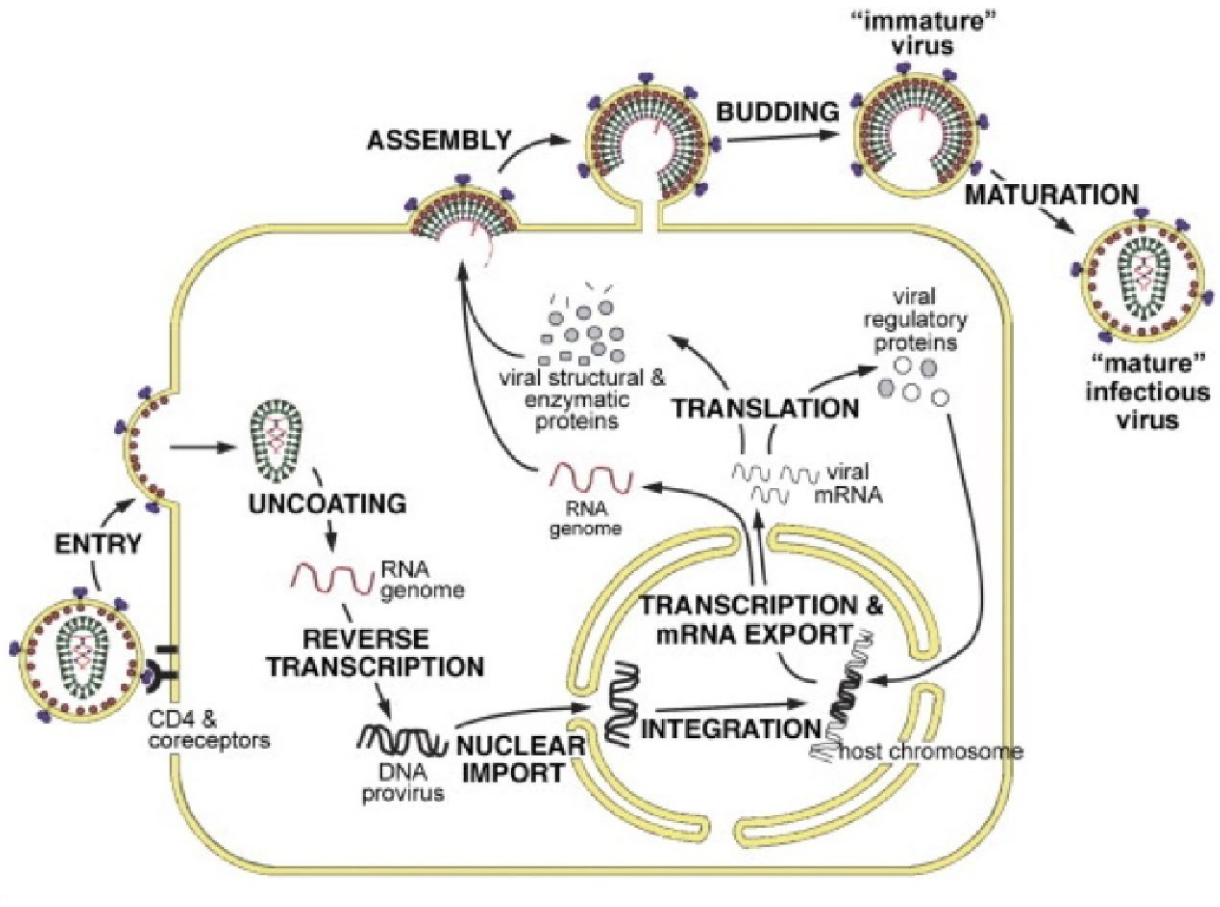

Figure 6. The HIV-1 virus life cycle. Env glycoprotein expressed on the surface of the HIV-1 virion attaches to CD4 expressed on the surface of the host cell, leading to fusion of the virion and host cell membranes and the release of the capsid into the host cell cytoplasm. The capsid uncoats in conjunction with the reverse transcription of the viral RNA genome into double stranded DNA, which is imported into the nucleus and integrated into the host chromosome. The provirus is transcribed into viral mRNA and the full-length RNA genome, which are exported from the nucleus and transcribed into viral proteins. The viral RNA genome and proteins are trafficked to the cell membrane for assembly and budding of an immature virus particle. Viral protease cleaves the structural and enzymatic polyproteins, condensing the capsid and producing a mature, infectious virus particle. Reprinted from (Ganser-Pornillos et al., 2008) **(206)**, Copyright © 2008, with permission from Elsevier.

functions in host cell processes, viral processes or both. Discussion of these collections of host factors is well beyond the scope of this work; however, their mention serves to demonstrate that the virus-host interactions involved with HIV-1 infection are numerous and complex, as well as to note that additional research is necessary to understand the mechanisms behind these interactions and how they might be subverted or enhanced to counter HIV-1 infection.

1.3.7.1 Attachment, Fusion, and Entry

As an enveloped virus, the initial step of HIV-1 infection of a target cell relies on the virion attaching to and fusing with the host cell membrane, thereby permitting deposition of the virion contents into the cell (188). This is accomplished through a multistep, sequential process coordinated by the Env glycoprotein trimer expressed on the virion surface (207). The Env trimer surface gp120 subunits engage the CD4 receptor expressed on the target cell surface, leading to a conformational change of Env, which then permits its binding to the CCR5 or CXCR4 co-receptor expressed in close proximity to CD4. An additional conformational change reveals the transmembrane gp41 core of the Env trimer, which inserts into the host cell membrane and refolds into a six-helix bundle to drive the membrane fusion process (208). Upon fusion, the viral membrane becomes continuous with the cell membrane, permitting the free diffusion of virion contents into the cytoplasm (209).

Multiple factors can limit or impede the process of host cell attachment, fusion, and entry. Env expression on the viral membrane, which varies among virus strains, is typically low and as such is a limiting factor in successful attachment (190). Similarly, the levels of CD4 and CCR5/CXCR4 expression on the target cell will influence the rate of attachment (210). As the only viral component expressed on the surface of virions, Env is the major target of antibodies

produced in response to HIV-1 infection (118, 211). To counter this humoral immune response, there are five hypervariable regions (V1-V5) on the Env surface (210), which are the most variable and genetically diverse parts of the virus (212). Mutations in these hypervariable regions result in immune evasion (120), as do alterations to the extensive glycans shield on Env (208). In addition, it is the V3 region of Env that is primarily responsible for R5/X4 co-receptor tropism (213). To overcome the limitations of Env-mediated host cell entry, *in vitro* HIV-1 studies frequently pseudotype virus, replacing Env with the vesicular stomatitis virus glycoprotein (VSV-G), which permits efficient entry into a wide range of host cell types (214).

1.3.7.2 Intracellular Trafficking

After deposition into the host cell cytoplasm, the HIV-1 conical capsid is actively trafficked toward the nucleus (215). This retrograde, inward movement is accomplished using the cell's stable microtubule network (216-218) by associating with and binding to the retrograde motor protein dynein (219) and its cargo adapters, including bicaudal D2 (BICD2) (220). Contrary to intuition, this net inward motion also requires use of the anterograde motor protein kinesin-1 and adapter protein fasiculation and elongation factor zeta 1 (FEZ1) for successful trafficking to the nucleus (221). While traversing the cytoplasm, the HIV-1 capsid must undergo two closely related viral processes, reverse transcription and capsid uncoating (215).

1.3.7.3 Reverse Transcription

A defining characteristic of retroviral infection is the conversion of the RNA viral genome to double-stranded DNA. While this process may be able to begin within a mature, cell-free virion (222, 223), the vast majority of reverse transcription occurs within the capsid deposited in the cytoplasm of an infected host cell (224). Multiple viral components have been reported to

constitute the reverse transcription complex (RTC) (225-227), though the structure of the RTC is uncertain and is closely associated with competing models of capsid uncoating (192, 228-230).

Reverse transcription is performed by the HIV-1 RT enzyme, which possesses DNA polymerase activity to synthesize DNA from either an RNA or DNA template and ribonuclease H (RNase H) activity, which degrades the RNA template from the RNA-DNA hybrid formed during the first DNA strand synthesis (231). Being a noncircular template, the full reverse transcription of the linear viral genome requires the performance of two strand transfer events in order to relocate DNA synthesis from one end of the template to the other (224). The presence of two copies of the RNA genome permits strand transfer to switch between the co-packaged genomes and recombine (232, 233), which can overcome genome damage (234, 235). If the genomes are genetically distinct, this recombination can generate a chimeric genome (224).

DNA synthesis begins with a primer annealed to the RNA genome template, for the purpose of which lysine transfer RNA isoacceptor 3 ($tRNA^{Lys3}$) from the virus particle's parent host cell is packaged, bound to the aptly-named primer binding site (PBS), located approximately 180 bases from the 5' end of the viral genome (224). Reverse transcription proceeds the short distance to the 5' end, where the first strand transfer operation is performed to transfer synthesis to the 3' end of the genome, facilitated by complementarity between the direct repeat "R" region located on each end of the viral genome (231). Following strand transfer, first strand DNA synthesis continues the length of the RNA genome, accompanied by RNase H degradation of the RNA template. This degradation is imperfect and leaves multiple, small RNA fragments annealed to the DNA strand, in particular at two polypurine tracts (PPT) located in the central (cPPT) and

3’ (3’PPT) portions of the genome (231). This PPT RNA serves as a primer for initiating synthesis of the second DNA strand. Synthesis from the cPPT produces the second strand of DNA up to the 3’PPT. Synthesis from the 3’PPT leads to the second strand transfer operation to transfer synthesis to the 5’ end of the genome, assisted by complementarity between the PBS and the still-attached $tRNA^{Lys3}$ primer, which is cleaved in the process (236). Second strand synthesis proceeds until the cPPT is reached but doesn’t terminate until after overrunning and displacing approximately 100 nucleotides of cPPT-primed second strand DNA, resulting in the formation of a “central flap” (237). It has been suggested this flap promotes capsid uncoating (230) and viral DNA nuclear import (238, 239); however, the necessity of the DNA flap for HIV-1 infectivity is debated (240-242).

After the completion of reverse transcription, the terminal ends of the double-stranded DNA genome are associated with and processed by a higher-order structure of the HIV-1 IN enzyme in preparation for integration (243). This intasome complex contains 16 copies of IN arranged in a tetramer-of-tetramers architecture, with each tetrameric complex contributing IN subunits to the conserved intasomal core, where DNA processing occurs (244, 245). The 3’ strand on each end is trimmed by two nucleotides to a conserved CA dinucleotide, exposing a reactive hydroxyl group (CA_{OH}-3’) that will be utilized during integration (231). The end-processed, double-stranded viral DNA associated with IN and other viral proteins is now referred to as the pre-integration complex (PIC) (246).

Being a viral process with no analog in the host cell, HIV-1 reverse transcription and its intermediate products are ideal candidates for immune recognition and restriction (247).

Hypermutation can be induced in newly reverse transcribed DNA by the host cell deaminase apolipoprotein B messenger RNA (mRNA)-editing enzyme-catalytic polypeptide-like 3G (APOBEC3G) resulting in degradation of the viral DNA and/or loss of infectivity (248). This is countered by the HIV-1 protein Vif either during virus particle assembly (249) or in the newly-infected host cell (248, 250, 251). As HIV-1 reverse transcription requires a pool of dNTPs to synthesize DNA, depletion of dNTP pools in non-cycling myeloid cells, such as macrophages, by SAMHD1 serves to stall reverse transcription and restrict HIV-1 infectivity (91, 92). Unlike HIV-2 and some SIV viruses, HIV-1 lacks a virus protein X (Vpx), which can target SAMHD1 for degradation and restore dNTP levels (252, 253), resulting in limited HIV-1 infection in these cells (254). Numerous host cell cytosolic pattern recognition receptors (PRRs) are tuned to detect double-stranded DNA, DNA/RNA hybrids and non-messenger RNA, all indicative of viral infection, leading to the degradation of these products and/or heightening the immune activation of the infected and surrounding cells (255). A fully or partially intact viral capsid masks these pathogen-associated molecular patterns (PAMPs) and evades immune recognition (256, 257).

1.3.7.4 Nuclear Entry

While an intact nuclear membrane prevents most retroviruses from accessing the host genome (148, 258) until it is disassembled during the cell division process of mitosis (259), lentiviruses like HIV-1 are able to translocate their PIC into an intact nucleus (148, 260) by way of transport through nuclear pore complexes (NPC) (261), selective gateways for nucleocytoplasmic exchange interspersed across the membrane (259). NPCs have a small diffusion limit, requiring most cargo, including HIV-1 PICs, to be actively transported through the pore (262), through interactions with nucleoporin (Nup) proteins that line the pore (259) and transport receptor proteins such as the karyopherins (importins, exportins, and transportins), which specialize in shuttling cargo in and

out of the nucleus (262). The directionality of this transport is established by the presence of a nuclear localization signal (NLS) on the cargo (263).

Multiple elements of the HIV-1 PIC have been shown to possess an NLS and contribute to the nuclear import of the PIC, including MA, Vpr, and IN (261, 264). However, the significance and necessity of these signals for import are questionable (265-267). More widely accepted is the role of CA as the major viral determinant of PIC nuclear import (268), which has been shown to interact with multiple nucleoporins upon which HIV-1 infectivity is dependent (267, 269), most notably nucleoporin 358 (Nup358, also known as Ran binding protein 2, or RanBP2) (270-272) and nucleoporin 153 (Nup153) (273-275), which reside at the external and internal boundary of the NPC, respectively (259). The karyopherin transportin3 (TNPO3, also known as transportin-SR2, or TRN-SR2) (276, 277) ferries cargo proteins containing serine-arginine (SR) repeat domains into the nucleus, including cleavage and polyadenylation specificity factor 6 (CPSF6) (278, 279). TNPO3 has also been shown to promote trafficking of HIV-1 PICs into the nucleus (280), ostensibly indirectly by its canonical transport of CPSF6 (281, 282), which binds to CA and mediates the dependence on TNPO3 (266, 283). While a model of HIV-1 PIC nuclear import via interactions with CPSF6/TNPO3, Nup358, and Nup153 fits these numerous observations (284), other potential pathways through the nuclear pore appear to exist (261, 266, 267, 269, 270). Additional research is necessary to determine elements of this alternative pathway.

1.3.7.5 Capsid Uncoating

One of the more enigmatic aspects of the HIV-1 virus life cycle is the process by which the intact conical capsid core becomes dissociated, or uncoated, to permit the release of the PIC into the nucleus for integration (284, 285). The large size of the intact core relative to nuclear pores dictates

that successful deposition of the PIC into the nucleus requires a shedding of some or most CA from the capsid (192, 286). Absent capsid uncoating, PICs accumulate at the cytoplasmic face of the nuclear membrane, unable to transit the NPC and enter the nucleus (230, 272, 287). This is countered by the need to shield the PIC from immune recognition and restriction while transiting the cytoplasm (256, 257), which supports retention of all or most CA until the nuclear membrane is reached. Studies have suggested that there is an optimal window in which capsid uncoating may occur, with shedding CA too early or retaining it too long resulting in a loss of virus infectivity (228, 288). A more comprehensive discussion on capsid uncoating will be deferred until a later section (**Section 1.5.3**).

1.3.7.6 Integration

The hallmark of retroviral infection is the deliberate, stable integration of the reverse transcribed DNA genome into the host cell genome that establishes persistent infection of the cell and its progeny (289). Once translocated into the nucleus, the PIC is targeted to the chromosomal genome, where HIV-1 IN performs the DNA strand transfer reaction that effects integration (290). The CA_{OH}-3' processed ends of the viral DNA genome are used to catalyze the hydrolysis of opposing chromosomal DNA strands, each end attacking one strand, offset 5 base pairs (bp) from one another, resulting in the covalent attachment of these 3' proviral ends to the host genome (291, 292). The remaining single strand gaps and 5' viral DNA overhangs are left to be resolved by the host DNA repair machinery (289), which also produces unintegrated, circularized forms of proviral DNA (2-LTR circles) (293) from PICs that fail to integrate (294).

Integration always occurs at the ends of the viral DNA genome but can occur at many positions within the host genome, with most positions being able to serve as acceptor sites, though

there are regional preferences. Specifically, HIV-1 preferentially integrates into transcriptionally active sites (295), which may be located near the periphery (296, 297) or the interior (298, 299) of the nucleus. While HIV-1 IN is competent on its own to perform the integration reaction, it requires assistance from host factors to target particular locations in the host genome. CPSF6, a pre-mRNA splicing factor, binds to CA and directs the PIC to transcriptionally active chromatin (300, 301). Lens epithelium-derived growth factor / transcriptional coactivator p75 (LEDGF/p75) binds to IN and tethers it to chromosomal DNA, directing the position of integration within gene bodies (301-303).

1.3.7.7 Latency

The integration of HIV-1 viral DNA represents the midpoint of the virus life cycle, in which the target cell is successfully infected and possesses the potential to produce progeny virus particles, if stimulated to do so (304). Absent such production, the host cell infection is deemed latent (305) and host cells in a latent state are referred to collectively as the latent reservoir (306, 307). Viral latency differs from clinical latency, the latter being a stage of infection where no clinical signs of disease are discernable, but in which virus particles are nonetheless being produced (60, 116). The latent reservoir does not include defective proviruses that are not replication-competent (308), which account for the majority of proviruses (309), as these lack the potential to produce infectious virus. True latent infection is rarely established (305), but results in a persistent population of infected host cells, most commonly among resting memory CD4+ T cells (310).

Mechanistically, latency involves the establishment of host cell conditions unfavorable for transcription of provirus (305). This can be due to sequestration of host transcription factors or components of the transcription machinery (29), or to epigenetic chromatin modifications (311),

particularly in proximity to the U3 region of the 5'-LTR (312), which acts as the promoter for HIV-1 provirus transcription (313). Alleviating the block(s) to provirus transcription can shift the infected host cell from latency to active production of virus (311). However, many proviruses (including replication-competent ones) are not induced to produce virus upon stimulation (309).

1.3.7.8 Transcription and Translation

Production of progeny virus particles from an infected host cell begins with transcription of the HIV-1 provirus, which is performed by cellular machinery (314), but depends highly upon the viral regulatory protein Tat, without the expression of which transcription is generally non-processive (315). Tat binds to the *cis*-acting RNA element trans-activation response element (TAR) that is present at the 5' end of all HIV-1 viral transcripts (316) and promotes elongation. The initial expression of small amounts of Tat results in a positive feedback loop (317) that leads to the efficient production of viral transcripts.

While all HIV-1 viral transcripts are initiated in the 5'-LTR, alternative splicing is used to alter the mRNAs that are produced, with more than 40 different splice variants possible (312). Alternate splicing is used to control the temporal expression of HIV-1 regulatory, accessory, enzymatic, and structural mRNAs and proteins and full-length genomic viral RNA (318). Completely spliced mRNAs for Tat, Rev, and Nef protein expression are produced early, followed by the intermediate production of partially spliced mRNAs for Env and the accessory proteins Vif, Vpr, and Vpu, and finally the late production of unspliced, full-length viral RNA that serves as mRNA for Gag and Gag-Pol and also as the genomic RNA for progeny virus (312). Rev binds to the Rev-response element (RRE) located in the *env* gene, promoting the nuclear export of partially

spliced and unspliced viral RNAs containing the RRE (319), which would otherwise normally be degraded in the nucleus (312).

As with transcription, HIV-1 uses host cell machinery to translate viral mRNAs into viral proteins (320). While most of these mRNAs contain a single open reading frame and can be translated simply, two of the mRNAs are bicistronic, encoding proteins in multiple reading frames, necessitating programmed ribosomal frameshifting based upon primary mRNA sequence and secondary structural signals to access downstream open reading frames (321). In this manner the Gag and Gag-Pol polyproteins are synthesized from the full-length viral RNA in a 20:1 stoichiometric ratio (322) and the Env and Vpu proteins are synthesized from the same single-spliced mRNA (323).

As the Env protein is being translated, it is translocated into the endoplasmic reticulum (ER), where it enters the cell secretory pathway and undergoes post-translational modifications including glycosylation, assembly into trimers, and cleavage into gp120 and gp41 subunits by the cellular enzyme furin before being trafficked to the plasma membrane (324). While in the ER, Env can become trapped by newly synthesized CD4 and subsequently degraded (323). This sequestration is countered by the HIV-1 accessory protein Vpu, which downregulates expression of newly synthesized CD4 (325).

1.3.7.9 Packaging, Assembly, Budding, Release, and Maturation

The packaging of HIV-1 virus particle contents is orchestrated by the Gag polyprotein, which contains all the necessary information and signals to directly or indirectly incorporate the remaining viral and host factors (191). The viral RNA genome binds to the NC domain of Gag

(326) by way of a packaging signal (Psi, Ψ) (327) in coordination with adjacent stem-loop structures (328) located near the 5' end of the genome. Two copies of the RNA genome are packaged in the vast majority of virions (329), which is accomplished by a non-covalent, Watson-Crick base-paired association of the two genomes mediated by the so-called "kissing-loop dimer" stem-loop structure (330). Cellular RNAs are also packaged into the virion (324), including the lysine transfer RNA ($tRNA^{Lys3}$) used as the primer to initiate reverse transcription (331). Viral accessory proteins (250, 332) and numerous host factors are packaged as well (333, 334).

The N-terminal MA domain of the Gag and Gag-Pol polyproteins is co-translationally myristoylated, which, combined with an adjacent basically-charged region, serves to target and anchor these polyproteins to the plasma membrane in lipid raft regions enriched with the phospholipid phosphatidylinositol-4,5-bisphosphate [$PI(4,5)P_2$] (335). The gradual congregation (336) of approximately 2,500 Gag molecules at the plasma membrane (337) leads to the formation of a spherical bulge in the membrane with the Gag and Gag-Pol polyproteins assuming a "beads on a string" hexameric lattice conformation, with their C-terminal ends extending inwards from the membrane (191). This spherical bud remains attached to the cell membrane by an unclosed stalk, which requires recruitment of the cellular endosomal sorting complex required for transport (ESCRT) machinery to perform membrane scission and release the nascent virus particle (322).

During budding and release, noninfectious, immature virus particles begin to undergo maturation, in which dimeric HIV-1 PR cleaves the Gag and Gag-Pol polyproteins into their constitutive functional domains (324). This proteolytic cleavage proceeds at distinctly different rates for each PR cleavage site (338) and results in an ordered disassembly of the immature Gag

lattice (191). The freeing of Gag domains leads to the molecular transformation of the individual CA monomers into the approximately 240 hexamers and exactly 12 pentamers that comprise the characteristic conical capsid (191), which encloses the condensed viral RNA genome, encased in NC, and the viral RT and IN enzymes (338, 339). Prior to maturation, nascent virus particles are impaired for cell membrane fusion to prevent immature, noninfectious particles from depositing their contents into host cells, via a transmembrane interaction between MA and Env gp41, which is mediated by PR cleavage of MA from Gag (340, 341). Once mature, cell-free virions are competent to infect target host cells and start a fresh round of HIV-1 infection.

1.3.8 HIV-1 Replication Kinetics, Mutation, and Genetic Diversity

HIV-1, like other RNA-based viruses, ensures its survival by having a short replication cycle that produces a large number of virus particles with a relatively high rate of mutation (342). Most of these mutations occur through the reverse transcription process, though some studies have suggested that the host RNA polymerase II enzyme, which transcribes the HIV-1 provirus from the host genome, could also make an appreciable contribution (343). The reduced fidelity of reverse transcription is frequently cited as being due to a lack of proofreading activity in the HIV-1 RT enzyme (231), but is also in part attributable to mutations in RT (343), abnormal strand transfer (344), recombination (224), and the activity of the APOBEC3G host restriction factor (248, 251). The single-step point mutation rate of reverse transcription is about $3x10^{-5}$ mutations per base per round of replication (344), which, when combined with the approximate 10 kb size of the viral genome, suggests that on average about one third of HIV-1 genomes contain a mutation after each round of replication (107).

The HIV-1 virus replication cycle time has been observed to take on average one to two days (107), with infected cells producing between 100 and 1,000 virions each per cycle (345). With more than one billion new cells estimated to be infected daily (346) and accounting for a rapid turnover of infected cells every 2 to 3 days (347), an HIV-1 infected individual can produce 10 billion virus particles each day (347). Combined with the above mutation rate, this suggests that statistically every possible single point mutation would occur between 10,000 and 100,000 times in an infected individual (346). This is supported by the observation that while most patients are initially infected with a single virus (348), a diverse population of viruses is found within infected individuals (224), indicating that mutations that arise during the virus life cycle within an individual drive this viral diversity (346).

This broad intra-host diversity means that HIV-1, like most RNA viruses, exists as a quasispecies – a population of genetically diverse but linked mutant viruses that collectively contribute to its overall characteristics and behaviors (349). No single virus can explain or account for all of the phenotypes observed; instead, the entire diverse mutant population has to be considered as a whole (350). Such genetic diversity permits HIV-1 to adapt rapidly to the host immune response, contributing to the ineffectiveness of immune control of viral replication (351, 352). Additionally, this diversity increases the likelihood that mutations conferring resistance to one or more antiretroviral therapeutics will already exist within an infected individual prior to treatment or may arise during therapy (346).

1.4 Antiretroviral Therapy

In the early days of the HIV/AIDS epidemic, a diagnosis of HIV-1 infection was a near-certain, albeit generally prolonged, death sentence (131). That began to change in 1987, with the release of the first HIV-1 ART pharmaceutical, zidovudine (or azidothymidine, AZT) (353). This breakthrough has been followed by the development of multiple generations of ART, divided into several different classes of drugs, targeting multiple virus components, and taken in combination (25). The deployment of combination antiretroviral therapy (cART) ushered in a new phase of the HIV/AIDS epidemic, punctuated by the conversion of HIV-1 infection into a manageable, chronic condition where, with diligent adherence to treatment, life expectancy of HIV-1 infected individuals can approach that of the general population (354, 355).

1.4.1 ART Medications and Drug Resistance

Current United States Federal Drug Administration (FDA)-approved ART medications fall into one of seven classes, targeting one of the viral enzymes, the viral Env surface glycoprotein, the cellular CD4 receptor, or the cellular CCR5 co-receptor (356). An additional class of medication, pharmacokinetic enhancers (ritonavir and cobicistat), may be included to increase bioavailability of those drugs metabolized by cytochrome P450 3A (CYP3A) enzymes (357). Almost two dozen bivalent and trivalent formulations have also been approved that contain drugs directed against at least two different molecular targets (356) to forestall the development of drug resistance mutations (25), which readily emerge during monotherapy (346), frequently from preexisting resistant viral populations (358). Poor adherence to ART dosing schedules, frequently due to poor tolerance of side effects and/or patient behavior factors (38), can lead to treatment failure and the

development of resistance, necessitating a change in ART regimen (25). As the virus continues to evolve and resist treatment, additional ART medications are required to effectively treat HIV-1 infected individuals (359).

1.4.1.1 Nucleoside/Nucleotide Reverse Transcription Inhibitors

Nucleoside/nucleotide reverse transcriptase inhibitors (NRTIs) represent the initial class of ART pharmaceuticals (353). As the name implies, NRTIs inhibit the function of HIV-1 RT by mimicking and competing with the dNTP substrates incorporated by RT into the nascent reverse transcribed viral genome (360). Key to their function is the lack of a 3'-hydroxyl group on the 2'-deoxyribosyl sugar that is required for forming a 3'-5'-phosphodiester bond with a subsequently appended dNTP, thereby preventing further incorporation of dNTPs and prematurely terminating reverse transcription of the viral genome (360-362). Resistance to NRTIs results in either improved discrimination of natural dNTPs from NRTI analogs or a reversal of chain termination by the excision of the NRTI (363-365). Current FDA-approved NRTIs include zidovudine (AZT), lamivudine (3TC), abacavir (ABC), tenofovir (TDF), and emtricitabine (FTC) (356).

1.4.1.2 Non-Nucleoside Reverse Transcriptase Inhibitors

Non-nucleoside reverse transcriptase inhibitors (NNRTIs) take a different approach at inhibiting RT non-competitively by acting upon the enzyme itself (366). NNRTIs bind to RT in a hydrophobic pocket adjacent to the polymerase catalytic active site, inducing conformational changes to RT and impairing the polymerization reaction (366-369). Despite considerable chemical diversity among NNRTIs, resistance to one drug, which can arise quickly after initiation of treatment, tends to result in cross-resistance to other NNRTIs (370). NNRTIs currently approved

for clinical use include nevirapine (NVP), efavirenz (EFV), etravirine (ETR), rilpivirine (RPV), and doravirine (DOR) (356).

1.4.1.3 Protease Inhibitors

Protease inhibitors (PIs) target the late virus life cycle stage of maturation by inhibiting HIV-1 PR cleavage of Gag and Gag-Pol (371). Virus particles lacking proper processing by PR are rendered noninfectious (372). Resistance to PIs comes from mutations in PR near the enzymatic active site (371, 373) and to changes in the protease cleavage sites in *gag* and *pol* to overcome fitness deficiencies in mutated PR (374). Protease inhibitors saquinavir (SQV), atazanavir (ATV), fosamprenavir (FPV), tipranavir (TPV), and darunavir (DRV) are currently approved for clinical use (356).

1.4.1.4 Integrase Strand Transfer Inhibitors

Integrase strand transfer inhibitors (INSTIs) prevent the integration of the HIV-1 DNA genome into the host genome by inhibiting the strand transfer reaction catalyzed by HIV-1 IN (375, 376). Inhibition is accomplished through active site binding and chelation of magnesium ions that are requisite cofactors of the reaction (377). Mutations in or near the IN catalytic core can lead to INSTI resistance (378). Only two INSTIs, raltegravir (RAL) and dolutegravir (DTG) are currently approved (356).

1.4.1.5 Entry Inhibitors

The final three classes of ART medications are designed to inhibit the attachment and fusion of a virus particle to a host cell. Post-attachment inhibitors bind noncompetitively to host cell CD4 receptors and prevent post-attachment conformational changes to the complex of CD4 and the

HIV-1 Env gp120 subunit that are required for co-receptor engagement (379). CCR5 antagonists are allosteric inhibitors of CCR5 agonists and the HIV-1 Env glycoprotein which alter CCR5 conformation and prevent the Env-CCR5 interaction necessary to promote stable attachment and subsequent fusion (380, 381). Fusion inhibitors prevent the Env gp41 subunit from promoting the fusion of the viral and cell membranes by mimicking the gp41 leucine zipper domain, preventing conformational changes to gp41 that are required for fusion (25, 382-384). Only one medication in each of these categories is currently approved for clinical use: post-attachment inhibitor ibalizumab (IBA), fusion inhibitor enfuvirtide (T-20), and CCR5 antagonist maraviroc (MVC) (356).

1.4.2 HIV-1 Capsid as a Target for Antiretroviral Therapy

The continued development of drug resistance mutations to current HIV-1 ART drives the pursuit of new therapeutic targets (25, 38). While the viral enzymes represent the principal targets of ART and account for the vast majority of presently approved pharmaceuticals (25, 385), attention has turned toward other viral components, including the Gag structural proteins (386). Among these, CA or capsid represents a viable therapeutic target, for which numerous small molecule inhibitors serve as a proof of concept (387).

CA plays a critical role in all post-entry events of the early virus life cycle, shielding the viral genome from cytoplasmic innate immune sensors, regulating the completion of reverse transcription, governing the use of nuclear trafficking and import pathways, and assisting in integration site targeting (192, 285, 388, 389). As an RNA virus, HIV-1 is prone to develop mutations during its replication cycle (390). Viable mutations are generally confined to certain

regions of the viral genome, particularly in Env and the accessory proteins (212, 391). Other parts of the genome are relatively intolerant to mutation, with sequence alterations compromising viral viability (392). CA exhibits some of the strongest sequence conservation across the viral genome (212, 391) and displays a high degree of mutational fragility, with most amino acid changes resulting in dysfunctional CA and severely impaired virus infectivity (393, 394). The HIV-1 capsid is not analogous to any host protein or complex and offers multiple interfaces within the capsid lattice that could be targeted by protein-protein interaction inhibitors (395). This combination of critical function, mutational fragility, and absence of host analogs makes the capsid a desirable target for antiretroviral intervention (386, 387).

An increasing number of small molecule compounds have been identified that target CA in its immature or mature form and inhibit HIV-1 virus infectivity (387). The majority of these compounds act on the late stages of the virus life cycle, inhibiting virus particle assembly (396-404) or maturation (405-408). Several CA-targeting compounds, however, impair early virus life cycle events, primarily reverse transcription and capsid uncoating (395, 404, 409-415), but also integration (416). Interestingly, several of these early-acting small molecules (404, 409-411, 413) target the same binding pocket on CA at which CA interacts with host dependency factors CPSF6 and Nup153 (417, 418). This has led to speculation that one mode of operation of these compounds is to inhibit CA interactions with these host factors, particularly at low doses (419), though ample evidence suggests that altering capsid stability is the primary mechanism of restriction (417-420).

While these compounds targeting CA or capsid have proven to be useful research tools, their therapeutic development has been impaired by *in vivo* selection of drug resistance mutations,

the prevalence of resistance-conferring polymorphisms, and challenges in translation into clinical use (387). A better understanding of how the HIV-1 capsid interacts with host factors and facilitates early and late virus life cycle events can inform on targetable aspects of capsid functionality and help direct intelligent design of novel therapeutics.

1.5 The Many Roles of HIV-1 Capsid

The HIV-1 capsid has been previously introduced and presented within the context of the virus life cycle, where it was shown to be involved in every post-entry step of the early life cycle (**Section 1.3.7**). Here, a brief synopsis of capsid assembly and structure will be provided along with an examination of how many of these roles of capsid can be described by considering capsid to function both as an interaction surface and as a protective shell.

1.5.1 HIV-1 Capsid Assembly and Structure

When initially released from an infected host cell, a nascent HIV-1 virus particle is immature and uninfectious (324). Encased within and attached to the lipid bilayer envelope is a protein lattice consisting of 3,000 to 5,000 copies of the Gag structural polyprotein (421, 422). Gag is comprised of four independently-folded structural domains, principally composed of alpha helices, linked by flexible regions (191) (**Figure 7A and 7B**). The N-terminal MA domain is co-translationally myristylated and links the Gag lattice to the envelope membrane (335). MA is linked on its C-terminal side to CA, consisting of the two separate functional domains CA^{NTD} and CA^{CTD} (in reference to their amino-terminal [NTD] and carboxy-terminal [CTD] orientation), a spacer

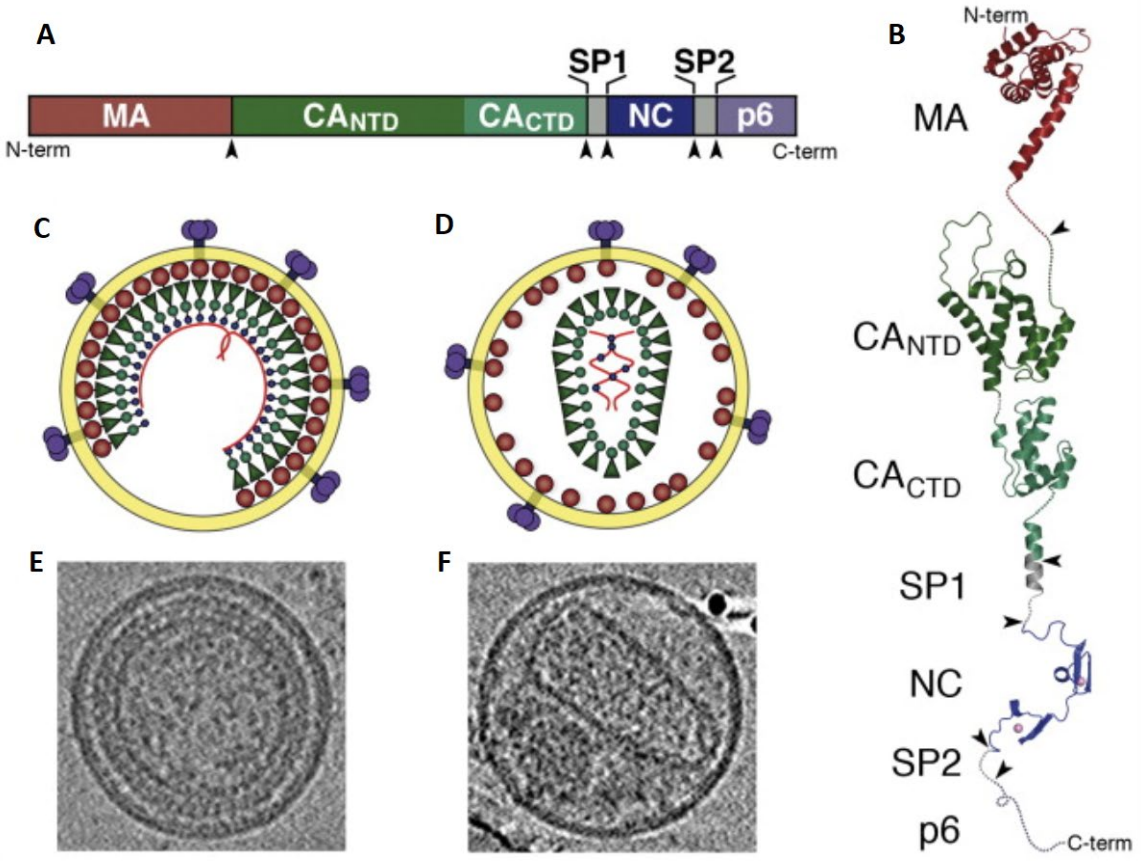

Figure 7. Assembly and maturation of the HIV-1 virion. (A) Schematic of the HIV-1 Gag structural polyprotein domain structure showing the relative positions of the MA, CA_{NTD}, CA_{CTD}, SP1, NC, SP2, and p6 functional units. (B) Structural model of the Gag polypeptide represented in (A), derived from high resolution structures and models of each domain. Dashed lines represent linker and unstructured regions. Arrowheads show PR cleavage sites in (A) and (B). Schematic models of immature (C) and mature (D) virions. Electron cryotomographic slices through the central plane of immature (E) and mature (F) virions. The spherical virus particles are approximately 130 nm in diameter. Reprinted from (Ganser-Pornillos et al., 2008) **(206)**, Copyright © 2008, with permission from Elsevier.

peptide (SP1), NC, a second spacer peptide (SP2), and the C-terminal p6 region (421). The immature Gag lattice (**Figure 7C and 7E**) is formed by interactions in the CA and SP1 regions, with CA^{NTD} and CA^{CTD} forming stacked, homo-hexameric rings (191) stabilized by an SP1 six-helix bundle (423, 424) that coordinates an inositol hexakisphosphate (IP_6) molecule (425).

The cleavage of Gag by PR into its constituent proteins drives the virus particle maturation process. Thus freed, the structural proteins undergo a dramatic reorganization, culminating in the condensation of about 1,500 CA monomers into a closed shell, encasing the viral genome (324). The immature CA hexamers undergo conformational adjustment, facilitated by the refolding of the CA N-terminal 13 residues into a β-hairpin upon CA^{NTD} cleavage from MA and CA^{CTD} cleavage from SP1 (191), and the re-engagement of IP_6 within the CA^{NTD} hexamer (425). This rearrangement results in the disassembly of the immature Gag lattice and the formation of the mature capsid lattice (**Figure 7D and 7F**). While the manner in which the mature capsid is formed remains uncertain (426), most models suggest a disassembly-reassembly pathway in which the capsid is synthesized *de novo* from individual CA monomers and/or small multimers (427).

The mature capsid (**Figure 8**) is modeled as a fullerene cone, consisting of a two-dimensional lattice of approximately 250 CA hexamers that incorporate exactly 12 pentamers to form a closed shell (428). The placement of the pentamers dictates the three-dimensional shape of this shell, with five pentamers located on one end and seven on the other end, resulting in the distinctive cone-shaped HIV-1 capsid (191). The asymmetry inherent to this arrangement is principally accommodated by the flexible linker between the CA^{NTD} and CA^{CTD} domains, which permits the inter-hexameric interfaces to adopt the necessary range of interface angles (429, 430).

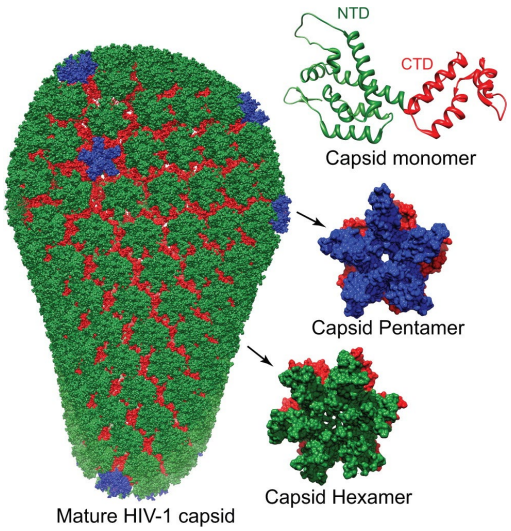

Figure 8. HIV-1 capsid assembly. The HIV-1 capsid monomer (top right) is comprised of NTD (green) and CTD (red) domains. Approximately 1,500 monomers assemble into hexamers (bottom right) and exactly 12 pentamers (middle right). NTDs are shown in green and blue for hexamers and pentamers, respectively, and CTDs are shown in red for both oligomers. A model of the fully assembled mature capsid (left) with adjacent hexamers and pentamers connected by CTD dimers. Reprinted with permission from (Deshmukh et al., 2013) **(431)**. Copyright © 2013 American Chemical Society.

The CA hexamers consist of an inner six-fold symmetric CA^{NTD} ring, which is stabilized by NTD-NTD interactions among ring members, and an outer CA^{CTD} "girdle" that is stabilized by NTD-CTD interactions between adjacent ring members (432, 433). The CA^{CTD} girdle interacts with neighboring hexamers at two-fold and three-fold symmetric CTD-CTD interfaces, stabilizing the overall capsid structure (430, 432). In this manner, the CA^{CTD} girdles act as the glue that holds the core together as a protective shell while the CA^{NTD} rings protrude from the surface of the core like small hexameric crowns, forming an interaction surface with the surrounding environment.

1.5.2 HIV-1 Capsid as an Interaction Surface

HIV-1 cannot rely only upon its own devices to successfully infect a host cell. Virus infectivity depends on utilizing a wide array of host factors to complete each of the virus life cycle steps (197). Three independent small interfering RNA (siRNA) screens (198-200) identified many such host dependency factors, which interact with various virus components at each step of the life cycle to facilitate infection (201, 434). Interestingly, the three screens each utilized a different strain of HIV-1 infecting a different host cell type (HIV-1_{IIIB} in HeLa-derived TZM-bl cells (198), HIV-1_{NL4-3} in HEK 293T cells (200), and HIV-1_{HXB2} in HeLa P4/R5 cells (199)) and produced little overlap of identified host dependency factors (201), suggesting that different HIV-1 strains can interact with distinct sets of host factors in different cell types.

Host factors that have been shown to interact with CA, including a small subset of factors identified in the above screens, will be considered below in two categories: factors identified fairly recently that primarily influence intracellular trafficking and may show effects on downstream events such as capsid uncoating or nuclear entry; and factors that have been well-characterized over a number of years and that have been shown primarily to affect nuclear entry and integration site preference, though they might also influence capsid uncoating. Numerous point mutations in CA have been identified that specifically impair interaction with one or more host dependency factors (267), particularly with well-characterized host factors. While these mutations are not necessarily of clinical significance, they facilitate the study of particular host factors that affect virus infectivity. A table summarizing the CA mutations described below is provided (**Table 1**).

Table 1. HIV-1 CA mutations and associated phenotypes

Mutation	Phenotype	Reference
T54A	Infects independently of CypA Cell cycle dependent in some cell types	(von Schwedler, 2003) (393)
N57A	Infects independently of CPSF6, Nup153, and Nup358 Cell cycle dependent in all cell types tested	(Yamashita, 2007) (268)
N57S	Infects independently of CPSF6, Nup153, and Nup358 Cell cycle dependent in all cell types tested Sensitive to treatment with CsA	(Rihn, 2013) (394)
N74D	Infects independently of CPSF6, Nup153 and Nup358 Infection restricted in macrophages prior to reverse transcription Sensitive to treatment with CsA	(Lee, 2010; Ambrose, 2012) (266, 435)
A77V	Infects independently of CPSF6, Nup153, and Nup358 Infects macrophages efficiently	(Saito, 2016) (436)
G89V	Does not bind to CypA Infects independently of Nup153 and Nup358	(Yoo, 1997) (437)
P90A	Does not bind to CypA Infects independently of Nup153 and Nup358	(Yoo, 1997) (437)
A92E	Infects independently of CypA Cell cycle dependent in some cell types	(Aberham, 1996; Braaten, 1996) (438, 439)
G94D	Infects independently of CypA Cell cycle dependent in some cell types	(Aberham, 1996; Braaten, 1996) (438, 439)
N121K	Infects independently of CypA	(Takemura, 2013) (440)
R132K	Infects independently of CypA Cell cycle dependent in some cell types	(Schneidewind, 2007) (441)

A set of recently identified capsid-interacting host dependency factors are all involved in microtubule-related trafficking and have been shown to be necessary for proper movement of HIV-1 cores within the host cell. Knockdown of microtubule stabilizing proteins diaphanous (Dia)-related formins (DRFs) Dia1 and Dia2 reduces core retrograde trafficking and impairs capsid uncoating (218). Depletion of microtubule-associated proteins 1 (MAP1) inhibits retrograde movement of the core and PIC nuclear entry (217). Dynein adapter protein BICD2 depletion delays capsid uncoating and impairs retrograde trafficking and nuclear entry (220, 442). FEZ1, a kinesin-1 adapter protein, binds to both CA and kinesin-1 and promotes net retrograde trafficking of the capsid, which is abrogated with a loss of interaction between FEZ1 and CA or between FEZ1 and kinesin-1 (221).

1.5.2.1 CypA

A set of five capsid interacting host dependency factors have been particularly well characterized, though their contributions to HIV-1 infectivity are complex, interdependent, and frequently cell type specific. Cyclophilins are host factors that were originally identified by their binding to the immunosuppressant drug cyclosporine A (CsA) (443). One family member, cyclophilin A (CypA), is among the earliest characterized HIV-1 host dependency factors that interact with CA, having been identified more than 25 years ago (444). CypA binds to CA on the prominent, extended loop between CA^{NTD} helices 4 and 5 that protrudes from the surface of the capsid and is eponymously known as the CypA binding loop (445). Functionally a peptidylprolyl isomerase, CypA catalyzes the cis/trans isomerization of the peptide bond between CA amino acids G89 and P90, which lies directly in the enzymatic active site when CypA is bound to CA (445, 446). This isomerization introduces conformational changes in CA distal to the CypA binding loop (446). A second,

noncanonical binding site on CypA has been suggested to also engage a separate CA monomer in an adjacent CA hexamer, stabilizing the capsid (447).

CypA is incorporated into nascent virus particles during assembly by binding to the CA^{NTD} domain of uncleaved Gag (448, 449). However, multiple studies have shown that it is CypA expression in target cells and not producer cells that governs its effects on HIV-1 infectivity (450, 451). Mutating the two key CA amino acids recognized by the CypA binding pocket to G89V or P90A abrogates CA-CypA interaction (437) and substantially attenuates infectivity (448, 452). Treatment with CsA or similar drugs inhibits the CA-CypA interaction (452-454), resulting in reduced virus infectivity (450, 451). Selection *in vivo* in the presence of CsA and mutagenesis studies have identified multiple CA mutations that permit HIV-1 replication in the presence of CsA, most notably A92E and G94D within the CypA binding loop (438, 439), but also at other, distal locations within the CA^{NTD} domain (285), including T54A in helix 3 (455), N121K between helices 6 and 7 (440), and R132K in helix 7 (441). These mutations do not prevent CypA binding to CA (439, 456), though in some cell types CypA binding impairs virus infectivity, rendering these CA mutants dependent upon CsA for proper infectivity (438, 439, 457, 458). In other cell types, however, CypA binding to these mutants has minimal impact on infectivity (439, 450, 451, 456, 457, 459), making them resistant to but not dependent upon CsA.

CypA can modulate all post-entry early virus life cycle events (388). Knockdown or knockout of CypA or drug inhibition of CypA binding to HIV-1 CA impairs reverse transcription at an early stage (439, 449, 452, 453, 460). This effect may be attributable to alterations in capsid stability, and by extension capsid uncoating, though contradictory results make determining the

role of CypA in HIV-1 capsid stability challenging. In *in vitro* studies, CypA has been shown to both stabilize capsids (461) and destabilize CA-NC tubes (462). Similar contradictory results have also been obtained with host cell infection (456). One possible explanation is that different levels of CypA produce different outcomes. A recent study observed that low, sub-stoichiometric amounts of CypA stabilize CA assemblies *in vitro* but high concentrations of CypA destabilize them (447). There has been some suggestion that this might be true in host cells as well (456, 457, 463).

Perhaps the most complex role for CypA lies with its effect on HIV-1 PIC nuclear entry, which correlates well with its overall effect on virus infectivity (459). Interestingly, several CsA-dependent CA mutants (T54A, A92E, G94D, and R132K) are also impaired for nuclear entry in nondividing HeLa cells but not HOS cells or macrophages (458, 463, 464), supporting CypA involvement in nuclear entry. CA has been identified as the key viral determinant (268) in permitting HIV-1 infection of nondividing cells (148, 260), which requires active transport of the PIC through the NPC (261). This transport depends upon CA interacting with multiple host factors, including NPC components Nup358 (270-272) and Nup153 (273-275), karypherin TNPO3 (280), and the CFI_m complex factor CPSF6 (266, 283) (all discussed below). CypA may regulate the dependence upon Nup358 (270) and Nup153 (273) for nuclear import, with inhibition of CA-CypA interaction by CsA treatment, CA mutants G89V and P90A, or CypA depletion permitting successful PIC nuclear entry in the absence of these host factors in some cell types (270, 273) but not in others (278). CypA has also been implicated in integration site selection, with inhibition of CA-CypA binding resulting in increased targeting of HIV-1 DNA to gene-dense chromosomal regions (270).

1.5.2.2 TNPO3

TNPO3 is an importin β karyopherin that transports SR-rich proteins into the nucleus (276, 277). Identified as an HIV-1 host dependency factor in two siRNA screens (198, 200), it was originally characterized as binding HIV-1 IN (280, 465). Subsequent studies, however, determined the dependence upon TNPO3 for virus infectivity to map to CA (466, 467). Depletion of TNPO3 restricts HIV-1 virus infectivity at or after nuclear import (198, 266, 280, 461, 466, 468-470) but prior to integration (198, 469, 470).

While TNPO3 has been shown *in vitro* to bind CA-NC assemblies (470) and accelerate capsid uncoating (461), it is more likely that TNPO3 mediates HIV-1 infectivity indirectly through interaction with another host dependency factor, SR-rich protein CPSF6, as TNPO3 mutants defective for binding to CPSF6 demonstrated poor virus infectivity (278, 282). This is further supported by multiple studies demonstrating that CA mutant N74D, which does not bind to CPSF6 (266, 283), is not restricted by TNPO3 depletion (266, 461, 466, 469). It was also shown that the TNPO3 cargo binding domain is necessary for HIV-1 infection (468), suggesting a viral or cellular component must act as a cargo for TNPO3 for it to promote infectivity.

1.5.2.3 CPSF6

CPSF6 is a member of the host nuclear CFI_m complex that is responsible for the 3' end processing of pre-mRNA transcripts (471). Cellular expression of CPSF6 is mostly nuclear (266, 281, 472), but CPSF6 has also been shown to shuttle between the nucleus and cytoplasm (473, 474). Nuclear import is accomplished through a C-terminal, SR-rich NLS (475) of the type imported by TNPO3 (276, 277). A truncated form of CPSF6 lacking this NLS (CPSF6-358) is mostly mislocalized to the cytoplasm and restricts HIV-1 infectivity by inhibiting nuclear entry (266), which can be

rescued by equipping CPSF6-358 with an alternative NLS (281). Similar restriction is obtained if full-length CPSF6 is equipped with a nuclear export signal (281, 282), indicating that it is the mislocalization of CPSF6-358 that is responsible for HIV-1 restriction and not some other effect of the protein truncation. It is also likely that cytoplasmic mislocalization of CPSF6 explains HIV-1 infectivity restriction by depletion of TNPO3, which results in higher levels of CPSF6 retention in the cytoplasm (281). Dual depletion of CPSF6 and TNPO3 rescues HIV-1 infectivity (281, 282, 298), further supporting a CPSF6/TNPO3 linked function in promoting HIV-1 infectivity.

CPSF6 has been shown to bind CA tubes *in vitro* (266, 283, 476) and the binding interface has been identified on CPSF6 (477) and on CA (266, 417, 418), the latter which is also the CA binding pocket for Nup153 (417). Depletion of CPSF6 results in marginally higher levels of HIV-1 infectivity (266, 301, 476) but alters the integration site landscape, reducing integration into gene-dense regions, transcriptionally active genes, and intron-rich genes (301). CPSF6 also appears to facilitate PIC nuclear import and penetration, with depletion reducing the nuclear localization of CA and viral DNA (298) and preventing PIC penetration into the interior of the nucleus (299).

In vivo selection for resistance to CPSF6-358 restriction resulted in a virus bearing CA mutation N74D (266), for which binding to CPSF6 is abrogated (266, 283). While able to robustly infect HeLa and CD4+ T cell lines independently of CPSF6, TNPO3, Nup358, and Nup153 (266, 270, 273, 435), N74D HIV-1 infectivity is restricted in terminally-differentiated macrophages at or before initiation of reverse transcription (435), with an associated activation of a type I interferon immune response (257). Another CA mutation, A77V, shares the same host factor

independence as N74D but retains the ability to infect macrophages (436), suggesting a mechanism other than host factor independence is responsible for N74D restriction in macrophages. N74D HIV-1 is also more sensitive to CsA treatment than WT HIV-1, which is partially rescued by the CsA-dependent CA mutation G94D and fully rescued by the G89V CA mutation (435), which prevents CypA binding to CA (437).

1.5.2.4 Nup358

Nup358 is a component of the cytoplasmic portion of the NPC, forming filaments that project from the NPC into the cytoplasm (261). A series of phenylalanine-glycine (FG) repeats form a hydrogel meshwork (478), by which Nup358 serves as a docking platform for nuclear transport proteins and their cargo (261). Nup358 also has a C-terminal cyclophilin homology domain (Nup358Cyp), with which it has been shown to bind to CA (270, 271). Like CypA, Nup358Cyp is competent for cis/trans isomerization of the CA G89-P90 peptide bond (479); however, Nup358Cyp binding is not inhibited by CsA, permitting a separate interrogation of function of CypA and Nup358Cyp (270). Knockdown or knockout of Nup358 impairs HIV-1 infectivity at nuclear entry (270, 271, 479, 480) and has also been demonstrated to delay capsid uncoating (481). Capsid mutants deficient for binding Nup358Cyp (G89V and P90A) or CPSF6 (N74D and N57A) are able to infect independently of Nup358 (266, 270, 480). Deletion of the Nup358Cyp domain does not impair HIV-1 virus infectivity (480), suggesting other aspects of Nup358 are sufficient to engage CA for proper nuclear import.

1.5.2.5 Nup153

Nup153 is a nucleoplasmic counterpart to Nup358 whose FG-repeat filaments extend into the nucleus from the NPC (261), though unlike Nup358 it lacks a cyclophilin homology domain. The

requirement for Nup153 engagement maps to CA (273), to which it binds (274, 482) with its FG repeats (275) in the same binding pocket that CA uses to bind to CPSF6 (274). Depletion of Nup153 restricts HIV-1 infectivity at nuclear import (274, 296, 482). CA mutants defective for binding CPSF6 and Nup358 (N74D, N57A, and N57S) also infect independently of Nup153 (266, 273-275), as do CA mutants defective for binding CypA (P90A) (273). While these mutants are infectious without engaging Nup153, they exhibit altered integration site preferences (275, 297, 483).

1.5.3 HIV-1 Capsid as a Protective Shell

Perhaps the most obvious role for the HIV-1 capsid is to serve as an enclosed shell that isolates the viral genome and enzymes from the intracellular environment. This isolation serves multiple purposes that facilitate virus infectivity. After being released into the host cell cytoplasm, the RNA viral genome and enzymes are trafficked to the nucleus for the eventual integration of the reverse transcribed viral DNA genome into the host cell genome (484). During this journey, all of the RTC components within the core need to be kept and trafficked together to allow reverse transcription and the transformation of the RTC into the PIC to occur (286). The capsid serves as a convenient vehicle for the consolidated trafficking of the core contents. The confined space within the core keeps the genome, enzymes, and other contents in close proximity, better permitting their interaction (286). The capsid is not perfectly sealed, but instead has a small pore at the center of each CA^{NTD} hexameric ring that is selectively permeable to small molecules, such as dNTPs and polyanions (429), which are present within the capsid at physiological concentrations (414), resulting in the start of endogenous reverse transcription within the intact capsid (414, 485).

The capsid also serves as a barrier to prevent contact between core contents and the intracellular environment. The HIV-1 RNA viral genome, the double-stranded DNA genome, and the RNA/DNA hybrid and other intermediate products of reverse transcription are all targets of antiviral cytosolic immune sensors (247, 255). Viral DNA is sensed in the cytosol by cyclic guanosine monophosphate-adenosine monophosphate (GMP-AMP) synthase (cGAS) and interferon gamma-inducible factor 16 (IFI16) (486), while HIV-1 genomic RNA is detected by retinoic acid-inducible gene I (RIG-I) (487, 488). Triggering any of these sensors leads to type I interferon immune activation and/or cell death (486, 489). The protective capsid shell serves to shield these nucleotides from detection and thereby evade a restrictive immune response (256, 257, 486).

For all the benefits of an intact capsid, there comes a point in the early virus life cycle in which a closed capsid proves detrimental to virus infectivity, requiring some or most of CA to be shed from the capsid through the process of capsid uncoating (285). Perhaps ironically, the capsid reaches a point at which it is simultaneously too large and too small. An intact capsid is too large to pass through the NPC (192, 286), which the PIC must transit in order to reach the host genome (230, 272, 287). Conversely, while reverse transcription can begin within an intact capsid, it cannot complete until uncoating has started (228), most likely owing to the increased rigidity of DNA compared to RNA, resulting in a need for additional space to accommodate the RNA/DNA hybrid or double-stranded DNA genome beyond what the intact capsid can provide (285). While originally viewed as a passive, metastable shell that spontaneously disassembles (389), capsid has come to be appreciated as a dynamic, active structure that undergoes a highly regulated process of CA removal, the correct execution of which is critical to successful virus infectivity (285, 490).

There are several unresolved questions pertaining to the capsid uncoating process (192, 285). Precisely how capsid uncoating is triggered remains uncertain; however, it has been suggested that reverse transcription mechanically initiates capsid uncoating (491). This is supported by the requirement for RNase H degradation of the RNA virus genome and the first strand transfer of reverse transcription to occur for capsid uncoating to be initiated (490), as well as the delaying of reverse transcription preventing the start of uncoating (196, 492, 493).

The timing and location of capsid uncoating are likewise currently undetermined, though there appears to be a window in which uncoating should optimally occur, with early/fast or late/slow capsid uncoating negatively impacting virus infectivity (228, 286, 288). Multiple, competing models for capsid uncoating have been proposed (192, 286). Early *in vitro* assays for capsid uncoating suggested that CA was shed shortly after host cell entry, owing to a lack of CA detected in RTCs and PICs (494-497). However, differences in results among these studies coupled with the reverse transcription, cytoplasmic trafficking, and nuclear entry processes being CA dependent hint that experimental conditions may have led to loss of CA in these assays and that the capsid may be more fragile than originally suspected (285, 286).

More recently, two promising models have been supported by numerous independent studies utilizing a range of assays. One model suggests that uncoating may occur while the RTC/PIC is in transit to the nucleus (219), facilitated by components of the microtubule trafficking machinery (215, 218, 498, 499), with CA being shed in a gradual or biphasic manner such that a slimmed down PIC arrives at the nuclear pore with some amount of CA still intact (492, 500, 501). Alternatively, uncoating may take place at the NPC (230, 481), with the capsid remaining mostly

or fully intact until reaching the nuclear membrane (272, 287). Given the uncertainty of what capsid uncoating even entails – whether CA is removed as individual hexamers, in small patches, or in large chunks; whether it is shed from the entire capsid surface or from discrete locations; whether dissociation occurs gradually or simultaneously; whether or not an initial loosening or permeabilization of the capsid precedes actual loss of CA; and how much CA remains associated with the PIC – it is entirely possible that both leading models are at least partially correct (192), or may describe distinct populations of capsids undergoing different forms of uncoating (287, 501, 502). As multiple, distinct populations of intracellular capsids have been observed, many of which are destined for non-infectious degradation (195, 286), it is still debatable if one or both of these uncoating processes ultimately lead to successful nuclear entry, integration, and new virus production (287, 501).

Additional research is required to address these outstanding unknowns with capsid uncoating. This is complicated by the lack of a definitive assay for uncoating (490), owing to such factors as the dynamic nature of uncoating (503), the fragility of intact capsid (286), the inability to tag the CA protein without loss of capsid integrity and/or function (394, 504), insufficient sensitivity to detect small losses of CA from the capsid (285), a general heterogeneity of cores that are frequently defective (285), and technical challenges in electron microscopy deep within infected host cells (230, 505). Numerous uncoating assays have been developed that all have some benefits, but also limitations (192, 285, 490). A particularly useful addition would be a capsid uncoating assay able to observe capsid uncoating in real time in live cells that is compatible with the latest super-resolution light microscopy techniques and conducive to pairing with electron microscopy in correlative light-electron microscopy.

2.0 Research Plan and Specific Aims

Using molecular and cellular tools and techniques, fluorescence microscopy, and virologic assays, we will examine how changes to virus capsid sequence alters HIV-1 infectivity, early virus life cycle events, and host factor interactions in different virus strains and host cell types. We will also develop novel imaging-based methods for assaying capsid uncoating to improve our understanding of this elusive process.

2.1 Specific Aims

2.1.1 Aim 1: Determine how changes in the capsid of different HIV-1 strains influence post-entry, pre-integration steps of infection in different cell types

Hypothesis: HIV-1 reverse transcription, capsid uncoating, and nuclear entry will differ in virus strains HIV-1$_{NL4-3}$ and HIV-1$_{LAI}$ and in HeLa, GHOST, and primary human CD4+ T cells.

HIV-1 CA has been shown to be the primary viral determinant that permits the virus to infect nondividing cells (265, 506), which is impaired by the CA mutation N57A (268), but the specific mechanism by which this occurs remains unclear. While cell type dependent differences in HIV-1 infectivity have been widely reported (435, 439, 457, 459, 507, 508) and some recent studies have observed capsid-dependent differences in restriction by host factors myxovirus resistance protein B (MxB) and Sad1 and UNC84 domain containing proteins 1 and 2 (SUN1 and SUN2)

when utilizing different virus strains (509-511), the role of the virus capsid in generating different infectivity phenotypes has not been closely examined and the broader implications of these strain-specific observations have not been explored. Using N57A HIV-1 as a tool to explore viral cell cycle dependence, HIV-1 infectivity will be examined for virus strains HIV-1_{NL4-3} and HIV-1_{LAI} in HeLa and GHOST human cell lines and in primary human CD4+ T cells. Observed differences in infectivity will be further characterized to identify early virus life cycle steps that exhibit virus strain-specific phenotypes. The role of capsid in these phenotypes will be explored and specific differences between capsid sequences examined to identify those amino acid differences that contribute to the observed phenotypes. Applicability of these observations to the broader collection of HIV-1 strains, in particular clinical isolates, will also be considered.

2.1.2 Aim 2: Determine how disruption of interactions between HIV-1 capsid and host proteins alters virus infectivity

Hypothesis: HIV-1 infectivity is sensitive to interactions with host factors CypA, CPSF6, and Nup153, and disruption of these interactions will alter virus infectivity in a virus strain and host cell dependent manner.

Host factors CypA, CPSF6, and Nup153 have been demonstrated to interact with the HIV-1 capsid and their disruption has been shown to impact overall virus infectivity and early virus life cycle processes (266, 267, 275, 283, 409, 439, 453). However, virus strain specific differences have not been explored, particularly within the context of different host cells. The interaction of HIV-1 capsid with each of these host factors will be individually disrupted and the impact on both overall virus infectivity and specific early virus life cycle processes will be examined. Virus bearing capsid

from strains HIV-1_{NL4-3} and HIV-1_{LAI} will be utilized to explore strain-specific phenotypes. Infections will be performed in HeLa and GHOST human cell lines to characterize cell type dependencies.

2.1.3 Aim 3: Develop novel methods to visualize HIV-1 capsid uncoating in infected host cells in real time

Hypothesis: The combination of an HIV-1 capsid impermeable fluorogen dye and a fluorogen activating protein or RNA aptamer will permit visualization of capsid permeabilization in cells.

While multiple assays for capsid dissociation currently exist, no one assay captures all aspects of the dynamic and variable nature of uncoating and gaps exist in our current capabilities to examine the uncoating process (192, 285, 286). Previous studies have produced different potential models for capsid uncoating based on indirect evidence of uncoating (230, 272, 287, 492, 500, 501). Visual confirmation of the status of capsid integrity during trafficking to the nucleus is required to discern the proper model for capsid uncoating. Leveraging a previously published fluorescence imaging assay (500), a new capsid permeabilization assay will be developed to address shortcomings in existing techniques. Design rationale will be provided, reagents developed, and initial validation testing performed.

3.0 Determine How Changes in the Capsid of Different HIV-1 Strains Influence Post-Entry, Pre-Integration Steps of Infection in Different Cell Types

This chapter is primarily adapted from the published manuscript:

Douglas K. Fischer, Akatsuki Saito, Christopher Kline, Romy Cohen, Simon C. Watkins, Masahiro Yamashita, Zandrea Ambrose. CA Mutation N57A Has Distinct Strain-Specific HIV-1 Capsid Uncoating and Infectivity Phenotypes. Journal of Virology Apr 2019, 93 (9) e00214-19; DOI: 10.1128/JVI.00214-19. Copyright © 2019 American Society for Microbiology (ASM).

With the following exceptions, the data presented herein is published in the *Journal of Virology* and is reprinted with permission from ASM. Figure 14 is part of a manuscript in preparation. Figures 16 and 17 are adapted from a co-author manuscript in revision that is included in its entirety in Appendix A.

3.1 Introduction

The HIV-1 capsid is a closed conical structure composed of hexamers and pentamers of the viral CA protein (428) that performs an essential set of functions in the early virus life cycle, shielding the viral RNA genome from cytoplasmic innate immune sensors, regulating the completion of reverse transcription, and governing use of nuclear trafficking and import pathways (192). Capsid has been shown to interact with numerous host factors including cyclophilin A (CypA) (444),

cleavage and polyadenylation specificity factor 6 (CPSF6) (266), the karyopherin transportin-3 (TNPO3) (470), and nucleoporins Nup153 (273) and Nup358 (270). Inhibition of these interactions impairs early virus life cycle events, including completion of reverse transcription, capsid uncoating, and nuclear trafficking and entry, and attenuates virus infectivity (198, 200, 271, 280, 281, 435, 439, 453, 466, 479, 482). Overall, HIV-1 CA is poorly tolerant of mutation, with most amino acid changes resulting in a dysfunctional capsid and severely impaired virus infectivity (393, 394), limiting the ability of HIV-1 to adapt to capsid-targeting therapies. The combination of its critical function, specific host factor interactions, and mutational fragility make the capsid a desirable target for antiretroviral intervention (386, 387).

HIV-1 is a lentivirus that is able to transduce nondividing cells, which allows infection of terminally-differentiated macrophages (148, 260, 512) and microglial cells (80). While CD4+ T cells are the principal target of HIV-1 infection, macrophages and microglia express CD4 and CCR5 (513, 514) and become HIV-infected in lymphoid, mucosal, and central nervous system tissues (79, 515). While not as efficiently infected as CD4+ T cells (516), macrophages are less prone to the cytopathic effects of HIV-1 infection (83). Combined with the widespread distribution of macrophages throughout the body and their long lifespan (517), macrophages can serve as a long-term HIV-1 reservoir (518, 519). It was previously shown that CA is the major viral determinant that permits HIV-1 infection of nondividing cells (265, 506), but the specific mechanism by which this occurs remains unclear.

The CA mutation N57A together with T54A renders HIV-1 cell cycle dependent in all cell types tested, unlike other CA mutants examined, which were only cell cycle dependent in certain

cell types (268, 458). N57 resides within a pocket of the N-terminal domain formed by alpha helices 3, 4, and 5 (**Figure 9A**). This pocket has been identified as the CA binding site for host factors CPSF6 (283) and Nup153 (274) and the CA-binding compound PF3450074 (PF74) (409). Mutating the asparagine to an alanine (N57A) renders HIV-1 infection independent of CPSF6 (281, 283), TNPO3 (466), Nup153 (274), and Nup358 (270), and prevents binding to and restriction by PF74 (283, 419). N57A was originally created in combination with cyclosporin A (CsA)-dependent CA mutation T54A (455) as part of an alanine-scanning surface mutation panel (393). We reasoned that N57A could serve as a useful tool for examining the mechanism by which HIV-1 is able to infect nondividing cells independent of any cell type specific attributes and sought to characterize the viral infectivity defect caused by N57A.

Here, we present the results of the early life cycle infectivity defect of N57A HIV-1 and our observation of distinct differences in infectivity and capsid permeabilization phenotypes in multiple cell types when N57A is incorporated into two widely used and closely related lab-adapted virus strains, HIV-1_{NL4-3} and HIV-1_{LAI}, which differ in only four amino acids within CA. Phenotypic differences that are dependent upon CA polymorphisms can be useful for elucidating early virus life cycle mechanisms but also raise the question of the applicability of observations with a single HIV-1 molecular clone.

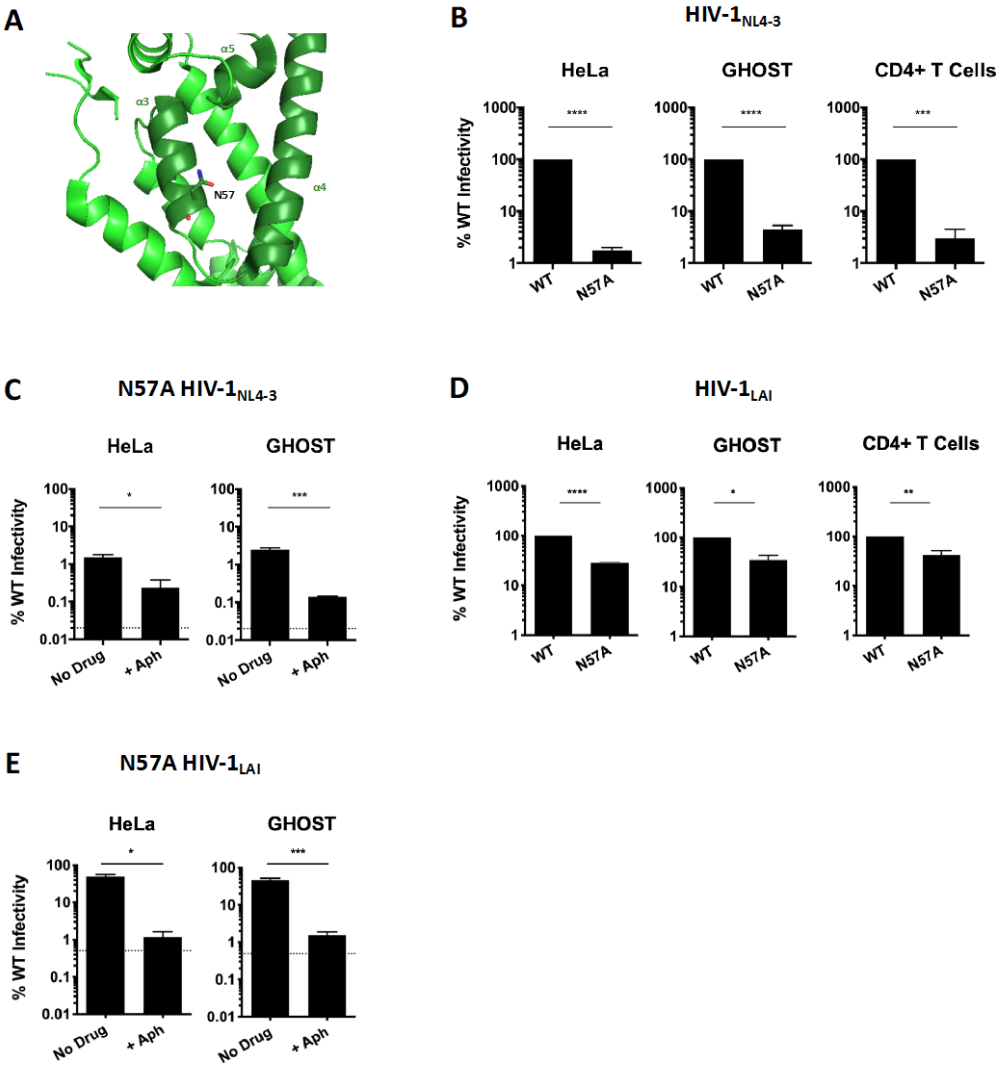

Figure 9. HIV-1 CA mutation N57A exhibits an infectivity defect that differs between HIV-1$_{LAI}$ and HIV-1$_{NL4-3}$. (A) Protein Data Bank structure 3H47 of a portion of HIV-1 CA showing the location of N57 within the pocket formed by alpha helices 3, 4, and 5. (B) Indicated cell types were infected with equal amounts of WT or N57A VSV-G pseudotyped, single-cycle HIV-1$_{NL4-3}$ expressing luciferase and assayed after 48h for luciferase activity. (C) Indicated cell types were infected with viruses from (B) with and without aphidicolin treatment. Dotted line represents average luciferase signal of uninfected cells. (D) Indicated cell types were infected with equal amounts of WT or N57A VSV-G pseudotyped, single-cycle HIV-1$_{LAI}$ expressing GFP and assayed after 48-72h for GFP expression. (E) Indicated cell types were infected with viruses from (D) with and without aphidicolin treatment. Dotted line represents average GFP signal of uninfected cells. **** $p < 0.0001$, *** $p < 0.001$, ** $p < 0.01$, * $p < 0.05$. Error bars indicate standard error of the mean (SEM) for 2-4 experiments.

3.2 Results

3.2.1 HIV-1 CA mutation N57A exhibits an infectivity defect that differs between common lab-adapted strains HIV-1_{NL4-3} and HIV-1_{LAI}

Based upon the previous observation that T54A/N57A HIV-1 was cell cycle dependent in all cell types tested (268), we sought to characterize N57A HIV-1 infectivity in different cell types. N57A HIV-1_{NL4-3} had a significant infectivity defect in HeLa and GHOST cell lines and in primary human CD4+ T cells (33- to 100-fold; **Figure 9B**) that was further exacerbated in nondividing cells (300- to 1,000-fold; **Figure 9C**). This defect is similar to that observed by other groups in HIV-1_{NL4-3} (270, 274, 283). HIV-1_{NL4-3} and HIV-1_{LAI} are two of the most widely used lab-adapted HIV-1 strains (178). Unexpectedly, when incorporated into HIV-1_{LAI}, the infectivity defect caused by N57A was considerably attenuated in HeLa and GHOST cell lines and in primary human CD4+ T cells (2- to 5-fold), though nonetheless significant when compared to WT virus (**Figure 9D**). N57A HIV-1_{LAI} infectivity was further reduced in the presence of aphidicolin (65- to 150-fold; **Figure 9E**).

3.2.2 The magnitude of reduced N57A HIV-1 infectivity is CA dependent

HIV-1_{NL4-3} was originally constructed in 1986 as a chimera between the 5' half of isolate NY5 (*gag* through most of *vpr*) and the 3' half of isolate LAV (180), which is also known as LAI (520). To determine the cause of phenotypic differences of N57A in HIV-1_{NL4-3} and HIV-1_{LAI}, two chimeric viruses were created by swapping the BssHII to ApaI restriction fragment between the NL4-3 and LAI reporter viruses (**Figure 10A**). This fragment spans the majority of the *gag* gene,

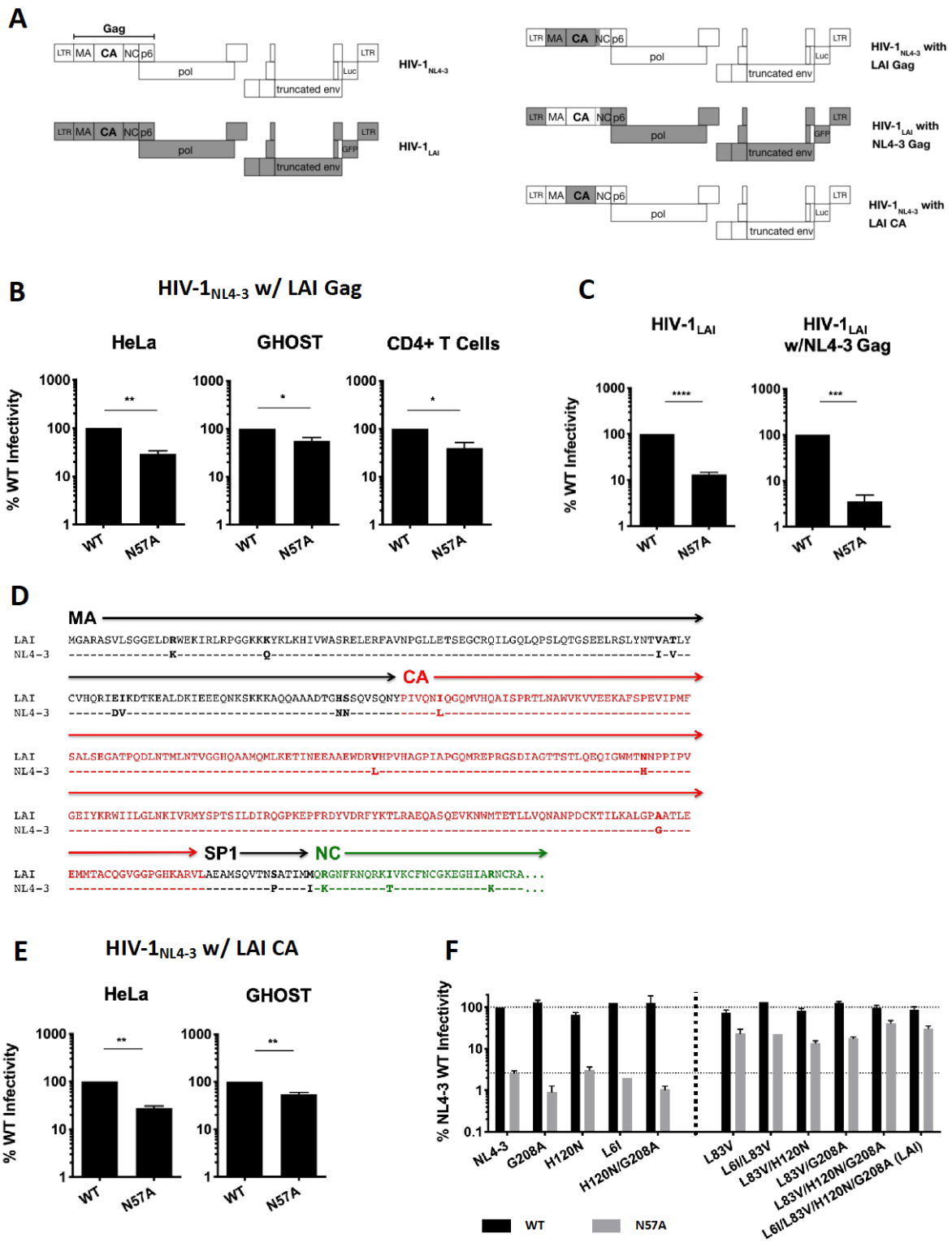

Figure 10. The magnitude of reduced N57A HIV-1 infectivity is CA dependent. (A) Schematic of the chimeric reporter viruses constructed from HIV-1_{NL4-3} and HIV-1_{LAI}. Indicated cell types were infected with equal amounts of

(B) WT or N57A HIV-1_{NL4-3} luciferase reporter virus with LAI Gag or (C) HIV-1_{LAI} GFP reporter virus with LAI or NL4-3 Gag and assayed after 48h for luciferase or GFP expression in MT-4 cells. (D) Amino acid sequences of the Gag fragment in HIV-1_{LAI} and HIV-1_{NL4-3} with CA shown in red. (E) Indicated cell types were infected with equal amounts of WT or N57A HIV-1_{NL4-3} with LAI CA and assayed after 48h for luciferase activity. (F) GHOST cells were infected with WT or N57A HIV-1_{NL4-3} bearing the indicated CA mutations and assayed after 48h for GFP expression. *** $p < 0.001$, ** $p < 0.01$, * $p < 0.05$. Error bars indicate SEM for 2-4 experiments.

including MA, CA, SP1, and a portion of NC. The difference in infectivity of N57 and A57 in HIV-1_{NL4-3} encoding LAI Gag was 2-5-fold in HeLa and GHOST cell lines and in primary human CD4+ T cells (**Figure 10B**), similar to what was observed with HIV-1_{LAI} (**Figure 9C**). Conversely, the difference in infectivity of WT and N57A in HIV-1_{LAI} encoding NL4-3 Gag was approximately 30-fold in MT-4 cells (**Figure 10C**), similar to that observed with HIV-1_{NL4-3} (**Figure 9B**), and in contrast to the 8-fold difference in infectivity of WT and N57A in HIV-1_{LAI} encoding LAI Gag (**Figure 10C**). Taken together, these data reveal that the difference in the levels of N57A HIV-1_{NL4-3} and N57A HIV-1_{LAI} infectivity is encoded within *gag*.

A total of 17 amino acids differ between the BssHII/ApaI *gag* fragment of HIV-1_{NL4-3} and HIV-1_{LAI} (**Figure 10D**). Only four amino acids vary within CA between HIV-1_{NL4-3} and HIV-1_{LAI}: L6I, L83V, H120N, and G208A. To determine the role of these CA amino acid differences in HIV-1_{NL4-3} and HIV-1_{LAI} on the infectivity phenotype of N57A, all four LAI residues were introduced into HIV-1_{NL4-3}, generating HIV-1_{NL4-3} with LAI CA (**Figure 10A**). As with the *gag* chimeric virus, the N57A infectivity defect in HIV-1_{NL4-3} with LAI CA phenocopied the defect in HIV-1_{LAI} (**Figure 10E**), demonstrating that the observed N57A infectivity phenotypes are attributable to

four amino acid substitutions in CA between the two virus strains. To ascertain the specific residue(s) responsible for the strain-specific N57A infectivity phenotypes, CA mutant viruses were created in HIV-1_{NL4-3} containing the four CA substitutions alone or in combination, with and without the N57A mutation. The L83V CA mutation alone was sufficient to confer the attenuated HIV-1_{LAI} N57A infectivity defect in HIV-1_{NL4-3} (**Figure 10F**).

3.2.3 The magnitude of N57A HIV-1 infectivity defects correspond with strain-specific defects in capsid permeabilization and reverse transcription

Alterations in capsid uncoating, caused by inhibitors or CA mutations, lead to diminished HIV-1 infectivity (285). To characterize the nature of the infectivity defect caused by N57A in HIV-1_{NL4-3} and HIV-1_{LAI}, we compared early capsid uncoating kinetics of WT and N57A HIV-1 in both virus strains, using our previously published capsid permeabilization assay (500, 521). In brief, HeLa cells were infected with HIV-1, in which the viral RNA was labeled with 5-ethynyl uridine (EU). Staining of the modified HIV-1 RNA was measured at different time points, which occurs after initial dissociation of the capsid. Capsid permeabilization of N57A HIV-1_{NL4-3} with LAI CA was similar to that of WT HIV-1_{NL4-3} with LAI CA (**Figure 11A**). In contrast, the capsid permeabilization kinetics of N57A HIV-1_{NL4-3} were significantly different from WT HIV-1_{NL4-3}, with viral RNA staining peaking at an earlier time point and diminishing more rapidly over time (**Figure 11B**).

Alterations in HIV-1 capsid uncoating often affect reverse transcription (228). Thus, we measured early and late reverse transcription products and 2-LTR circles in cells infected with HIV-1_{NL4-3}, HIV-1_{NL4-3} with LAI CA, and HIV-1_{LAI}. There were no appreciable differences in

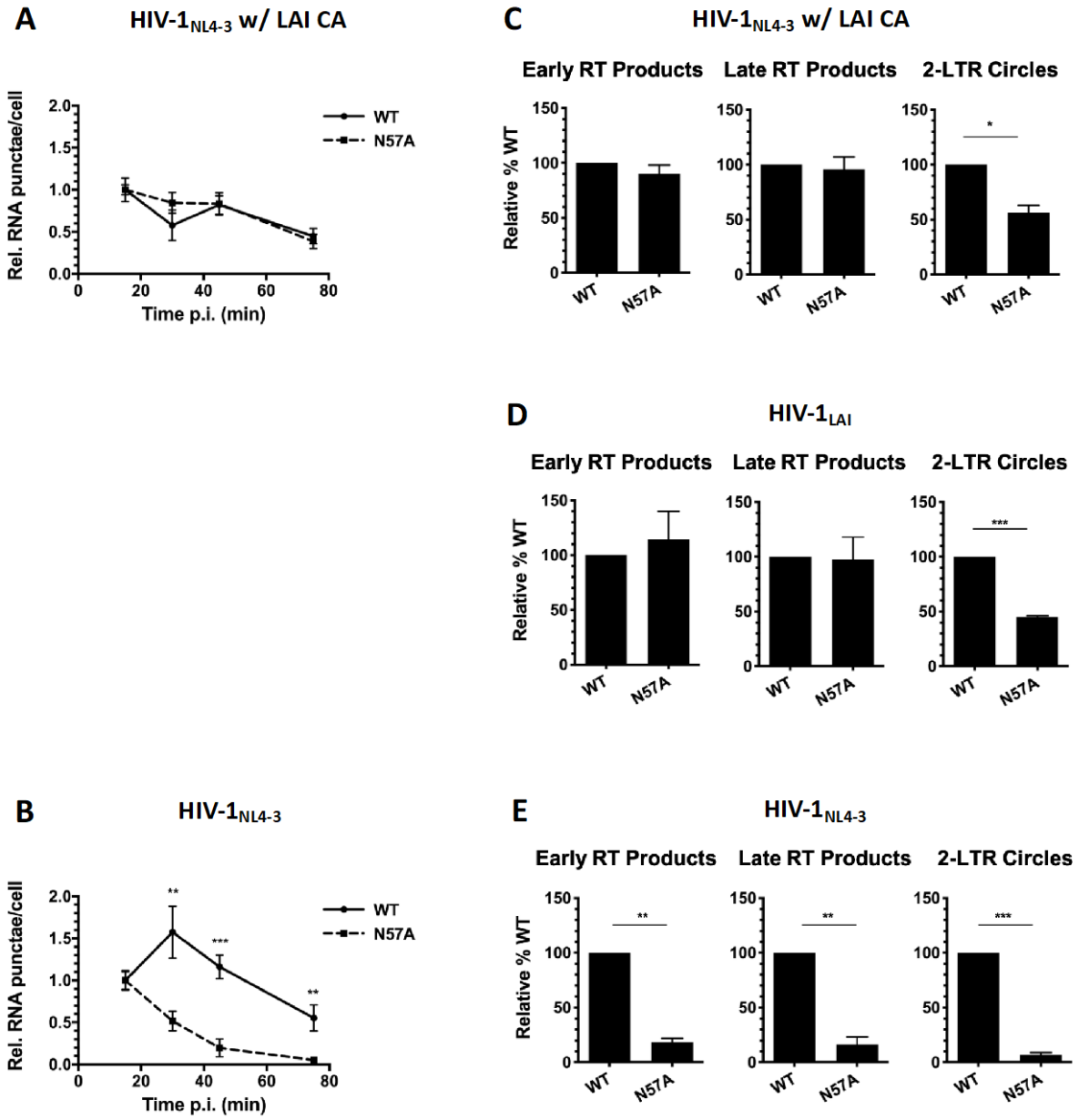

Figure 11. Gag-dependent infectivity defects caused by N57A occur before or after reverse transcription for HIV-1$_{NL4-3}$ and HIV-1$_{LAI}$, respectively. HeLa cells were infected with equal amounts of WT or N57A HIV-1$_{NL4-3}$ luciferase reporter virus with (A) LAI CA or (B) NL4-3 CA and assayed for capsid permeabilization at indicated time points. HeLa cells were infected with equal amounts of (C) viruses from (A), (D) WT or N57A HIV-1$_{LAI}$ GFP reporter virus, or (E) viruses from (B) and reverse transcription products and 2-LTR circles were measured. *** $p < 0.001$, ** $p < 0.01$, * $p < 0.05$. Error bars indicate SEM for at least 2 experiments.

early or late reverse transcripts between WT and N57A HIV-1_{NL4-3} with LAI CA (**Figure 11C**) or between WT and N57A HIV-1_{LAI} (**Figure 11D**); however, in HIV-1_{NL4-3}, N57A early and late reverse transcripts were significantly diminished 7-10-fold compared to WT (**Figure 11E**). Similar to the infectivity data, there were 2-3-fold lower levels of 2-LTR circles produced in cells infected with N57A HIV-1_{NL4-3} with LAI CA compared with WT HIV-1_{NL4-3} with LAI CA (**Figure 11C**) and in cells infected with N57A HIV-1_{LAI} compared with WT HIV-1_{LAI} (**Figure 11D**), but 20-fold lower levels of 2-LTR circles in cells infected with N57A HIV-1_{NL4-3} compared with WT HIV-1_{NL4-3} (**Figure 11E**). Taken together, these data further demonstrate that the N57A HIV-1_{NL4-3} and N57A HIV-1_{LAI} phenotypes are CA-dependent and suggest that the nature of the infectivity defect caused by N57A differs when the mutation is in the two strains, with the mutation leading to an infectivity defect prior to reverse transcription in HIV-1_{NL4-3} and after reverse transcription in HIV-1_{LAI}.

3.2.4 N57A HIV-1 infectivity is partially rescued by CA mutation G94D in a virus strain and host cell type dependent manner

While impaired only 2- to 5-fold in infectivity compared to WT virus, we hypothesized that N57A HIV-1_{LAI} could be amenable to adaptation to improve replication. Therefore, serial passaging of replication-competent N57A HIV-1_{LAI} was performed in MT-4 cells until robust replication was detected. Sequencing of the virus after outgrowth revealed a second CA mutation, G94D, in addition to N57A. Addition of this mutation to N57A HIV-1_{LAI} resulted in the partial rescue of N57A HIV-1_{LAI} infectivity in both spreading (**Figure 12A**, top panel) and single-cycle infection (**Figure 12A**, bottom panel). A similar positive effect of G94D on infectivity of N57A HIV-1_{LAI}

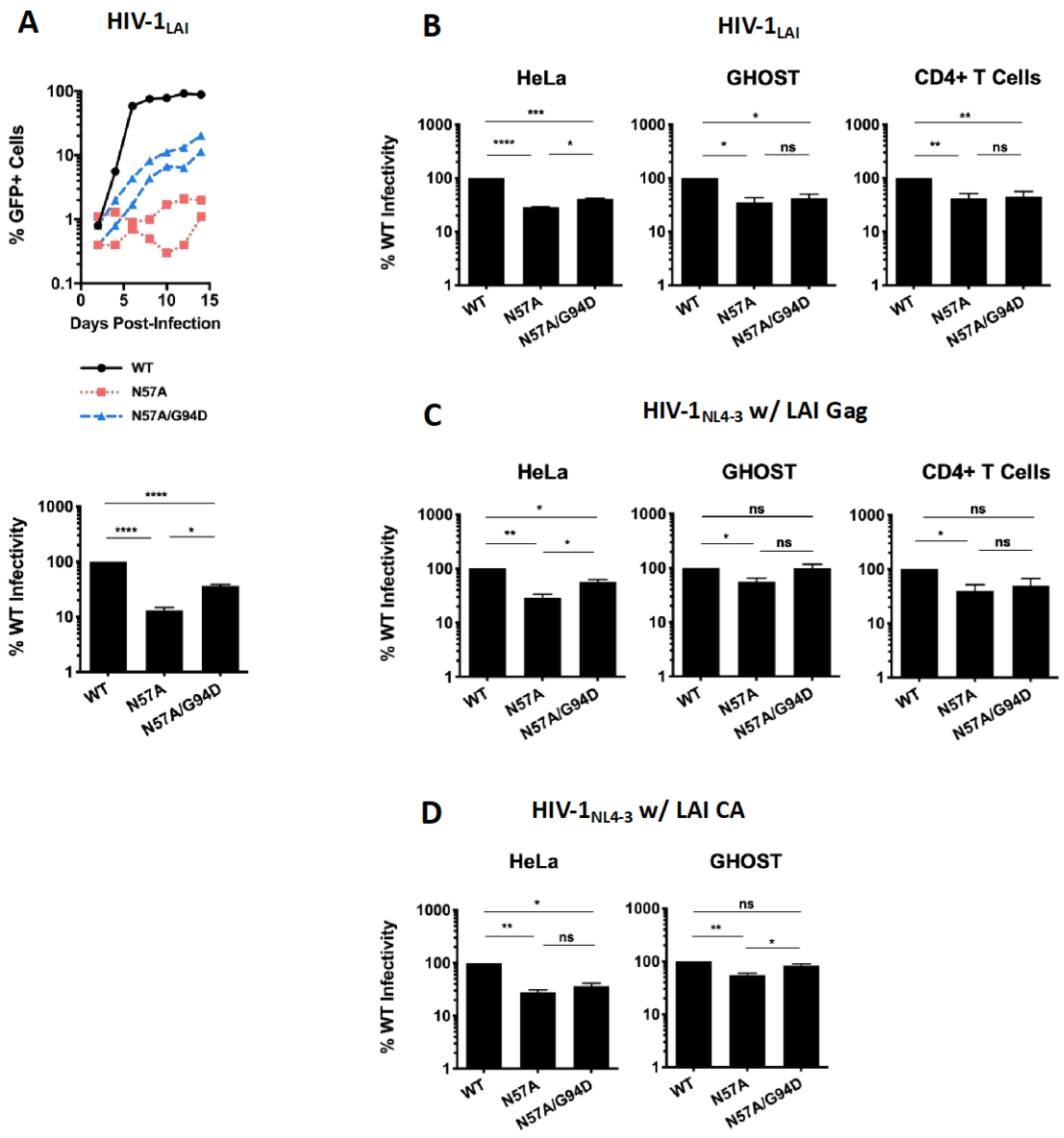

Figure 12. N57A HIV-1$_{LAI}$ infectivity is rescued by CA mutation G94D in a cell type dependent manner. (A) MT-4 cells were infected with equal infectious units of WT, N57A, or N57A/G94D HIV-1$_{LAI}$ full-length (top panel) or single-cycle (bottom panel) GFP reporter virus. Virus replication was measured by GFP expression for 2 weeks (top panel). Single-cycle infectivity was determined after 48-72h by GFP expression (bottom panel). (B) Indicated cell types were infected with equal amounts of WT, N57A, or N57A/G94D HIV-1$_{LAI}$ single-cycle GFP reporter virus and assayed after 48-72h for GFP expression. (C) Indicated cell types were infected with equal amounts of WT, N57A, or N57A/G94D HIV-1$_{NL4-3}$ single-cycle luciferase reporter virus with LAI Gag or LAI CA (D). **** $p < 0.0001$, *** $p < 0.001$, ** $p < 0.01$, * $p < 0.05$. Error bars indicate SEM for 2-4 experiments.

virus was observed for other cell types (**Figure 12B**). To determine if the rescue of N57A HIV-1_{LAI} infectivity by G94D differs between the two virus strains, the G94D mutation was combined with N57A in HIV-1_{NL4-3} containing either LAI Gag (**Figure 12C**) or LAI CA (**Figure 12D**). As with HIV-1_{LAI}, G94D partially rescued infectivity in these viruses in HeLa, GHOST, and primary human CD4+ T cells. While the degree of rescue varied with cell type and was less apparent in single-cycle infection than spreading infection, G94D consistently increased infectivity of N57A HIV-1_{NL4-3} with LAI CA.

In contrast, the addition of G94D to N57A in HIV-1_{NL4-3} did not rescue the N57A infectivity defect in HeLa, GHOST, or primary human CD4+ T cells (**Figure 13A**). While N57A/G94D HIV-1_{NL4-3} had significantly higher infectivity compared to N57A HIV-1_{NL4-3} in GHOST cells, the level of N57A/G94D HIV-1_{NL4-3} infectivity was still greater than 1 log lower than WT virus. Surprisingly, while the addition of the L83V CA mutation in HIV-1_{NL4-3} was sufficient to rescue the N57A infectivity defect in HIV-1_{NL4-3} similar to that in HIV-1_{LAI} (**Figure 10F**), L83V in HIV-1_{NL4-3} did not rescue the N57A/G94D infectivity defect (**Figure 13B**).

3.2.5 Partial rescue of N57A/G94D HIV-1_{NL4-3} infectivity requires multiple CA mutations

The failure of the L83V CA mutation to rescue N57A/G94D HIV-1_{NL4-3} infectivity suggested that additional CA residues differing between HIV-1_{NL4-3} and HIV-1_{LAI} contribute to the rescue of N57A HIV-1_{NL4-3} infectivity by the addition of CA mutation G94D. To determine what additional CA mutation(s) among L6I, H120N, and/or G208A would be necessary, in combination with L83V, to rescue the N57A/G94D HIV-1_{NL4-3} infectivity defect, each of these mutations was added with L83V to N57A HIV-1_{NL4-3} and N57A/G94D HIV-1_{NL4-3}. Interestingly, adding either L6I,

H120N, or G208A to L83V resulted in partial rescue of the N57A/G94D HIV-1_{NL4-3} infectivity defect in both GHOST and HeLa cells (**Figure 14**). Excluding the L83V CA mutation eliminates infectivity rescue by G208A (**Figure 14**), indicating that the attenuated N57A HIV-1 infectivity defect conferred by L83V is a prerequisite for one of the other CA mutations to rescue N57A/G94D HIV-1 infectivity.

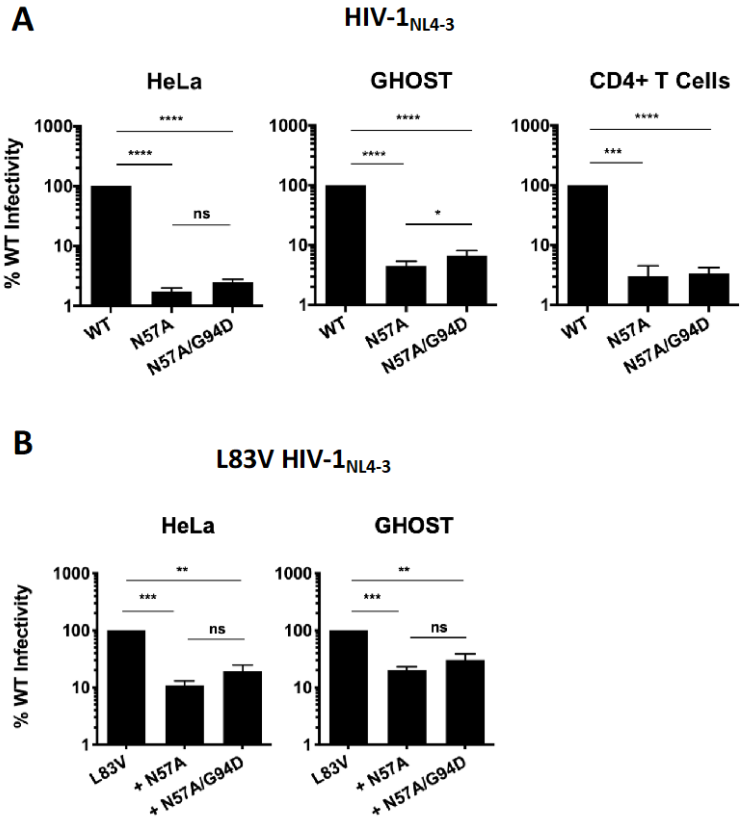

Figure 13. N57A HIV-1_{NL4-3} infectivity is not rescued by CA mutation G94D. (A) Indicated cell types were infected with equal amounts of WT, N57A, or N57A/G94D HIV-1_{NL4-3} luciferase reporter virus and assayed after 48h for luciferase activity. (B) Cells were infected with L83V, N57A/L83V, or N57A/L83V/G94D HIV-1_{NL4-3} and assayed after 48h for luciferase activity. **** $p < 0.0001$, *** $p < 0.001$, ** $p < 0.01$, * $p < 0.05$. Error bars indicate SEM for 2-4 experiments.

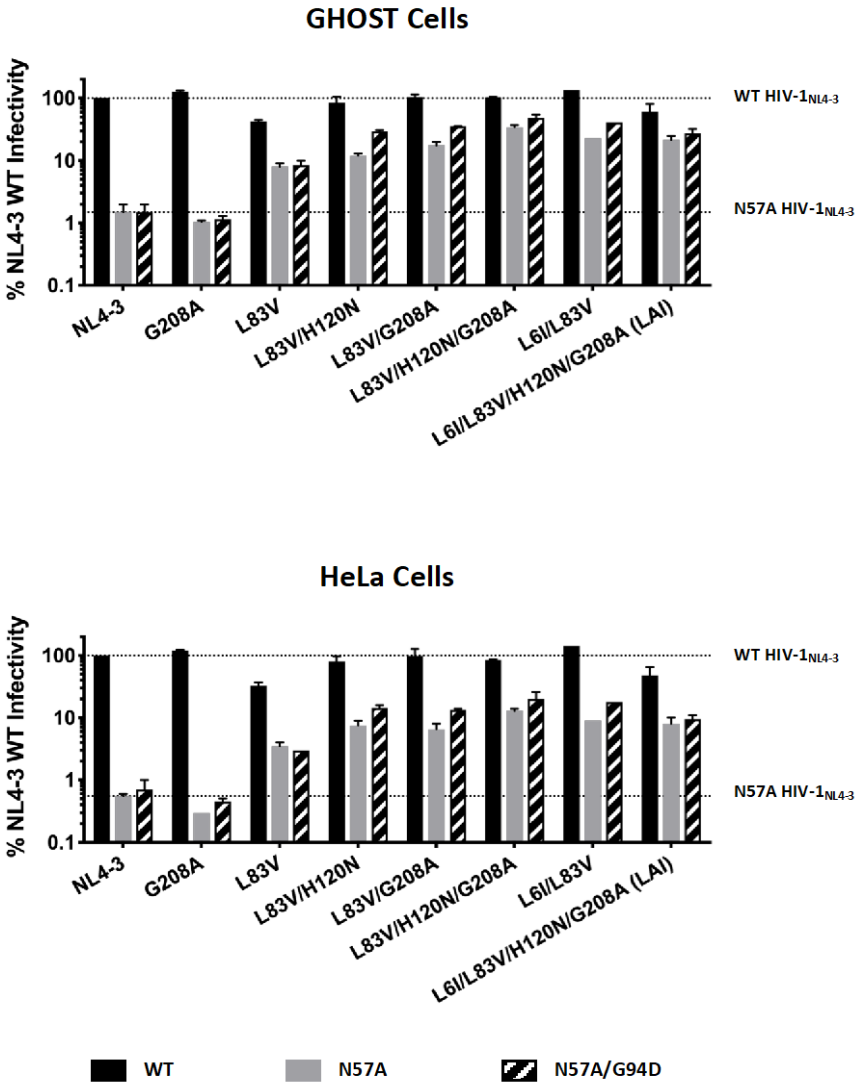

Figure 14. Rescue of N57A/G94D HIV-1_{NL4-3} infectivity depends upon multiple CA mutations. Indicated cell types were infected with equal amounts of WT, N57A, or N57A/G94D HIV-1_{NL4-3} luciferase reporter virus bearing the indicated CA mutations and assayed after 48h for luciferase activity. Error bars indicate SEM for 2 experiments.

3.2.6 HIV-1_{NL4-3} and HIV-1_{LAI} CA sequences are representative of HIV-1 clinical isolate sequences

Given the strikingly different CA-dependent N57A infectivity phenotypes observed in lab-adapted strains HIV-1_{NL4-3} and HIV-1_{LAI}, which differ by only four amino acids in CA (residues 6, 83, 120, and 208), we determined whether the CA sequences of these HIV-1 strains were representative of clinical isolates, including non-B subtypes. Over 40,000 Gag sequences from the Los Alamos National Laboratory (LANL) HIV-1 sequence database were analyzed, of which approximately 14,000 were subtype B. The results showed that CA amino acids 6, 83, 120, and 208 are polymorphic within subtype B (**Figure 15A**) and across multiple subtypes (**Figure 15B**). These 4 amino acids in HIV-1_{NL4-3} and HIV-1_{LAI} are most predominant and, with the exception of position 120 analyzed across all subtypes, collectively represent the majority of primary isolate sequences, though their relative prominence varies. An examination of a panel of 10 subtype B transmitted/founder viruses (522) similarly demonstrated that at CA residues 6, 83, 120, and 208 the HIV-1_{NL4-3} and HIV-1_{LAI} amino acids together represent 70-100% of the amino acids found at these positions in the transmitted/founder virus panel (data not shown). Furthermore, more than 90% of CA sequences within subtype B (**Figure 15C**) and across all subtypes (**Figure 15D**) matched HIV-1_{NL4-3} and HIV-1_{LAI} at the vast majority of CA positions, with a greater degree of diversity observed when comparing non-B sequences. Taken together, these data demonstrate that HIV-1_{NL4-3} and HIV-1_{LAI} CA sequences are both representative of CA in HIV-1 primary isolates.

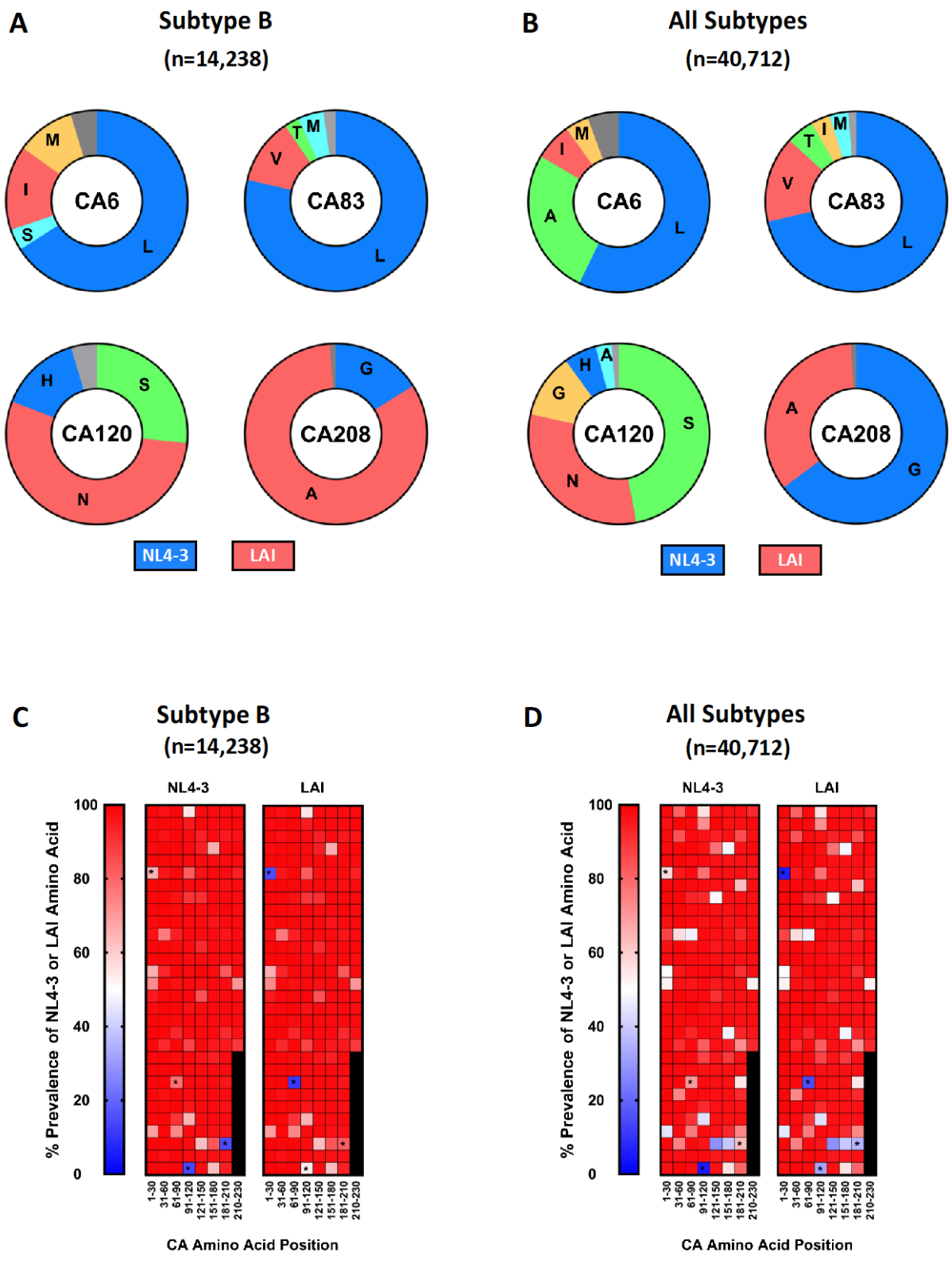

Figure 15. CA positions differing between HIV-1$_{NL4-3}$ and HIV-1$_{LAI}$ are polymorphic and represented in most HIV-1 clinical isolates. HIV-1 Gag sequences from the LANL HIV-1 database were compared at residues 6, 83, 120,

and 208 in (A) subtype B and (B) multiple subtypes with NL4-3 (blue) and LAI (red) amino acids generally the most predominant. Amino acids comprising at least 2% of sequences are indicated in the graphs. Grey segments represent the combination of amino acids at <2% prevalence. HIV-1_{NL4-3} and HIV-1_{LAI} amino acid prevalence at each CA position compared to (C) subtype B or (D) all subtype HIV-1 clinical isolate sequences. The four residues at which HIV-1_{NL4-3} and HIV-1_{LAI} differ are marked with asterisks.

3.2.7 A single amino acid polymorphism in a transmitted/founder virus enhances HIV-1 capsid stability

To explore clinically relevant consequences of minor CA sequence differences between HIV-1 virus strains, a panel of 10 subtype B transmitted/founder (T/F) viruses were examined (**Appendix A**) that are representative of a minority of HIV-1 strains that are able to be transmitted and serve as a founder virus in a newly infected host (522). The capsid-targeting compound PF74 has been shown to destabilize the HIV-1 capsid at high doses (410, 500) and inhibit virus infectivity (409, 410). Infecting TZM-bl cells with these virus strains in the presence of a range of concentrations of PF74, one strain (CH040) exhibited resistance to high doses of PF74 (**Figure 16A and 16B**). To examine the CA dependence of this PF74 resistance, HIV-1_{CH040} CA was cloned into HIV-1_{LAI}. Similar to HIV-1_{CH040}, HIV-1_{LAI} with CH040 CA exhibited resistance to high doses of PF74 in TZM-bl and MT-4 cells, which was not observed in WT HIV-1_{LAI} (**Figure 16C**), demonstrating that this PF74 resistance is CA dependent. Utilizing a novel capsid integrity assay, we further demonstrated that resistance to high doses of PF74 is accompanied by a significant increase in RT activity of isolated capsid cores (**Appendix A**), suggesting that HIV-1_{CH040} capsid has increased stability compared to HIV-1_{LAI} capsid.

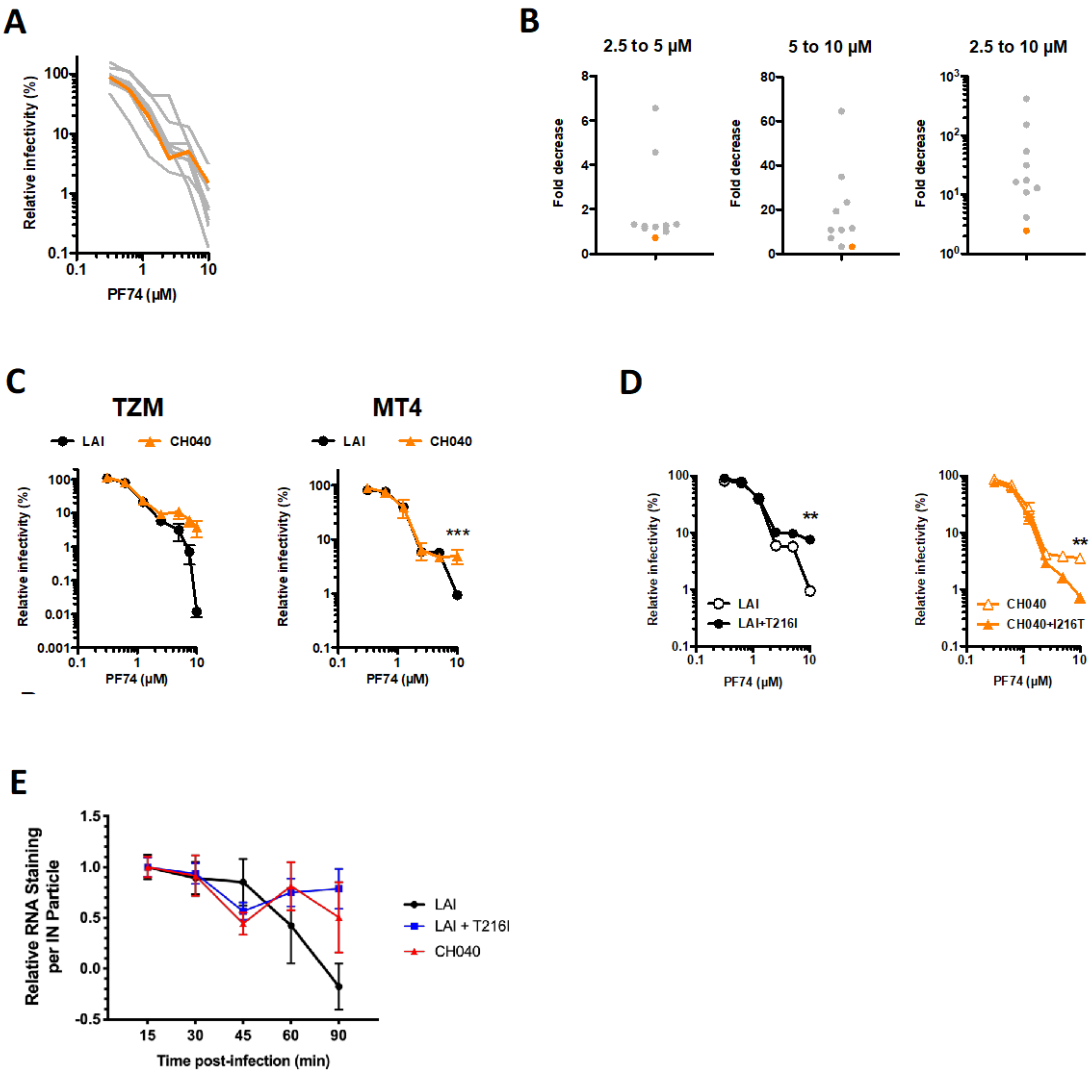

Figure 16. CA mutation T216I enhances HIV-1 capsid stability. (A) TZM-bl cells were infected with a panel of T/F viruses in the presence of a range of PF74 concentrations and assayed for luciferase production. HIV-1_{CH040} is shown in orange. Results shown are the average of 2-3 experiments. (B) Magnitude of PF74 effect on infectivity from (A) was quantified at three ranges of drug concentrations. (C) Indicated cell types were infected with HIV-1_{LAI} GFP reporter virus with LAI or CH040 CA in the presence of a range of PF74 concentrations and assayed for luciferase production (TZM, n=2) or GFP expression (MT-4, n=4-7). (D) MT-4 cells were infected with HIV-1_{LAI} GFP reporter viruses bearing the indicated CA strains and mutations as in (C), n=3-7. (E) HeLa cells were infected with equal amounts of HIV-1_{LAI} luciferase reporter virus with indicated CA and assayed for capsid permeabilization at indicated time points. Data were compiled from three experiments and normalized with the dataset for the first time point (15m post-infection). ** $p < 0.01$. Error bars indicate SEM.

Nine CA amino acids differ between HIV-1_{LAI} and HIV-1_{CH040}, with one amino acid in the C-terminal of CA particularly suggestive of potentially influencing capsid stability. Residue 216, which is a threonine in HIV-1_{LAI} and an isoleucine in HIV-1_{CH040}, is located within the trimeric interface governing CA hexamer-hexamer interactions (430, 523, 524). To determine if CA amino acid 216 is responsible for the observed PF74 resistance phenotypes, the T216I CA mutation was made in HIV-1_{LAI} and the corresponding I216T CA mutation was made in HIV-1_{LAI} with CH040 CA. The T216I mutation conferred resistance to high doses of PF74 to WT HIV-1_{LAI} similar to that observed in HIV-1_{LAI} with CH040 CA (**Figure 16D**, left), while I216T made HIV-1_{LAI} with CH040 CA sensitive to high doses of PF74 (**Figure 16D**, right), as was observed with WT HIV-1_{LAI}. Similarly, isolated T216I HIV-1_{LAI} capsid cores exhibited increased RT activity compared to WT HIV-1_{LAI} (**Appendix A**). Taken together, these data suggest that HIV-1_{CH040} differs from HIV-1_{LAI} in capsid stability as a consequence of the T216I CA amino acid substitution.

To examine the capsid stability of HIV-1_{LAI} and HIV-1_{CH040}, we utilized a previously reported capsid permeabilization assay that takes advantage of the dependence of viral RNA staining on the opening of the viral capsid (500, 521). Previous work showed that EU incorporated into HIV-1 RNA during virus production could be stained in cells after virus infection of cells with a decrease in RNA detection over time (500, 521). The rate of RNA staining is affected by capsid stability, such that viruses with hyperstable capsids had slower RNA staining kinetics compared to WT HIV-1 capsid and viruses with hypostable capsids showed faster RNA staining. In this study, RNA staining of HIV-1_{LAI} with CH040 capsid was distinct from that of virus with WT LAI capsid (**Figure 16E**). WT HIV-1_{LAI} virus had a steady decrease in RNA staining after the initial time point, similar to previous results (**Figure 11A**). In contrast, higher numbers of RNA-positive

particles were observed at 60 and 90 minutes post-infection for HIV-1_{LAI} with CH040 capsid than the WT HIV-1_{LAI} virus. The T216I substitution in the LAI capsid phenocopied the CH040 capsid in this capsid permeabilization assay (**Figure 16E**). These results were validated using an orthogonal imaging-based assay that uses a fusion of cyclophilin A and DsRed (CypA-DsRed) to label the virus capsid and monitor its loss from single cores *in vitro* and in infected host cells (287, 525) (**Appendix A**). These results suggest that the capsid of HIV-1_{CH040} is more stable than that of HIV-1_{LAI} and that this difference is regulated by the T216I substitution.

3.2.8 The T216I CA amino acid substitution permits HIV-1 evasion of viral DNA host innate immune sensing

One potential consequence of increased capsid stability is enhanced evasion of cytosolic viral DNA sensors, thereby avoiding an interferon-driven antiviral immune state in infected and neighboring host cells (247). To examine this possibility, a previously described experimental system was utilized, in which HIV-1 infection activates cGAS-mediated IFN signaling in the monocytic cell line THP-1 (526) (**Appendix A**). Infecting THP-1 cells with HIV-1_{LAI} led to a robust production of type I IFN across a range of doses, which was abrogated by the addition of the T216I CA mutation (**Figure 17A and 17B**). Conversely, HIV-1_{LAI} with CH040 CA failed to induce type I IFN production in THP-1 cells but adding the I216T CA mutation generated a strong dose-dependent type I IFN response (**Figure 17A and 17B**). Thus, the same CA amino acid substitution that confers increased capsid stability also prevents type I IFN production in response to HIV-1 infection. Interestingly, an examination of the CA sequence of the other viruses in the T/F panel showed that none contained I216 as found in HIV-1_{CH040}. To examine IFN induction by these T/F viruses, CA from each virus was cloned into HIV-1_{LAI} and used to infected THP-1 cells

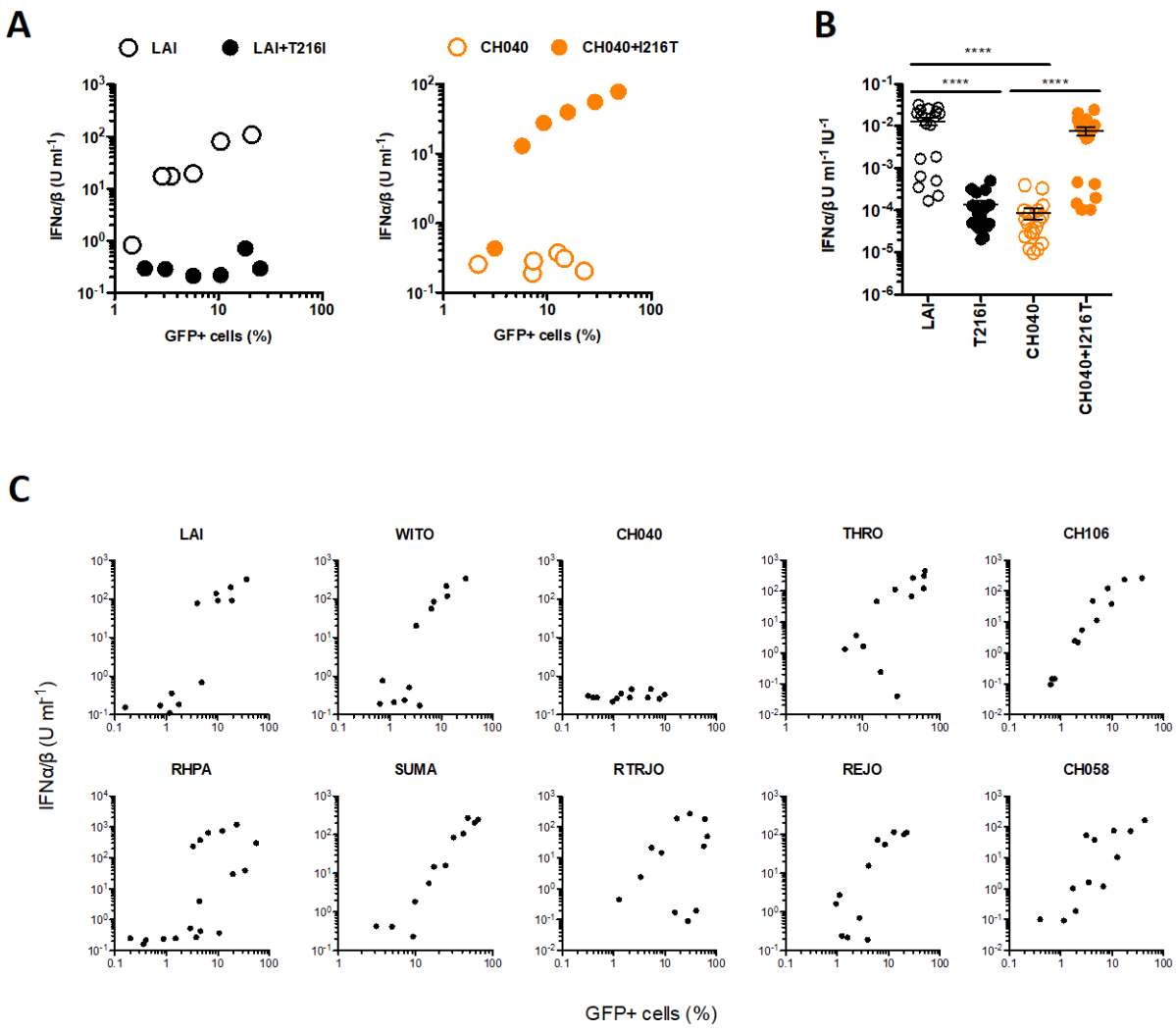

Figure 17. HIV-1 CA mutation T216I inhibits induction of type I IFN production. THP-1 cells were infected with HIV-1_{LAI} GFP reporter viruses bearing the indicated CA strains and mutations. Concentrations of IFN in culture supernatant were measured using a reporter cell line together with known amounts of IFN for generating standard curves and normalized to the numbers of infected cells. (A) Representative results from one of three independent experiments and (B) compiled results from all experiments (n=18, 3 experiments with 6 infectious doses) are shown. (C) HIV-1_{LAI} GFP reporter virus bearing WT CA or CA from the indicated T/F strains were used to infect THP-1 cells as in (A), with results compiled from two experiments. **** $p < 0.0001$. Error bars indicate SEM.

across a range of doses. Infection with each of the T/F viruses except HIV-1_{CH040} resulted in a robust generation of type I IFN similar to that observed with HIV-1_{LAI} (**Figure 17C**), suggesting that CA amino acid I216, while effective at evading innate immune response in monocytic cells, is relatively rare among transmitted/founder viruses.

3.3 Discussion

Here, we characterize the unexpected difference in infectivity of N57A HIV-1 in two of the most widely used lab-adapted HIV-1 strains, HIV-1_{NL4-3} and HIV-1_{LAI}, and offer a model to summarize our findings (**Figure 18**). While N57A has been previously examined in HIV-1_{NL4-3} (270, 274, 283) and found to have an infectivity defect similar to our results in HIV-1_{NL4-3}, this is, to the best of our knowledge, the first study to examine N57A in HIV-1_{LAI} and the first observation of an attenuated (2-7.7-fold) infectivity defect with N57A. Our results were consistent across multiple cell lines and in primary human CD4+ T cells, and while cell type specific variation in overall infectivity was observed here as in previous studies (270, 274, 283), the N57A infectivity defect was always significantly attenuated in HIV-1_{LAI} compared to HIV-1_{NL4-3}.

Our use of *gag* chimeric viruses demonstrated that the N57A infectivity phenotypes in HIV-1_{NL4-3} and HIV-1_{LAI} are CA dependent, with the infectivity phenotype observed in each chimera corresponding to the phenotype observed in the *gag* source strain and not the background strain (i.e. HIV-1_{NL4-3} with LAI Gag exhibited the same N57A infectivity phenotype as HIV-1_{LAI} and HIV-1_{LAI} with NL4-3 Gag phenocopied HIV-1_{NL4-3}). We focused on CA to account for the observed differences in N57A infectivity phenotypes between HIV-1_{NL4-3} and HIV-1_{LAI} because

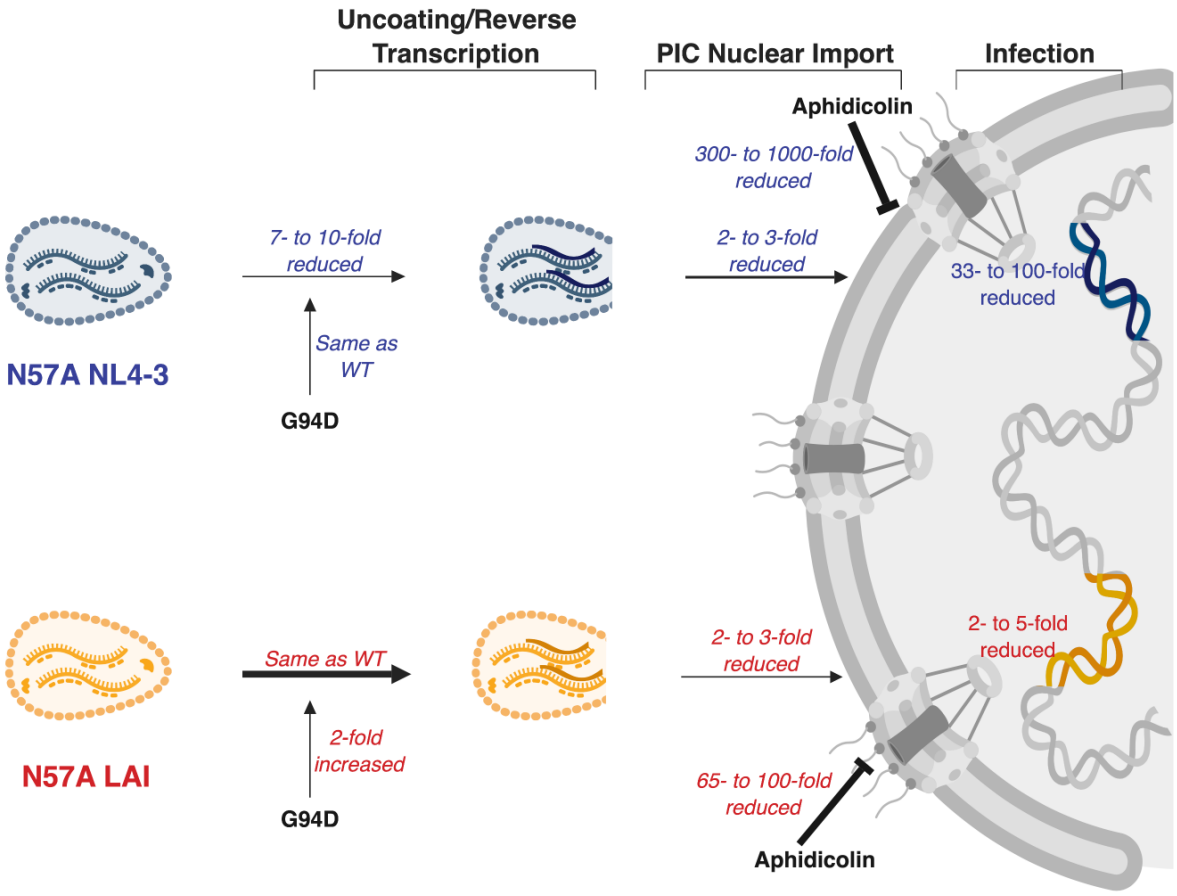

Figure 18. Model of N57A HIV-1_{NL4-3} and N57A HIV-1_{LAI} phenotypes. The differences in capsid permeabilization, reverse transcription, nuclear import, and infection of N57A HIV-1 compared to WT virus in either HIV-1_{NL4-3} (top) or HIV-1_{LAI} (bottom) are shown. The effects of cell cycle arrest (via aphidicolin treatment) and the addition of the G94D CA mutation are included.

N57A was previously shown to affect interactions with CA-dependent host factors CPSF6 (281, 283), TNPO3 (466), Nup153 (274), and Nup358 (270). Indeed, mutation of CA amino acids 6, 83, 120, and 208 in HIV-1_{NL4-3} to those of HIV-1_{LAI}, thereby producing HIV-1_{NL4-3} with LAI CA, resulted in N57A infectivity phenotypes in these strains that are CA dependent.

Examining subsets of these mutations in combination with N57A further refined this CA dependence to a single requisite amino acid substitution, L83V. Residue 83 resides within helix 4 of the N-terminal domain of CA, proximal to the CypA binding loop. It has been suggested that this residue in combination with residues 120 and 122 is involved in the modulation of restriction by tripartite motif containing protein 5α (TRIM5α) (527). Maillard et al. demonstrated that mutating these three residues in HIV-$1_{R8.74}$ to their HIV-2 equivalents (V83Q, H120R and P122Q) conferred sensitivity to restriction by human TRIM5α. However, there are no published reports characterizing a specific role for CA residue 83, particularly one modulated by the presence of leucine versus valine. This residue is located on an external surface within the N-terminal CA domain that interacts with multiple host factors and could be involved with one or more host factor interactions that are altered by the L83V mutation. Alternatively, mutation of residue 83 could be involved with proximal or distal CA conformational changes that vary based upon the amino acid.

As CA was shown to alter the N57A infectivity phenotypes in HIV-1_{NL4-3} and HIV-1_{LAI}, capsid permeabilization kinetics of N57A in HIV-1_{NL4-3} and HIV-1_{NL4-3} with LAI CA were examined. N57A capsid permeabilization was accelerated in HIV-1_{NL4-3} but not in HIV-1_{NL4-3} with LAI CA, suggesting a fundamental difference in the nature of the N57A infectivity defect in these two HIV-1 strains. This was supported by the observation that production of reverse transcripts

was significantly reduced for N57A HIV-1_{NL4-3} compared to WT HIV-1_{NL4-3} but not for N57A in the context of HIV-1_{LAI} CA. N57A in all virus backgrounds led to a significant reduction in 2-LTR circles compared with WT, which is consistent with previous observations of other N57 CA mutations in HIV-1_{NL4-3} (275). The relative level of N57A 2-LTR circles compared to WT in HIV-1_{NL4-3} (20-fold) is considerably lower than the level of N57A 2-LTR circles compared with WT in HIV-$_{NL4-3}$ with LAI CA and HIV-1_{LAI} (2-3-fold), which might suggest, if taken on its own, that N57A HIV-1_{NL4-3} has a more appreciable nuclear entry defect than N57A HIV-1_{LAI}. However, when observed within the context of the accompanying defect in N57A HIV-1_{NL4-3} reverse transcription products versus WT virus (7-10-fold), the 20-fold reduction in 2-LTR circles for N57A HIV-1_{NL4-3} is consistent with a combination of the same 2-3-fold nuclear entry defect of N57A HIV-1_{LAI} and an earlier 7-10-fold reverse transcription defect. In other words, these data suggest that N57A causes a similar nuclear entry defect in both HIV-1_{NL4-3} and HIV-1_{LAI} but has an additional, earlier infectivity defect that results in accelerated capsid permeabilization and reduction in reverse transcription in HIV-1_{NL4-3} and not in HIV-1_{LAI}.

The emergence of G94D as a compensatory mutation in N57A HIV-1_{LAI} hints at a role for CypA interaction in N57A HIV-1 infectivity. CA interaction with CypA has been shown to impact all post-entry steps of the early virus life cycle, including reverse transcription, capsid stability, and modulating the use of other capsid-interacting host factors (388). CA mutation G94D originally emerged as a resistance mutation that permits robust virus replication in the presence of CsA, a competitive inhibitor of CA-CypA binding (438, 439). Similar to N57A, CA mutant N74D HIV-1 (266) infects cells independently from host factors CPSF6, TNPO3, Nup358, and Nup153 (266, 273, 435), though it is not cell cycle dependent. N74D is sensitive to inhibition of CA-CypA

interaction, which is partially rescued by the addition of CA mutation G94D (435). Coupled with the observed rescue of N57A HIV-1_{LAI} infectivity by the addition of G94D, this is highly suggestive of a dependency on CypA interaction for N57A HIV-1 infectivity, which might be altered by G94D. Another possible mechanism of N57A/G94D HIV-1_{LAI} infectivity rescue could be the restoration of one or more host factor interactions. While multiple studies have demonstrated that N57A HIV-1_{NL4-3} infects independently of CPSF6, TNPO3, Nup153, and Nup358 (270, 274, 281, 283, 466), similar studies have not been conducted on N57A HIV-1_{LAI} and, importantly, on N57A/G94D HIV-1_{LAI}. Examining capsid host factor interactions within the context of these CA mutations in both HIV-1_{NL4-3} and HIV-1_{LAI} could assist in understanding the nature of the N57A infectivity defect and the mechanism of its rescue by G94D.

The inability of CA mutation L83V to induce the infectivity rescue of N57A HIV-1_{NL4-3} by G94D was unexpected, given the ability of the addition of the L83V CA mutation to HIV-1_{NL4-3} to convert the N57A HIV-1_{NL4-3} infectivity phenotype to that of N57A HIV-1_{LAI}. Intriguingly, the further mutation of any one of the other three amino acids that differ between HIV-1_{NL4-3} and HIV-1_{LAI}, when added to L83V, led to rescue of N57A/G94D HIV-1_{NL4-3} infectivity. Infectivity rescue depends upon both L83V and any one of the other CA mutations, as excluding L83V abolishes rescue. This suggests that there are separate CA-dependent mechanisms responsible for the increased infectivity of N57A HIV-1_{LAI} compared to N57A HIV-1_{NL4-3} and for the rescue of N57A HIV-1_{LAI} by G94D, with the L83V mutation alone responsible for the former and L83V together with the L6I, H120N, and/or G208A mutation(s) contributing to the latter. It is curious that three separate mutations at discrete locations in CA can each alter the N57A/L83V/G94D HIV-1_{NL4-3} infectivity phenotype in a similar manner. This is suggestive of an induced change to

the conformation of CA, which could alter host factor engagement, or an alteration to capsid stability. Additional research will be required to determine the mechanism through which infectivity rescue is obtained.

While originally derived from one or more clinical isolates, HIV-1_{NL4-3} (180) and HIV-1_{LAI} (520) are lab-adapted virus strains. Adaptation by serially passaging in cell lines selects for phenotypes, such as CD4 affinity and coreceptor tropism, that differ substantially from infectivity phenotypes observed in HIV-1 clinical isolates, particularly transmitted/founder strains (178). While the primary viral determinant for these lab-adapted infectivity phenotypes was shown to map to changes to gp120 (528, 529), it is possible that lab adaptation could also result in changes to CA. HIV-1_{NL4-3} and HIV-1_{LAI} CA differ at only four positions (residues 6, 83, 120, and 208), three of which (residues 6, 83, and 120) are among the most polymorphic positions within CA (394, 530). Indeed, an analysis of over 40,000 Gag sequences from primary isolates of multiple subtypes demonstrated the polymorphic nature of all four of these CA positions, including the residues present in HIV-1_{NL4-3} and HIV-1_{LAI}. Within subtype B, Gag (including CA) shows low overall sequence diversity (391) and across all subtypes the N-terminal region of CA, along with IN, contains the lowest levels of amino acid diversity within the HIV-1 genome (212). The frequency of HIV-1_{NL4-3} and HIV-1_{LAI} amino acids across all CA positions showed strong conservation, with over 90% of CA sequences matching HIV-1_{NL4-3} and HIV-1_{LAI} at the vast majority of the positions. The high degree of similarity of CA sequences from HIV-1_{NL4-3}, HIV-1_{LAI}, and clinical isolates suggests that CA-dependent phenotypes, such as observed with N57A, could differ among other HIV-1 lab-adapted strains and primary isolates.

Only a small percentage of HIV-1 virus strains are able to be effectively transmitted to an uninfected individual and become established, and as such represent a population of virus strains of high clinical significance (36). The ability to evade host cell innate immune responses enhances the likelihood of successful transmission, while conversely a better understanding of how evasion is accomplished informs on how it might be subverted (247). HIV-1_{CH040}, while unique among the small panel of T/F viruses examined for increased capsid stability and concomitant avoidance of cytosolic viral DNA sensors, is likely representative of additional T/F virus strains. The phenotypically critical I216 amino acid can be found in 1% of the approximately 14,000 HIV-1 subtype B sequences examined in the LANL HIV-1 database, and an additional 3% of the sequences have a different, non-threonine amino acid at this position, which could potentially possess a similar phenotype. That such a consequential phenotype can be modulated by a single CA amino acid substitution speaks to both the flexibility and fragility of HIV-1 and demonstrates that a minor alteration to the stability of the virus capsid is sufficient to appreciably impact virus infectivity and clinical transmissibility.

We have shown that two closely related and widely used HIV-1 molecular clones (HIV-1_{NL4-3} and HIV-1_{LAI}) can exhibit significantly different infectivity phenotypes due to four CA amino acid differences and that these clones are both represented in HIV-infected individuals. Thus, careful consideration should be given to drawing conclusions from one particular HIV-1 clone used in post-entry infection studies and the potential for significant variation in results with the use of multiple strains. While phenotypic differences in HIV-1 subtypes and host cell types have been acknowledged for many aspects of the virus life cycle, differences among closely related subtype B strains, such as HIV-1_{NL4-3} and HIV-1_{LAI}, or for CA-dependent host factors have

garnered less attention. It is hoped that this study highlights the significance that minor differences in closely related HIV-1 strains may impart significant infectivity differences and that consideration should be given to examining the effects of natural polymorphisms on specific results.

3.4 Materials and Methods

Cell Lines

HEK 293T cells, GHOST cells, TZM-bl cells, and HeLa cells were maintained at 37° C with 5% CO_2 in Dulbecco's Modified Eagle Medium (DMEM, Gibco) supplemented with 10% Fetal Bovine Serum (FBS, Atlanta Biologicals), 100 units (U)/mL Penicillin, 100 µg/mL Streptomycin, and 2 mM L-Glutamine (Thermo Fisher). GHOST cells were additionally supplemented with 500 µg/mL Geneticin G418 (Gibco), 500 µg/mL Puromycin (Invitrogen), and 100 µg/mL Hygromycin B (Invitrogen). THP-1 and MT-4 cells were cultured in Roswell Park Memorial Institute medium (Cellgro) supplemented with 10% FBS (Sigma), 1× penicillin-streptomycin (Cellgro) and 2 mM 2-glutamine (Cellgro). Human peripheral blood mononuclear cells (PBMCs) were isolated from leukopheresis obtained from the Central Blood Bank (Pittsburgh, PA) via Ficoll-Paque Plus (GE Healthcare) density gradient centrifugation, following manufacturer's instructions. PBMCs were maintained at 37° C and 5% CO_2 in RPMI-1640 medium (Gibco) supplemented with 10% FBS, 100 U/mL Penicillin, 100 µg/mL Streptomycin, 2 mM L-Glutamine, and 20 U/mL recombinant interleukin-2 (IL-2, Thermo Fisher). PBMCs were stimulated with 50 U/mL IL-2 and 5 µg/mL phytohaemagglutinin (PHA, Gibco) for 48-72h prior to infection.

Viruses

Proviral plasmid pNLdE-luc (266) was used to produce HIV-1_{NL4-3} and plasmids pBru3ori-ΔEnv-luc2 and pBru3ori-ΔEnv-GFP3 (268) were used to produce HIV-1_{LAI}. CA mutations were generated via the Q5 (New England BioLabs) or QuikChange (Agilent) site-directed polymerase chain reaction (PCR) mutagenesis kits following manufacturers' instructions and verified by Sanger sequencing. The pNLdE-LAI-luc chimeric plasmids (HIV-1_{NL4-3} with LAI Gag) were created by cloning the Gag fragment from pBru3ori-ΔEnv-GFP3 into pNLdE-luc using the restriction enzymes BssHII and ApaI. The pBru3ori-ΔEnv-NL43-GFP3 chimeric plasmids (HIV-1_{LAI} with NL4-3 Gag) were created by cloning the Gag fragment from pNLdE-luc into pBru3ori-ΔEnv-GFP3 using BssHII and ApaI. A BssHII-ApaI fragment containing the entire capsid-encoding segment was PCR amplified using a panel of full-length T/F HIV-1 infectious molecular clones obtained through the National Institutes of Health (NIH) AIDS Reagent Program as template and cloned into pBru3ori-ΔEnv-GFP3. The following molecular clones for T/F viruses were used: RHPA.c/2635, WITO.c/2474, CH040.c/2625, CH058.c/2960, CH077.t/2627, CH106.c/2633, THRO.c/2626, REJO.c2864, RTRJO.c2851 and SUMA.c/2821 (522).

HEK 293T cells were plated overnight and transfected with Lipofectamine 2000 (Invitrogen) or with polyethylenimine (PolySciences) using the following plasmids: the proviral plasmids described above, pL-VSV-G or pHCMV-G, and, for imaging studies, pcDNA5-TO-Vpr-mRuby3-IN (521). Supernatants were harvested 48h later, filtered or centrifuged to remove cells, concentrated via Lenti-X Concentrator (Clontech), and stored in aliquots at -80° C. For virus stocks used in the capsid permeabilization assay, 293T producer cells were supplemented with 1 mM EU (Invitrogen) for 12-16h, which was replaced with regular media for the remainder of the 48h

incubation. Viruses were titered by infection of GHOST cells as previously described (531) and quantified for p24 by HIV-1 p24 enzyme-linked immunosorbent assay (ELISA) kit (XpressBio). Virus yields were also quantified by measuring virion-associated RT activity using a SYBR green-based quantitative PCR assay (532).

Infectivity Assays

HeLa cells, GHOST cells, and PBMC were plated overnight in 24-well plates, challenged with equal p24 amounts of virus for 2h, washed with phosphate buffered saline (PBS), and given fresh media. Virus infectivity was determined by luciferase production (Promega) after 48h using a 1450 MicroBeta TriLux microplate luminescence counter (PerkinElmer). For assays including treatment with aphidicolin, cells were treated with aphidicolin (2 μg/mL) at time of plating and remained in drug-containing media throughout the assay. For green fluorescent protein (GFP) reporter virus, infection of HeLa cells and MT-4 cells was performed with equal amounts of virus input normalized by RT activity. Spinoculation (1,200 × g for 30 min) was used to enhance infection of HeLa cells. The number of GFP-expressing cells was counted using either Guava easyCyte (Millipore) or LSRII flow cytometer (BD Biosciences) 2 to 3 days after infection. Assessment of PF74 resistance and type I IFN induction were perform as described in Appendix A.

Measurement of reverse transcripts and 2-LTR circles

HeLa cells were plated in 6-well plates and infected with 50 ng p24 of virus treated with deoxyribonuclease I (DNase I, Roche) for 30m at 37° C. After 24h, cells were washed with PBS, trypsinized, and pelleted. Control infections were performed in the presence of 150 nM of efavirenz or 25 nM of rilpivirine. DNA was extracted using the Blood Mini Kit (Qiagen), Early

(RU5) and late (*gag*) HIV-1 reverse transcripts and 2-LTR circles were measured by quantitative PCR as previously described (533).

Capsid Permeabilization Assay and Confocal Imaging

The capsid permeabilization assay was performed as previously described (500, 521). Briefly, HeLa cells were plated overnight in 35 mm glass bottom dishes (MatTek), synchronously infected with EU-labeled HIV-1 virus particles, and incubated for the indicated time periods at 37° C. Cells were washed with PBS, fixed with 2% paraformaldehyde (PFA), and permeabilized with 0.1% Triton X-100 (Fisher Scientific). Viral RNA was stained using the Click-iT RNA Imaging Kit (Invitrogen), washed with PBS, stained with Hoechst 33342 (Molecular Probes), and mounted with coverslips. Confocal imaging was performed on a Nikon A1 laser scanning confocal microscope, with 8-10 image Z-stacks per sample. Viral RNA staining was enumerated using Imaris image analysis software (Bitplane).

Sequence Analysis

Aligned HIV-1 p24 (CA) protein sequences were retrieved from the Los Alamos National Laboratory HIV-1 sequence database (https://www.hiv.lanl.gov) in May 2018. The vast majority (99.5%) of the 40,712 sequences were classified as group M with 35% subtype B, 29% subtype C, 22% circulating recombinant forms, 10% subtype A, 3% subtype D, and <1% each subtypes F, G, H, J and K. At each CA amino acid position, sequences were compared to the NL4-3 and LAI amino acids and the prevalence of the NL4-3 and LAI amino acid (0-100%) was calculated. The frequencies of amino acids present at residues 6, 83, 120, and 208 were measured by Perl scripts, with amino acids representing less than 2% of sequences aggregated into an “other” category.

Statistics

Results were analyzed for statistical significance by two-sided student t test with Prism software (GraphPad). Grubbs' Extreme Studentized Deviate test was used to exclude significant outliers from capsid permeabilization assay data sets. A p-value of less than or equal to 0.05 was used to indicate statistical significance. For the capsid permeabilization assay, capsid permeabilization kinetics were analyzed by multiple linear regression modeling using the SAS software to test if the slopes were equivalent. Using the F statistic with the Bonferroni correction for pairwise comparisons, p values less than 0.0167 were considered statistically significant.

3.5 Acknowledgements

We would like to thank Callen Wallace and Samantha Teng for technical assistance. This work was supported by the National Institutes of Health P50 grant GM082251 (SCW, MY, ZA), the National Institutes of Health R01 grant AI100720 (MY), and the National Institutes of Health T32 training grant AI065380 (DKF).

4.0 Determine How Disruption of Interactions Between HIV-1 Capsid and Host Proteins Alters Virus Infectivity

This chapter includes data adapted from the following published manuscripts:

Douglas K. Fischer, Akatsuki Saito, Christopher Kline, Romy Cohen, Simon C. Watkins, Masahiro Yamashita, Zandrea Ambrose. CA Mutation N57A Has Distinct Strain-Specific HIV-1 Capsid Uncoating and Infectivity Phenotypes. Journal of Virology Apr 2019, 93 (9) e00214-19; DOI: 10.1128/JVI.00214-19. Copyright © 2019 American Society for Microbiology (ASM).

Jiying Ning, Zhou Zhong, **Douglas K. Fischer**, Gemma Harris, Simon C. Watkins, Zandrea Ambrose, Peijun Zhang. Truncated CPSF6 Forms Higher-Order Complexes That Bind and Disrupt HIV-1 Capsid. Journal of Virology Jun 2018, 92 (13) e00368-18; DOI: 10.1128/JVI.00368-18. Copyright © 2018 American Society for Microbiology.

Figures 19, 20, and 21 are published in the *Journal of Virology* (Fischer et al., 2019) and are reprinted with permission from ASM. Figures 22, 23, and 25 include data that is published in the *Journal of Virology* (Ning et al., 2018) and are reprinted with permission from ASM. Figures 24, 26, 27, and 28 are part of a manuscript in preparation.

4.1 Introduction

Successful target cell infection by HIV-1 requires interaction with numerous host proteins (198-201) that facilitate each step of the virus life cycle (197). Among these are host factors that have been shown to interact with the viral capsid, including CypA (444), CPSF6 (266), and Nup153 (273). Disruption of these interactions has a deleterious effect on viral infectivity (271, 281, 435, 439, 453, 534), making them an attractive target for therapeutic intervention (386, 387).

We have shown that HIV-1 CA mutation N57A exhibits an infectivity defect that differs between common lab-adapted strains HIV-1_{NL4-3} and HIV-1_{LAI}, the magnitude of which is CA dependent and corresponds with strain-specific defects in capsid permeabilization and reverse transcription (**Chapter 3**). The N57A HIV-1 infectivity defect is partially rescued in HIV-1_{LAI} but not in HIV-1_{NL4-3} by the addition of CA mutation G94D (**Chapter 3**). The mechanisms behind these infectivity defects and partial infectivity rescue have not been explored, but these could include strain-specific differences that affect host factor interactions. While N57A HIV-1_{NL4-3} has been demonstrated to infect independently of CPSF6 and Nup153 (270, 274, 281, 283), infectivity of N57A HIV-1_{LAI} and N57A/G94D HIV-1_{LAI} have not been examined for independence from these host factors.

A truncated form of host protein CPSF6 that is missing the C-terminal nuclear localization signal (CPSF6-358) has previously been shown to be mislocalized to the cytoplasm and to restrict WT HIV-1 infection (266) but not infection of N74D HIV-1 (266) or A77V HIV-1 (436), which do not bind to CPSF6 (266, 283, 436). This selective restriction of HIV-1 infectivity by CPSF6-358 based upon capsid binding can serve as a useful tool for examining the ability of HIV-1_{NL4-3}

and HIV-1_{LAI} bearing CA mutations N57A and N57A/G94D to interact with CPSF6. In addition, the mechanism by which CPSF6-358 restricts WT HIV-1 infectivity is not entirely clear. CPSF6-358 restricts WT HIV-1 infection after reverse transcription and before nuclear entry (266) and *in vitro* observations show that CPSF6-358 forms higher order complexes, which can bind to and disrupt CA tubes (521). Whether or not this represents the mode of action of CPSF6-358 within infected host cells remains to be determined.

Here, we present the results of our examination of HIV-1 interaction with host proteins CPSF6, CypA, and Nup153 using genetic approaches to introduce mutations into CA and to affect host factor expression and/or HIV-1 capsid-binding in cells. First, we extend the *in vitro* observations of CPSF6-358 higher order complex formation through cell-based studies, suggesting a plausible mechanism by which CPSF6-358 restricts HIV-1 infectivity. We demonstrate a dependence on CypA binding to CA for N57A HIV-1 infectivity and its partial rescue by CA mutation G94D in a virus strain and host cell type dependent manner. In addition, we show that N57A HIV-1 and N57A/G94D HIV-1 infect independently of CPSF6 and Nup153.

4.2 Results

4.2.1 Formation of CPSF6-358 higher order complexes in cells is induced by and restricts WT HIV-1 infection

CPSF6-358 has been observed to form higher order complexes *in vitro* that bind to and disrupt CA tubular assemblies (521), suggesting a mechanism by which CPSF6-358 restricts WT HIV-1

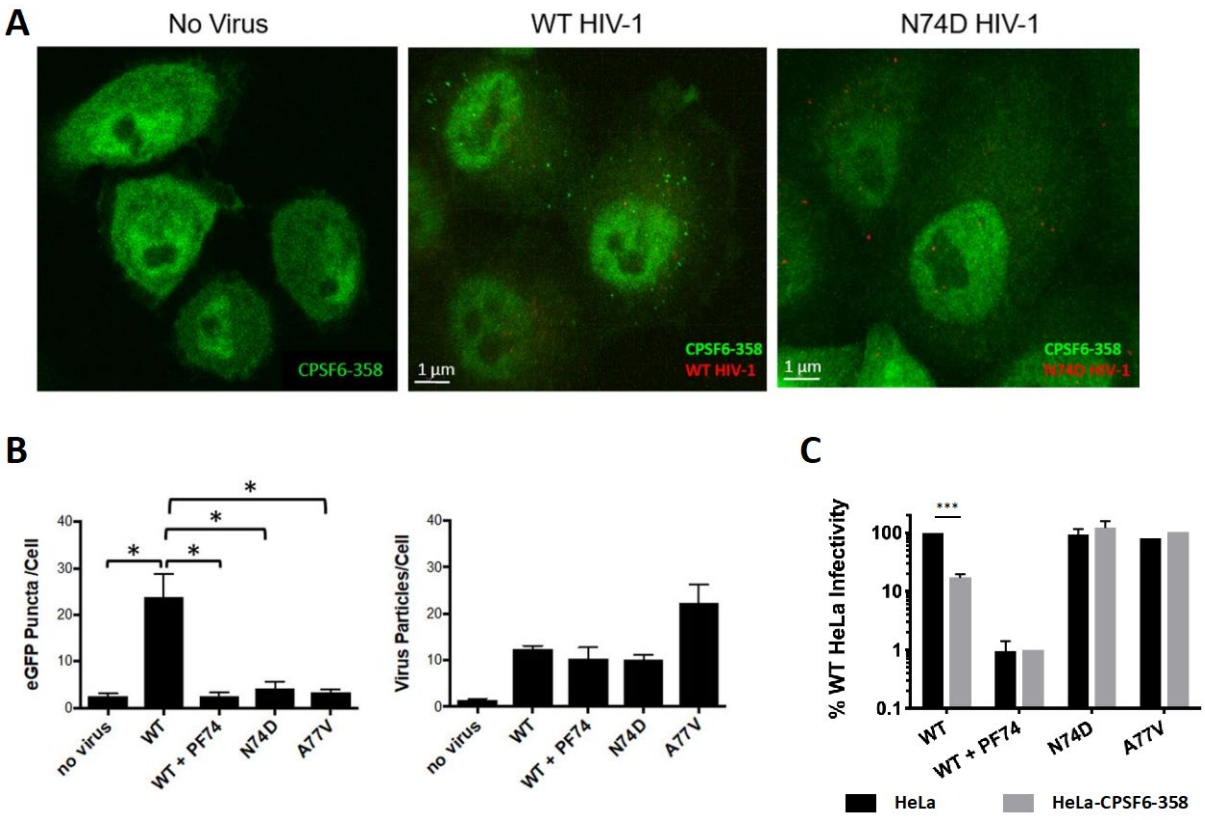

Figure 19. WT HIV-1 infection induces formation of CPSF6-358 higher-order complexes in HeLa cells. (A) Confocal images of HeLa cells stably expressing CPSF6-358-eGFP before or 30 min after infection with WT HIV-1 or N74D HIV-1. (B) CPSF6-358-eGFP puncta and mRuby-IN particles were quantified per cell (n ≥ 25 z-stacks) at 30 min post-infection with WT HIV-1 in the presence or absence of 10 µM PF74, N74D HIV-1, or A77V HIV-1. (C) HeLa cells and HeLa cells stably expressing CPSF6-358-eGFP were infected with equal amounts of WT HIV-1 in the presence or absence of 10 µM PF74, N74D HIV-1, or A77V HIV-1 and assayed after 48h for luciferase activity. * $p < 0.05$, *** $p < 0.001$. Error bars indicate SEM for at least 2 experiments. Panels (A) and (B) reprinted from Ning et al. (2018) with permission from ASM.

infectivity. To determine if the *in vitro* observations could be visualized in cells, HeLa cells stably expressing CPSF6-358 with eGFP fused to the C-terminus (CPSF6-358-eGFP) were infected with WT or N74D HIV-1 and examined by confocal microscopy. Cells infected with WT HIV-1 exhibited distinct green cytoplasmic puncta that were not observed with N74D HIV-1 infection or in uninfected cells (**Figure 19A**). To verify that capsid binding is necessary for formation of puncta, infection and confocal imaging were repeated with WT HIV-1, WT HIV-1 in the presence of 10 μM PF74 (a pharmacologic competitive inhibitor of CPSF6 binding to CA (417)), N74D HIV-1, or A77V HIV-1. Inhibiting CPSF6 interaction with CA through drug treatment or CA mutation prevented the formation of CPSF6-358-eGFP puncta (**Figure 19B**, left), despite the presence of similar numbers of virus particles in each sample (**Figure 19B**, right). To confirm that the formation of CPSF6-358-eGFP puncta corresponded with restriction of virus infectivity, HeLa cells and HeLa cells stably expressing CPSF6-358-eGFP were infected with WT HIV-1, WT HIV-1 in the presence of 10 μM PF74, N74D HIV-1, or A77V HIV-1. CPSF6-358-eGFP expression did not restrict N74D HIV-1 or A77V HIV-1 infectivity and did not augment PF74 restriction of WT HIV-1 but restricted WT HIV-1 infectivity 6-fold (**Figure 19C**). These data suggest that HIV-1 binding to CPSF6-358 induces the formation of higher order complexes in cells and restriction of infectivity.

4.2.2 CPSF6-358 higher-order complexes associate with HIV-1 particles and lead to accelerated permeabilization of HIV-1 capsid

The requirement for CPSF6 interaction with CA to induce the formation of CPSF6-358-eGFP puncta suggested CPSF6-358-eGFP complexes might form in association with WT HIV-1 virus particles. To examine this possibility, HeLa cells stably expressing CPSF6-358-eGFP were

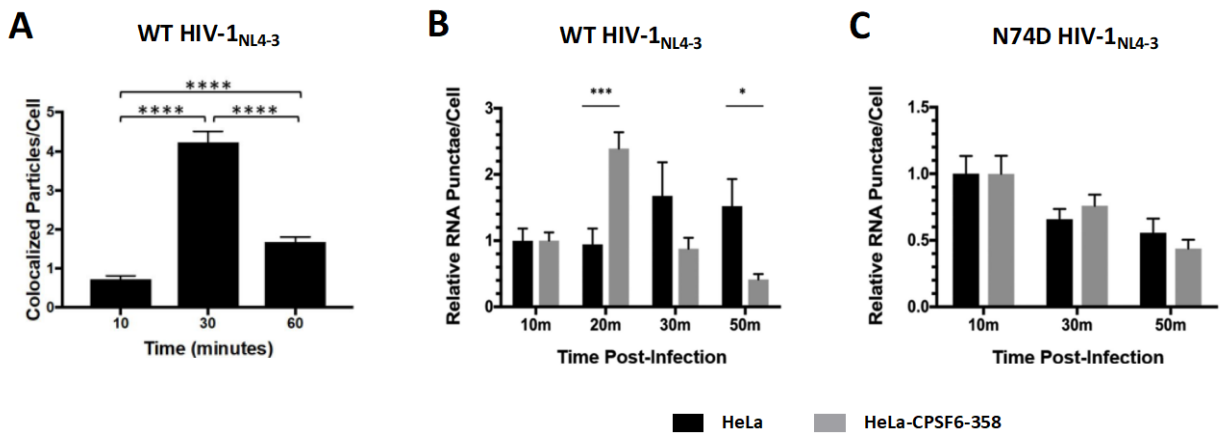

Figure 20. WT HIV-1 particles associate with CPSF6-358 and undergo capsid permeabilization more quickly in its presence. (A) Live-cell frustrated TIRF microscopy images were obtained after synchronized infection of HeLa cells stably expressing CPSF6-358-eGFP with WT HIV-1 and colocalized CPSF6-358-eGFP and mRuby3-IN particles were quantified at 10, 30, and 60 minutes post-infection. (B) HeLa cells and HeLa cells stably expressing CPSF6-358-eGFP were infected with WT HIV-1 or (C) N74D HIV-1 and stained for viral RNA at indicated times. * $p < 0.05$, *** $p < 0.001$, **** $p < 0.0001$. Error bars indicate SEM. Adapted from Ning et al. (2018) with permission from ASM.

synchronously infected with WT HIV-1 packaging Vpr-mRuby3-IN *in trans*, live cell frustrated total internal reflection fluorescence (TIRF) imaging was performed, and colocalization of CPSF6-358-eGFP and mRuby3-IN particles was quantified. CPSF6-358-eGFP puncta, which formed as early as 10 minutes post-infection, frequently colocalized with mRuby3-IN virus particles, peaking in number at 30 minutes post-infection, and generally separated by 60 minutes post-infection (**Figure 20A**). These data, combined with the prior observation of CPSF6-358 disruption of CA tubes *in vitro*, led to the hypothesis that CPSF6-358-eGFP causes more rapid capsid permeabilization. To test this idea, the EU capsid permeabilization assay (500) was performed with HeLa cells and HeLa cells stably expressing CPSF6-358-eGFP infected with WT HIV-1 or

N74D HIV-1. In the absence of CPSF6-358-eGFP, WT HIV-1 capsid permeabilization occurred at 30 minutes post-infection (**Figure 20B**), similar to previous observations (500) (**Chapter 3**). In the presence of CPSF6-358-eGFP, WT HIV-1 capsid permeabilization occurred at 20 minutes post-infection (**Figure 20B**). CPSF6-358-eGFP did not alter capsid permeabilization of N74D HIV-1 (**Figure 20C**). Together, these data suggest that CPSF6-358 complexes form in association with WT HIV-1 virus particles and lead to accelerated capsid permeabilization.

4.2.3 CPSF6-358 does not restrict N57A or N57A/G94D HIV-1 infection

N57A HIV-1 infectivity, more specifically N57A HIV-1_{NL4-3}, has been shown to infect cells independently of host factors CPSF6 (281, 283), Nup358 (270), and Nup153 (270, 274), which have been suggested to form a pathway for PIC nuclear entry and integration targeting (284). The increased infectivity of N57A HIV-1_{LAI} compared to N57A HIV-1_{NL4-3} or the partial rescue of N57A HIV-1_{LAI} infectivity by the CA mutation G94D that we observed (**Chapter 3**) could be explained by restoration of N57A HIV-1 interaction with one or more of these host factors. To determine if CPSF6 interaction is altered between N57A HIV-1_{NL4-3} and N57A HIV-1_{LAI} or restored by N57A/G94D HIV-1_{LAI}, HeLa cells and HeLa cells stably expressing CPSF6-358-eGFP were infected with WT, N57A, or N57A/G94D HIV-1_{NL4-3} or HIV-1_{NL4-3} with LAI CA. WT HIV-1 was significantly restricted by CPSF6-358 with both NL4-3 CA (8-fold, **Figure 21A**) and LAI CA (12-fold, **Figure 21B**). N57A HIV-1 with both NL4-3 CA (**Figure 21A**) and LAI CA (**Figure 21B**) showed similar infectivity with and without CPSF6-358 expression, indicating that N57A HIV-1_{LAI}, like N57A HIV-1_{NL4-3}, infects independently of CPSF6. N57A/G94D HIV-1_{NL4-3} infectivity was likewise unaffected by CPSF6-358 (**Figure 21A**). CPSF6-358 expression also did

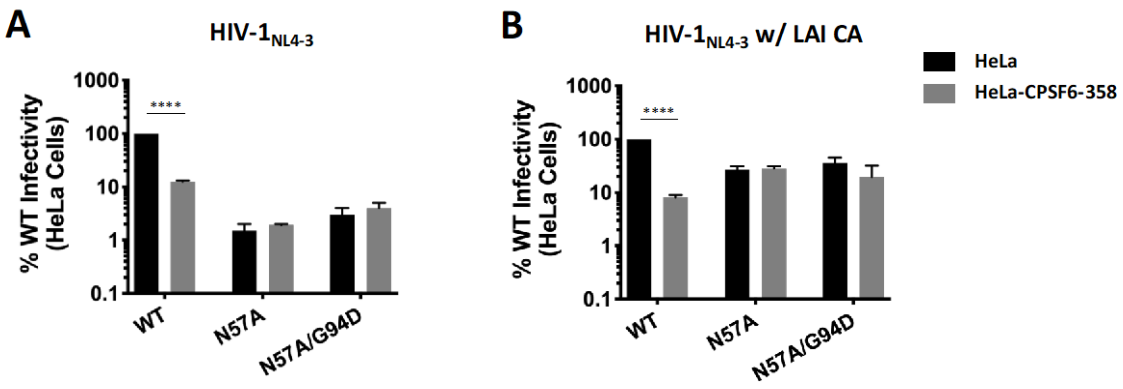

Figure 21. CPSF6-358 does not restrict N57A HIV-1 or N57A/G94D HIV-1 infection. HeLa cells and HeLa cells stably expressing CPSF6-358-eGFP were infected with equal amounts of WT, N57A, or N57A/G94D HIV-1_{NL4-3} luciferase reporter virus with (A) WT or (B) LAI CA and assayed after 48h for luciferase activity. **** $p < 0.0001$. Error bars indicate SEM for 2 experiments.

not significantly impact infectivity of N57A/G94D HIV-1_{NL4-3} with LAI CA (**Figure 21B**), suggesting that G94D does not restore interaction of N57A HIV-1_{LAI} with CPSF6.

4.2.4 CsA treatment leads to faster formation of CPSF6-358 higher-order complexes

CPSF6-358-eGFP puncta did not all form simultaneously upon synchronous infection with WT HIV-1 but appeared over time, which could be caused by another host factor preventing CPSF6-358-eGFP from gaining immediate access to the capsid. We hypothesized that CypA, which has long been known to bind to CA (444), might shield the capsid from CPSF6-358 and delay formation of puncta. To examine this possibility, HeLa cells stably expressing CPSF6-358-eGFP were infected with WT or N74D HIV-1 packaging mRuby3-IN *in trans* in the presence or absence of CsA treatment. With WT HIV-1 infection, a greater number of puncta were observed with CsA

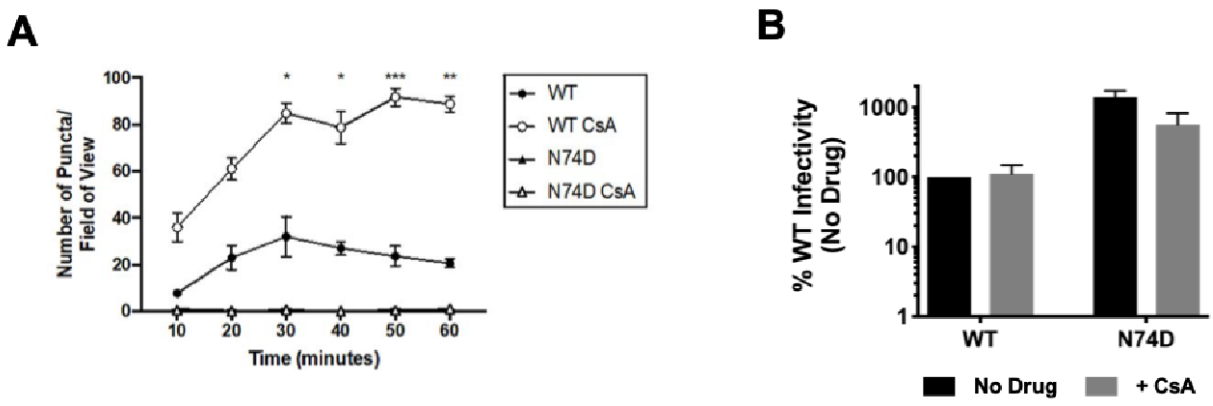

Figure 22. CsA treatment accelerates formation of CPSF6-358 higher-order complexes. (A) HeLa cells stably expressing CPSF6-358-eGFP were treated (open symbols) or not (solid symbols) with 2 μM CsA and synchronously infected with WT HIV-1 or N74D HIV-1. The number of CPSF6-358-eGFP puncta per confocal imaging field of view was determined at indicated times post-infection. (B) HeLa cells stably expressing CPSF6-358-eGFP were infected with equal amounts of WT HIV-1 or N74D HIV-1 in the presence or absence of 2 μM CsA and assayed after 48h for luciferase activity. * $p < 0.05$, ** $p < 0.01$, *** $p < 0.001$. Error bars indicate SEM. Panel (A) reprinted from Ning et al. (2018) with permission from ASM.

treatment than without at all time points examined (**Figure 22A**), despite similar numbers of mRuby3-IN particles (data not shown), and significantly more puncta were observed with CsA treatment starting at 30 minutes post-infection (**Figure 22A**). No puncta were observed with N74D HIV-1 infection with or without CsA treatment (**Figure 22A**). The increase in WT HIV-1-induced CPSF6-358-eGFP puncta upon CsA treatment did not correspond to greater restriction of virus infectivity, as HeLa cells stably expressing CPSF6-358-eGFP and infected with WT HIV-1 with and without CsA treatment showed similar levels of infection (**Figure 22B**). N74D HIV-1 infectivity, while not restricted by CPSF6-358, was sensitive to CsA treatment (**Figure 22B**), as

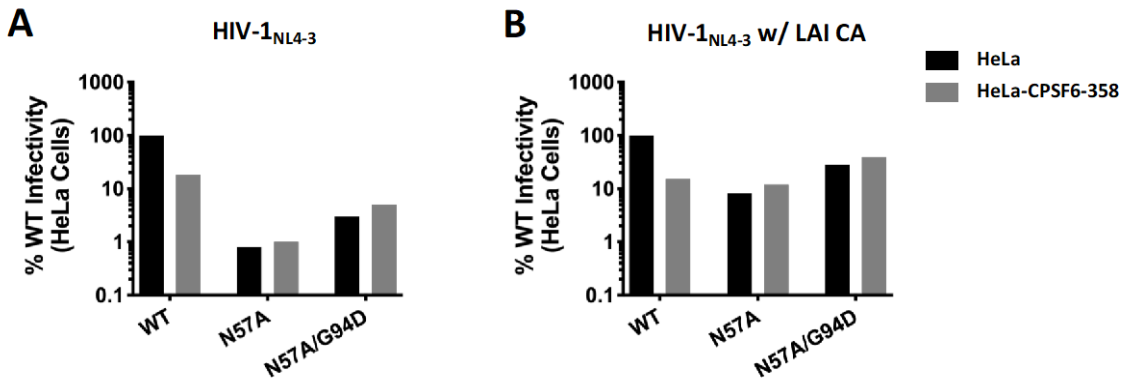

Figure 23. CsA treatment does not alter N57A HIV-1 or N57A/G94D HIV-1 resistance to CPSF6-358 restriction. HeLa cells and HeLa cells stably expressing CPSF6-358-eGFP were treated with 2 μM CsA and infected with equal amounts of WT, N57A, or N57A/G94D HIV-1_{NL4-3} luciferase reporter virus with (A) WT or (B) LAI CA and assayed after 48h for luciferase activity.

previously reported (435). These data suggest that CsA treatment leads to more rapid formation of CPSF6-358 complexes.

4.2.5 CsA treatment does not alter N57A HIV-1 or N57A/G94D HIV-1 resistance to CPSF6-358 restriction

Given the effect of CsA treatment on the formation of CPSF6-358-eGFP puncta, the hypothesis that CypA might shield CPSF6-358 from accessing the capsid, and the dependence of N57A HIV-1 and N57A/G94D HIV-1 infectivity on CypA interaction, we wanted to revisit the question of N57A HIV-1 and N57A/G94D HIV-1 infecting independently of CPSF6 in the context of CsA treatment. To determine if CsA treatment altered N57A HIV-1 or N57A/G94D HIV-1 resistance to CPSF6-358 restriction in either HIV-1_{NL4-3} or HIV-1_{LAI}, HeLa cells and HeLa cells stably

expressing CPSF6-358-eGFP were treated with CsA and infected with WT, N57A, or N57A/G94D HIV-1_{NL4-3} with WT or LAI CA. As previously observed without CsA treatment, WT HIV-1 infectivity was restricted with CsA treatment by CPSF6-358 with both NL4-3 CA (6-fold, **Figure 23A**) and LAI CA (7-fold, **Figure 23B**). Infectivity of neither N57A HIV-1 nor N57A/G94D HIV-1 was restricted by CPSF6-358 in the presence of CsA treatment with NL4-3 CA (**Figure 23A**) or LAI CA (**Figure 23B**). These results show that CsA treatment does not alter N57A HIV-1 or N57A/G94D HIV-1 infecting independently of CPSF6.

4.2.6 N57A HIV-1 infectivity is dependent upon capsid interaction with CypA

It was previously observed that N57A relieves the CsA dependence of T54A in HIV-1 (458), suggesting that N57A might influence the interaction between CA and the host factor CypA. To determine the effect of CypA binding on N57A HIV-1 infectivity, HeLa and GHOST cells were infected with WT and N57A HIV-1_{NL4-3} and WT and N57A HIV-1_{NL4-3} with LAI CA in the presence and absence of CsA treatment. While WT HIV-1_{NL4-3} (**Figure 24A**) and WT HIV-1_{NL4-3} with LAI CA (**Figure 24B**) showed only a minimal reduction in infectivity with CsA, infectivity was significantly reduced for both N57A HIV-1_{NL4-3} (**Figure 24C**) and N57A HIV-1_{NL4-3} with LAI CA (**Figure 24D**) in the presence of CsA. This was particularly noticeable for N57A in the context of HIV-1_{LAI} CA, in which infectivity was only reduced 2- to 5-fold compared to WT virus in the absence of CsA but was reduced 10- to 30-fold compared to WT virus in the presence of CsA.

Given the attenuated infectivity of N57A HIV-1 in nondividing cells (**Chapter 3**), the impact of CsA treatment on WT and N57A HIV-1 infectivity was examined in growth arrested

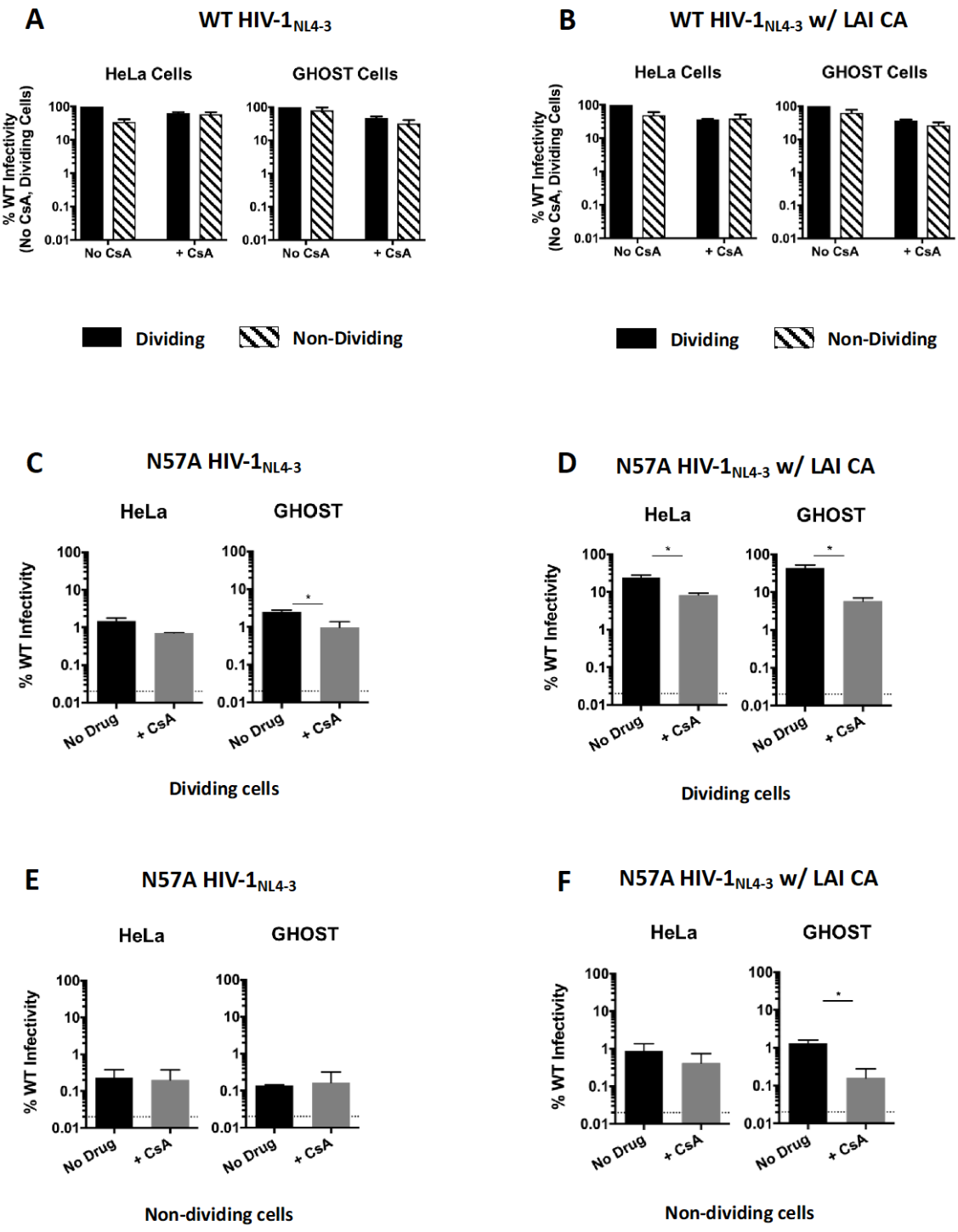

Figure 24. N57A HIV-1 infectivity is dependent upon capsid interaction with CypA. Indicated cell types were infected with equal amounts of WT (A) HIV-1_{NL4-3} or (B) HIV-1_{NL4-3} with LAI CA with or without aphidicolin treatment and in the presence or absence of CsA treatment and assayed after 48h for luciferase activity. Indicated cell types were infected with WT or N57A (C) HIV-1_{NL4-3} or (D) HIV-1_{NL4-3} with LAI CA in the presence or absence of

CsA. Indicated cell types were infected with WT or N57A (E) HIV-1_{NL4-3} or (F) HIV-1_{NL4-3} bearing LAI CA treated with aphidicolin and in the presence or absence of CsA. N57A HIV-1 infectivity is shown relative to the corresponding WT virus infectivity for each treatment. Dotted line represents average luciferase signal of uninfected cells. * $p < 0.05$. Error bars indicate standard error of the mean (SEM) for 3 experiments.

HeLa and GHOST cells. As with dividing cells, WT HIV-1_{NL4-3} (**Figure 24A**) and WT HIV-1_{NL4-3} with LAI CA (**Figure 24B**) showed little change in infectivity of nondividing cells with the addition of CsA. The already low infectivity of N57A HIV-1_{NL4-3} in nondividing cells was not further reduced by CsA treatment in either cell line (**Figure 24E**). In HIV-1_{NL4-3} with LAI CA, N57A infectivity in nondividing cells was reduced with CsA to varying degrees depending on the cell type (**Figure 24F**). In HeLa cells, the reduction in infectivity was only 2-fold. However, in GHOST cells the reduced infectivity of N57A HIV-1_{NL4-3} with LAI CA was 10-fold, which was similar to what was observed in dividing GHOST cells. Thus, N57A HIV-1 infectivity is dependent upon CA binding of CypA, particularly in dividing cells, and more prominently with HIV-1_{LAI} CA than with HIV-1_{NL4-3} CA.

4.2.7 Inhibiting CypA-capsid interaction restricts N57A HIV-1 infectivity at nuclear entry

To examine the mechanism through which CypA promotes N57A HIV-1 infectivity, we measured early and late reverse transcription products and 2-LTR circles in HeLa cells infected with WT and N57A HIV-1_{NL4-3} and WT and N57A HIV-1_{NL4-3} with LAI CA in the presence and absence of CsA treatment. For WT HIV-1_{NL4-3}, early and late reverse transcripts were reduced 1.6-fold and 2.3-fold, respectively, and 2-LTR circles were reduced 1.4-fold with CsA treatment (**Figure 25A**),

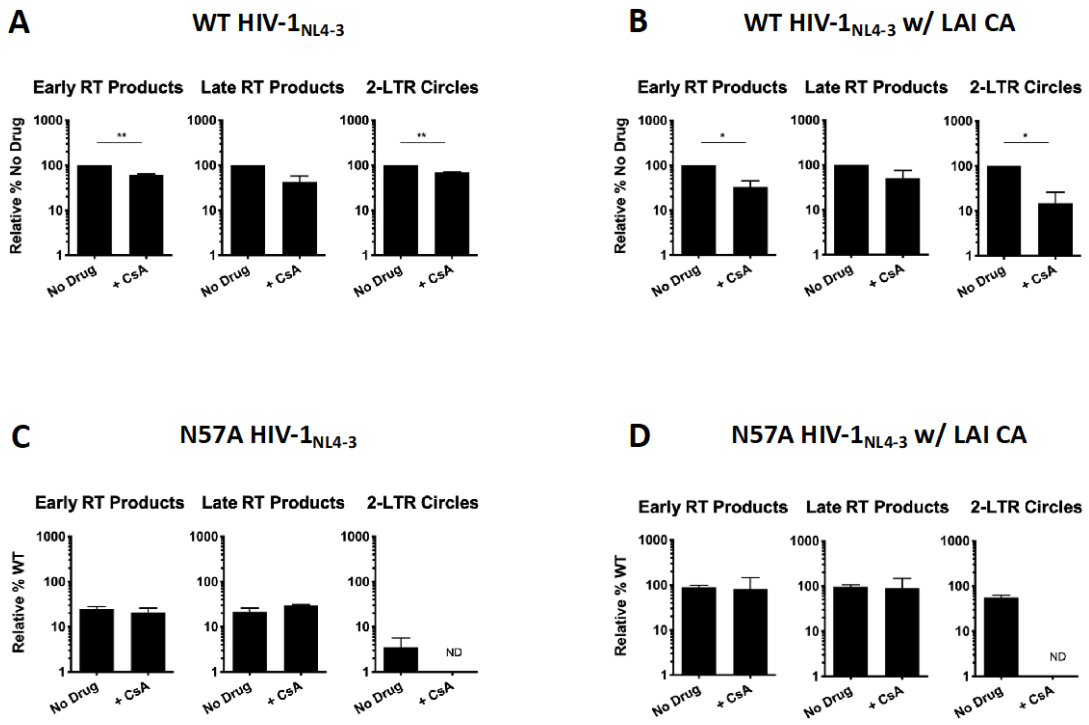

Figure 25. Inhibiting CypA-capsid interaction restricts N57A HIV-1 infectivity at nuclear entry. HeLa cells were infected with equal amounts of (A) WT HIV-1_{NL4-3}, (B) WT HIV-1_{NL4-3} with LAI CA, (C) N57A HIV-1_{NL4-3}, or (D) N57A HIV-1_{NL4-3} with LAI CA in the presence or absence of CsA treatment and reverse transcription products and 2-LTR circles were measured. ND indicates no qPCR product detected. ** $p < 0.01$, * $p < 0.05$. Error bars indicate SEM for 2 experiments.

corresponding to a 1.6-fold reduction in infectivity of WT HIV-1_{NL4-3} with CsA treatment (**Figure 24A**). Similarly, early and late reverse transcripts were reduced 3-fold and 2-fold, respectively, during CsA treatment of WT HIV-1_{NL4-3} with LAI CA infection (**Figure 25B**). However, 2-LTR circles were reduced 7-fold for HIV-1_{NL4-3} with LAI CA (**Figure 25B**), corresponding to a 5-fold reduction in infectivity of WT HIV-1_{NL4-3} with LAI CA upon CsA treatment (**Figure 24B**). These results are consistent with previous observations (459).

CsA treatment did not alter production of early or late reverse transcripts for N57A HIV-1_{NL4-3} (**Figure 25C**) nor for N57A HIV-1_{NL4-3} with LAI CA (**Figure 25D**) compared to WT viruses. However, no 2-LTR circles were detected during CsA treatment for either N57A HIV-1_{NL4-3} (**Figure 25C**) or N57A HIV-1_{NL4-3} with LAI CA (**Figure 25D**). Taken together, these data suggest that inhibiting CypA binding to capsid restricts WT HIV-1 prior to or at reverse transcription. In contrast, N57A HIV-1 infection is inhibited by CsA treatment at the step of nuclear entry.

4.2.8 G94D rescue of N57A HIV-1 infectivity depends on CA binding to CypA

N57A HIV-1 infectivity is partially rescued by the addition of CA mutation G94D in HIV-1_{LAI} but not in HIV-1_{NL4-3} (**Chapter 3**). G94D HIV-1 has been previously shown to infect cells independent of capsid binding to CypA, becoming CsA dependent in some cell lines (438, 450, 507). To determine whether CsA treatment would affect the rescue of N57A HIV-1 infectivity by addition of G94D, HeLa and GHOST cells were infected with WT, N57A, and N57A/G94D HIV-1_{NL4-3} or HIV-1_{NL4-3} with LAI CA in the presence or absence of CsA treatment. As expected, there was no appreciable difference in the infectivity of HIV-1_{NL4-3} viruses during CsA treatment and no rescue of N57A HIV-1_{NL4-3} infectivity by G94D (**Figure 26A**). Whereas G94D partially rescued infectivity of N57A HIV-1_{NL4-3} with LAI CA in both HeLa and GHOST cells, treatment with CsA prevented this rescue (**Figure 26B**). In HeLa cells, there was a non-significant increase in infectivity with the addition of G94D to N57A HIV-1_{NL4-3} with LAI CA in the presence of CsA. In GHOST cells, the infectivity of N57A/G94D HIV-1_{NL4-3} with LAI CA was significantly decreased 15-fold compared to virus with N57A alone in the presence of CsA.

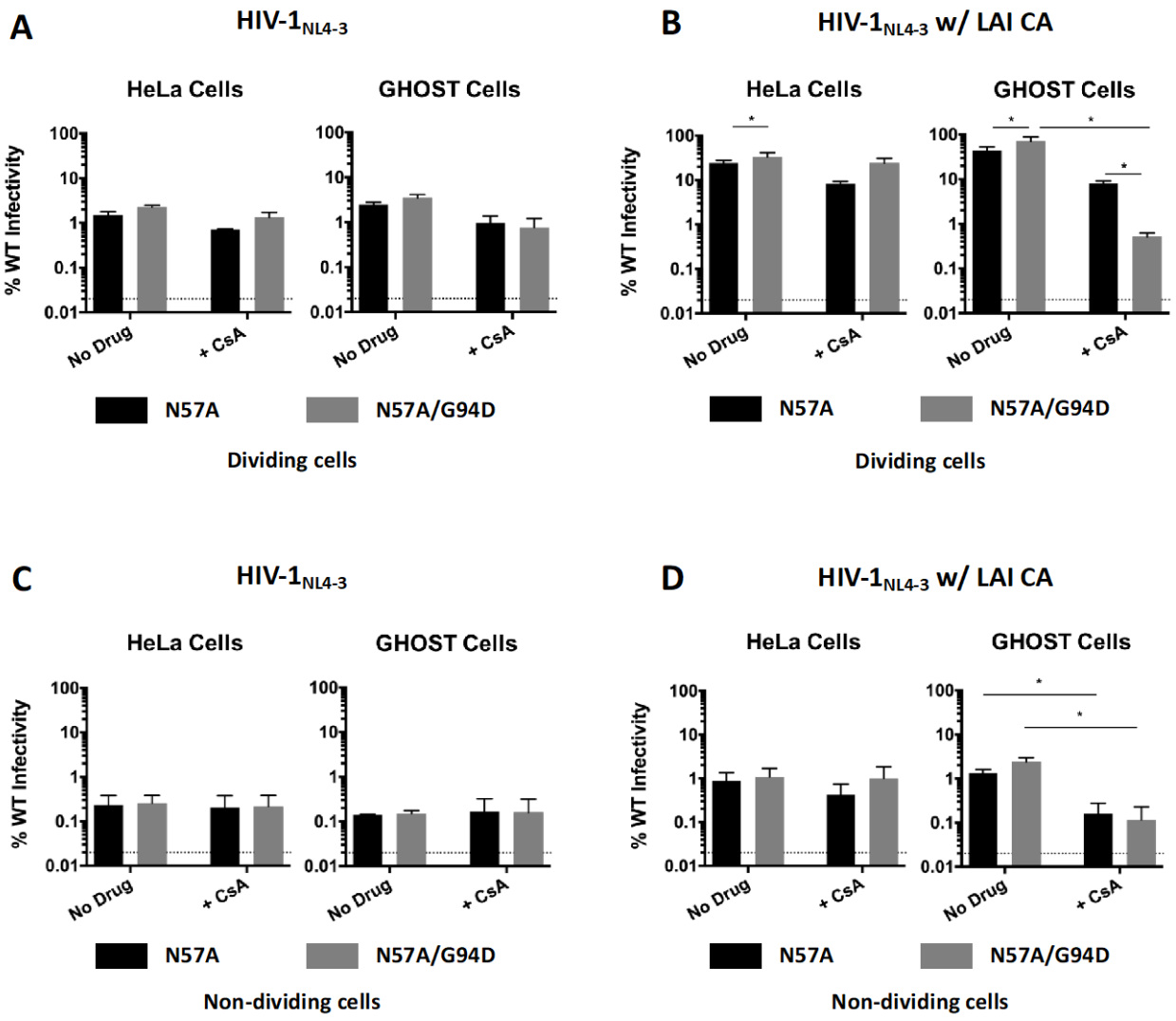

Figure 26. G94D rescue of N57A HIV-1$_{LAI}$ infectivity is dependent upon capsid binding to CypA in a cell-type specific manner. Indicated cell types were infected with equal amounts of WT, N57A, or N57A/G94D HIV-1$_{NL4-3}$ luciferase reporter virus with (A) WT or (B) LAI CA in the presence or absence of CsA treatment and assayed after 48h for luciferase activity. (C and D) Cells treated with aphidicolin were infected with viruses from (A) and (B), respectively. N57A and N57A/G94D HIV-1 infectivity is shown relative to the corresponding WT virus. Dotted line represents average luciferase signal of uninfected cells. * $p < 0.05$. Error bars indicate SEM for 3 experiments.

In growth-arrested cells, CsA treatment did not change the rescue of N57A infectivity by G94D compared to N57A alone in either HIV-1_{NL4-3} or HIV-1_{NL4-3} with LAI CA. Infectivities of N57A and N57A/G94D HIV-1_{NL4-3} were similar with and without CsA treatment in both nondividing HeLa and GHOST cells (**Figure 26C**). In HIV-1_{NL4-3} with LAI CA, no appreciable difference was observed between N57A and N57A/G94D viruses in nondividing HeLa cells with and without CsA treatment (**Figure 26D**). However, N57A/G94D HIV-1_{NL4-3} with LAI CA showed a 10-fold reduction in infectivity in GHOST cells in the presence of CsA compared to N57A HIV-1_{NL4-3} with LAI CA (**Figure 26D**). Altogether, these data demonstrate that the rescue of the N57A infectivity defect by G94D in HIV-1_{NL4-3} with LAI CA is both cell cycle and, in some cell types, CypA dependent. In contrast, N57A HIV-1_{NL4-3} infectivity is not rescued by G94D, with or without CypA interaction, in dividing or nondividing cells.

4.2.9 N57A HIV-1 and N57A/G94D HIV-1 infect independently of Nup153

In addition to CPSF6, N57A HIV-1_{NL4-3} has been shown to infect independently of Nup153 (270, 274), which shares the same CA binding pocket as CPSF6 (417). To determine if N57A HIV-1_{LAI} also infects independently from Nup153 and if the G94D CA mutation alters this independence, we first validated specific, transient knockdown (KD) of Nup153 by siRNA. To do this, we utilized a HeLa cell line stably expressing both CPSF6-eGFP and iRFP670-Nup153. An siRNA directed against GFP was used as a non-specific control siRNA, alongside the siRNA directed against Nup153. The stable expression cell line permitted examination of siRNA KD specificity by flow cytometry. After 72h of transient siRNA expression, 83% of Nup153 KD cells were negative for iRFP670-Nup153 expression compared with 26% of siRNA untransfected cells (**Figure 27A**). 88% of GFP KD cells were negative for CPSF6-eGFP expression compared with 61% of siRNA

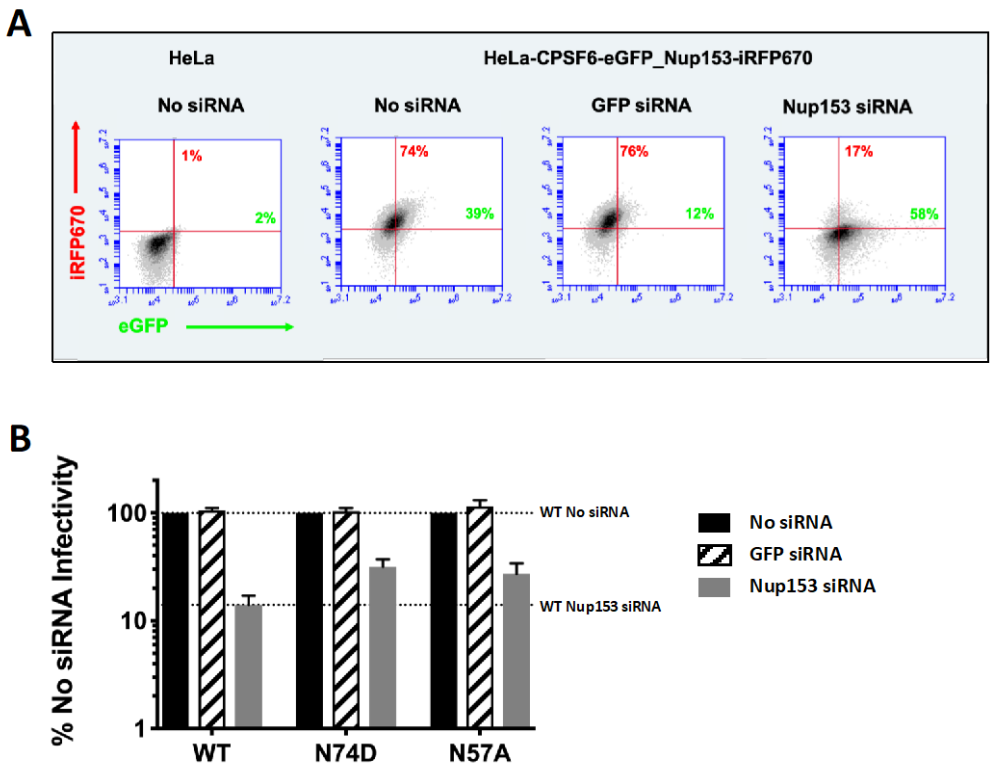

Figure 27. Validation of Nup153 siRNA KD. (A) HeLa cells stably expressing CPSF6-eGFP and iRFP670-Nup153 were transfected with siRNA targeting GFP or Nup153 and examined after 72h for eGFP and iRFP670 expression. (B) HeLa cells transfected with siRNA targeting GFP or Nup153 were challenged after 72h with equal amounts of WT, N74D, or N57A HIV-1_{NL4-3} luciferase reporter virus and assayed after 48h for luciferase activity. Error bars indicate SEM for 2 experiments.

untransfected cells (**Figure 27A**). There was no KD of iRFP670-Nup153 expression with GFP-directed siRNA nor KD of CPSF6-eGFP expression with Nup153-directed siRNA, but rather an increase in expression was observed for both CPSF6-eGFP and iRFP670-Nup153 with untargeted siRNA (**Figure 27A**). This was likely due to siRNA KD alleviating competition between the constructs for cell resources for maximal expression. While specific KD was observed as early as 24h after siRNA transfection, KD levels reached their maximum around 72h post-transfection (data not shown).

To confirm that Nup153 KD caused the expected reduction in virus infectivity and that HeLa cells expressing only endogenous Nup153 had a similar phenotype to the stable expression cell line, siRNA KD of GFP and Nup153 was repeated in HeLa cells and HeLa cells stably expressing CPSF6-eGFP and iRFP670-Nup153. Cells were challenged after 72h with WT, N74D, and N57A HIV-1_{NL4-3}. Stable expression cell line samples were examined by flow cytometry at the time of infection to confirm successful siRNA KD (data not shown). Compared to untransfected control cells, Nup153 KD reduced WT HIV-1 infection 7-8-fold (**Figure 27B**). N74D and N57A HIV-1 infectivity was reduced 3-4-fold (**Figure 27B**), in agreement with previous reports (270, 476). GFP KD did not have an appreciable effect on the infectivity of any of the viruses (**Figure 27B**). Both HeLa cells and HeLa cells stably expressing CPSF6-eGFP and iRFP670-Nup153 showed sufficiently similar phenotypes to serve as paired experimental replicates. Together these results confirm transient siRNA KD of both stably expressed and endogenous Nup153 in HeLa cells.

To determine the effect of Nup153 depletion on N57A HIV-1_{LAI} and N57A/G94D HIV-1, siRNA KD of GFP and Nup153 was repeated in HeLa cells and HeLa cells stably expressing CPSF6-eGFP and iRFP670-Nup153. After 72h, cells were challenged with WT, N57A, or N57A/G94D HIV-1_{NL4-3} with WT or LAI CA. Stable expression cell line samples examined by flow cytometry at the time of infection confirmed successful siRNA KD (data not shown). Compared to untransfected control cells, WT HIV-1 infectivity was reduced 3-fold with Nup153 depletion for both HIV-1_{NL4-3} (**Figure 28A**) and HIV-1_{NL4-3} with LAI CA (**Figure 28B**). N57A HIV-1 and N57A/G94D HIV-1 infectivity was reduced 2-fold or less with Nup153 KD for HIV-1_{NL4-3} (**Figure 28A**) and HIV-1_{NL4-3} with LAI CA (**Figure 28B**). As with validation testing, GFP

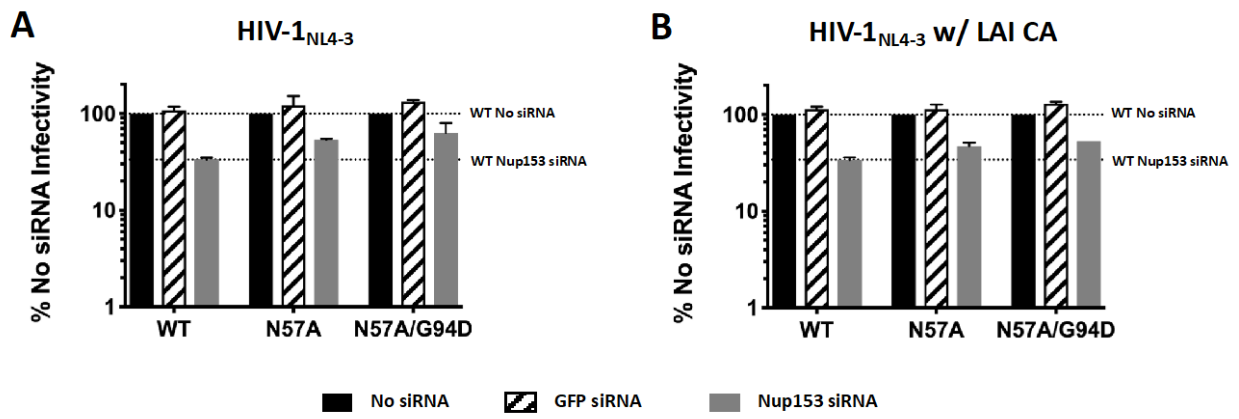

Figure 28. G94D does not alter N57A HIV-1 infectivity independence from Nup153. HeLa cells transfected with siRNA targeting GFP or Nup153 were challenged after 72h with equal amounts of WT, N57A, or N57A/G94D HIV-1_{NL4-3} luciferase reporter virus with (A) WT or (B) LAI CA and assayed after 48h for luciferase activity. Error bars indicate SEM for 2 experiments.

KD did not have an appreciable effect on the infectivity of any of the viruses (**Figure 28A and 28B**), and HeLa cells and HeLa cells stably expressing CPSF6-eGFP and iRFP670-Nup153 were sufficiently similar to be merged as experimental replicates. Combined, these data suggest that N57A HIV-1 infects independently of Nup153 in HIV-1_{NL4-3} and HIV-1_{LAI} and CA mutation G94D does not alter this independence.

4.3 Discussion

Here we explore the effects of disrupting HIV-1 capsid interactions with host proteins CPSF6, CypA, and Nup153 on virus infectivity, within the context of host cell infection by the commonly used lab-adapted strains HIV-1_{NL4-3} and HIV-1_{LAI} containing CA mutations N57A and

N57A/G94D. N57A shares several phenotypic attributes with another CA mutation on the opposite side of the same N-terminal domain binding pocket, the previously characterized N74D (266). Like N57A, N74D HIV-1 infects cells independently of CPSF6, TNPO3, and Nup153 (266, 273, 435). However, unlike N57A, there is no cell cycle dependence caused by N74D. N74D HIV-1 infectivity is sensitive to CsA treatment (435), indicating that CA interaction with CypA is important for N74D HIV-1 infectivity. Thus, we examined whether N57A also is dependent on CA binding to CypA. By inhibiting interaction of CA and CypA with CsA treatment, we demonstrated that N57A HIV-1 infectivity is dependent upon CypA in both dividing (HIV-1_{NL4-3} and HIV-1_{NL4-3} with LAI CA) and nondividing cells (HIV-1_{NL4-3} with LAI CA). This observation is in line with the CsA hypersensitivity of the N57S CA mutation (269), which is similar to N57A in cell cycle dependence for infection (394). The CypA dependence of two CPSF6-independent CA mutations would seem to suggest an inter-relationship between CypA and CPSF6 in terms of HIV-1 infectivity, which also has been suggested in other studies (476, 521). We further showed that CsA treatment does not affect reverse transcription in N57A HIV-1, but rather that 2-LTR circle production is reduced, suggesting that the loss of N57A capsid interaction affects nuclear entry. These results support a role for CypA influencing HIV-1 nuclear entry that has been previously proposed as a result of different studies (270, 459).

The emergence of G94D as a compensatory mutation in N57A HIV-1_{LAI} further demonstrates an interplay of CypA and other cellular factors on HIV-1 infection. Similar to N57A HIV-1 infectivity, G94D rescue is dependent upon CA interaction with CypA. Inhibiting this interaction via CsA treatment reduced (HeLa cells) or abrogated (GHOST cells) the G94D infectivity rescue of N57A HIV-1_{LAI}. In GHOST cells, CsA treatment significantly exacerbated

overall infectivity of N57A/G94D HIV-1_{LAI}, reducing it by more than 100-fold. These results are consistent with previous reports on cell type differences in HIV-1 infectivity upon CsA treatment with CA mutation G94D or the related CA mutation A92E (438, 450, 451, 456, 459, 507). The significant reduction in infectivity of N57A/G94D HIV-1_{LAI} in CsA-treated GHOST cells is similar to the 100-fold reduction in infectivity of CsA-dependent T54A HIV-1 with the addition of the N57A mutation (458). This suggests that the CypA dependence of N57A HIV-1 infectivity is not alleviated by the presence of a CypA-independent CA mutation (G94D) but is also dominant over the CypA-independent CA mutation, rendering the virus hypersensitive to CsA treatment.

Using the previously characterized C-terminal truncated form of CPSF6, CPSF6-358, as a tool to examine virus capsid interaction with CPSF6, we extended *in vitro* studies (521) and provided evidence for the formation of CPSF6-358 higher order complexes within WT HIV-1 infected host cells that restrict virus infectivity by promoting accelerated capsid permeabilization. The accelerated kinetics of capsid permeabilization observed with CPSF6-358 are reminiscent of the kinetics observed with the expression of HIV-1 restriction factor rhesus tripartite motif containing protein 5α (rhTRIM5α) (500), which has also been shown to bind HIV-1 capsids (535) and to disrupt CA tubular assemblies *in vitro* (536-538), restricting HIV-1 infectivity prior to reverse transcription (539). CPSF6-358, however, does not impair the kinetics or completion of reverse transcription in cells (266), suggesting that it might restrict HIV-1 infectivity in a different manner. While the EU-based capsid permeabilization assay signal indicates loss of capsid integrity by permitting the entry of a small dye to stain viral RNA (500), it does not measure the removal of CA from the capsid or exposure of the viral genome to the cytoplasm, and as such cannot differentiate between a mostly intact capsid with small openings and a disrupted capsid that has

lost structural integrity. The successful completion of reverse transcription in the presence of CPSF6-358, however, suggests the capsid, while permeabilized, could maintain some degree of protection for the genome.

The lack of N74D HIV-1 infectivity restriction by CPSF6-358 agrees with previous reports (266) and corresponds with an inability of CPSF6-358 to bind to and disrupt N74D HIV-1 CA tubular assemblies *in vitro* (521) and a failure of N74D HIV-1 to elicit the formation of CPSF6-358-eGFP puncta, as observed with WT HIV-1 infection. Unsurprisingly, N74D HIV-1 capsid permeabilization kinetics were not altered by CPSF6-358, given the lack of interaction with N74D CA. The kinetics of N74D HIV-1 capsid permeabilization did differ from WT HIV-1, however, suggesting that a lack of interaction with CPSF6 might influence capsid permeabilization.

While N57A HIV-1_{NL4-3} has previously been shown to infect independently of CPSF6 and Nup153 (270, 274, 281, 283), we are unaware of any study that has specifically examined interaction of N57A HIV-1_{LAI} with these host factors or determined the dependence of N57A/G94D HIV-1 infectivity on CPSF6 or Nup153 interaction. We did not observe virus strain-specific differences in N57A HIV-1 infectivity independence from CPSF6 and Nup153 or alteration of this independence by the addition of the G94D CA mutation The restriction of N57A/G94D HIV-1_{LAI} infectivity by CPSF6-358 would suggest that the addition of G94D to N57A HIV-1_{LAI} restores interaction of N57A HIV-1 with CPSF6 in a virus strain-specific manner and would offer a potential mechanism through which G94D partially rescues N57A HIV-1_{LAI} infectivity. The use of HeLa cells for this study, prompted by the previous establishment of a HeLa cell line stably expressing CPSF6-358-eGFP for imaging studies, was not ideal, given our previous

findings of a considerably more robust rescue of N57A HIV-1_{LAI} infectivity by G94D in GHOST cells (**Chapter 3**). Repeating the CPSF6-358 restriction experiments in GHOST cells would facilitate a clear determination of CPSF6 independence for N57A/G94D HIV-1_{LAI} infectivity.

Similarly, additional experiments should be performed with Nup153 to ensure the preliminary results are indeed reflective of N57A HIV-1 and N57A/G94D HIV-1 infectivity independence of Nup153, or the lack thereof. While the use of a CPSF6-eGFP/iRFP670-Nup153 stable expression HeLa cell line facilitated validation of Nup153 depletion, KD of Nup153 should be confirmed by Western blot. The attenuated reduction of virus infectivity observed in **Figure 28** compared to **Figure 27** is likely due to overexpression of Nup153 in the cell line used. As with CPSF6, examination of Nup153 independence for N57A/G94D HIV-1_{LAI} infectivity would benefit from the use of regular HeLa cells as well as GHOST cells. Given that Nup153 is critical for HIV-1 nuclear entry in nondividing cells (275), examining the effects of Nup153 depletion on N57A and N57A/G94D HIV-1 infection of nondividing cells might amplify the phenotypes observed in this study. Finally, previous reports have demonstrated that CsA treatment partially rescues WT HIV-1_{NL4-3} infectivity in Nup153-depleted HeLa cells (269, 270). It could be informative to examine how CsA treatment alters the effects of Nup153 KD on N57A and N57A/G94D HIV-1 infection in both HeLa and GHOST cells.

4.4 Materials and Methods

Cell Lines

HEK 293T cells, GHOST cells, and HeLa cells were maintained at 37° C with 5% CO_2 in Dulbecco's Modified Eagle Medium (DMEM, Gibco) supplemented with 10% Fetal Bovine Serum (FBS, Atlanta Biologicals), 100 U/mL Penicillin, 100 µg/mL Streptomycin, and 2 mM L-Glutamine (Thermo Fisher). GHOST cells were additionally supplemented with 500 µg/mL Geneticin G418 (Gibco), 500 µg/mL Puromycin (Invitrogen), and 100 µg/mL Hygromycin B (Invitrogen). HeLa cells stably expressing CPSF6-358-eGFP were created by transduction with a lentiviral vector encoding CPSF6-358 that had been tagged on the C-terminus with eGFP. HeLa cells stably expressing CPSF6-eGFP and iRFP670-Nup153 were created by transduction with lentiviral vectors either encoding CPSF6 that had been tagged on the C-terminus with eGFP or encoding Nup153 that had been tagged on the N-terminus with iRFP670.

Viruses

Proviral plasmid pNLdE-luc (266) was used to produce HIV-1_{NL4-3}. CA mutations were generated via the Q5 (New England BioLabs) or QuikChange (Agilent) site-directed PCR mutagenesis kits following manufacturers' instructions and verified by Sanger sequencing.

HEK 293T cells were plated overnight and transfected with Lipofectamine 2000 (Invitrogen) using the following plasmids: pNLdE-luc, pL-VSV-G, and, for imaging studies, pcDNA5-TO-Vpr-mRuby3-IN (521). Supernatants were harvested 48h later, filtered or centrifuged to remove cells, concentrated via Lenti-X Concentrator (Clontech), and stored in aliquots at -80° C. For virus stocks used in the capsid permeabilization assay, 293T producer cells

were supplemented with 1 mM 5-ethynyl uridine (EU, Invitrogen) for 12-16h, which was replaced with regular media for the remainder of the 48h incubation. Viruses were titered by infection of GHOST cells as previously described (531) and quantified for p24 by HIV-1 p24 ELISA kit (XpressBio).

Infectivity Assays

HeLa cells and GHOST cells were plated overnight in 24-well plates, challenged with equal p24 amounts of virus for 2h, washed with phosphate buffered saline (PBS), and given fresh media. Virus infectivity was determined by luciferase production (Promega) after 48h using a 1450 MicroBeta TriLux microplate luminescence counter (PerkinElmer) or a Synergy2 Multi-Detection microplate reader (BioTek). For assays including treatment with CsA and/or aphidicolin, cells were treated with CsA (2 μM) and/or aphidicolin (2 μg/mL) at time of plating and remained in drug-containing media throughout the assay. For assays including treatment with PF74, cells were treated with 10 μM PF74 2h prior to challenge and remained in drug-containing media throughout the assay.

Measurement of Reverse Transcripts and 2-LTR Circles

HeLa cells were plated in 6-well plates and infected with 50 ng p24 of virus treated with DNase I (Roche) for 30m at 37° C. After 24h, cells were washed with PBS, trypsinized, and pelleted. Control infections were performed in the presence of 150 nM of efavirenz or 25 nM of rilpivirine. For assays including treatment with CsA, cells were treated with CsA (2 μM) at time of plating and remained in drug-containing media throughout the assay. DNA was extracted using the Blood

Mini Kit (Qiagen), Early (RU5) and late (*gag*) HIV-1 reverse transcripts and 2-LTR circles were measured by quantitative PCR as previously described (533).

siRNA KD of Protein Expression

Duplexed siRNA oligonucleotides were synthesized (IDT) with target sequences directed against Nup153 or GFP. The Nup153 target sequence (NUP153#2) was previously published (273). The GFP target sequence (5'-GCCACAACGTCTATATCAT-3') was provided by Dharmacon. HeLa cells were seeded overnight in 6-well or 24-well plates, transfected with siRNA using Lipofectamine 2000 following manufacturer's directions, and incubated for 24-72h.

Flow Cytometry

Adherent cells were washed with PBS, dissociated with Trypsin-ethylenediaminetetraacetic acid (-EDTA) (Gibco), quenched with 2% FBS in PBS, and fixed with fresh 2% paraformaldehyde (PFA) for 15m. Cells were examined on an LSR-II (BD Biosciences) or Accuri C6 (BD Biosciences) flow cytometer. Cells were gated by forward and side scatter (FSC/SSC) to isolate single cells, which were analyzed for expression of fluorescent constructs using FACSDiva (BD Biosciences) or Accuri C6 Plus (BD Biosciences) software.

Synchronized Infection and Fixation of Cells

HeLa cells stably expressing CPSF6-358-eGFP (deposited in Addgene; no. 110693) were seeded in MatTek dishes overnight in FluoroBrite medium (Thermo Fisher Scientific) containing 10% FBS and penicillin, streptomycin, and glutamine at 37°C and 5% CO2. Prior to imaging, the cells were incubated with fresh medium with or without 2 μM CsA (Sigma-Aldrich) or 10 μM PF-74

(Sigma) for 1 h. Afterward, the cells were chilled at 4°C for 10 min. Virus was added to the microwell above the coverslip in the center of the MatTek dish and incubated at 37°C for 10 min. Before imaging, the cells were washed three times with medium to remove unbound virus. For fixation, the cells were washed with phosphate-buffered saline (PBS) and fixed with fresh 2% PFA for 15 min. The cells were washed with PBS and stained with Hoechst 33342 (Sigma) for 5 min. After washing off the Hoechst stain with PBS, Gelvatol mounting medium (Sigma-Aldrich) was added to the dish, and a coverslip was added on top of the cells.

Capsid Permeabilization Assay

HeLa cells and HeLa cells stably expressing CPSF6-358-eGFP were synchronously infected with EU-labeled HIV-1 (20 ng of p24, as determined by ELISA). The cells were fixed 10 to 50 min post-infection, permeabilized, stained for viral RNA (EU-AF647 Click-iT; Invitrogen) and cell nuclei (Hoechst 33342), and mounted with coverslips.

Confocal and Live-Cell Imaging

Fixed-cell images were collected with a Nikon A1 scanning confocal microscope. Z-stack images were collected at 0.5-μm steps up to 10 μm in 3 colors (408 nm, 488 nm, and 561 nm). For live-cell experiments, MatTek dishes containing cells were placed on a STX heat stage (Tokai Hit, Inc.) to maintain 37°C and 5% CO2. A Nikon Ti live-cell microscope was used to collect frustrated TIRF images using a Prime 95B scientific complementary metal-oxide-semiconductor (sCMOS) camera (Photometrics, Inc.) with an LBX-4C illumination module (Oxxius, Inc.). Images were collected at up to 3 frames per second with two colors (488 nm and 561 nm).

Quantification of Puncta and Virus Particles

Nikon Elements 5.0 was used to quantify the CPSF6-358 puncta during HIV-1 infection. Ten or more z-stacks (0.5-μm spacing) of confocal images were collected for each time point. In brief, a three-dimensional (3D) nucleus mask was made based on Hoechst staining. Both CPSF6-358 puncta and HIV-1 particles were detected using the 3D spot detection function. The number of CPSF6-358 puncta was determined by subtraction of the initial CPSF6-358 puncta from the signals within the nucleus mask. RNA puncta were enumerated with Imaris software. Grubbs' extreme Studentized deviate test was used to identify and exclude statistical outliers.

Statistics

Results were analyzed for statistical significance by two-sided student t test with Prism software (GraphPad). A p-value of less than or equal to 0.05 was used to indicate statistical significance.

4.5 Acknowledgements

We would like to thank Callen Wallace for technical assistance and Dr. Alan Engelman for the kind gift of a plasmid encoding Nup153. This work was supported by the National Institutes of Health P50 grant GM082251 (SCW, MY, ZA, PZ), the National Institutes of Health R01 grant AI100720 (MY), the National Institutes of Health T32 training grant AI065380 (DKF), and the United Kingdom (UK) Wellcome Trust Investigator Award 206422/Z/17/Z (PZ).

5.0 Develop Novel Methods to Visualize HIV-1 Capsid Permeabilization in Infected Host Cells in Real Time

This chapter is comprised of unpublished data, including data for two planned manuscripts. The overall author attribution is as follows:

Douglas K. Fischer[1], Christopher Kline[1], Austin Souryavong[1], Zhou Zhong[1], Simon C. Watkins[2], Zandrea Ambrose[1]

[1]Department of Microbiology and Molecular Genetics, University of Pittsburgh School of Medicine, Pittsburgh, Pennsylvania, USA; [3]Department of Cell Biology and Physiology, University of Pittsburgh School of Medicine, Pittsburgh, Pennsylvania, USA.

5.1 Introduction

The HIV-1 RNA genome is packaged inside a conical capsid that is released into the host cell cytoplasm after attachment and fusion of the enveloped virus particle (389). Once within the host cell, the genome must undergo reverse transcription into double stranded DNA, which is trafficked to the nucleus as part of the preintegration complex (PIC) for integration into the host genome (117). Successful completion of reverse transcription and nuclear entry of the PIC requires the timely and ordered dissociation of the capsid through the process of uncoating (285).

While a critical process in the retroviral life cycle, there are many unanswered questions about capsid uncoating. There is uncertainty about when and where within the host cell uncoating occurs, what viral and/or cellular events trigger uncoating, what viral and/or cellular factors are involved in promoting or inhibiting uncoating, and what host cell type or virus strain dependencies might influence the process (192, 286). Answering these questions has proven challenging owing to the dynamic nature of the uncoating process and to the inherent difficulty in directly examining capsid constituents within infected host cells (285, 503).

The earliest capsid uncoating assays involved isolation and purification of cores from infected host cells followed by *in vitro* biochemical analysis of core contents (494-497). Capsid fragility led to dissociation under these extraction conditions, such that little or no intact capsid was recovered, suggesting that capsid uncoating occurred shortly after release into the host cell cytoplasm (285, 286). Subsequent assays (discussed below), which handle capsid more gently, have largely shown this model to be unlikely, and multiple models for capsid uncoating have since been proposed (192). The two most prominent models suggest either a gradual, perhaps biphasic, removal of CA as the capsid transits the cytoplasm (492, 500, 501) or a retention of the vast majority of CA until the capsid reaches the nuclear pore complex (230, 272, 287). These models are not necessarily mutually exclusive and could describe different populations of capsids undergoing uncoating or might be observing different aspects of the same process.

Currently employed capsid uncoating assays can be divided into three categories based upon their underlying principle (**Table 2**). Biochemical and infectivity assays examine the composition or infectivity of virus particles within or extracted from infected host cells. While

Table 2. Current assays for HIV-1 capsid uncoating

Category	Assay (Lab) [Ref]	Principle	Pros	Cons
Biochemical	Fate of the capsid assay (Sodroski/Diaz-Griffero) [Stremlau, 2006] (536)	Western blot of pelletable vs soluble CA in cells	Theoretically not technically challenging and no special equipment needed Can use any cells (just need a lot of them)	Not amenable for studying kinetics Does not differentiate between cores or aggregated CA protein Population measurement, does not allow visualization of individual particles Several labs have been unable to reproduce results
Infectivity	CsA washout assay (Hope) [Hulme, 2011] (492)	Infect cells that express TRIMCyp in the presence of CsA, then wash out CsA at different time points and measure infectivity	Theoretically not technically challenging and no special equipment needed	Can only be performed in cells expressing TRIMCyp Population measurement, does not allow visualization of individual particles May not accurately reflect uncoating of CsA dependent CA mutants
Fixed Cell Imaging	CA staining assay (Hope/Campbell) [Lukic, 2014] (498)	Infect cells, fix, stain for CA protein	Can use any cells Is actually measuring CA/capsid	Staining may not appear to be very sensitive and is variable depending on antibody lot Requires cell fixation Shows loss of signal Moderately technically challenging, as it requires confocal microscopy
	EU staining assay (Ambrose) [Xu, 2013] (500)	Infect cells with virus made in the presence of 5-ethynyl uridine (EU) + second marker, fix, stain for RNA	Can use any cells Shows gain of signal	Moderately technically challenging, as it requires confocal microscopy Requires cell fixation

Table 2 continued

Category	Assay (Lab) [Ref]	Principle	Pros	Cons
Real Time Imaging	Gag-iGFP live cell imaging assay (Hope) [Mamede, 2017] (501)	Infect cells with Gag-internal GFP (Gag-iGFP) + second marker and image loss of signal	Can use any cells Uses live cell imaging, so can image kinetics of individual particles	Technically challenging, as it requires live cell confocal microscopy and has two-phase loss of signal Shows loss of signal
	CypA-DsRed live-cell imaging assay (Melikian) [Francis, 2016] (525)	Infect cells with virus made in the presence of CypA-DsRed + second marker and image loss of signal	Can use any cells Uses live cell imaging, so can image kinetics of individual particles	Technically challenging, as it requires live cell confocal microscopy and has two-phase loss of signal Shows loss of signal Unclear whether CypA-DsRed aggregation impacts capsid uncoating Will not reflect uncoating of CypA independent CA mutants
	In vitro single-molecular fluorescence imaging assay of Gag-iGFP (Böcking) [Marquez, 2018] (540)	Virus with Gag-iGFP is bound to a coverslip and loss of signal is imaged	Can image kinetics of many individual particles Can rather easily evaluate contribution of individual proteins on uncoating (if able to produce them)	Not a cell-based assay Technically challenging, as it requires single particle imaging Shows loss of signal

these assays offer straightforward measurement of virus properties, their greatest drawback is the combination of broad populations of virus particles in determining an average metric. Virus particles in infected cells may or may not lead to infection and can be categorized into distinct populations (195, 286). As these assays are incapable of examining individual particles this distinction is lost, and the average measurements calculated may not be reflective of infectious virus particle characteristics.

Fixed cell imaging assays offer an improvement over biochemical and infectivity assays by permitting examination of individual virus particles within infected host cells. By fixing and imaging infected cells, these assays provide location context and allow for visualization of different viral and host proteins using antibodies or protein tags. The CA protein, which is genetically fragile (393, 394), cannot be directly tagged without compromising capsid stability, requiring antibodies to be used for its visualization. However, fixation results in interactions and uncoating status being examined only at a few discrete points in time and does not permit following individual virus particles across time as the uncoating process evolves, which likely varies among virus particles. Virus-host interactions are frequently brief and rapid (481, 521, 541), and as such fixed cell imaging is likely to miss important events.

Real time (live cell and *in vitro*) imaging assays, while technically challenging, extend the benefits of fixed cell imaging assays by allowing rapid image acquisition and the ability to track individual virus particles over time. While offering the potential to unlock a wealth of information about the uncoating process, the current real time imaging assays available all suffer from dependence upon a loss of fluorescent signal to indicate capsid uncoating. A reliance on loss of

signal as proof of an event occurring has an inherent false positive component that is particularly appreciable with fluorescence, which can readily be caused by photobleaching (542) or quenching (543, 544). To more accurately detect and track virus capsids that have started the uncoating process, a definitive gain of signal is more desirable.

In addition to uncertainty surrounding the proper model for capsid uncoating, there is considerable debate as to what it actually means for the capsid to uncoat. While the nature and location of CA shed from the capsid is unknown, one property of uncoating is intrinsic to the loss of CA from the capsid in any form. An intact capsid, while selectively permeable to ions and small molecules such as dNTPs, is a closed container that is impermeable to the passage of all but the smallest molecules (414, 491, 545). A breach of the capsid barrier through initiation of uncoating will necessarily render the capsid permeable, and detection of this permeabilization can serve as an indicator of the start of the uncoating process.

To decouple from a specific form of CA removal from the capsid and to avoid the need to directly measure the loss of CA, multiple uncoating assays specifically measure capsid permeabilization (500, 501, 540). Among these assays, the EU-based capsid permeabilization assay (500) alone provides a gain of signal upon capsid permeabilization. While the EU assay requires fixed cells, the concepts underlying the assay are amenable to live cell imaging with some modifications. Here, we describe the design of a live cell capable capsid permeabilization assay, the development of reagents, and initial validation testing. This assay, inspired by the fixed cell EU assay, provides for real time visualization of virus particles undergoing capsid

permeabilization in infected host cells, potentially in conjunction with labeled virus and host proteins, with a gain of signal to definitively indicate capsid permeabilization.

5.2 Results

5.2.1 Conceptual adaptation of the EU-based capsid permeabilization assay for visualizing capsid permeabilization in infected host cells in real time

The EU capsid permeabilization assay, as used in **Chapter 3** in an updated form (**Figure 29A**), is based upon a dual signal system, consisting of a persistent signal that labels all virus particles and a permeabilization signal that indicates those capsids that have become permeabilized at a particular time point. The persistent signal is provided by fluorescently tagged IN (521), which is packaged *in trans* at the time of virus production. The permeabilization signal is provided by a two-part label based on click chemistry (546). 5-ethynyl uridine (EU), a uridine analog, is incorporated into the viral RNA genome (as well has host cell RNA) during virus production. A capsid impermeable fluorescent azide dye specifically binds to the ethynyl moiety of EU but is only able to access the EU-containing RNA genome once the capsid has become permeabilized (500).

The EU click system suffers from several shortcomings that prevent its use with live cell imaging. The click reaction requires a chemically reductive environment and copper catalyst that are not compatible with living cells. In addition, the azide dye is not cell permeable and has an intrinsic fluorescence that produces background signal, which limits the sensitivity of the assay.

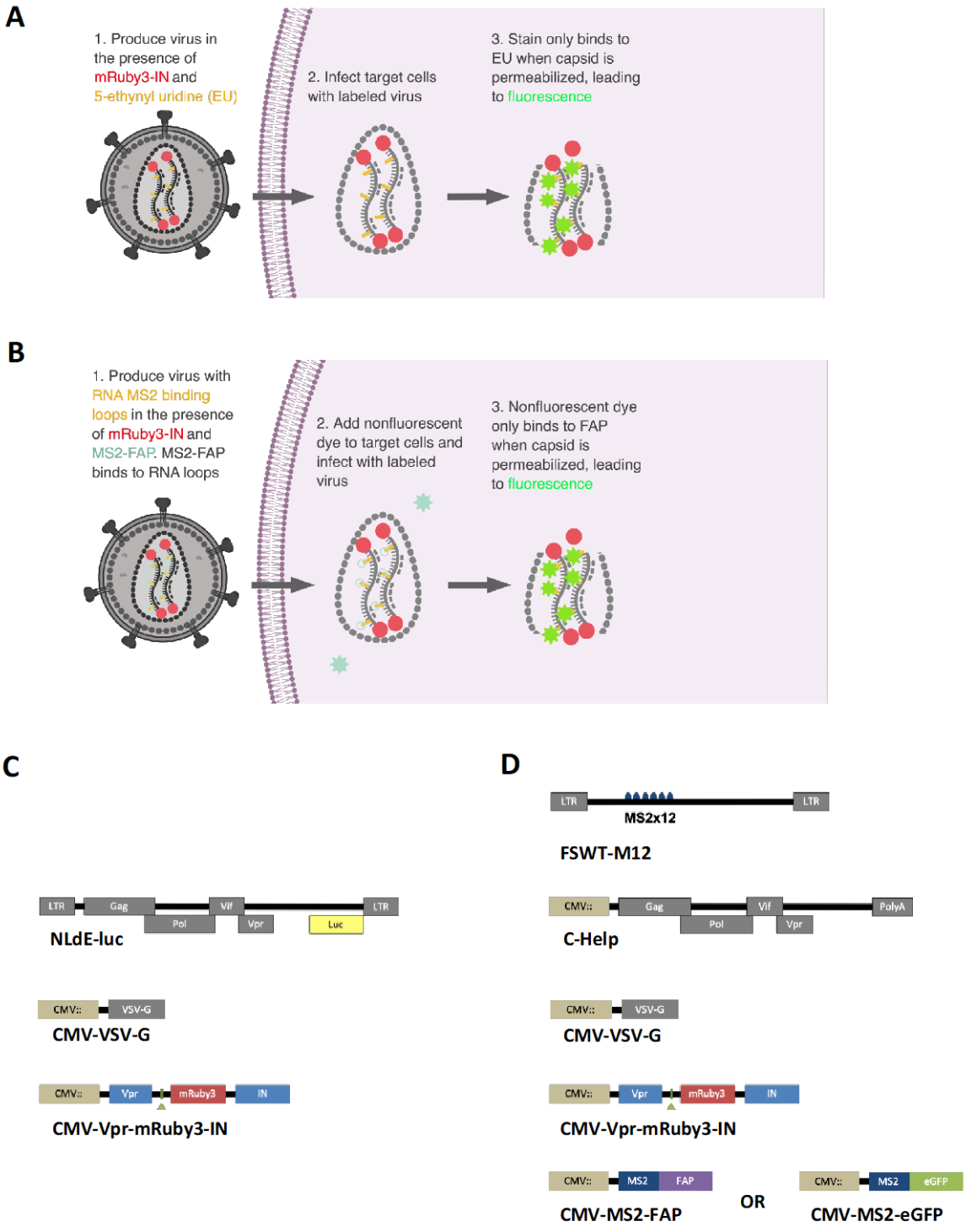

Figure 29. Concept of a new HIV-1 capsid permeabilization assay. Model for (A) the existing, modified EU-based capsid permeabilization assay and (B) an MS2-FAP-based capsid permeabilization assay. Schematic design of plasmids used to make virus for the (C) EU assay and (D) the MS2-FAP assay. MS2-FAP in (D) can be replaced with MS2-eGFP for system testing purposes.

The basic principles of the EU assay and labeling scheme, however, are sound and can be modified to produce a new live cell assay.

The EU-dye combination is conceptually a two-component sensor, with one component located on either side of an intact capsid barrier. Only by permeabilization of that barrier can the components be brought together to generate a signal. A similar two-component sensor can be designed for use within living cells. The sensor component within the capsid should be associated with or incorporated into the viral genome. The sensor component external to the capsid must be large enough and/or of appropriate charge to not pass through the hexamer pores of the intact capsid (414) (i.e., be impermeable to an intact capsid) but small enough to enter the capsid once permeabilization has started. This soluble component must also be cell permeable and non-toxic over the time of imaging.

The association of a fluorescent signal with RNA in living cells was pioneered by Bertrand et al. with the development of the MS2-GFP labeling system (547). The bacteriophage MS2 (548, 549) coat protein (550) binds to the phage RNA genome on sequence-specific hairpin loops (551-555). Introduction of these MS2 binding loops to an RNA target and expression of the MS2 coat protein fused to a fluorescent protein such as GFP (MS2-GFP) results in fluorescent tagging of the RNA target in living cells (547, 556). The MS2-GFP system has been used to examine HIV-1 transcription kinetics in infected host cells (313), to study HIV-1 RNA packaging into virions (329), and to label nascent HIV-1 virus particles (500). For the purposes of a capsid permeabilization signal, however, a fluorescent protein would be inappropriate, owing to a constant fluorescent signal that is not modulated by the capsid permeabilization state. Thus, while

the MS2 labeling system can provide targeting to sequence-specific RNA, an alternative to GFP or other fluorescent protein must be used for fluorescence.

Fluorogen activating proteins (FAPs) bind to and generate fluorescence from otherwise dark molecules (fluorogens) (557). Szent-Gyorgyi et al. developed a set of human single-chain antibody reporters that reversibly bind to fluorogen dyes with nanomolar affinity and increase their fluorescence thousands-fold to within the range of fluorescent proteins (557). The FAP-dye combination has been shown to work efficiently in living cells with flow cytometry (558) and live cell microscopy (559) with fluorogen dyes of different wavelengths and with different chemical properties (560). With an appropriately chosen fluorogen dye that is not permeable to an intact HIV-1 capsid and a FAP that is packaged inside the capsid, the FAP system could be used to monitor the permeabilization state of the capsid.

Combining the RNA targeting of the MS2 system and the two-component sensor properties of the FAP system may provide a capsid permeabilization signal that is compatible with living cells. The MS2-FAP capsid permeabilization assay (**Figure 29B**) would consist of a viral RNA genome that encodes a cassette of MS2 binding loops and, like the modified EU assay, package fluorescently labeled IN *in trans* as a persistent virus particle signal. A fusion of the MS2 coat protein and a FAP (MS2-FAP) are expressed in virus producer cells and incorporated into virus particles by binding to the MS2 loops in the viral genome. Target host cells are treated with fluorogen dye and infected with MS2-FAP virus. The dye is excluded from the capsid and remains dark until capsid permeabilization begins. Upon permeabilization, the dye gains access to the capsid interior, binds to the FAP, and produces a fluorescent signal.

5.2.2 Validation and optimization of the FSWT/MS2 system for production of infectious, fluorescently labeled virus particles

The production of labeled virus requires the transfection of multiple plasmids into virus producer cells. For the modified EU assay, a total of three plasmids are transfected (**Figure 29C**) that encode: a replication incompetent single cycle reporter virus (pNLdE-luc), a VSV-G pseudotyped envelope, and Vpr-mRuby3-IN for persistent labeling. Using existing reagents in our laboratory, the MS2-FAP assay increases the number of plasmids to five (**Figure 29D**) encoding: an HIV-1-based lentiviral vector encoding a cassette of MS2 binding loops (e.g. FSWT-12 that encodes 12 MS2 binding loops), HIV-1 packaging proteins (pC-Help), a VSV-G envelope, Vpr-mRuby3-IN, and MS2-FAP. The complex nature of this system suggested that validation testing of the underlying components was warranted to determine if double labeling of infectious virus particles could be achieved. To that end, the MS2-eGFP fusion protein was used in place of MS2-FAP.

To verify that the FSWT/MS2 system can produce virus particles, HEK 293T cells were transfected with the NLdE-luc plasmid set from the EU assay (without EU) or with the FSWT-12 plasmid set for the MS2-FAP assay (with MS2-eGFP in place of MS2-FAP) to produce viruses. TIRF microscopy revealed that FSWT-12 produced fluorescent particles similar to those made with NLdE-luc (**Figure 30A**). FSWT-12 virus was infectious, although it had 1 log lower specific infectivity (infectious units [IU] per ng p24) compared to NLdE-luc virus, likely due to increased numbers of plasmids used for transfection (**Figure 30B**). To examine the effect of different numbers of MS2 binding sites on fluorescent labeling and infectivity, FSWT lentiviral vector plasmids encoding 6, 12, or 24 binding sites (FSWT-6, FSWT-12, and FSWT-24, respectively) were used to produce virus in the presence of MS2-eGFP. TIRF imaging of these viruses showed

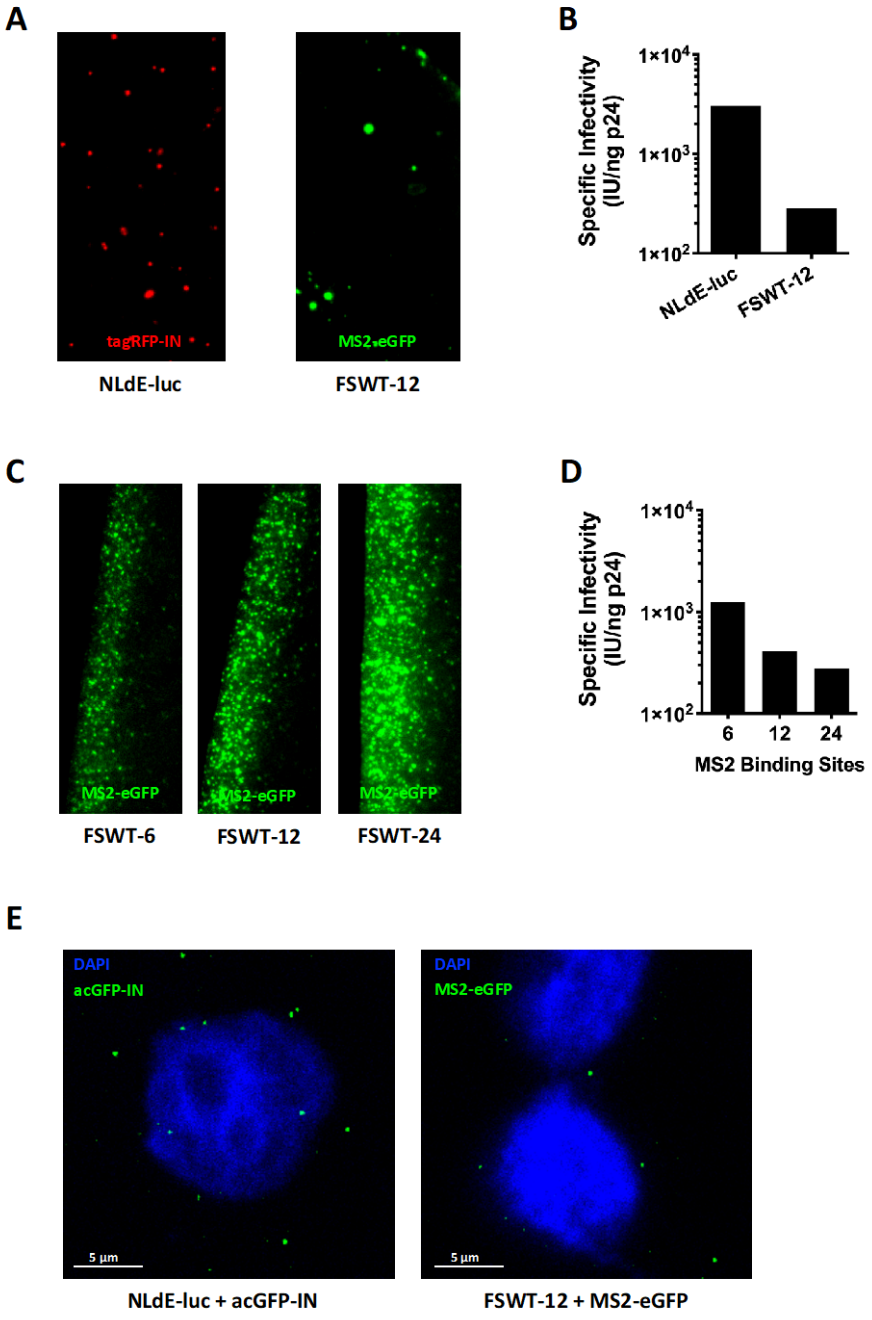

Figure 30. Validation of FSWT/MS2 virus system for production of fluorescent, infectious virus particles. (A) TIRF images of WT HIV-1 particles labeled with Vpr-tagRFP-IN (left) or with MS2-eGFP (right). (B) Specific infectivity (IU/ng of p24) of viruses shown in (A). (C) TIRF images of WT HIV-1 particles labeled with MS2-eGFP with 6, 12, or 24 MS2 binding loops. (D) Specific infectivity of viruses shown in (C). (E) Confocal imaging of HeLa cells 15m after infection with WT HIV-1 labeled with Vpr-acGFP-IN (left) or MS2-eGFP (right). Cell nuclei were stained with DAPI.

increased labeling and particle brightness proportional to the number of binding sites (**Figure 30C**), with decreased infectivity as the number of binding sites increased (**Figure 30D**). A total of 12 binding sites offered a reasonable compromise between efficient labeling and infectivity. To determine if fluorescent FSWT-12 virus particles could be imaged in infected host cells, HeLa cells were infected with either NLdE-luc virus packaging acGFP-IN or FSWT-12 virus packaging MS2-eGFP and fixed 15m post-infection. Confocal imaging showed that although fewer in number than NLdE-luc virus particles, fluorescent FSWT-12 virus particles could be observed in HeLa cells (**Figure 30E**). Differential interference contrast (DIC) imaging showed that the fluorescent signal overlapped with the cell cytoplasm, suggesting virus particles were located within the cells (data not shown). Taken together, these data demonstrate that the FSWT/MS2 system can be used to produce infectious, fluorescently labeled virus particles that can be visualized in infected host cells.

The efficient production of labeled virus particles from a plasmid-based system requires the successful transfection of multiple plasmids into each producer cell. Only those cells that express all components are able to produce labeled virus particles. Increasing the number of co-transfected plasmids decreases overall transfection efficiency (561). As the MS2-FAP assay requires co-transfection of five plasmids (**Figure 29D**), we surmised that decreasing the number of plasmids to be transfected would improve both transfection and particle labeling efficiencies. One method to reduce the number of transfected plasmids is to stably express one or more plasmids in producer cells. To examine the feasibility of MS2-eGFP stable expression, HEK 293T producer cells were transfected with MS2-eGFP expressed from the herpes simplex virus thymidine kinase (HSV-TK) promoter in a vector that contained a puromycin resistance gene (pALTIP), cultured

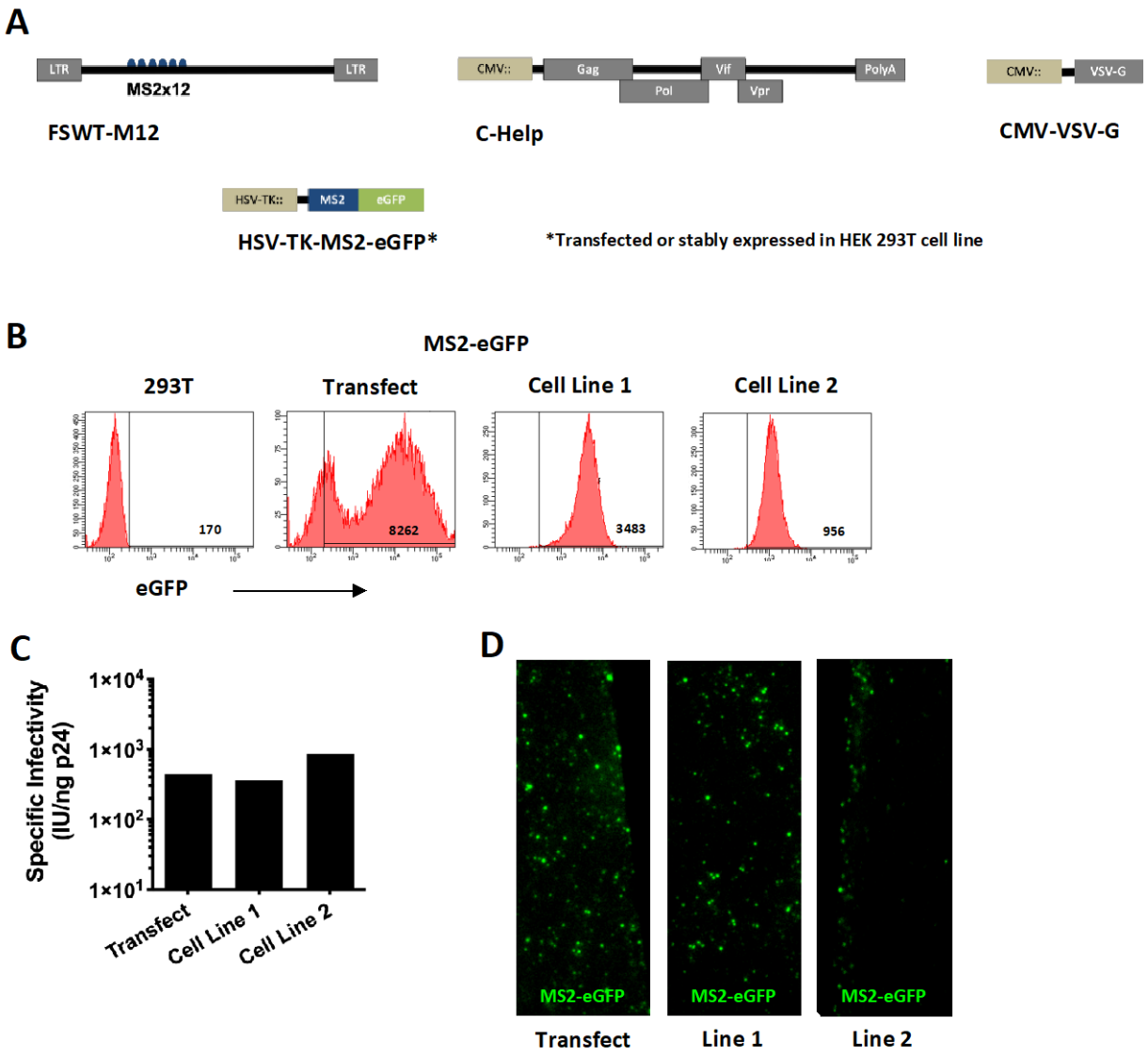

Figure 31. Creation of MS2-eGFP stable expression cell lines. WT HIV-1 was produced and labeled with MS2-eGFP either by transfection into HEK 293T cells or using HEK 293T cell lines stably expressing MS2-eGFP. (A) Schematic of plasmids used to produce virus. (B) MS2-eGFP expression in producer cells was examined by flow cytometry with median fluorescent intensity (MFI) indicated. (C) Specific infectivity and (D) TIRF imaging of viruses produced in (A).

under antibiotic selection, and clonally expanded. Stable expression cell lines were made from two clones that expressed MS2-eGFP at different levels, and FSWT-12 virus was produced in both cell lines and in HEK 293T cells expressing MS2-eGFP transiently via transfection (**Figure 31A**). Examining producer cells by flow cytometry for MS2-eGFP expression demonstrated the expected broad range of expression levels from MS2-eGFP transfection and the narrow range of expression in each cell line (**Figure 31B**), with cell line 1 expressing MS2-eGFP 4-fold higher than cell line 2, but at a 2.5-fold lower median expression level than observed with transient transfection. All cells produced virus particles of similar specific infectivity (**Figure 31C**). TIRF imaging revealed that while virus produced from transfected cells and cell line 1 had similar MS2-eGFP particle labeling, cell line 2 exhibited considerably less labeling (**Figure 31D**), owing to the lower level of MS2-eGFP expression or perhaps to a deficiency in that particular clone. As such, stable expression cell line 1 was used for future experiments.

While the increase in MS2-eGFP virus particle labeling with increased MS2 binding sites (**Figure 30C**) suggests specific packaging of MS2-eGFP in virus particles, it does not rule out non-specific incorporation in the absence of MS2 binding sites. To determine if MS2-eGFP is non-specifically packaged, NLdE-luc virus with tagRFP-IN (which lacks MS2 binding sites) was produced in HEK 293T cells and in the HEK 293T cell line stably expressing MS2-eGFP. TIRF imaging showed a very small but persistent number of green fluorescent particles in virus produced in the presence of MS2-eGFP (**Figure 32A**), typically one or two particles per field of view, which were not present in virus produced in its absence. No particles were double labeled with tagRFP-IN and MS2-eGFP, and the vast majority of particles observed were labeled with only tagRFP-IN. This suggests that while a small amount of non-specific MS2-eGFP incorporation may occur,

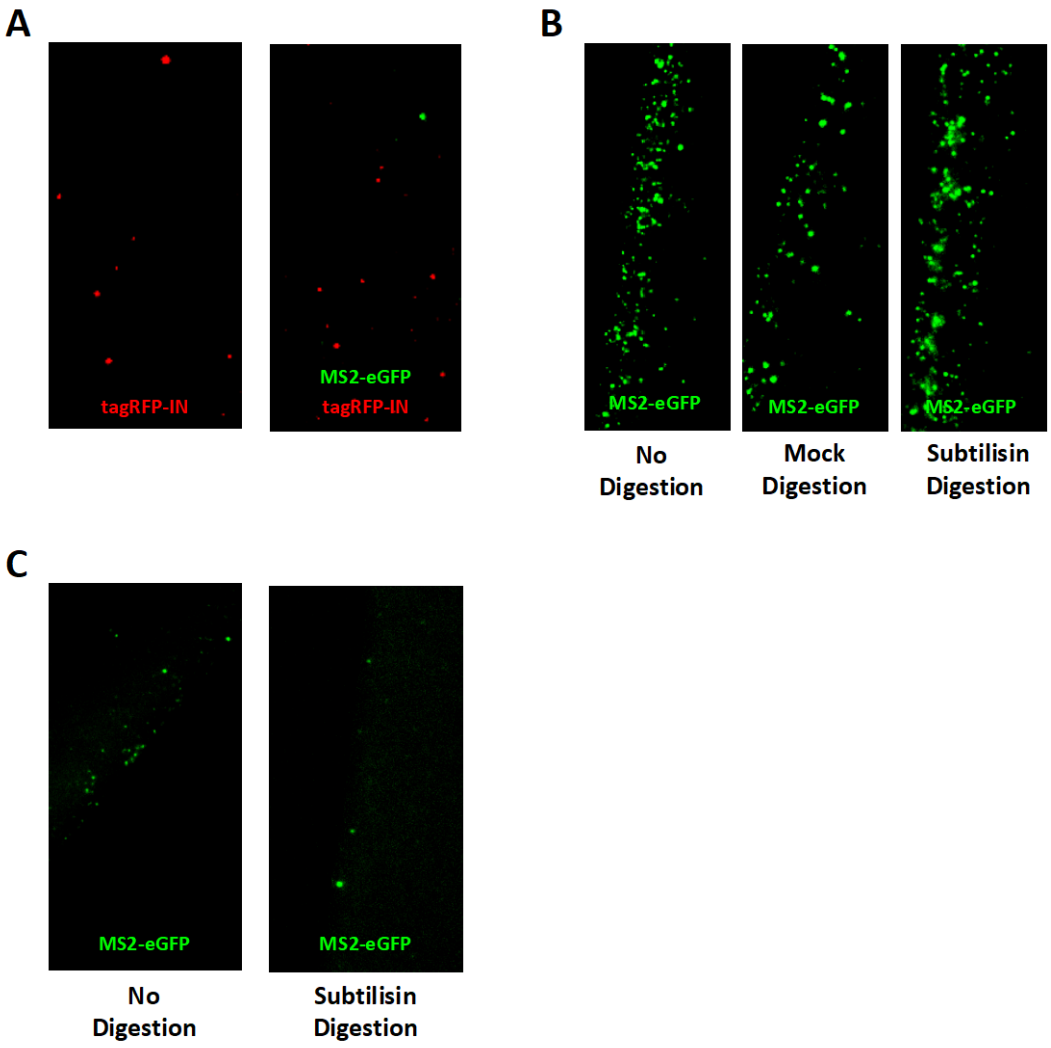

Figure 32. MS2-eGFP is packaged into HIV-1 particles with high specificity. (A) TIRF imaging of WT HIV-1 lacking MS2 binding loops, labeled with Vpr-tagRFP-IN, without (left) and with (right) expression of MS-eGFP in HEK 293T producer cells. (B) TIRF imaging of WT HIV-1 labeled with MS2-eGFP without digestion (left), with mock digestion in buffer (middle), and with subtilisin digestion (right). (C) TIRF imaging of supernatant from HEK 293T cell line stably expressing MS2-eGFP without (left) and with (right) subtilisin digestion.

packaging of MS2-eGFP into virus particles is predominantly associated with MS2 binding loops in the RNA genome.

While the observation of fluorescent particles in virus producer cell supernatant would be expected to predominantly represent virus particles, exosomes and/or microvesicles are likely also present and constitute an unquantified population of these particles. To determine the proportion of fluorescent particles in the virus preparation that may be exosomes/microvesicles, FSWT-12 virus produced in the presence of MS2-eGFP was subjected to subtilisin digestion. Subtilisin is a non-membrane permeable protease that will cleave external proteins from particles. Exosomes/microvesicles that have been so treated will not pellet with virus particles upon ultracentrifugation, allowing the purification of actual virus (562). While virus that was mock digested in buffer without subtilisin retained infectivity, the specific infectivity of virus digested by subtilisin was below the limit of detection, despite having a comparable p24 concentration (data not shown), demonstrating that subtilisin digestion was successful in cleavage of external proteins from particles. Examining virus without digestion, with mock digestion, or with subtilisin digestion by TIRF imaging showed similar populations of fluorescent particles (**Figure 32B**), suggesting the population of exosomes/microvesicles in the virus stock was relatively small.

To further support these observations, cell culture supernatant from HEK 293T cells stably expressing MS2-eGFP was digested with subtilisin. TIRF imaging of supernatant with and without digestion revealed that the cell supernatant contained an appreciable but small population of fluorescent particles, the vast majority of which were depleted by subtilisin digestion (**Figure 32C**). While the proportion of non-virus fluorescent particles appeared to be low, there remained

the potential for these particles to confound imaging of infected host cells, if the particles were taken up by cells in a similar manner to virus particles. To determine the propensity for these non-virus fluorescent particles to interfere with imaging of infected host cells, HeLa cells were mock inoculated with cell culture supernatant from HEK 293T cells stably expressing MS2-eGFP and fixed after 15m. Confocal imaging revealed the mock inoculated cells were indistinguishable from untreated negative control cells (data not shown). Taken together, these data suggest that while there is a small population of non-infectious, fluorescent particles present in virus made with MS2-eGFP, these particles do not impact imaging of virus or infected host cells.

A failure of HIV-1 to successfully complete reverse transcription would abrogate virus infectivity, and a capsid permeabilization assay system with impaired reverse transcription would have limited utility. The presence of MS2-eGFP bound to MS2 binding loops within the RNA genome presents a potential inhibitor of reverse transcription, as RT would need to dislodge MS2-eGFP in order for reverse transcription to proceed through the MS2 binding loop cassette. While it has been demonstrated that RNA translation is not impeded by the presence of MS2 coat protein bound to RNA (563) and we show that these viruses are infectious (**Figures 30 and 31**), the ability of RT to displace MS2 coat protein has not been determined. To examine this, FSWT virus was produced with and without the presence of MS2-eGFP, with either 6 or 12 MS2 binding sites used to package MS2-eGFP, and reverse transcription products were quantified in infected HeLa cells at multiple time points post-infection. Early and late reverse transcription products were readily detected with and without MS2-eGFP present (**Figure 33A and 33B**) and at similar levels with 6 or 12 MS2 binding sites (**Figure 33C and 33D**). This suggests that RT is able to successfully complete reverse transcription in the presence of MS2 coat protein bound to the RNA binding

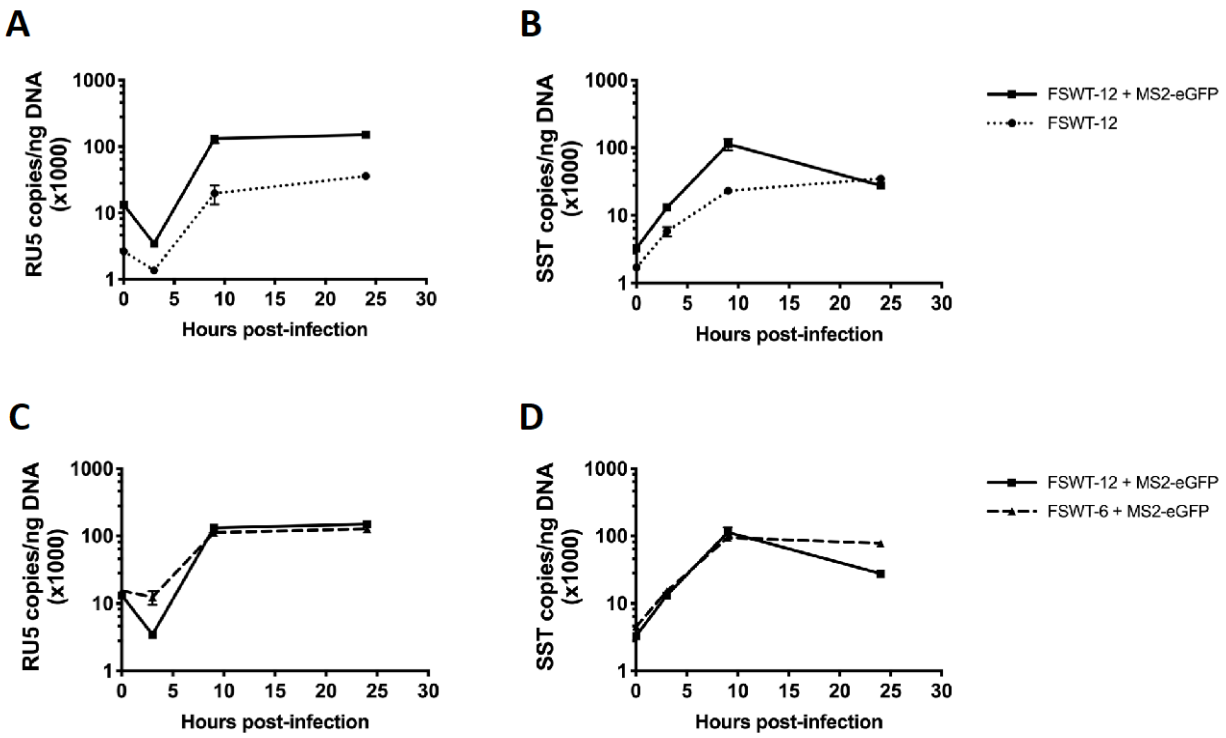

Figure 33. MS2-eGFP bound to viral RNA does not inhibit reverse transcription. HeLa cells were infected with equal amounts of WT HIV-1 with and without labeling by MS2-eGFP (A and B) or with labeling by 6 or 12 copies of MS2-eGFP (C and D). Early (A and C) and late (B and D) reverse transcription products were measured at indicated times post-infection.

loops. Collectively, these data validate the use of the FSWT/MS2 system for producing infectious, fluorescent virus particles that are specifically labeled and undergo reverse transcription, suitable for use in a live cell capsid permeabilization assay.

5.2.3 Creation and testing of the MS2-FAP fusion construct

MS2-FAP was created by replacing eGFP in MS2-eGFP with dL5, a single chain antibody FAP. To verify proper functionality of the FAP, MS2-FAP was transfected into HEK 293T cells and its expression was examined by flow cytometry after 48h, with the malachite green (MG)-Ester fluorogen dye added 30m prior to examination. Compared to untransfected negative control cells, a majority (72%) of cells expressing MS2-FAP showed a strong fluorescent signal with a broad range of expression levels (**Figure 34A**). To confirm that the fluorescent signal was specific to the combination of FAP and fluorogen dye, HeLa cells were transfected with or without MS2-FAP and fixed after 48h, and with or without MG-Ester dye added 30m prior to fixation. Confocal microscopy showed that cells expressing MS2-FAP without MG-Ester dye or regular cells treated with MG-Ester dye had no fluorescent signal and were indistinguishable from untransfected, untreated negative control cells (**Figure 34B**). In contrast, the combination of MS2-FAP expression and MG-Ester dye treatment produced a strong fluorescent signal (**Figure 34C**). Additionally, application of the MG-Ester dye to cells expressing MS2-FAP post-fixation produced a similar fluorescent signal to application prior to fixation (data not shown), indicating that either method could be used with fixed cell samples.

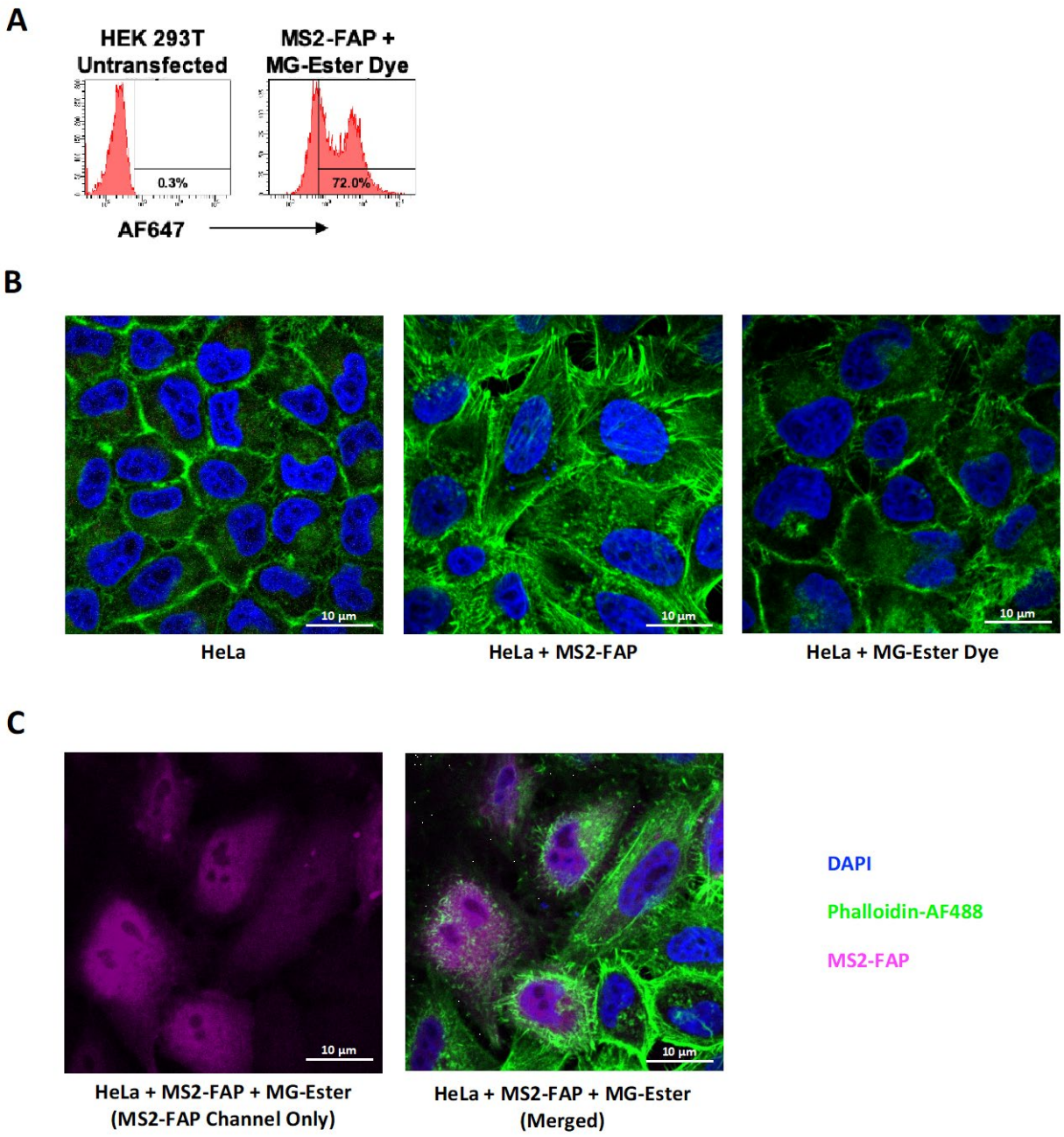

Figure 34. Creation and testing of the MS2-FAP fusion protein. (A) HEK 293T cells were transfected with MS2-FAP and examined after 48h by flow cytometry for MS2-FAP expression. (B) Confocal imaging of HeLa cells that were untransfected (left), transfected with the MS2-FAP plasmid but without addition of MG-Ester dye (middle), or untransfected with MG-Ester dye added (right). (D) Confocal imaging of HeLa cells expressing MS2-FAP with MG-Ester dye added (purple). All cells were stained with phalloidin-AF488 (green) and DAPI (blue).

While fixed cell imaging demonstrated proper functionality of MS2-FAP and MG-Ester dye, the capsid permeabilization assay would require use in living cells. To confirm that the reagents function properly with live cell imaging, HEK 293T cells were transfected with MS2-FAP and imaged by live cell confocal microscopy after 48h, with MG-Ester dye added 30m prior to imaging. Compared to untransfected, untreated negative control cells, cells expressing MS2-FAP and treated with MG-Ester dye produced a strong fluorescent signal in the majority of cells (**Figure 35A**). To demonstrate that the application of MG-Ester dye did not impact cell viability, cells were cultured for an additional 72h after dye treatment with no apparent detrimental effect (data not shown).

To verify that MS2-FAP could be used to produce fluorescent virus particles, FSWT-12 virus was produced in the presence of MS2-FAP. MG-Ester dye was added either to the producer cells (to ensure binding to MS2-FAP prior to virus particle maturation and capsid closure) or to the collected virus (to determine if MG-Ester dye is capsid permeable). TIRF imaging revealed that MS2-FAP produced fluorescent virus particles regardless of when MG-Ester dye was added (**Figure 35B**), additionally demonstrating that MG-Ester dye is capsid permeable. Virus lacking either addition of MG-Ester dye or packaging of MS2-FAP did not produce fluorescent virus particles (data not shown). Fluorescence of MS2-FAP + MG-Ester virus particles was still present after subjecting the virus to a freeze-thaw cycle and re-imaging (data not shown). The addition of MG-Ester dye did not alter the specific infectivity of the virus, with similar infectivity of virus lacking dye or virus in which dye was added during or after virus production (**Figure 35C**). Initial attempts to image host cells infected with MS2-FAP virus suffered from a failure to add additional MG-Ester dye to the cells (beyond the amount present in the treated virus) to ensure a constant dye

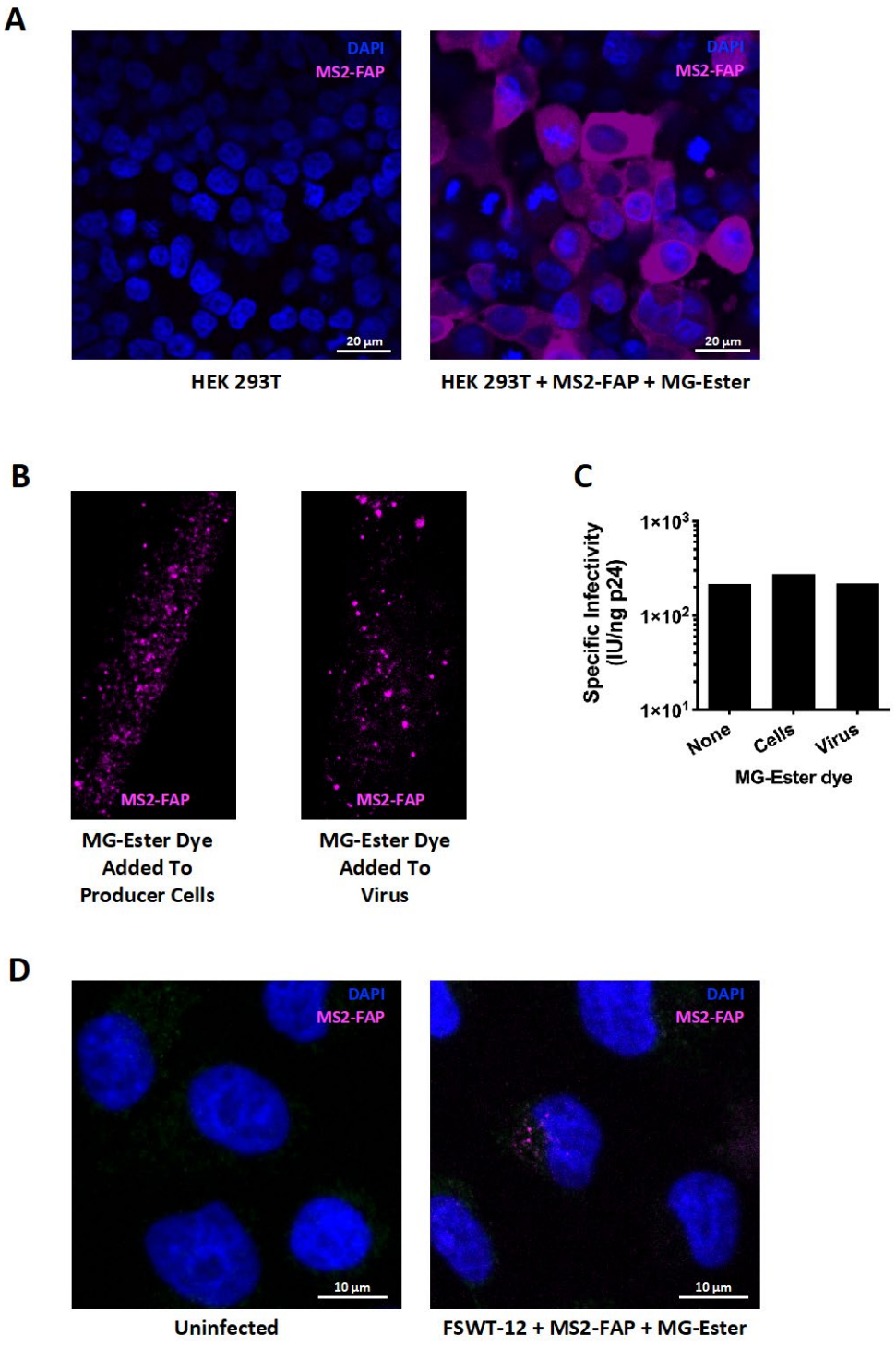

Figure 35. MS2-FAP can be used with live cell imaging and to make infectious, fluorescent virus. (A) Live cell confocal imaging of HEK 293T cells with and without expression of MS2-FAP and addition of MG-Ester dye. (B) TIRF imaging of WT HIV-1 labeled with MS2-FAP and with MG-Ester dye added either to producer cells (left) or to the virus (right). (C) Specific infectivity of viruses in (B) and the same virus without MG-Ester dye added. (D)

Confocal imaging z-stack maximum intensity projection of HeLa cells 15m after infection with WT HIV-1 virus labeled with MS2-FAP and MG-Ester dye.

concentration. Nonetheless, fluorescent virus particles were observed (**Figure 35D**), similar to those observed with virus packaging MS2-eGFP (**Figure 30E**). Altogether, these data confirm the functionality of MS2-FAP and the ability to make fluorescent, infectious virus particles.

5.2.4 MS2 binding site competition impairs efficient packaging of two MS2-based imaging constructs

The final element of the MS2-FAP assay system to be tested was the persistent virus particle signal, provided by Vpr-mRuby3-IN packaged *in trans*. While efficient Vpr-mRuby3-IN packaging was consistently obtained with NLdE-luc virus, repeated attempts to co-package either Vpr-tagRFP-IN or Vpr-mRuby3-IN with MS2-eGFP in FSWT-12 virus were unsuccessful (data not shown). As MS2-eGFP was efficiently packaged into FSWT-12 virus, it was hypothesized that a second MS2-based construct could be packaged with a persistent fluorescent signal in place of Vpr-mRuby3-IN. MS2-tagRFP was created by replacing eGFP in MS2-eGFP with tagRFP and used in place of Vpr-mRuby3-IN (**Figure 36A**). To verify efficient co-expression of two MS2-based constructs, HeLa cells were transfected with both MS2-eGFP (used in place of MS2-FAP for simplicity) and MS2-tagRFP and imaged after 48h. Confocal imaging revealed that most cells expressed both constructs at similar levels (**Figure 36B**). FSWT virus with either 12 or 24 MS2 binding sites was made in cells expressing both MS2-eGFP and MS2-tagRFP. TIRF imaging showed that while an appreciable population of FSWT-12 fluorescent particles were double

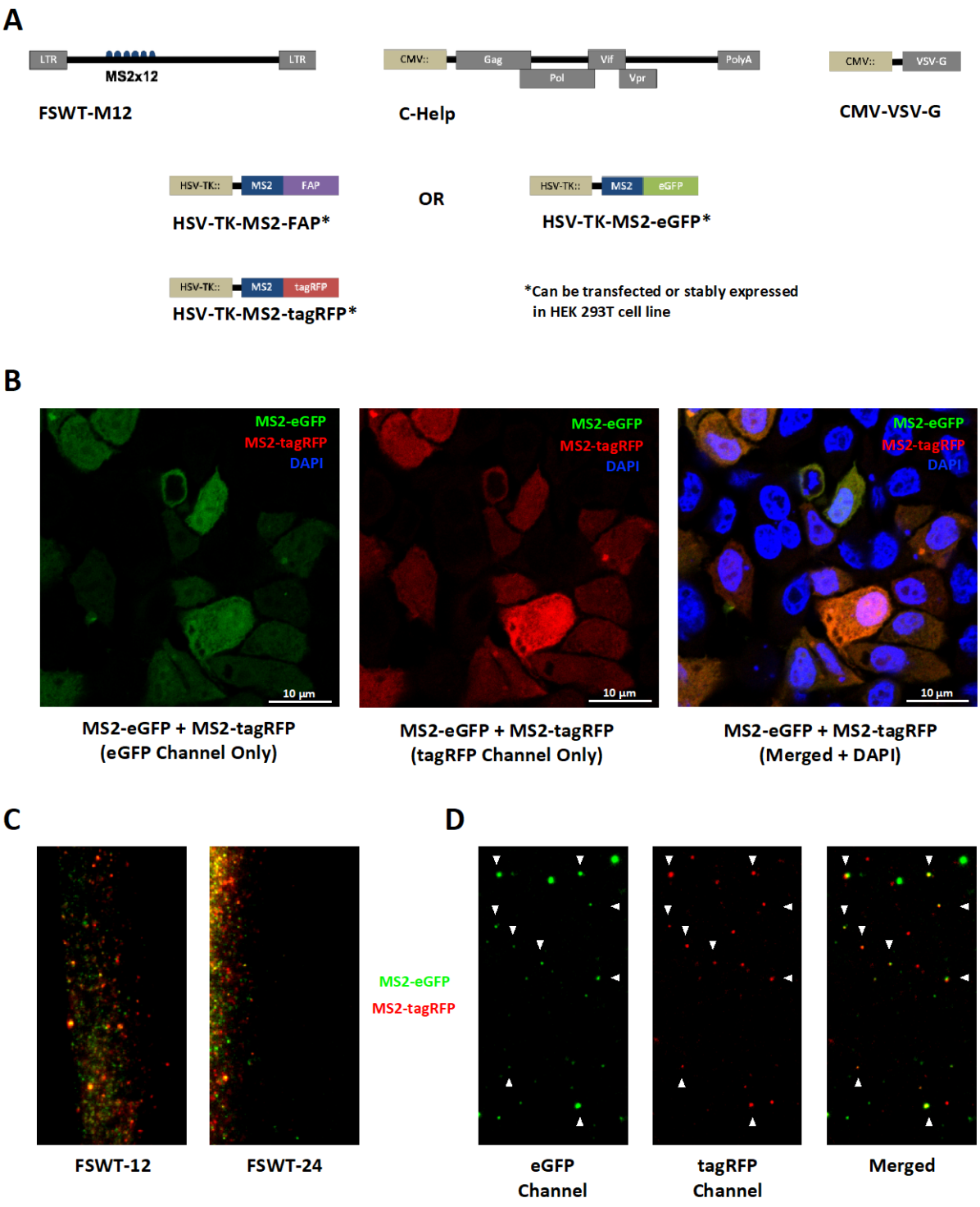

Figure 36. MS2 binding site competition impedes labeling of virus particles with two different MS2-based fluorescent constructs. (A) Schematic design of MS2 system with dual MS2-based labels. MS2-FAP can be replaced with MS2-eGFP for system testing purposes. (B) Confocal imaging of HeLa cells expressing MS2-eGFP and MS2-tagRFP. (C) TIRF imaging of WT HIV-1 virus labeled with MS2-eGFP and MS2-tagRFP with either 12 (left) or 24

(right) MS2 binding loops. (D) TIRF imaging of WT HIV-1 labeled with MS2-eGFP and MS2-tagRFP with 24 MS2 binding loops. White arrowheads indicate virus particles labeled with both fluorescent constructs.

labeled with MS2-eGFP and MS2-tagRFP, the majority of particles were labeled with only one construct (**Figure 36C**, left). Increasing the number of MS2 binding sites to 24 produced a commensurate increase in double labeled particles (**Figure 36C**, right); however, the double labeled population still only accounted for about 50% of the fluorescent particles. A closer examination of the double labeled particles revealed that packaging of each construct was biased on a per-particle basis, with some particles predominantly packaging MS2-eGFP and others MS2-tagRFP, with only a small proportion having roughly equivalent labeling (**Figure 36D**). These data collectively suggest that MS2 binding site competition impedes efficient packaging of two different MS2-based constructs.

5.2.5 Bacteriophage PP7 coat protein offers an alternative to a second MS2-based imaging construct but fails to package efficiently

Successful co-labeling with two MS2-based constructs in the presence of MS2 binding site competition would require equivalent levels of expression of both constructs and would still be subject to stochastic fluctuations in packaging, which would result in biased labeling as previously observed. Deeming a consistently acceptable balance of MS2-eGFP and MS2-tagRFP packaging unlikely, an alternative approach was considered. Similar to MS2, the bacteriophage PP7 coat protein binds to RNA genome hairpin loops, the sequence of which are distinct from those of MS2 (564). Efficient co-labeling of target RNA with fluorescent MS2 and PP7 constructs has been

previously reported (563), suggesting a similar labeling scheme for HIV-1 virus particles (**Figure 37A**) would be reasonable. The FSWT-12 lentiviral vector was modified to add 12 PP7 binding loops either after or before the MS2 binding loop cassette (FSWT-M12-P12 and FSWT-P12-M12, respectively), and a fusion of the PP7 coat protein and the red fluorescent protein mCherry (PP7-mCherry) was cloned into the pcDNA3.1 (cytomegalovirus [CMV] promoter) and pALTIP (HSV-TK promoter) vectors.

FSWT-M12-P12 viruses produced in cells expressing either MS2-eGFP, PP7-mCherry, or both were equally infectious (**Figure 37B**). TIRF imaging revealed that while MS2-eGFP labeling of fluorescent particles was similar to that previous obtained with FSWT-12 virus, minimal PP7-mCherry labeling was observed either alone or in conjunction with MS2-eGFP (**Figure 37C**). Similar results were obtained with FSWT-P12-M12 viruses, in which the MS2 and PP7 binding loops cassettes were in the reversed orientation (data not shown). Failure to observe PP7-mCherry labeled particles was not due to lack of expression of PP7-mCherry in producer cells, a lack of fluorescence from mCherry, or errors in the sequence of either PP7 coat protein or the PP7 binding loop cassette (data not shown). HEK 293T cells stably expressing both MS2-eGFP and PP7-mCherry under selection of different antibiotics showed strong expression of both constructs in the vast majority of cells by confocal imaging (**Figure 37D**). A deeper examination of the PP7 coat protein and binding loop cassette revealed that the sequence originally provided for the PP7 binding loop cassette (565), which was used to synthesize the FSWT-M12-P12 and FSWT-P12-M12 genomes, did not include optimizations that were subsequently reported (563). The authors noted significant problems with the PP7 binding cassette in the absence of these optimizations (563), suggesting a cause for the poor incorporation of PP7-mCherry into virus particles.

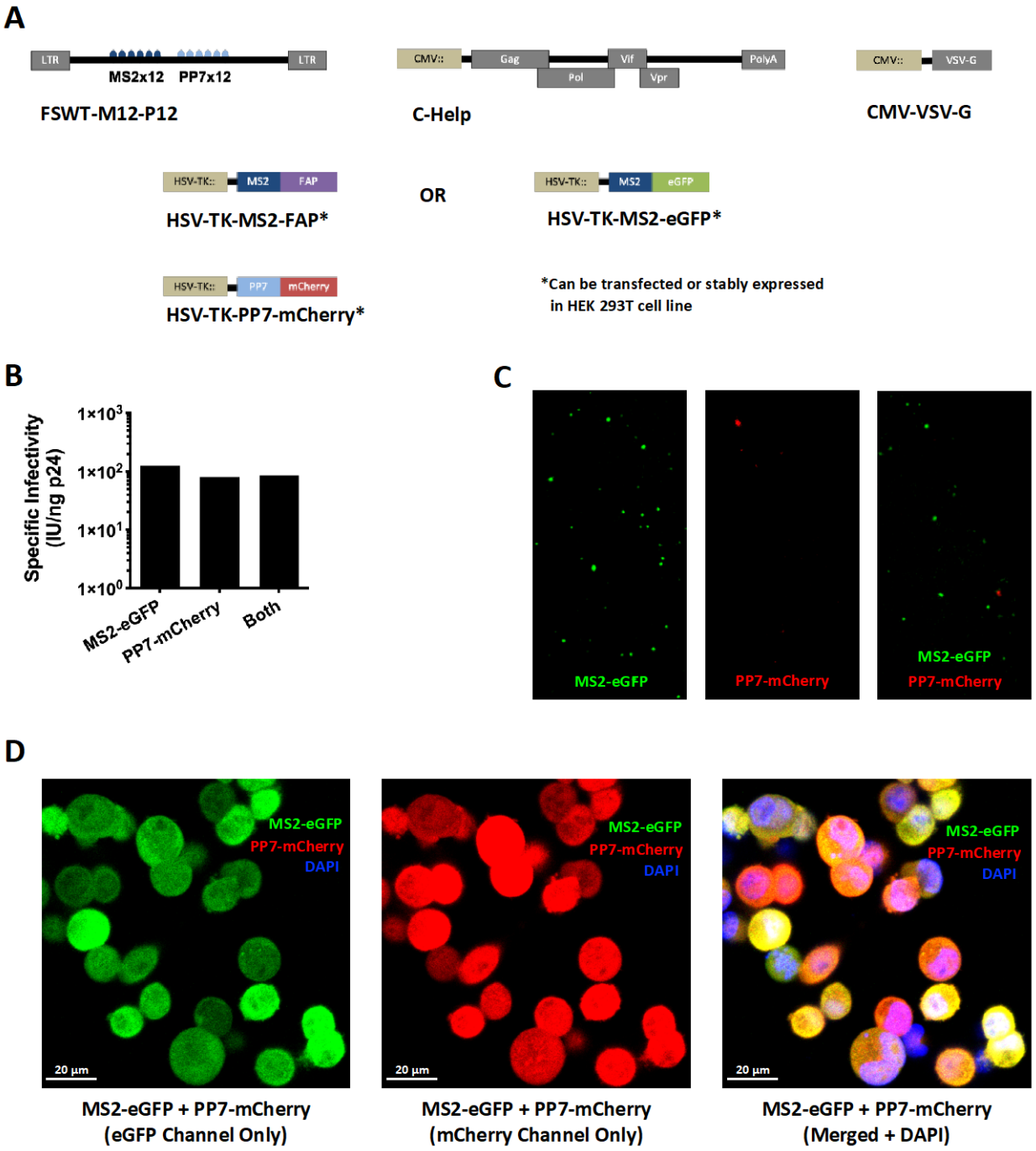

Figure 37. MS2/PP7 labeling system fails to package PP7 construct efficiently. (A) Schematic design of dual MS2/PP7 virus particle labeling system. MS2-FAP can be replaced with MS2-eGFP for system testing purposes. (B) Specific infectivity and (C) TIRF imaging of WT HIV-1 labeled with MS2-eGFP, PP7-mCherry, or both MS2-eGFP and PP7-mCherry. (D) Confocal imaging of HEK 293T cells stably expressing MS2-eGFP and PP7-mCherry.

5.2.6 Development of two simplified versions of the live cell compatible capsid permeabilization assay

The discovery of the unoptimized PP7 binding loop cassette incorporated into the FSWT lentiviral vector offered a potential solution to the inefficient packaging of the PP7-mCherry persistent signal into virus particles, with a plan devised to clone the optimized cassette into FSWT. However, the pause in development also offered the opportunity for reflection on the state of the MS2-FAP assay system, how it deviated from the modified EU assay plasmid set, and the further complications introduced in an attempt to overcome problems with the persistent signal originally provided by Vpr-mRuby3-IN. Some of the early choices made in reagent use were based upon availability in the laboratory and did not necessarily reflect the optimal architecture. It was recognized that simplifying the assay would be highly beneficial and improve the likelihood of success in development. As such, a revised plan was made for the MS2-FAP assay (**Figure 38A**) that would see a return to the NLdE-luc virus system used in the EU assay, with the firefly luciferase reporter gene replaced with an MS2 binding loop cassette (NLdE-MS2). The use of NLdE-MS2 would permit efficient packaging of Vpr-mRuby3-IN and alleviate alternatives for its replacement. Finally, MS2-FAP could be stably expressed in a cell line, reducing the number of plasmids for transfection to the original three (**Figure 38B**).

Further consideration of the MS2-FAP assay architecture revealed an additional aspect that might be simplified. The permeabilization signal, while based on a two-component sensor, consisted of four discrete subunits: MS2 binding loops incorporated into the RNA genome, MS2 coat protein, FAP, and fluorogen dye. The first three items collectively performed the role of the

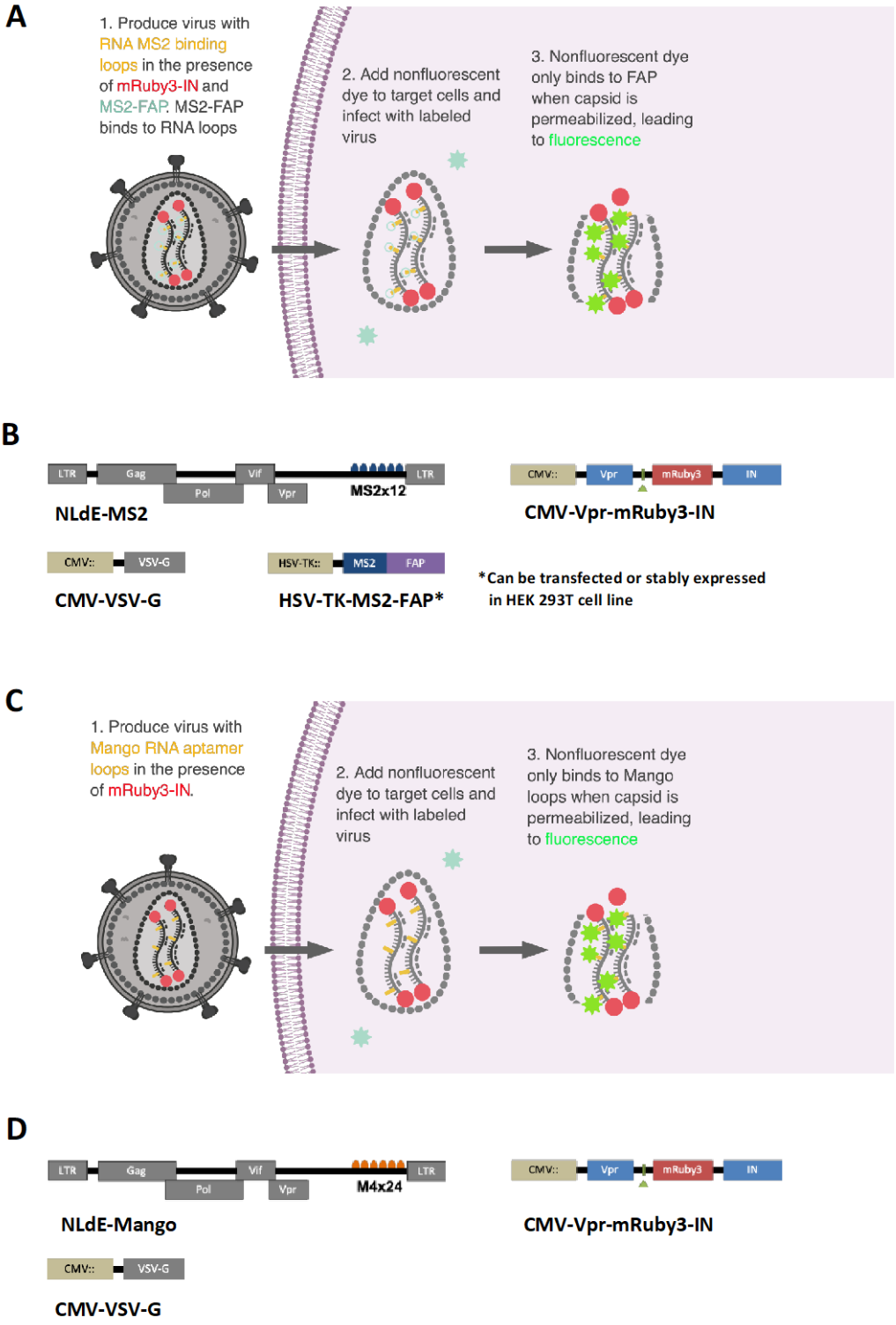

Figure 38. Designing simplified MS2- and RNA aptamer-based HIV-1 capsid uncoating assays. MS2-FAP capsid permeabilization assay updated model (A) and plasmid design (B). Model (C) and plasmid design (D) for the Mango RNA aptamer capsid permeabilization assay.

sensor component internal to the intact capsid. Redevelopment of the nature of the two-component sensor could see these three subunits merged into one.

FAPs are not the only biological structures that can specifically activate fluorogen dyes to fluoresce. RNA-based fluorescent light-up aptamers (FLAPs) are RNA sequences that operate in a similar fashion, binding to fluorogen dyes and increasing their fluorescence by 3-4 orders of magnitude (566). The FLAP secondary structure forms stem loops that contain a lidded, multi-tiered guanine (G)-quadruplex into which the fluorogen dye reversibly binds and adopts a confined conformational state that induces fluorescence (567). Following the discovery of the first FLAP, Spinach (568), multiple generations of FLAPs have been developed (567) including Mango (569), which binds to a commercially-available thiazole orange (TO)-derived fluorophore, TO1-Biotin, with nanomolar affinity (570). Competitive ligand binding microfluidic selection has produced new versions of Mango with optimized fluorescence properties (571). Two of these, Mango2 and Mango4, have been demonstrated to perform well in both fixed and live cell imaging (571) and, with 25-bp and 27-bp loop cores, respectively, can readily be arranged in loop cassettes to provide an amplified fluorescent signal for the target RNA (David Rueda, personal communication).

Based upon the above, the Mango capsid permeabilization assay was devised (**Figure 38C**). Similar in principle to the MS2-FAP assay, the Mango assay simplifies the permeabilization signal into a set of Mango2 or Mango4 RNA aptamer loops that are incorporated into the NLdE-luc virus plasmid in place of the firefly luciferase gene, producing NLdE-Mango, combined with a capsid impermeable fluorogen dye. Permeabilization of the capsid results in a fluorescent signal when the fluorogen dye binds the Mango loops. As with the MS2-FAP assay, the persistent virus

particle signal is provided by Vpr-mRuby3-IN. No additional plasmids are required, resulting in a three-plasmid transfection set (**Figure 38D**).

5.2.7 Upgrading the fluorescently tagged IN construct for super-resolution imaging and stable cell line expression

Persistent virus particle labeling with Vpr-mRuby3-IN has found use in numerous assays and studies within our laboratory. Use of stimulated emission depletion (STED) microscopy for super-resolution imaging (572, 573), which could potentially include the Mango capsid permeabilization assay, are unable to utilize this reagent due to the poor visualization of red fluorescent proteins by STED (574). To provide a STED-friendly version of fluorescently tagged IN that can be packaged into HIV-1 virus particles *in trans*, the mRuby3 fluorescent protein was replaced with the dL5 FAP, which has been demonstrated to provide an effective far red fluorescent signal with STED (559).

To verify that Vpr-FAP-IN is fully functional in all domains, NLdE-luc virus was produced packaging either Vpr-mRuby3-IN or Vpr-FAP-IN *in trans* (**Figure 39A**), with MG-Ester dye added to the Vpr-FAP-IN virus producer cells. Both viruses had similar infectious titer (**Figure 39B**) and p24 concentration (**Figure 39C**). Packaging either Vpr-mRuby3-IN or Vpr-FAP-IN *in trans* complemented and rescued infectivity of HIV-1 lacking integrase activity due to the D116N mutation in the IN active site (575), confirming proper function of the IN domain (**Figure 39D**). Vpr-FAP-IN fluorescently labeled virus particles similarly to Vpr-mRuby3-IN, as demonstrated by TIRF imaging of virus (**Figure 39E**) and confocal imaging of HeLa cells fixed 15m after virus

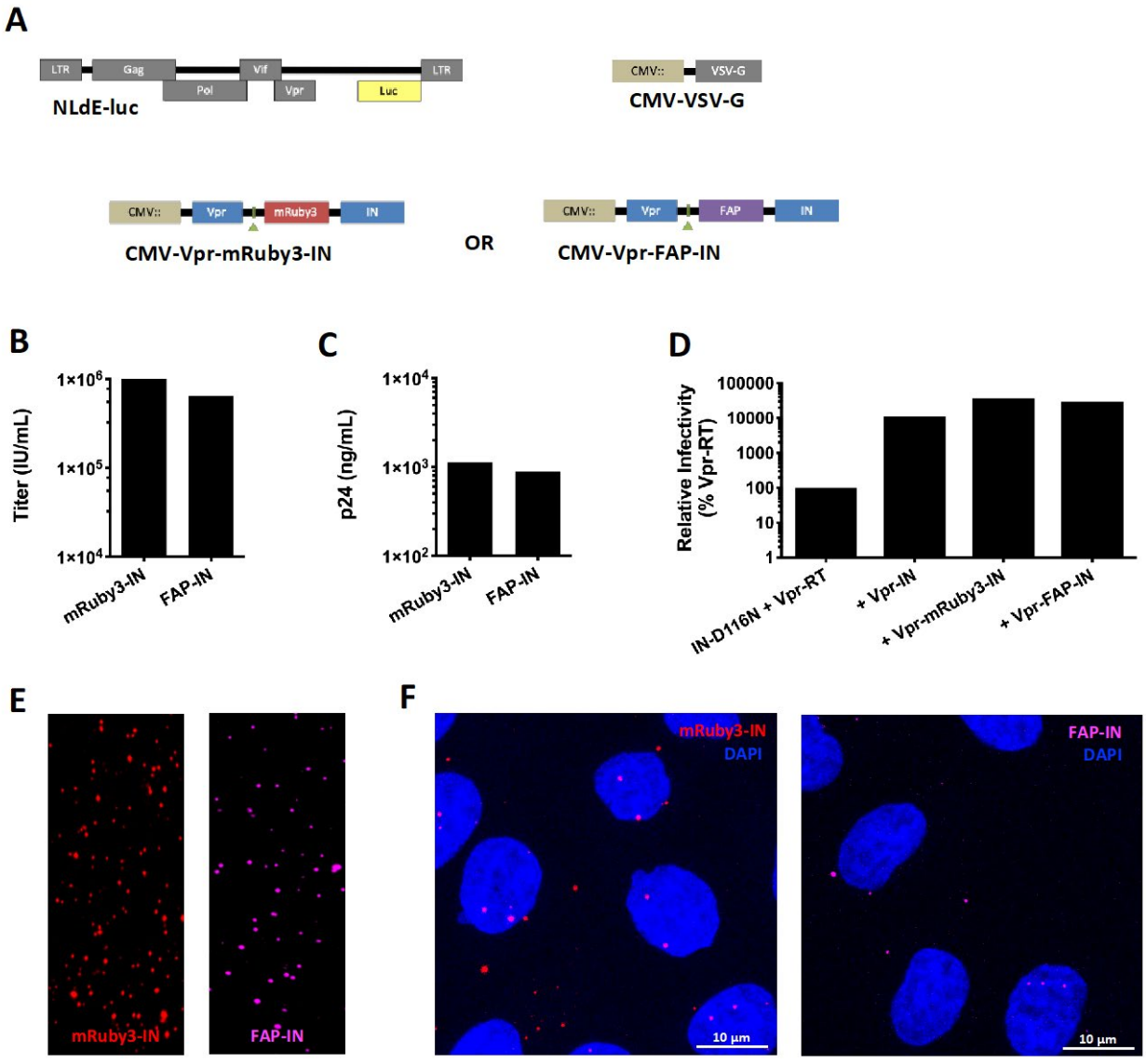

Figure 39. Creation and Testing of Vpr-FAP-IN. (A) Schematic of NLdE-luc virus labeled with Vpr-mRuby3-IN or Vpr-FAP-IN *in trans*. (B) Infectious titer and (C) p24 concentration of WT HIV-1 labeled with Vpr-mRuby3-IN or Vpr-FAP-IN. (D) HeLa cells were infected with equal amounts of D116N HIV-1 complemented *in trans* with the indicated plasmids and assayed after 48h for luciferase activity. (E) TIRF imaging of WT HIV-1 labeled with Vpr-mRuby3-IN or Vpr-FAP-IN. (F) Confocal imaging of HeLa cells 15m after infection with viruses from (E).

infection (**Figure 39F**). Vpr-FAP-IN-labeled virus particles were further shown to be visible in infected HeLa cells with STED microscopy (data not shown). Collectively, these data show that Vpr-FAP-IN can be used for far red fluorescent HIV-1 virus particles compatible with STED super-resolution imaging.

To optimize production of labeled virus particles by reducing the number plasmids for virus production, a cell line stably expressing Vpr-mRuby3-IN would be useful. Initial attempts at stable expression of Vpr-mRuby3-IN in HEK 293T cells through transfection and antibiotic selection resulted in widespread cell death or silencing of the Vpr-mRuby3-IN gene (i.e. cells survived antibiotic selection but expressed no Vpr-mRuby3-IN; data not shown). The inability to stably express Vpr-mRuby3-IN could be caused by Vpr, which has demonstrated cytotoxic characteristics. Vpr has been shown to induce G_2/M cell cycle arrest both during HIV-1 infection and when independently expressed (576, 577), leading to apoptosis (578, 579). This cell cycle arrest is modulated by phosphorylation of Vpr on serine 79 (580) by protein kinase A (581), with arrest abrogated by mutating this serine to an alanine (S79A) (580). Vpr mutants lacking the ability to arrest the cell cycle, however, retain cytopathicity (582) through the recruitment of the CUL4-$DDB1^{DCAF1}$ E3 ubiquitin ligase complex (583-586), inducing K48-linked polyubiquitination and proteasomal degradation of host cell proteins (587). Mutating Vpr glutamine 65 to arginine (Q65R) inhibits binding to DDB1 and CUL4-associated factor 1 (DCAF1) (584, 588) and prevents localization of Vpr to the nuclear membrane and induction of cell cycle arrest (589). Due to one or both of these cytopathic functions, Vpr has been shown to prevent establishment of HIV-1 chronic infection cell lines (590), which correlates with our observations.

Based upon the above, we hypothesized that the inability to establish a cell line stably expressing Vpr-mRuby3-IN was caused by Vpr cytopathicity and the abrogation of Vpr-induced cell cycle arrest and proteasome-mediated degradation of host cell proteins would permit stable expression. A previous study demonstrated that the Q65R/S79A mutations negated the cytopathic effects of Vpr expression and permitted the formation of hygromycin-resistant cell colonies by episomal maintenance of a plasmid expressing Vpr and a hygromycin resistance cassette (591). This suggested that Q65R/S79A Vpr should permit stable expression of Vpr-mRuby3-IN. However, it was also imperative that Vpr retain the ability to be packaged into nascent virus particles by engaging the C-terminal p6 domain of Gag (592) to direct *trans*-packaging of the Vpr-mRuby3-IN construct. This packaging is dependent upon the Vpr N-terminal α-helix (592) and upon Vpr oligomerization (593). While the N-terminal region of Vpr mediates oligomerization (594), a previous study suggested the Q65R mutant was defective for proper oligomerization (587). As such, it would be necessary to validate the functionality of the mutated construct prior to attempting to establish a stable expression cell line.

The Q65R and S79A point mutations were accordingly made in the Vpr domain of Vpr-mRuby3-IN to generate a putatively non-cytotoxic version of the construct, ncVpr-mRuby3-IN (**Figure 40A**), and NLdE-luc virus was produced packaging either Vpr-mRuby3-IN or ncVpr-mRuby3-IN *in trans*. Examining HEK 293T producer cells for each virus by flow cytometry demonstrated that both constructs were expressed at similar levels (**Figure 40B**). The relatively low overall levels of expression observed with flow cytometry were due to the absence of a 561 nm light source in the cytometer, requiring attenuated excitation of mRuby3 at 488 nm. Viruses packaging each construct had similar infectious titers (**Figure 40C**) and p24 concentrations

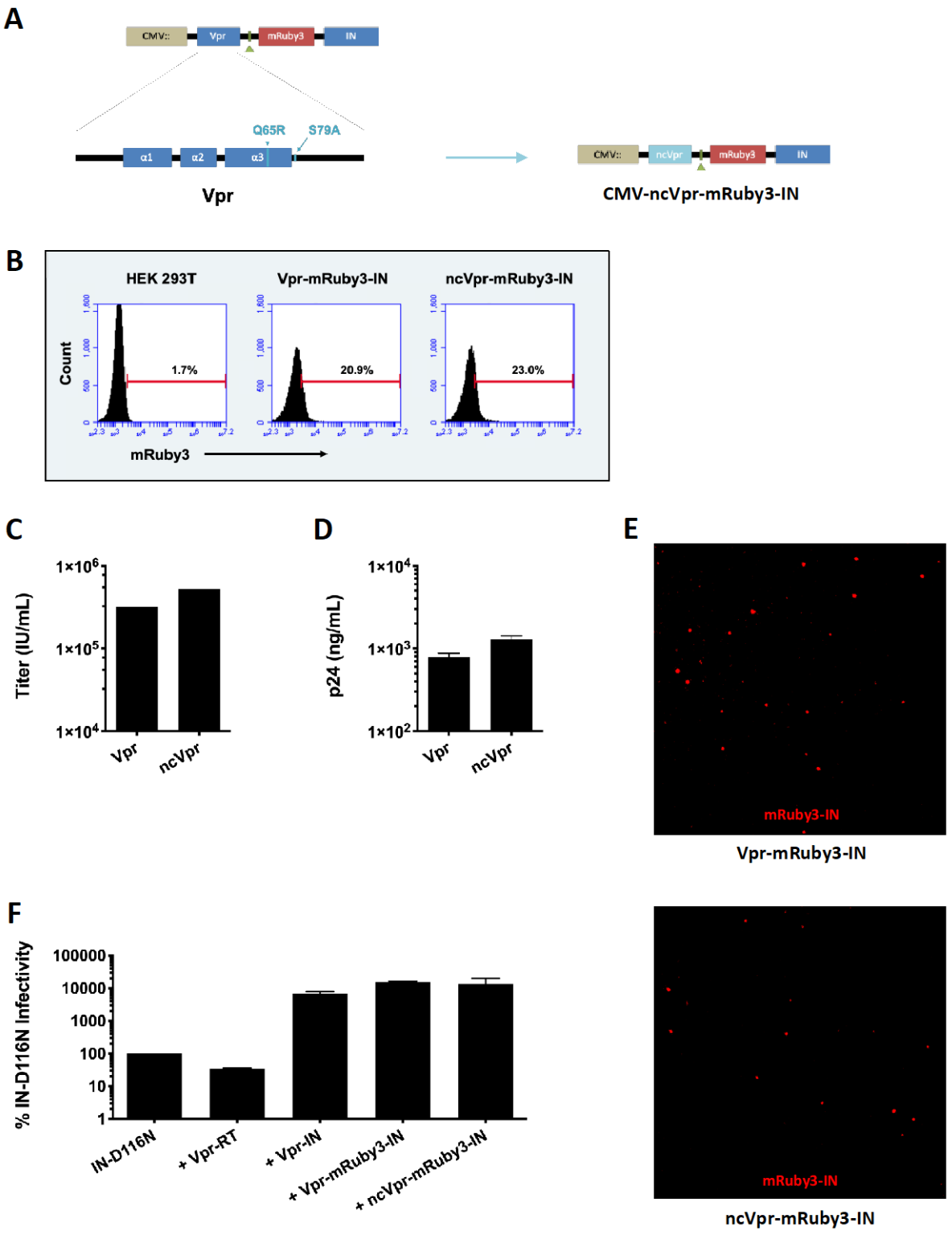

Figure 40. Creation and Testing of a non-cytotoxic Vpr-mRuby3-IN (ncVpr-mRuby3-IN). (A) Schematic design of ncVpr-mRuby3-IN with specific Vpr point mutations indicated. (B) WT HIV-1 was produced and labeled with Vpr-mRuby3-IN or ncVpr-mRuby3-IN. Expression of mRuby3-IN in HEK 293T producer cells was examined by

flow cytometry. (C) Infectious titer, (D) p24 concentration, and (E) TIRF imaging of viruses produced in (B). (F) HeLa cells were infected with equal amounts of D116N HIV-1 complemented *in trans* with indicated plasmids and assayed after 48h for luciferase activity. Error bars represent standard error of the mean for two experiments.

(**Figure 40D**). TIRF imaging showed similar fluorescent particles for both viruses (**Figure 40E**). Both Vpr-mRuby3-IN and ncVpr-mRuby3-IN complemented D116N HIV-1 when packaged *in trans* and rescued virus infectivity (**Figure 40F**). Taken together, these data demonstrate that ncVpr-mRuby3-IN retains the full functionality of Vpr-mRuby3-IN and could be used to produce a stable cell line.

5.3 Discussion

The dynamic nature of capsid uncoating and the involvement of virus-host protein interactions in promoting or inhibiting uncoating require an assay capable of rapid examination of virus particles in infected host cells to advance our understanding of this complex, required viral process. Capsid permeabilization provides a marker for the loss of capsid integrity and a gain-of-signal indicator of permeabilization facilitates accurate assessment and tracking of virus particles that have begun uncoating. Here, we provide the design, development, and initial validation steps for such a real time capsid permeabilization assay. While assay development is ongoing, the steps performed thus far serve to validate the approach taken and lay the necessary groundwork for assay completion and system integration testing.

A dual particle labeling system facilitates the tracking of all virus particles within infected host cells and allows imaging to focus upon regions of interest that are shown to contain particles, denoted by the persistent signal, in anticipation of permeabilization of these particles, as evidenced by the gain of the permeabilization signal. Subsequent loss of the permeabilization signal, upon RNase cleavage of the viral RNA genome, can likewise be tracked, with the persistent fluorescent IN signal remaining associated with the PIC, permitting visualization of the particle up to and into the nucleus. In this manner, virus particle permeabilization profiles can be paired with other characteristics of trafficking, host protein interactions, and infectivity to provide context for how permeabilization relates to these other processes.

Using bacteriophage coat proteins to direct fused reporters to target RNA containing sequence-specific binding loops is a decades old technology that, despite its longevity, continues to require optimization. This is particularly true in cases where a high degree of sensitivity is required to detect a signal with single-molecule resolution (563). Our initial efforts with MS2- and PP7-based constructs utilized preexisting reagents that lacked more recent improvements that might have alleviated the experienced shortcomings, such as increased inter-loop spacing and altered stem sequences that minimize inter-loop folding errors and improve binding site occupancy (563). The use of newer, brighter fluorescent proteins such as mNeonGreen (595) can also reduce the number of bound fluorescent proteins required for detection, offering further optimization of this system. While current efforts are focused on the Mango version of the capsid permeabilization assay, the availability of such upgrades to the MS2 system make it a viable approach to consider both as an alternative to Mango and for other potential imaging-based assays in the future.

Eliminating the MS2 coat protein and FAP fusion from the capsid permeabilization assay system by replacing MS2 RNA hairpin loops with Mango RNA aptamer loops not only simplifies the number of components required to detect capsid permeabilization but also minimizes the amount of foreign proteins being packaged into nascent virus particles. Virus infectivity is negatively impacted by increasing amounts of *trans*-packaged proteins. Reducing the amount of foreign protein required in the assay minimizes perturbation to the system being measured and makes the results obtained more likely to reflect the characteristics of unlabeled virus.

Modeling the capsid permeabilization signal on a two-component sensor overcomes the need to use a fluorescent protein to detect loss of capsid integrity by way of dispersion and loss of the fluorescent signal, which is the method used by other live cell capsid permeabilization assays. The challenge of this approach is the need to identify or design a fluorogen dye that will not permeate an intact capsid yet is diminutive enough that it can enter the capsid with only a small breach to the barrier. Both FAP and Mango systems offer alternatives in this regard. The developers of the dL5 FAP have produced an array of fluorogen dyes with varying chemical properties and molecular sizes (Marcel Bruchez, personal communication). The fluorogen dye bound by the Mango RNA aptamer, TO1-Biotin, is commercially available and multiple TO1 dye derivatives have also been created with varying sizes and chemical properties (569). These panels of dyes offer a foundation for screening for HIV-1 capsid impermeability. Hamiltonian replica exchange molecular dynamics (H-REMD) simulations to profile the translocation of molecules through the HIV-1 capsid hexamer pore can also be used for intelligent, model-driven screening of potential dye modifications that might render the dye capsid impermeable (Juan Perilla, personal communication), thereby directing any chemical synthesis efforts toward likely successful

candidates. Altogether, these resources and techniques increase the likelihood of finding or fabricating a capsid impermeable dye with either system.

Validation testing of the integrated Mango capsid permeabilization assay will, as with the assay design, take inspiration from the original EU assay, as well as from results obtained with the modified EU assay presented in **Chapters 3 and 4**. *In vitro* visualization of virus particles with and without cell lysate is expected to show an increase in permeabilization signal in the presence of cell lysate, which should be further increased in lysate from cells expressing rhTRIM5α or TRIMCyp (500). Cell-based imaging should demonstrate similar permeabilization kinetics to those previously observed with HIV-1_{NL4-3} and HIV-1_{LAI} viruses (**Chapter 3**), with hyperstable and hypostable CA mutants (500), and in the presence of CPSF6-358 (**Chapter 4**). As the Mango capsid permeabilization assay can function in fixed samples, it should also be possible to merge the Mango assay with the EU assay (i.e. treat NLdE-Mango virus with EU) in fixed samples and observe colocalized permeabilization signals. Alternatively, *in situ* hybridization assays with RNA probes can be performed. These and additional tests can be conducted to satisfactorily demonstrate the validity of the Mango assay results and permit its use in answering novel, biologically relevant questions.

5.4 Materials and Methods

Plasmids and Constructs

pcDNA3.1-MS2-eGFP, a kind gift from Dr. Jeremy Luban, was engineered to contain an AfeI restriction site immediately 5’ of eGFP via the Q5 (New England BioLabs) site-directed PCR

mutagenesis kit following manufacturers' instructions and verified by Sanger sequencing. pcDNA3.1-dL5-mCer, a gift from Dr. Marcel Bruchez, was engineered to contain an AfeI restriction site immediately 5' of dL5 and a stop codon and BamHI restriction site immediately 3' of dL5 via Q5 and verified by Sanger sequencing. pcDNA3.1-MS2-FAP was created by cloning the dL5 FAP from pcDNA3.1-dL5-mCer into pcDNA-3.1-MS2-eGFP using AfeI and BamHI restriction sites. pcDNA3.1-MS2-tagRFP was created by synthesis and cloning of the tagRFP gene (Genscript) into pcDNA3.1-MS2-eGFP using AfeI and BamHI restriction sites. pALTIP-MS2-eGFP, pALTIP-MS2-tagRFP, and pALTIP-MS2-FAP were created by cloning MS2-eGFP, MS2-tagRFP, or MS2-FAP, respectively, from pcDNA3.1 into pALTIP using XbaI and BamHI restriction sites.

pALTIP(hygro) was created by replacing the puromycin resistance gene in pALTIP with the hygromycin resistance gene from pcDNA5-TO-DsRed (596) (a gift from Dr. Anton Bennett, Addgene plasmid # 16340). pALTIP(hygro)-PP7-mCherry was created by amplifying and cloning PP7-mCherry (565) (a gift from Dr. Daniel Larson, Addgene plasmid # 61763) without the N-terminal NLS into pALTIP(hygro) using XbaI and BamHI restriction sites.

pcDNA3.1-Vpr-tagRFP-IN was created by cloning tagRFP into the previously described Vpr-IN fusion construct (597), a kind gift from Dr. John Kappes, using AleI and BspEI restriction sites. pcDNA3.1-Vpr-acGFP-IN was created by cloning acGFP into pcDNA3.1-Vpr-tagRFP-IN using AleI and BspEI restriction sites. pcDNA5-TO-Vpr-mRuby3-IN has been previously described (521). pcDNA5-TO-Vpr-FAP-IN was created by cloning the dL5 FAP from pcDNA3.1-MS2-FAP into pcDNA5-TO-Vpr-mRuby3-IN using AfeI and BamHI restriction sites. pALTIP-

Vpr-mRuby3-IN was created by amplifying and cloning Vpr-mRuby3-IN into pALTIP using NheI and XhoI restriction sites. pcDNA5-TO-ncVpr-mRuby3-IN was created by introduction of the Vpr mutations Q65R and S79A into pcDNA5-TO-Vpr-mRuby3-IN via Q5, which were verified by Sanger sequencing.

pFSWT-MS6, pFSWT-MS12, and pFSWT-MS24, kind gifts from Dr. Jeremy Luban, are lentiviral vectors containing 6, 12, or 24 bacteriophage MS2 coat protein binding loops, respectively. pFSWT-M12-P12 and pFSWT-P12-M12 were created by synthesis and cloning of a cassette containing 12 bacteriophage PP7 coat protein binding loops (565) (Genscript) into FSWT-MS12 on either the 3' or 5' side of the MS2 binding loop cassette, respectively. Lentiviral vector packaging plasmid pC-HelpΔvif, a gift from Dr. Klaus Strebel, has been previously described (598).

Cell Lines

HEK 293T cells, GHOST cells, and HeLa cells were maintained at 37° C with 5% CO2 in Dulbecco's Modified Eagle Medium (DMEM, Gibco) supplemented with 10% Fetal Bovine Serum (FBS, Atlanta Biologicals), 100 U/ml Penicillin, 100 µg/ml Streptomycin, and 2 mM L-Glutamine (Thermo Fisher). GHOST cells were additionally supplemented with 500 µg/ml Geneticin G418 (Gibco), 500 µg/ml Puromycin (Invitrogen), and 100 µg/ml Hygromycin B (Invitrogen). HEK 293T cell lines stably expressing MS2-eGFP, MS2-FAP, or PP7-mCherry were created by transfecting HEK 293T cells with pALTIP-MS2-eGFP, pALTIP-MS2-FAP, or pALTIP(hygro)-PP7-mCherry, respectively, which were placed under puromycin (MS2-eGFP and MS2-FAP) or hygromycin (PP7-mCherry) antibiotic selection after 48h and clonally expanded.

For stable expression of both MS2-eGFP and PP7-mCherry, HEK 293T cells stably expressing MS2-eGFP were transfected with pALTIP(hygro)-PP7-mCherry, placed under puromycin and hygromycin selection after 48h, and clonally expanded.

Viruses

HEK 293T cells were plated overnight and transfected with Lipofectamine 2000 (Invitrogen) using the following plasmids: for NLdE-luc virus the proviral plasmid pNLdE-luc (266), pL-VSV-G, and one of the fluorescently tagged IN plasmids described above; for FSWT virus one of the aforementioned FSWT lentiviral vector plasmids, the pC-Help packaging plasmid, pL-VSV-G, and one or more of the MS2- and/or PP7-based fluorescent constructs described above. In place of transfection, fluorescent constructs were also stably expressed in virus producer cells, as indicated in the main text. For virus containing MS2-FAP prepared with MG-Ester dye added to producer cells, MG-Ester (a kind gift of Dr. Marcel Bruchez) diluted 1:2,000 to 1:5,000 was added to cell culture media after 6-9h post-transfection. Supernatants were harvested 48h after transfection, filtered or centrifuged to remove cells, and stored in aliquots at -80° C. Producer cells were examined for fluorescent construct expression by flow cytometry, as described below. Viruses were titered by infection of GHOST cells as previously described (531) and quantified for p24 by HIV-1 p24 ELISA kit (XpressBio).

Subtilisin Digestion

Virus stocks and cell culture supernatants were incubated in digest buffer with and without addition of subtilisin as previously described (562). Briefly, 2X digest buffer (40 mM Tris-HCl, 2 mM $CaCl_2$, pH 8.0) with or without subtilisin (2 mg/ml) was added to virus and supernatants at a

1:1 ratio and incubated overnight at 37° C. Subtilisin was inactivated by addition of 2000X phenylmethylsulfonyl fluoride (PMSF) followed by 15m incubation at room temperature. Virus stocks and supernatants were purified by ultracentrifugation through a 20% sucrose cushion at 100,000 x g for 2h, resuspended in cell culture media, and stored in aliquots at -80° C.

Infectivity Assays

HeLa cells were plated overnight in 24-well plates, challenged with equal p24 amounts of virus for 2h, washed with phosphate buffered saline (PBS), and given fresh media. Virus infectivity was determined by luciferase production (Promega) after 48h using a 1450 MicroBeta TriLux microplate luminescence counter (PerkinElmer) or a Synergy2 Multi-Detection microplate reader (BioTek).

Measurement of Reverse Transcripts

HeLa cells were plated in 6-well plates and infected with 50 ng p24 of virus treated with DNase I (Roche) for 30m at 37° C. At indicated times post-infection, cells were washed with PBS, trypsinized, and pelleted. Control infections were performed in the presence of 150 nM of efavirenz or 25 nM of rilpivirine. DNA was extracted using the Blood Mini Kit (Qiagen). Early (RU5) and late (SST) HIV-1 reverse transcripts were measured by quantitative PCR as previously described (533).

Transfections

HeLa or HEK 293T cells were plated overnight in plastic 6-well plates (for flow cytometry samples) or 35 mm MatTek dishes with glass bottom inserts (for imaging samples) and transfected

with Lipofectamine 2000 or PolyJet (SignaGen Laboratories) using one or more of the aforementioned fluorescent construct plasmids. Cells had media replaced after 6-9h and were incubated for an additional 16-48h prior to examination by flow cytometry, fixed cell imaging, or live cell imaging.

Flow Cytometry

Adherent cells were washed with PBS, dissociated with Trypsin-EDTA (Gibco), quenched with 2% FBS in PBS, and fixed with fresh 2% paraformaldehyde (PFA) for 15m. Cells were examined on an LSR-II (BD Biosciences) or Accuri C6 (BD Biosciences) flow cytometer. Cells were gated by forward and side scatter (FSC/SSC) to isolate single cells, which were analyzed for expression of fluorescent constructs using FACSDiva (BD Biosciences), Accuri C6 Plus (BD Biosciences), or FlowJo (FlowJo) software.

TIRF Imaging

Viruses were examined for fluorescent construct packaging by placing a 20 µl droplet of virus stock on a glass MatTek dish insert and imaged by total internal reflection fluorescence microscopy on a Nikon Ti microscope equipped with a Nikon Apochromat TIRF 1.49 numerical aperture (NA) 100X objective and an iXon EM+ DU-897 electron multiplying charge-coupled device (EMCCD) camera (Andor Technology).

Synchronized Infection

HeLa cells were plated in glass bottom MatTek dishes overnight in FluoroBrite medium (Thermo Fisher Scientific) supplemented with 10% Fetal Bovine Serum, 100 U/ml Penicillin, 100 µg/ml

Streptomycin, and 2 mM L-Glutamine. Cells were chilled for 10m at 4° C prior to being inoculated with 100 µl virus, incubated at 4° C for 30m, washed with 37° C medium, and incubated at 37° C for the indicated time period prior to fixation and confocal imaging.

Cell Fixation and Staining

For samples including pre-fixation treatment with MG-Ester dye, cell media was replaced with media containing MG-Ester diluted 1:2,000 to 1:5,000 and cells were incubated for 30m at 37° C. Cells were washed three times with PBS, fixed with fresh 2% PFA for 15m, then washed three additional times with PBS. For samples including phalloidin staining, cells were permeabilized with 0.1% Triton X-100 for 20m, washed three times with PBS, stained with phalloidin conjugated with Alexa Fluor 488 diluted 1:250 in PBS for 30m, and washed three times with PBS. For samples including post-fixation treatment with MG-Ester dye, cells were stained with MG-Ester diluted 1:2,000 to 1:5,000 in PBS for 30m and washed three times with PBS. Cells were stained with Hoechst 33342 (Sigma) diluted 1:2,000 in PBS for 15m, washed three times with PBS, mounted with a glass coverslip using Gelvatol mounting media, incubated overnight at room temperature in the dark to cure, then stored in the dark at 4° C.

Confocal Imaging

Fixed and live cell images were collected on a Nikon A1 laser scanning confocal microscope. Z-stack images were collected at 0.5-µm steps up to 10 µm. For live cell imaging that included MG-Ester treatment, MG-Ester diluted 1:2,000 to 1:5,000 was added to cell culture media 30m prior to imaging.

5.5 Acknowledgements

We would like to thank Dr. Anton Bennett, Dr. Marcel Bruchez, Dr. John Kappes, Dr. Daniel Larson, Dr. Jeremy Luban, and Dr. Klaus Strebel for the aforementioned reagents; Callen Wallace and Jordi Yahr for technical assistance; and Drs. David Rueda and Peter Unrau for valuable discussions about RNA aptamers. This work was supported by the National Institutes of Health P50 grant GM082251 (SCW, ZA) and the National Institutes of Health T32 training grant AI065380 (DKF).

6.0 Conclusions and Future Directions

The HIV-1 capsid is involved in every post-entry step of the early virus life cycle, shields the viral genome from innate immune recognition, and is instrumental in permitting infection of nondividing cells. Each function of the capsid involves interaction with host factors that promote or impair viral infectivity. A greater understanding of how virus-host protein-protein interactions contribute to virus infectivity phenotypes and how those phenotypes differ among cell types and with different virus strains are needed to provide further insight into both viral and host cell processes and assist in the development of novel therapeutic targets. As the early life cycle progresses, the capsid must uncoat in a dynamic and directed, yet currently nebulous, process. New reagents and techniques are needed to assist in a more comprehensive examination of capsid uncoating to clarify this vital aspect of the virus life cycle.

In this dissertation, we sought to examine the influence of capsid from different HIV-1 strains on early post-entry virus life cycle steps in different cell types. We characterized the infectivity defect of the cell cycle dependent CA mutant N57A in the two widely used and closely related lab-adapted strains HIV-1_{NL4-3} and HIV-1_{LAI}. We analyzed the prevalence of NL4-3 and LAI amino acids in Gag sequences from subtype B isolates and from isolates across multiple subtypes to consider the broader implications of our findings with NL4-3 and LAI. We investigated the resistance of the transmitted/founder virus strain HIV-1_{CH040} to high doses of the capsid-targeting drug PF74 and explored the capsid stability and innate immune evasion phenotypes associated with this resistance.

We also endeavored to characterize the effect of disrupting host protein interactions with capsid on virus infectivity. We examined the formation of higher order complexes of the previously characterized CPSF6-358 in HIV-1 infected host cells and used CPSF6-358 as a tool to explore the interaction of CPSF6 with HIV-1_{NL4-3} and HIV-1_{LAI} bearing CA mutations N57A and N57A/G94D. We continued our characterization of N57A and N57A/G94D HIV-1 by investigating the effects of pharmacologic inhibition of CA binding to CypA and siRNA depletion of Nup153 on infection by viruses with these CA mutations in HIV-1_{NL4-3} and HIV-1_{LAI}.

Finally, we aimed to develop novel methods of visualizing capsid uncoating in real time in infected host cells. We leveraged the existing EU-based fixed cell capsid permeabilization assay to design a live cell capable capsid permeabilization assay. We performed extensive validation testing and optimization, which led to simplification of the assay design. We also modified the Vpr-mRuby3-IN virus particle labeling construct to create a version that would function with STED super resolution imaging and a version that could be used to create a stable expression cell line.

6.1 Conclusions

6.1.1 Aim 1: Determine how changes in the capsid of different HIV-1 strains influence post-entry, pre-integration steps of infection in different cell types

We showed that HIV-1 CA mutation N57A exhibits an infectivity defect that differs between common lab-adapted strains HIV-1_{NL4-3} and HIV-1_{LAI}, the magnitude of which is CA dependent.

Among the four CA amino acids that differ between NL4-3 and LAI, amino acid 83 is sufficient to modulate the N57A HIV-1 infectivity phenotype. Mutating this amino acid in HIV-1_{NL4-3} from leucine to the valine present in HIV-1_{LAI} (L83V) confers upon N57A HIV-1_{NL4-3} the attenuated infectivity defect observed in N57A HIV-1_{LAI}. Our findings were consistent across multiple human cell lines and in human CD4+ T cells and represent, to the best of our knowledge, the first observation of an attenuated N57A HIV-1 infectivity defect.

The magnitude of the N57A HIV-1 infectivity defects correspond with strain-specific defects in capsid permeabilization and reverse transcription. While both N57A HIV-1_{NL4-3} and N57A HIV-1_{LAI} exhibit a defect in nuclear entry, as evinced by a significant reduction in the generation of 2-LTR circles, only N57A HIV-1_{NL4-3} additionally exhibits a significant reduction in early and late reverse transcription products and accelerated capsid permeabilization compared with WT HIV-1. This suggests a fundamental difference in the nature of the N57A infectivity defects in these strains.

The N57A HIV-1 infectivity defect is partially rescued by the addition of the CA mutation G94D in HIV-1_{LAI} but not in HIV-1_{NL4-3}. The L83V CA mutation, while sufficient to shift the N57A HIV-1_{NL4-3} infectivity phenotype to that of N57A HIV-1_{LAI}, is not sufficient to induce partial rescue by G94D, but requires the additional mutation of at least one of the three other CA amino acids that differ between NL4-3 and LAI (amino acids 6, 120, and 208). This suggests that different mechanisms are responsible for the N57A HIV-1 infectivity phenotype and the partial rescue of N57A HIV-1 infectivity by G94D. The fact that three different CA mutations in three discrete locations within both CA functional domains can each individually, combined with L83V, induce

partial rescue of N57A HIV-1_{NL4-3} infectivity by G94D suggests each of these mutations might cause a change to the conformation of CA that could alter capsid stability and/or engagement of host factors. A change in CA binding to host factors, which may be differentially expressed in different cell types, could further explain cell type dependent differences in virus infectivity.

N57A HIV-1 is a useful tool for examining the mechanism through which HIV-1 is able to infect nondividing cells. CA has been shown to be the major viral determinant permitting cell cycle independent host cell infection (265, 506), and while other CA mutants lose this capability in certain cell types (268, 458), only N57A and the similar mutation N57S are rendered cell cycle dependent in all cell types tested (268, 275). Understanding the mechanisms by which the N57A HIV-1 infectivity defect is attenuated in HIV-1_{LAI} and partially rescued by G94D could provide further insight into why N57A is limited to cell cycle dependent infection in all cell types and, by extension, help clarify the mechanism by which WT HIV-1 infects nondividing cells.

An examination of over 40,000 Gag sequences from primary isolates demonstrated that there is strong conservation of CA amino acids across most CA positions, such that HIV-1_{NL4-3} and HIV-1_{LAI} bear a close resemblance to primary isolates at the vast majority of positions. The four CA residues that differ between HIV-1_{NL4-3} and HIV-1_{LAI} are among the most polymorphic CA residues, and the amino acids present in NL4-3 and LAI at these positions are highly prevalent among clinical isolates. This suggests that, similar to our observations with N57A, other CA-dependent phenotypes could differ among HIV-1 lab-adapted strains and clinical isolates.

N57A itself does not appear to be a clinically relevant CA mutation, as only one Gag sequence among 40,000 examined bore this mutation. However, expanding HIV-1 ART to include capsid-targeting therapies could increase its prevalence. The experimental drug PF74 targets capsid (409, 410), acts as a competitive inhibitor for capsid binding to host proteins CPSF6 and Nup153 (417-419) and, at high doses, impairs capsid stability (417-420). Virus resistant to PF74 was selected by *in vitro* adaptation, bearing either five (409) or four (508) CA mutations. Interestingly, N57A HIV-1 has also been shown to be resistant to PF74 (274, 419). With the attenuated N57A HIV-1_{LAI} infectivity defect modulated by CA amino acid V83, it is tempting to hypothesize that N57A could arise as a resistance mutation to capsid-directed therapies that target the same binding pocket as PF74 (417, 418) in virus strains that bear CA amino acid V83.

In extending our studies of lab-adapted strains to include clinically relevant strains, we showed that a single CA amino acid polymorphism in the transmitted/founder strain HIV-1_{CH040} enhances capsid stability compared with HIV-1_{LAI}. Mutating amino acid 216 from threonine to isoleucine (T216I) in HIV-1_{LAI} conferred similar increased capsid stability on HIV-1_{LAI} as observed with HIV-1_{CH040} CA. The T216I amino acid substitution further permits evasion of viral DNA host innate immune sensing, as demonstrated by a lack of type I IFN production in THP-1 cells infected with HIV-1_{CH040} or T216I HIV-1_{LAI}, but a robust dose-dependent induction of type I IFN upon infection with HIV-1_{LAI} or I216T HIV-1_{CH040}. This evasion of innate immune viral DNA sensing by HIV-1_{CH040} was unique among the panel of 10 transmitted/founder strains examined, but the presence of I216 in 1% of over 14,000 subtype B Gag sequences examined suggests this phenotype might be present in a small but appreciable subset of clinical isolates.

Collectively, these studies demonstrate that significant differences in HIV-1 infectivity phenotypes can be modulated by one or few CA amino acid substitutions. That such minor differences in CA sequences of closely related virus strains can appreciably alter infectivity phenotypes suggests that care must be taken in extrapolating results from studies that utilize single isolates and could help explain differences in results of similar studies that use different strains. These altered phenotypes might include differences in host factor interactions or could cause similar virus strains to exhibit different phenotypes in a cell type dependent manner. We explored these possibilities in the second aim of the dissertation.

6.1.2 Aim 2: Determine how disruption of interactions between HIV-1 capsid and host proteins alters virus infectivity

We demonstrated that the formation of CPSF6-358 higher order complexes in infected host cells is induced by and restricts WT HIV-1 infection. Formation of these complexes is induced by the specific recognition of WT capsid, as complexes do not form upon infection with N74D HIV-1, which does not bind to CPSF6, nor is N74D HIV-1 infection restricted by CPSF6-358. CPSF6-358 complexes were shown to associate with WT HIV-1 particles and lead to accelerated permeabilization of the HIV-1 capsid, suggesting the mechanism of infection restriction involves premature capsid permeabilization. However, our results also raise several questions about how this restriction might work, which are addressed under **Future Directions**. Using CPSF6-358 as a tool to interrogate interaction of CPSF6 with HIV-1_{NL4-3} and HIV-1_{LAI} CA, we showed that neither N57A HIV-1 nor N57A/G94D HIV-1 infection was restricted by CPSF6-358 with CA from either virus strain, indicating that the attenuated N57A HIV-1_{LAI} infectivity defect and the partial rescue

of N57A HIV-1_{LAI} infectivity by CA mutation G94D were not due to restoring N57A HIV-1 interaction with CPSF6.

We observed that inhibiting CypA binding to capsid by CsA treatment leads to more rapid formation of CPSF6-358 higher order complexes but does not alter N57A HIV-1 or N57A/G94D HIV-1 resistance to CPSF5-358 restriction. Examining capsid-CypA interaction without the presence of CPSF6-358, we demonstrated that N57A HIV-1 infectivity is dependent upon capsid interaction with CypA. Inhibiting CypA-capsid interaction restricts N57A HIV-1 infectivity at nuclear entry with both N57A HIV-1_{NL4-3} and N57A HIV-1_{LAI}. Further, G94D rescue of N57A HIV-1 infectivity is also dependent upon CA binding to CypA. This latter result was particularly surprising, given that G94D HIV-1 infects independently of CypA and in some cell types is dependent upon CsA treatment to inhibit CypA binding (438, 439, 457, 458). The dependence of N57A HIV-1 on CypA is reminiscent of N74D dependence on CypA (435), and raises several questions, such as: what is the mechanism by which CA mutations that render HIV-1 infection independent of CPSF6, Nup153, and Nup358 become dependent upon CypA? What does CypA binding provide to these CA mutants and why do they require it? How do these CA mutations render a CypA-independent mutation (e.g. G94D) dependent upon CypA?

It has previously been suggested that there might be a relationship between CypA and CPSF6 interacting with the HIV-1 capsid (436, 521) (Vineet KewalRamani, personal communication), perhaps with CypA shielding the capsid from CPSF6 engagement, regulating when and where CA-CPSF6 interaction may occur. Our study provides additional support for this model. The lack of a crystal structure for full length CPSF6, however, makes it difficult to

understand the overall manner in which full length CPSF6 engages CA and how its engagement might influence, and be influenced by, other CA-interacting host factors.

We also showed that N57A HIV-1 and N57A/G94D HIV-1 infect independently of Nup153 with both HIV-1_{NL4-3} and HIV-1_{LAI}, indicating that, similar to CPSF6, Nup153 interaction is not restored in either N57A HIV-1_{LAI} or N57A/G94D HIV-1_{LAI}. This suggests that the mechanisms behind the attenuated N57A HIV-1_{LAI} infectivity defect and G94D rescue of N57A HIV-1_{LAI} infectivity lie elsewhere.

6.1.3 Aim 3: Develop novel methods to visualize HIV-1 capsid uncoating in infected host cells in real time

We demonstrated that the concepts underlying the EU-based capsid permeabilization assay can be adapted for visualizing capsid permeabilization in infected host cells in real time. We presented the live cell capable MS2-FAP assay design utilizing bacteriophage MS2 coat protein-based RNA recognition/binding coupled with a FAP binding to a capsid impermeable fluorogen dye for indication of capsid permeabilization. We performed extensive validation and optimization of the FSWT/MS2 system for the production of infectious, fluorescently labeled virus particles, along with the creation and testing of the MS2-FAP fusion construct.

Technical challenges impaired packaging of a persistent fluorescent virus particle label, which led to the consideration of alternative labeling strategies and ultimately to the redesign and simplification of the assay. The Mango capsid permeabilization assay was presented, based on the use of the Mango RNA aptamer and a capsid impermeable fluorogen dye. We further upgraded

the Vpr-mRuby3-IN virus particle labeling construct for STED super-resolution imaging and stable cell line expression.

The Mango capsid permeabilization assay will permit the examination of capsid permeabilization in real time in infected host cells. It can be combined with fluorescent signals associated with viral or host proteins to demonstrate how capsid permeabilization relates to other viral and host processes. Importantly, it can help answer some of the outstanding questions associated with the initial steps of capsid uncoating, as evidenced by permeabilization, including when and where within the host cell uncoating begins, what viral and host factors are involved in initiating uncoating, and what effects various CA mutations, inhibition of host factor interactions, or pharmacological treatments have on the initiation of uncoating.

6.2 Future Directions

6.2.1 The N57A HIV-1 infectivity defect and related phenotypes

Our observations associated with the CA-dependent N57A HIV-1 infectivity defect and partial rescue by G94D revealed multiple related infectivity phenotypes that would benefit from further exploration and suggest several questions for future study. While each of these phenotypes might be produced by a separate mechanism, they should also be considered collectively, as similar techniques and avenues of inquiry might be used in pursuing each of these mechanisms. These questions are:

1. How does CA mutation L83V attenuate the N57A HIV-1_{NL4-3} infectivity defect?

2. How does CA mutation G94D partially rescue the N57A HIV-1_{LAI} infectivity defect?
3. How do CA mutations L6I, H120N, and G208A work in conjunction with L83V to effect N57A/G94D HIV-1_{NL4-3} rescue?

While we observed that adding L83V to N57A HIV-1_{NL4-3} confers the attenuated infectivity phenotype of N57A HIV-1_{LAI} (**Chapter 3**), no clear mechanism was identified, and there have been no published reports characterizing a role for amino acid 83 in CA. Preliminary electron microscopy (EM) of N57A HIV-1_{NL4-3} and N57A HIV-1_{LAI} suggests L83V might improve capsid stability, which could also explain the early reverse transcription defect and accelerated capsid permeabilization observed with N57A HIV-1_{NL4-3}. Additional EM should be performed and should include N57A/L83V HIV-1_{NL4-3} to specifically examine the contribution of the L83V CA mutation in the differences observed in preliminary EM images between N57A HIV-1_{NL4-3} and N57A HIV-1_{LAI}. N57A/L83V HIV-1_{NL4-3} could also be examined for reverse transcription products and perhaps capsid permeabilization kinetics with the hypothesis that the L83V CA mutation corrects these defects observed in N57A HIV-1_{NL4-3}.

Our findings that the addition of CA mutation G94D partially rescues the N57A HIV-1_{LAI} infectivity defect but not the N57A/L83V HIV-1_{NL4-3} infectivity defect, despite both viruses having similar attenuated infectivity defects (**Chapter 3**), indicate that the G94D rescue is likely accomplished by a different mechanism than the attenuation of the N57A HIV-1_{LAI} infectivity defect. Mutating any one of the other three CA amino acids that differ between NL4-3 and LAI in addition to L83V results in partial rescue of N57A HIV-1_{NL4-3} infectivity by G94D, further complicating the characterization of these phenotypes. Collectively, however, two principle

scenarios should be considered in searching for a mechanism: changes to host factor interactions and changes to capsid stability and/or conformation.

Our examination of host factor interactions (**Chapter 4**) showed that N57A HIV-1_{LAI} infection is independent of CPSF6 and Nup153 interaction similar to N57A HIV-1_{NL4-3} infection, indicating that restoration of interaction with either of these host factors is not involved in attenuating the N57A HIV-1_{LAI} infectivity defect. Similar observations showed that N57A/G94D HIV-1 infection is also independent of CPSF6 and Nup153, demonstrating that neither of these host factors are involved in the G94D rescue of N57A HIV-1 infectivity. However, it should be noted that these studies were conducted only in HeLa cells. The most robust rescue of N57A HIV-1_{LAI} infectivity by G94D was observed in GHOST cells (**Chapter 3**), in which these experiments should be repeated. CD4+ T cells should also be examined, as they are the primary target of HIV-1 infection.

Other host protein interactions could be altered to produce these infectivity phenotypes. In addition to CPSF6 and Nup153, N57A HIV-1 also infects independently of Nup358 (270), which should be similarly examined in HeLa, GHOST, and CD4+ T cells. Nup358 includes a cyclophilin homology domain (Nup358Cyp) that has been shown to bind CA *in vitro* (270, 271), though the role of Nup358Cyp binding to CA in host cells is debated (270, 271, 480). While G94D HIV-1 infects independently of CypA (438, 439), in the context of N57A/G94D HIV-1_{LAI} CypA binding is necessary (**Chapter 4**). This raises the possibility that N57A/G94D HIV-1_{LAI} infection might require CA interaction with Nup358Cyp. It is also possible that G94D might provide N57A HIV-1_{LAI} access to an alternative pathway for infecting dividing cells. This idea is not unreasonable, as

a similar cell cycle dependent CA mutation, N57S, which also does not infect nondividing cells, relies on a particular set of nucleoporins for infection (269). Such alternative pathways have been proposed for a variety of HIV-1 CA mutant viruses that infect independently of one or more of the host factors that comprise the established, "canonical" nuclear import pathway (267, 270). However, identification of host factors belonging to these hypothesized noncanonical routes has been elusive.

Additional insight into the mechanism behind one or more of these infectivity phenotypes could be gained from collaborative efforts examining HIV-1 capsid assemblies by solid state nuclear magnetic resonance (SSNMR) spectroscopy (599), which could reveal differences in capsid stability or conformation. Previous studies have demonstrated that the capsid possesses fluid, dynamic conformational flexibility that is necessary for both formation of a stable assembled capsid and interactions with host factors (600). We are working with collaborators to examine assemblies of capsid from N57A HIV-1 and N57A/G94D HIV-1 from both NL4-3 and LAI strains to determine if any of these CA mutations induce changes to this conformational flexibility that might inform on a mechanism behind the observed phenotypes.

SSNMR spectroscopy can also help answer the related questions of how inhibiting CypA binding to CA impairs N57A HIV-1 nuclear entry and N57A/G94D HIV-1 infectivity. Prior studies have examined HIV-1 capsid assemblies in conjunction with bound CypA and have shown that CypA binding significantly attenuates the flexibility and mobility of the CypA binding loop of CA (601). The G94D CA mutation was also demonstrated to exhibit a similar loss of flexibility

without CypA bound (601). The N57A CA mutation in HIV-1_{NL4-3} and/or HIV-1_{LAI} might alter the observed CypA binding loop flexibility.

6.2.2 CPSF6-358 restriction

The formation of CPSF6-358 higher order complexes in association with HIV-1 infection and the commensurate acceleration of capsid permeabilization (**Chapter 4**) provides further insight into how CPSF6-358 restricts infection, but also poses additional questions. Mechanistically, how does CPSF6-358 restrict infectivity? We noted that the accelerated capsid permeabilization is similar to that observed with rhTRIM5α restriction (500). Does CPSF6-358 pull the capsid apart in a similar manner, or does the capsid stay together, albeit more loosely or in a larger structure? What is the basis of CPSF5-358 aggregate formation in cells? When purified, CPSF6-358 was observed to former oligomers in the absence of HIV-1 (521); however, this was not observed in HeLa cells stably expressing CPSF6-358-eGFP (**Chapter 4**), though we cannot rule out oligomers that incorporate too few copies of eGFP to be observed with confocal imaging. Does capsid nucleate aggregation of CPSF6-358 simply by offering numerous binding sites for high avidity or do CPSF6-358 monomers also bind to one another similar to oligomerization during purification? Does CPSF6-358 form any sort of lattice structure around the capsid akin to rhTRIM5α (535)? Answering these questions will likely require structural biology studies to more closely examine the manner in which CPSF6-358 engages capsid and, potentially, itself. A previous study used SSNMR to characterize the dynamic interaction of capsid with rhTRIM5α and observed global rigidification and loss of flexibility of the capsid upon engagement of rhTRIM5α, leading to conformational changes that altered capsid subunit interfaces and destabilized the capsid lattice

(602). A similar examination of capsid assemblies with CPSF6-358 might yield important clues as to what engagement of CPSF6-358 does to capsid flexibility and structure.

One key manner in which rhTRIM5α and CPSF6-358 restriction of HIV-1 infection differ is that rhTRIM5α restricts prior to reverse transcription (539) whereas CPSF6-358 does not prevent the completion of reverse transcription (266), which suggests different mechanisms of restriction. Interestingly, rhTRIM5α restriction is associated with the proteasomal degradation pathway, the inhibition of which alleviates the reverse transcription block imposed by rhTRIM5α, but still results in restriction of HIV-1 infection at nuclear entry (603). Impairing proteasomal degradation also permits visualization of HIV-1 associated with rhTRIM5α in cytoplasmic bodies (504), reminiscent of HIV-1 associated with CPSF6-358 puncta (**Chapter 4**). This suggests that the direct interactions of CPSF6-358 and rhTRIM5α with capsid could be similar, with rhTRIM5α additionally directing engaged virus particles toward proteasomal degradation and earlier restriction. This raises additional questions about CPSF6-358 restriction: what happens with CPSF6-358/capsid complexes after formation? Is there directed proteasomal degradation like with rhTRIM5α? Do these complexes lead to cytoplasmic sensing of capsid contents and innate immune activation? Finally, how similar is CPSF6-358 interaction with capsid to that of full length CPSF6? In other words, does full length CPSF6 engage capsid in the same manner as CPSF6-358 except perinuclearly as opposed to cytoplasmically, with localization being the determinant of whether that engagement promotes or restricts infection? Understanding the dynamics of CPSF6-358 interaction with capsid could inform on how endogenous CPSF6 may promote virus infection.

6.2.3 The Mango capsid permeabilization assay and future upgrades

Work continues on the development of the Mango capsid permeabilization assay with validation testing and initial use planned as previously described (**Chapter 5**). Once operational, there are several modifications or upgrades that can be considered to extend the capabilities of the assay. After identifying one or more small, capsid impermeable fluorogen dyes to identify the earliest stages of capsid permeabilization, we can form some idea of the size of the breach in the capsid using differently sized dyes that require larger openings to enter the core. Comparing the kinetics of capsid permeabilization with these different sized dyes can provide clues as to the nature of the openings in the capsid, e.g. whether large chunks or individual hexamers are removed, or if permeabilization rather results from gaps opening up between hexamers, etc.

Being able to observe capsid permeabilization in real time is more useful when permeabilization can be associated with other characteristics of viral infection. An important consideration is whether or not the observed capsid permeabilization phenotype is associated with successful infection. Many virus particles are destined for non-infectious pathways (195, 286) and one determinant of infectious potential for a virus particle might be when, where, and/or how it uncoats. To ascertain whether a particular virus particle leads to successful infection, some form of reporter functionality can be encoded in the viral genome, which is expressed after integration. This is, for example, how the NLdE-luc reporter virus used throughout this dissertation functions. In designing the Mango capsid permeabilization assay, the firefly luciferase reporter gene was replaced with the Mango RNA aptamer. However, if reporter functionality can be retained, it would be possible to observe infected cells over an extended period of time as the reporter gene becomes expressed, thereby revealing virus particle events that led to successful infection.

Designing a reporter virus that contains NanoLuc (604) or mNeonGreen (595) in addition to the Mango RNA aptamer would minimize the size increase of reporters compared with the existing NLdE-luc reporter virus, thereby minimizing the impact of the reporters on virus infectivity. Combining capsid permeabilization characteristics with a measure of success or failure in infection might reveal specific capsid permeabilization phenotypes that are associated with infection.

Using the Mango capsid permeabilization assay, as reverse transcription proceeds, RNase H degradation of the viral RNA genome would result in disruption of the RNA aptamer structure and concomitant loss of fluorescence. While this might limit the amount of time during which the capsid permeabilization signal is visible, it can also serve as the basis for a variation of the capsid permeabilization assay that focuses instead on the kinetics of reverse transcription. Altering the location of the RNA aptamer loops within the viral genome should also alter the duration of the capsid permeabilization fluorescent signal, providing information on the rate at which reverse transcription is proceeding, in relation to the time at which capsid permeabilization occurs. To separately examine reverse transcription kinetics from capsid permeabilization, the fluorogen dye could also be pre-loaded onto the RNA aptamer by producing virus in the presence of the dye in addition to treating the infected host cells with dye. To provide greater detail of reverse transcription kinetics, multiple sets of RNA aptamer loops could be incorporated at different locations within the viral RNA genome, utilizing different RNA aptamers that bind fluorogen dyes of different wavelengths. One important consideration in choosing where to potentially place RNA aptamer loops in the viral RNA genome is the critical role played by RNA secondary structure in HIV-1 replication (328, 605, 606), including several highly conserved structural motifs (607, 608) that should not be disrupted. Alternatively, a lentiviral vector system could be employed for a

reverse transcription assay, permitting a wider range of locations within the vector genome to be targeted for RNA aptamer loop placement.

The goal of specifically characterizing the loss of CA from the capsid during uncoating is fraught with technical challenges. The ability to quantitatively and sensitively measure CA loss requires the capability to either reliability and broadly label CA directly or has to use an orthogonal technique for quantifying the amount of CA at different time points. Also challenging is determining not only what amount of CA has been lost but from where on the capsid. Given the small size of the capsid and the resolution limit of confocal technologies, any imaging-based solution would likely require the use of super-resolution light imaging techniques and/or EM. EM has been used successfully to examine HIV-1 infected cells (219), particularly when combined with fluorescent light microscopy via correlative light electron microscopy (CLEM) and cryo-electron tomography (cryo-ET, cryo-CLEM) (505, 609, 610). The Mango capsid permeabilization assay is designed to be compatible with super-resolution light imaging and CLEM. An extension of the assay could be used in conjunction with these imaging techniques to permit the EM interrogation of virus particles that have become permeabilized, offering insight into the structure of the permeabilized capsid.

6.3 Final Thoughts

HIV-1 research is performed against the backdrop of the ongoing AIDS epidemic. Advances in our knowledge about the virus should also be examined in terms of how those gains can be leveraged in a way that might ultimately result in clinical benefits. Despite the miraculous

improvements in mortality conferred by adherence to ART, the continued development of drug resistance mutations and poorly tolerated side effects fuel the need for new pharmaceuticals and for new potential therapeutic targets. The viral capsid plays multiple critical roles in the virus life cycle and is unlike any host protein or complex, yet is genetically fragile, making it a strong candidate for antiviral intervention.

Through this dissertation we have added to the growing body of knowledge about the HIV-1 capsid, about capsid interactions with host factors, and how capsid mutations and differences in viral strains and cell types can alter virus infectivity. We have additionally developed reagents and techniques to improve our capabilities at examining the capsid and furthering our understanding of how this protective shell comes undone. Finally, we have suggested, through our observations of significantly different infectivity phenotypes among closely related virus strains and our analysis of capsid sequences of primary isolates, that care must be exercised when extrapolating the applicability of infectivity phenotypes observed in single isolates to broader virus populations. It is our sincere hope that these contributions might in some small part progress our efforts at combatting HIV-1 infection and AIDS and help bring us one step closer to ending this worldwide epidemic.

Appendix A A Novel Phenotype Links HIV-1 Capsid Stability to cGAS-Mediated DNA Sensing

Mohammad Adnan Siddiqui[1], Akatsuki Saito[1], Upul D. Halambage[2], Damien Ferhadian[1], Douglas K. Fischer[3], Ashwanth C. Francis[4], Gregory B. Melikyan[4,5], Zandrea Ambrose[3], Christopher Aiken[2], and Masahiro Yamashita[1]

[1]Aaron Diamond AIDS Research Center, New York, New York, USA

[2]Department of Pathology, Microbiology and Immunology, Vanderbilt University Medical Center, Nashville, Tennessee, USA

[3]Department of Microbiology and Molecular Genetics, University of Pittsburgh School of Medicine, Pittsburgh, Pennsylvania, USA

[4]Department of Pediatrics, Emory University, Atlanta, Georgia, USA

[5]Children's Healthcare of Atlanta, Atlanta, Georgia, USA

This appendix is a manuscript in revision included in its entirety in support of data presented in Chapter 3.

A.1 Introduction

The capsid of HIV-1, a cone-shaped shell, is made of capsid protein (CA) subunit and encases essential components, such as two copies of viral RNA and enzymes reverse transcriptase (RT)

and integrase (IN) (324, 611). Upon delivery into the cytoplasm, the viral capsid engages the host cytoskeleton network to migrate toward the nucleus, where the reverse transcribed viral DNA is inserted into the host chromatin (192, 503, 612). During this early phase of the viral replication cycle, the HIV-1 core transforms itself to physically distinct sub-viral structures, called reverse transcription complexes (RTCs) and pre-integration complexes (PICs), through a process called uncoating or capsid disassembly (285, 286). Uncoating, a temporally and spatially regulated process, results in the shedding of CA subunits from the core.

Molecular and mechanistic details of capsid disassembly remain incompletely understood, but a consensus view is that uncoating is exquisitely controlled by both intrinsic capsid stability and extrinsic elements, including capsid-binding cellular factors. Intrinsic capsid stability is governed by interactions between CA subunits that generate CA oligomers (hexamers and pentamers), the basic units of the viral capsid that interact with each other to form a capsid lattice in a fullerene cone (191, 613, 614). The N-terminal domain (NTD) and the C-terminal domain (CTD) of CA are linked with a short stretch of a flexible linker and involved in the assembly of viral capsids. Interactions between individual CA subunits, which are mediated by NTD-NTD, NTD-CTD and CTD-CTD interfaces (191), are critical for capsid stability (228, 430, 523, 615). To what extent each of these interfaces contributes to capsid stability is incompletely understood. As described above, capsid stability and uncoating are also regulated by cellular factors. At least a dozen host proteins are known to directly bind to the viral capsid (reviewed in (388)), although how each of the molecules either stabilizes or destabilizes the viral capsid is controversial. Nonetheless, a significant role played by capsid-interacting cellular proteins is well illustrated by the rhesus monkey variant of TRIM5α (539), a potent antiviral molecule that interacts with the

viral capsid and accelerates uncoating to prevent reverse transcription and, as a result, severely limits viral infection. In addition, a small molecule called inositol hexakisphosphate (IP_6), which has been recently shown to be a co-factor for HIV-1 assembly (425), displays the ability to regulate capsid stability (616).

Proper disassembly of the capsid is critical for nearly every step during the early phase of HIV-1 replication, up until viral integration into the host chromosomes. For instance, defects of CA mutations in viral DNA synthesis suggest a role for uncoating in the progression of reverse transcription (228, 617-619). These functional interplays are not unidirectional; post-entry steps also affect the progression of capsid disassembly. A notable example is the effect of reverse transcription on the extent and kinetics of uncoating (490-493). Functional roles of CA and its shedding from intracellular viral complexes are extended to the nucleus (272, 298, 472, 620, 621). Capsid is the major determinant for HIV-1 nuclear entry (266, 267, 270, 273, 274, 284, 622) and critically contributes to the unique preference of HIV-1 integration targeting (270, 301, 483, 623, 624). Thus, viral uncoating can be viewed as a complex series of events in which the viral capsid and its matured complexes shed CA subunits both in the cytoplasm and nucleus.

Another function of the viral capsid that has been proposed in the literature is to shield nascent viral DNA from innate immune sensors (625-627). HIV-1 reverse transcription takes place in the cytoplasm and thus viral DNA can be recognized by cytosolic DNA sensors to trigger an innate immune response (526). Cytoplasmic sensing of HIV-1 DNA appears to be context dependent: for example, HIV-1 infection of monocyte-derived macrophages does not appear to induce a robust innate immune response (628, 629). Nonetheless, macrophages are equipped with

functional cytosolic DNA sensing machinery, which consists of cyclic guanosine monophosphate–adenosine monophosphate synthase (cGAS) and the adaptor protein stimulator of interferon genes (STING), as well as other regulators and downstream effectors, such as interferon-gamma inducible factor 16 (IFI16), polyglutamine binding protein 1 (PQBP1), TANK-binding kinase 1 (TBK-1) and interferon regulatory factor 3 (IRF3) (526, 630, 631). The lack of a robust type I interferon (IFN) response upon HIV-1 infection of macrophages can be explained by the presence of the cytosolic exonuclease three prime repair exonuclease 1 (TREX1) (629), as well as negative regulation of host factors by viral accessory proteins (reviewed in (255)). Additionally, it has been proposed that the capsid cloaks viral DNA from being sensed by cytosolic DNA sensors (257, 632). Alterations in CA interactions with the host cellular factors cyclophilin A (CypA) and cleavage and polyadenylation specificity factor subunit 6 (CPSF6) triggered innate immune responses and IFN production in macrophages (257). The involvement of CypA in innate sensing of HIV-1 DNA was also extended to monocyte-derived dendritic cells (632).

Capsid stability is the major intrinsic property that regulates uncoating (285, 286). HIV-1 capsid stability, which is dictated by fine-tuned interactions between individual CA subunits, must be optimal to ensure proper uncoating that is critical for viral replication (228). Our current understanding of HIV-1 capsid stability is largely built upon biochemical characterization of viral cores prepared *in vitro* (228). Core yield, the quantity of CA that is associated with isolated cores, is a standard measure for capsid stability (633). A similar core isolation technique can be combined with microscopy-based observations of physical associations of CA with core particles (525). There is general agreement between biochemical and microscopic techniques on the behavior of representative CA mutants with altered capsid stability, although some discrepancy has been also

noted (492, 500, 525). An inevitable drawback of these powerful techniques is their laborious experimental procedure that precludes large-scale studies of various mutants or diverse naturally occurring variants. A complementary approach, such as a recently described assay exploiting the exposure of a virion-associated mRNA reporter (502), is needed to further deepen our understanding of capsid stability.

In the present work, we exploited PF-3450074 (PF74), a capsid-binding small-molecule compound (409), as a tool to study capsid functions. PF74 was shown to destabilize the viral capsid in certain assay systems (410, 418, 420, 500, 634), although PF74 did not affect capsid stability, and even stabilized cores, in imaging-based assays (525, 620, 635). We used the capsid-targeting activity of PF74, together with cell-free and cell-based assays, to reveal a novel naturally occurring phenotype of capsid stability that drastically alters cGAS-dependent sensing of HIV-1 DNA and highlights an underappreciated capacity of HIV-1 to accommodate phenotypic variation in the viral capsid.

A.2 Results

A.2.1 Resistance to effects of high doses of PF74

In the present study, we utilized PF74 to study capsid functions. A unique dose-response curve of PF74 (**Figure 41A**) corresponds to two distinct mechanisms of action in which low doses block a step following reverse transcription whereas high doses block reverse transcription (409, 410, 417, 419, 420, 472, 620, 634). Among a panel of CA mutants examined for their sensitivity to PF74

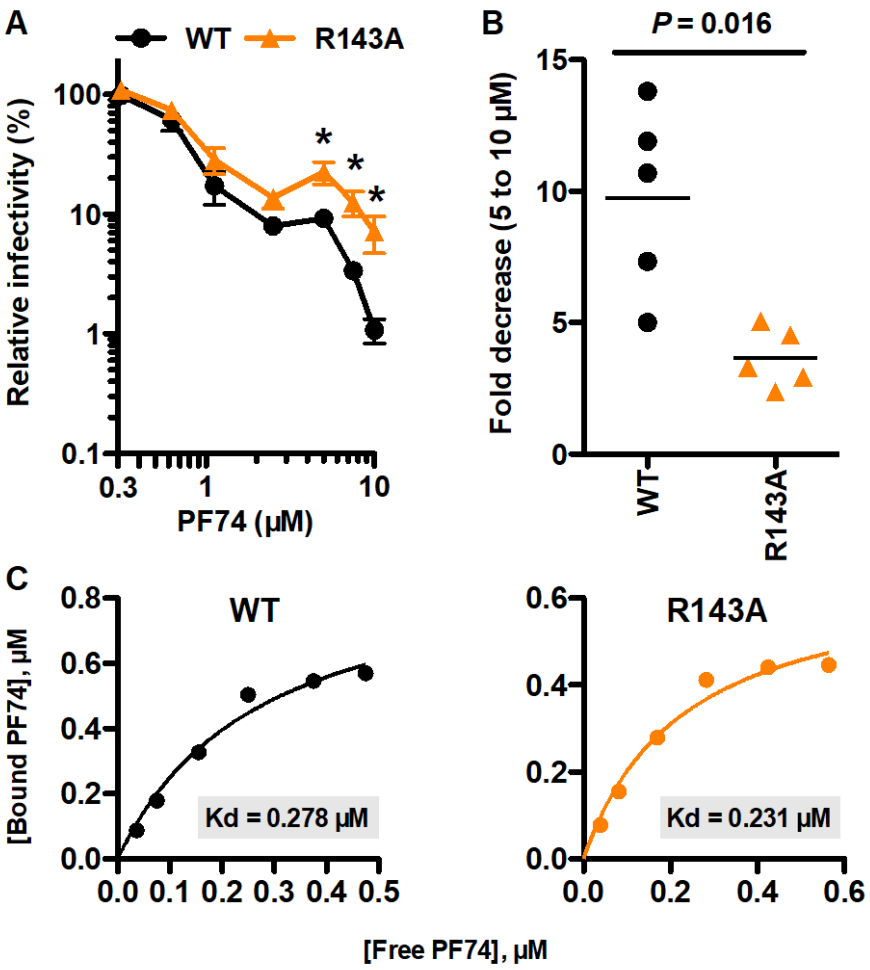

Figure 41. A CA mutation confers resistance to antiviral activity at high PF74 concentrations, while maintaining PF74 binding. (A) GFP-encoding reporter virus carrying either the WT or R143A capsid were used to infect HeLa cells transduced with the empty LPCX vector with increasing amounts of PF74. Relative infectivity was calculated by setting the number of GFP-positive cells without PF74 treatment as 100%. The mean values were obtained from five independent experiments. Error bars denote the standard error of mean (SEM). *P < 0.05 (calculated with the unpaired student t test). (B) The degree of PF74-mediated inhibition at high drug doses was quantified by the results shown in panel A. Individual dots correspond to data points from each experiment. Results were analyzed with the unpaired student t test. (C) The affinity of PF74 for WT and R143A hexamers was determined using equilibrium dialysis. One representative data from two independent experiments with similar results is shown here. A Kd value for R143A in the other experiment was 0.244 μM.

(unpublished results), the R143A mutant was distinct because its difference from the WT virus of the LAI strain was more pronounced at high drug concentrations (**Figure 41A**). Namely, antiviral activity by PF74 at 2.5, 5 and 10 μM against the R143A mutant was significantly less than for the WT virus (**Figure 41A and 41B**). However, when PF74 dissociation constants were measured using equilibrium dialysis, the R143A substitution did not markedly alter the affinity of CA hexamers to PF74 (**Figure 41C**). This finding suggests that PF74 can bind to the capsid of the R143A virus, although this idea should be viewed with caution as stabilized CA hexamers, but not cores, were used in the binding assay.

The R143A mutant specifically resisted antiviral activity at high PF74 concentrations, even though it did not exhibit substantially altered CA hexamer affinity for PF74 (**Figure 41**). As high drug concentrations were shown to destabilize the viral capsid in certain assays (410, 418, 420, 500, 634), one possible mechanism of the observations is that the R143A mutant neutralizes the core-destabilizing activity by PF74. To test this hypothesis, we examined effects of PF74 on purified HIV-1 cores using a biochemical approach (228). In control experiments performed to validate our experimental system, we observed that addition of a detergent, Triton X-100, in the core isolation procedure led to the appearance of a broad peak of reverse transcriptase (RT) in dense fractions (data not shown). The density of one of the fractions (1.25 g/ml) was within the range of densities known to contain retroviral cores in previous studies (228, 636-638). Furthermore, two representative CA mutant viruses that have either hyperstable (E45A) or unstable cores (Q219A) (228) behaved as expected in our experimental system (data not shown).

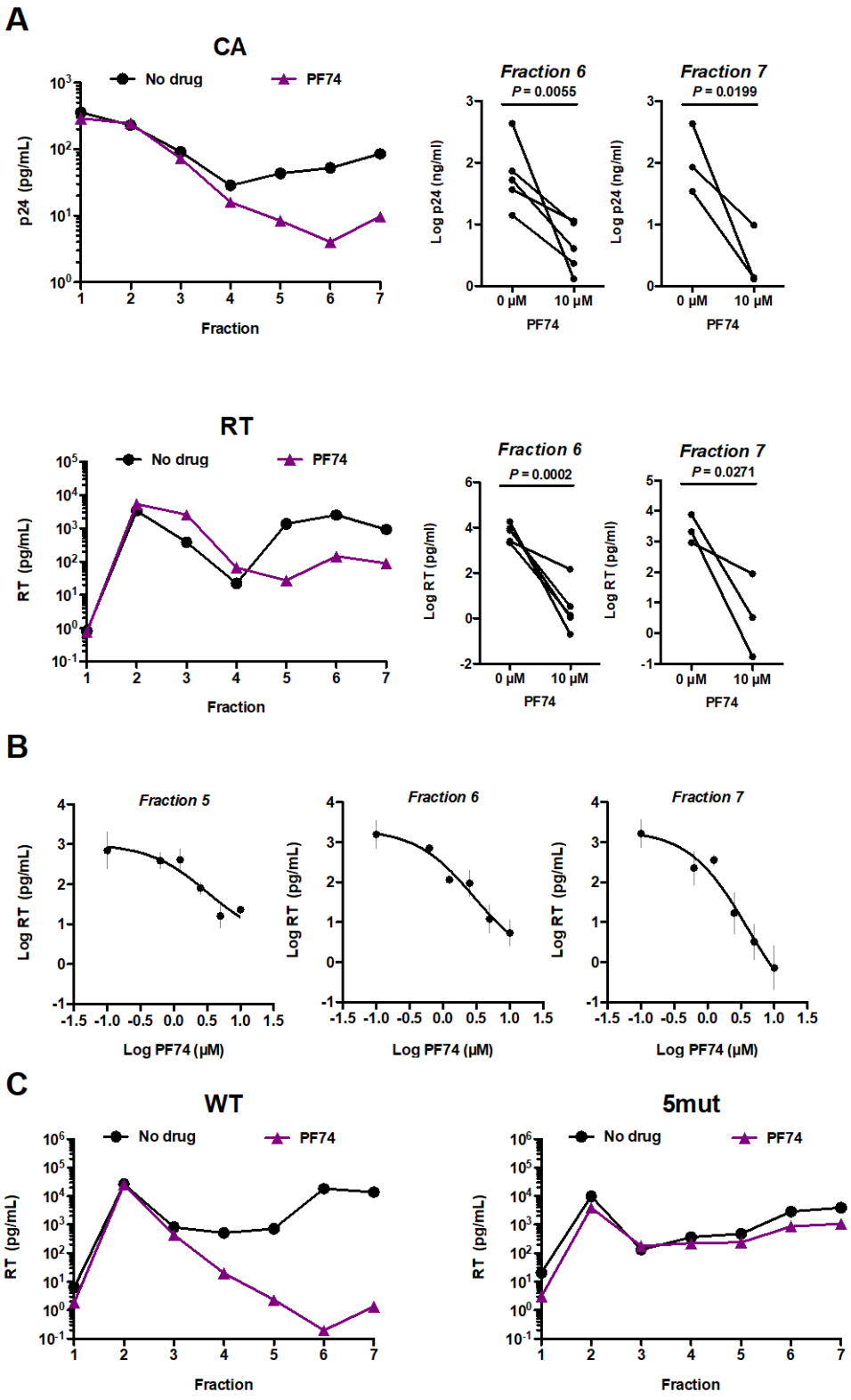

Figure 42. PF74 reduces CA and RT molecules in core-containing fractions. (A) HIV-1 cores were separated on a discontinuous sucrose gradient after incubation in the presence or absence of 10 µM of PF74 at 37 ºC for one hour.

The amount of CA (top panels) and RT (bottom panels) in each fraction was measured by p24 CA ELISA and the SG-PERT assay, respectively. A representative profile from two independent experiments is shown on the left. Additional experiments were performed to measure CA and RT for core-containing fractions 6 and 7. Each dot represents the measured amount in a single experiment. Dots that represent results originating from the same experiment are connected with lines. Differences between the two conditions were studied with the unpaired t test. (B) Virus particles were treated with increasing amounts of PF74 and subjected to the core isolation procedure. The amount of RT molecules in the indicated fractions was measured by the SG-PERT assay. The mean of three independent experiments is shown with error bars (shown in gray) denoting SEM. Best-fit curves were generated by nonlinear regression using log-transformed data. (C) A drug-resistant mutant (5mut) was compared to the WT virus as describe above. The data shown here is representative of two independent experiments.

Consistent with previous observations (410), pre-treatment of the virus with PF74 reduced the level of p24 CA in fractions that contain cores (**Figure 42A**, fractions 6 and 7). Furthermore, the quantity of RT molecules associated with similar high-molecular-weight complexes was substantially decreased upon PF74 treatment (**Figure 42A**, bottom panels) in a dose-dependent manner (**Figure 42B**). In contrast, the amount of RT in the same dense fractions was barely changed for the PF74-resistant mutant 5Mut, which encodes five amino acid substitutions (Q67H, K70R, H87P, T107N and L111I) (409, 410) (**Figure 42C**). Thus, consistent with the previous work (410), PF74 appears to destabilize the viral capsid in this particular assay.

We next asked how the R143A mutation affects the sensitivity to the capsid-destabilizing activity of PF74 (**Figure 43**). Having shown that PF74 decreases core-associated CA and RT molecules (**Figure 42**), we utilized the PCR-based RT assay in the following experiments, as it is more sensitive than the CA p24 ELISA assay. Consistent with the cell-based assay in which

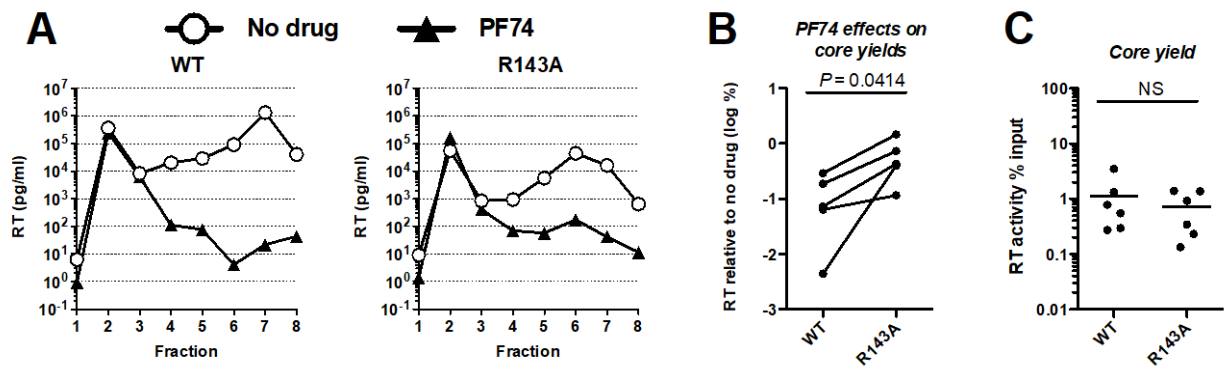

Figure 43. The R143A mutant virus partially resists the core-destabilizing activity of PF74. (A) Core yield of the R143A mutant was compared to that of the WT virus in the presence or absence of 10 μM PF74 by the method described in the legend to Figure 42. A representative result is shown from five independent experiments. (B) Core-destabilizing activity of PF74 against two viruses is depicted as the amount of RT in fraction 6 treated with 10 μM PF74 relative to no drug treatment. The data shown here are results of five independent experiments and were examined using the two-tailed paired t test. (C) Core yields are shown as the RT amount in fraction 6 normalized to the amount of input used in each experiment. Data was compiled from six experiments and analyzed by the two-tailed unpaired t test.

R143A was resistant to antiviral activity by high PF74 doses (**Figure 41A and 41B**), the R143A mutation partially neutralized the core-destabilizing activity of PF74 (**Figure 43**). Specifically, the magnitude of PF74-mediated reduction of RT molecules in core-containing fractions (fractions 6 and 7) was smaller for the R143A mutant as compared to the WT virus (**Figure 43A**). The difference was statistically significant across five independent experiments, although the magnitude of decrease varied between these experiments (**Figure 43B**). The amount of RT in fraction 6 in the absence of the drug, which appeared to correlate with capsid stability, did not differ between the two viruses (**Figure 43C**). These observations suggest that the R143A virus resists the antiviral activity of PF74 by counteracting its core-destabilizing activity.

A.2.2 A naturally occurring genetic polymorphism at the trimeric hexamer interface confers resistance to PF74-induced core destabilization

The results of our studies of the lab-generated mutant R143A uncovered a novel capsid-specific phenotype. We extended our study to primary strains for understanding natural phenotypic variation of the HIV-1 capsid. Ten T/F viruses (522), which were assessed for their sensitivity to PF74, displayed considerable variations in dose-response curves against PF74 (data not shown). Among them, one strain (CH040) was distinct because its resistance to antiviral activity was more pronounced at high drug concentrations, a phenotype similar to that of the aforementioned R143A mutant (**Figure 41**). Transfer of the DNA sequence encoding the entire CA domain of the Gag protein from CH040 to the LAI backbone conferred this phenotype in which PF74 lost its potency at high, but not low, drug concentrations (**Figure 44A**). Because the LAI-based chimeric virus carrying CA from CH040 was very similar to the R143A mutant virus in their PF74 resistance profile, we reasoned that the capsid of CH040 resists PF74-mediated inhibition by neutralizing its capsid-destabilization activity. To test this idea, PF74 effects on the core yield were examined by using the same "spin-through" procedure (**Figure 44B**). Similar to the R143A virus, the chimeric virus carrying CA from CH040 partially neutralized the core-destabilizing activity by PF74, as it yielded a higher level of RT molecules in core-containing fractions than the WT LAI strain (**Figure 44B**) with statistical significance (**Figure 44C**). The CH040 capsid had a two-fold higher yield than the LAI capsid in the absence of PF74 (**Figure 44D**).

The CA-coding sequence of CH040 differs from that of LAI (**Figure 45A**). Among nine amino acid differences between these two sequences, a threonine-to-isoleucine change (T216I; from LAI to CH040) was noticeable, as this change is located at the trimeric interface for CA

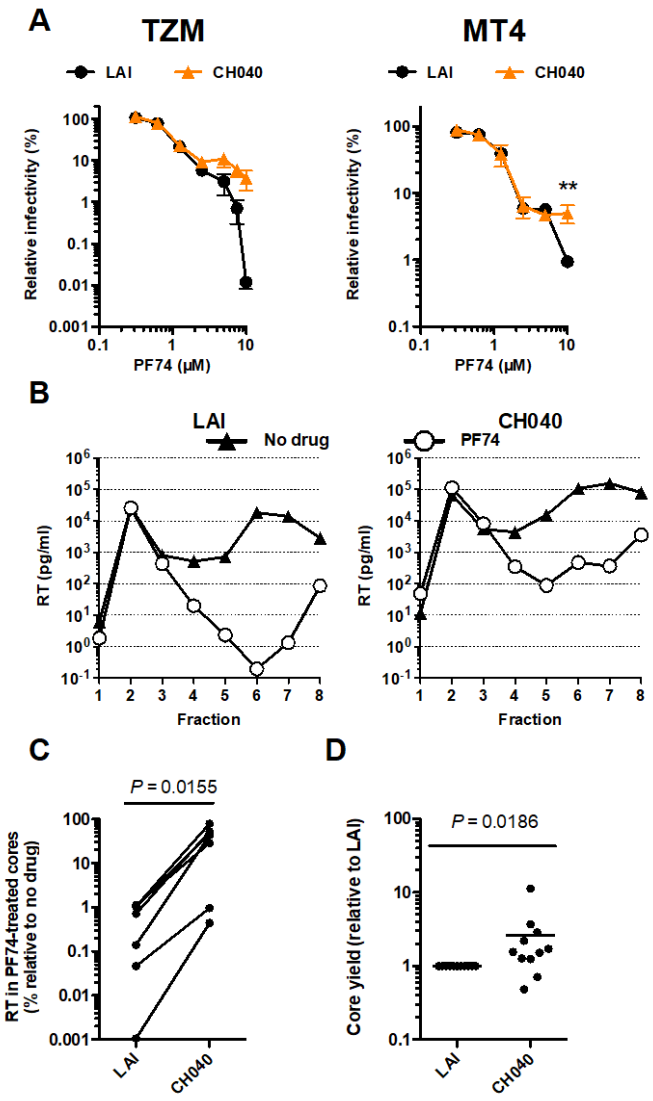

Figure 44. The capsid from a primary strain confers resistance to antiviral activity and core-destabilization effects of PF74. (A) Dose-response curves of LAI and LAI encoding CH040 CA were generated on TZM (left panel, n = 2) and MT4 (right panel, n = 7 for LAI, n = 4 for CH040) cells using env/nef-defective GFP-reporter virus. Luciferase activity was used as readout for TZM whereas the number of GFP-positive cells was used for MT4 cells. Relative infectivity was calculated by setting the data points without PF74 treatment as 100%. The average values are shown with error bars denoting SEM. **P < 0.01 (calculated with the unpaired student t test). (B) Core yields of the virus carrying the capsid from CH040 were compared to those of the parental LAI virus in the presence or absence of 10 μM PF74 by the method described in the legend to Figure 42. A representative result is shown from eight independent experiments. (C) Effects of PF74 on capsid stability were assessed by examining the amount of RT in

fraction 6 of PF74-treated samples as compared to those without PF74 treatment. Results from seven independent experiments are shown and were analyzed using the two-tailed, paired t test. Values obtained from the same experiment are connected by lines. (D) RT amounts in a core-containing fraction (fraction 6) were used to determine the core yield. Results are shown as relative values of core yields that were normalized to those by the LAI virus. The data was compiled from 11 independent experiments. The P value was derived using the Wilcoxon matched-pairs signed rank test.

hexamer-hexamer interactions (430, 523, 524) and the same T216I emerged as a second-site suppressor mutation to rescue the P38A CA mutant, the capsid of which is unstable (639). To determine whether this genetic polymorphism dictates the difference in core-related phenotypes between LAI and CH040 viruses, the T216I substitution was introduced into the LAI strain whereas the reciprocal isoleucine-to-threonine (I216T) substitution was introduced into the clone encoding the CH040 CA protein. These two new viruses exhibited opposing phenotypes; the T216I change conferred the LAI strain with PF74 resistance, specifically at high PF74 concentrations, whereas the I216T substitution rendered the chimeric virus carrying CH040 CA more susceptible to antiviral activity at high doses of PF74 (**Figure 45B**). We also compared the effects of PF74 on the core yields of LAI carrying the T216I mutation to those of the WT LAI strain (**Figure 46**). The LAI mutant carrying T216I substitution differed from the parental LAI virus (**Figure 46A**) but resembled the LAI chimera with CH040 CA (see **Figure 44B**) in the abundance of RT molecules associated with core-containing fractions (**Figure 46B**) in the presence of PF74. It was difficult to judge the effects of T216I on capsid stability in the absence of PF74 treatment due to the presence of an outlier (**Figure 46C**). Without the outlier, the core yield of the T216I mutant in the absence of PF74 was lower than that of the parental WT virus by 3-fold (P = 0.0048). These results indicate

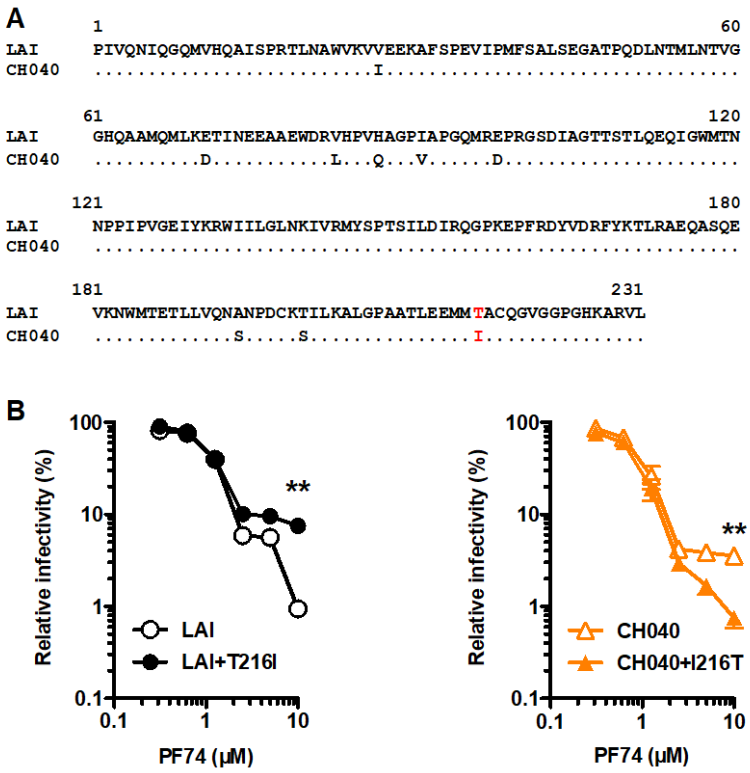

Figure 45. Amino acids at position 216 in CA govern the sensitivity to antiviral activity of high PF74 doses. (A) Alignment of HIV-1 CA amino acid sequences of LAI and CH040. Amino acids of CH040 that are identical to those of LAI are shown as dots. Amino acids at position 216 are highlighted in red. (B) Dose-response curves of PF74 for these viruses were generated by infecting MT4 cells with GFP-encoding reporter viruses in the presence of increasing amounts of PF74. Results are displayed as relative infectivity normalized to the infectivity in control cells without PF74. The mean values from at least three independent experiments are shown with error bars denoting SEM: n = 7 for LAI, n = 3 for LAI+T216I, n = 3 for CH040, and n = 5 for CH040+I216T. **P < 0.01 (two-tailed, unpaired t test).

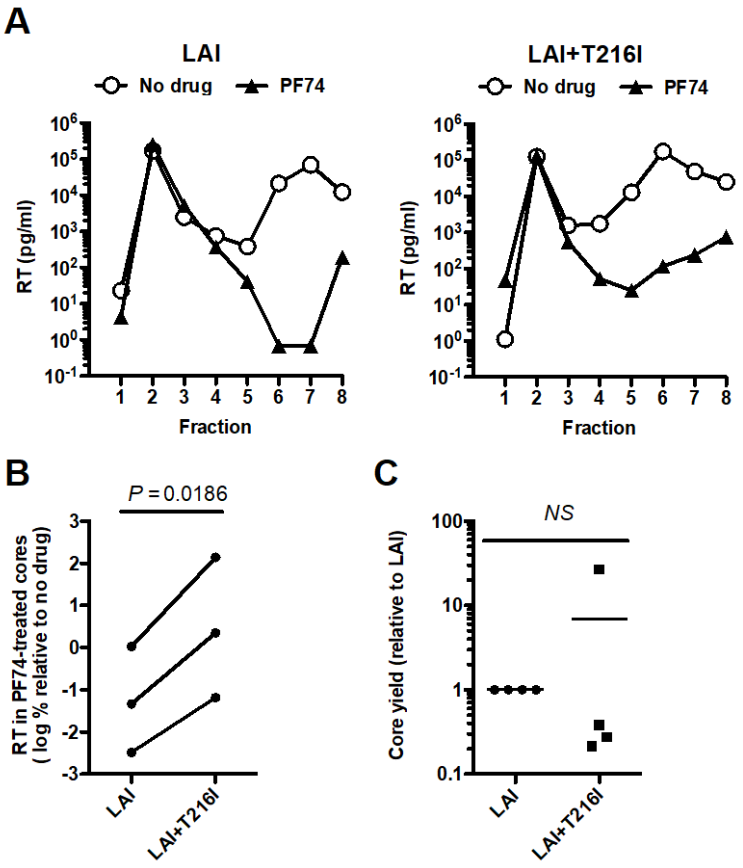

Figure 46. T216I substitution confers partial resistance to PF74-induced core-destabilization. (A) PF74 effects on HIV-1 cores. Virus particles of two LAI-based viruses were subjected to the "spin-thru" core isolation procedure after incubation with or without 10 μM PF74. (B) PF74 effects on the core yield are depicted as normalized values of RT amounts in fraction 6 relative to those without drug treatment. Log10-transformed values are shown and used for analysis by the two-tailed paired t test. (C) Core yields were derived by the amount of RT in fraction 6. The normalized amounts of core yield to the WT LAI virus are shown from four independent experiments. Data was analyzed by the two-tailed unpaired t test.

that a naturally occurring genetic polymorphism at the trimeric interface between CA hexamers allowed HIV-1 to gain PF74 resistance.

A.2.3 Single virus imaging studies *in vitro* and in cells reveal that PF74-resistant variants have stable capsids

Our observations suggested that CH040 differs from LAI in capsid stability and that the T216I substitution is responsible for the difference. To test this possibility, we utilized two complementary imaging assays established in previous work (500, 525). In the first approach, we co-labeled HIV-1 pseudoviruses by incorporating integrase fused to mNeonGreen (INmNeonGreen, INmNG) and cyclophilin A (CypA) tagged with DsRed (CypA-DsRed). We have previously demonstrated the utility of the CypA-DsRed fusion protein as a non-invasive marker for the viral capsid that allows monitoring loss of HIV-1 CA from single cores *in vitro* and in living cells (287, 525). To assess the core stability *in vitro*, double-labeled pseudoviruses were adhered to coverslips, permeabilized with saponin, and loss of CypA-DsRed from single virions was monitored by time-lapse imaging. These experiments revealed that the kinetics of CypA-DsRed loss from PF74-resistant viruses was delayed compared to the LAI virus (**Figure 47A and 47B**). Specifically, a significantly greater number of single INmNG labeled LAI cores lost CypA-DsRed than the PF74-resistant viruses (R143A, T216I and CH040, **Figure 47A and 47C**). In agreement with the previously published results, the number of INmNG spots remained relatively constant within 30 min after permeabilization. These observations imply that the capsids of PF74-resistant viruses are more stable than those of the WT LAI virus (**Figure 47B and 47C**).

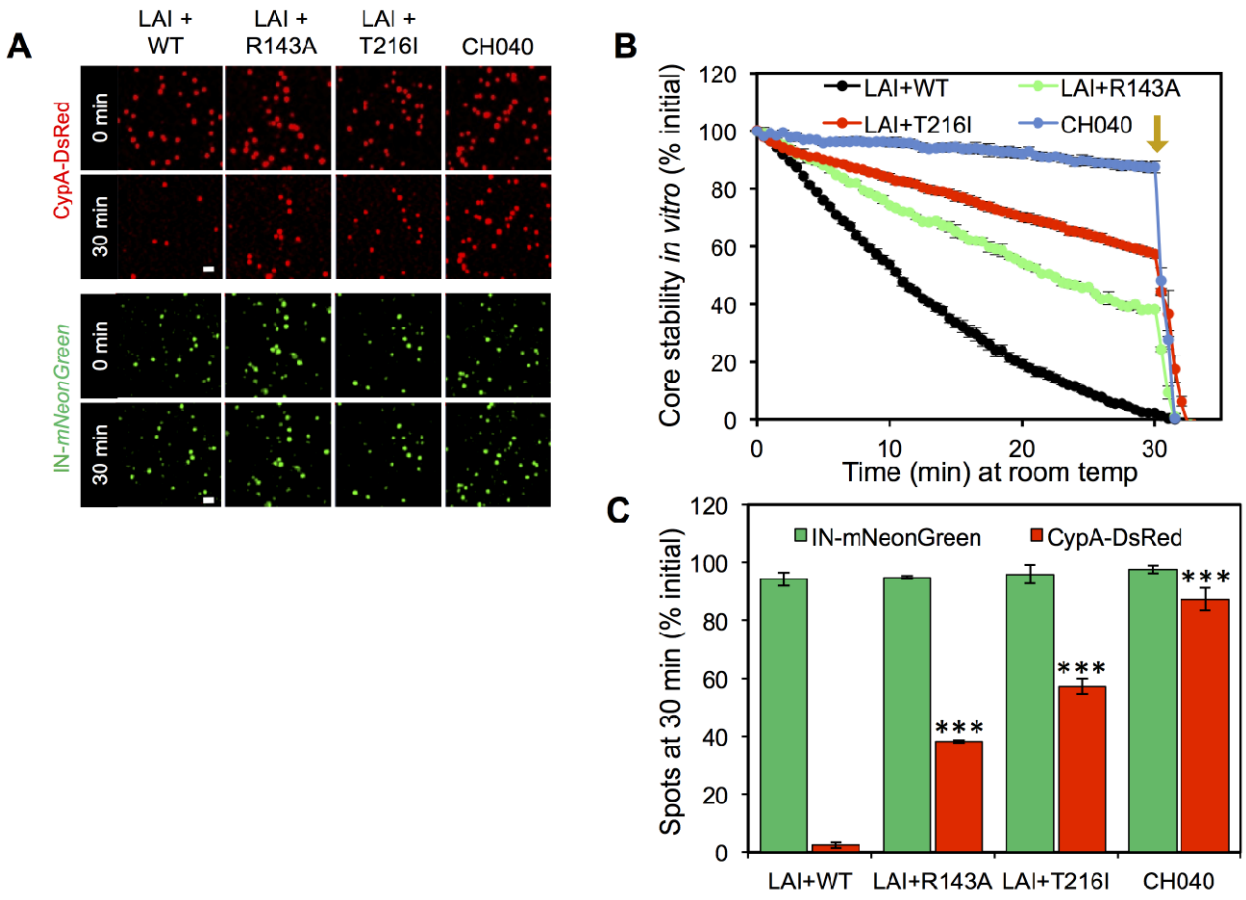

Figure 47. Microscopic analysis of HIV-1 core stability *in vitro*. (A) Images of single CypA-DsRed and INmNeonGreen spots at time 0 and 30 minutes after permeabilization with saponin (same field of view for both time points). Scale bar is 2 µm. (B) Kinetics of single virus uncoating *in vitro*, as measured by loss of CypA-DsRed spots. An arrow indicates the time of CsA addition. Error bars are SEM. A representative result of four experiments for LAI WT, LAI T216I and CH040 and two experiments for R143A is shown. (C) A bar chart shows the average stable fraction of CypA-DsRed and INmNeonGreen spots at 30 min after permeabilization in multiple experiments. ***P < 0.0001 (unpaired t test).

We next examined single HIV-1 uncoating in the cytoplasm using the same INmNG/CypA-DsRed labeled viruses pseudotyped with VSV-G (**Figure 48A and 48B**). In this cell-based assay, VSV-G-mediated viral fusion releases the HIV-1 cores into the cytoplasm where different outcomes are observed: (1) highly unstable cores exhibiting abrupt uncoating followed by proteasomal degradation of viral complexes; and (2) stable cores that survive for several hours in the cytoplasm and usually exhibit a very slow/gradual loss of CA/CypA-DsRed (525). The minor fraction of the relatively stable post-fusion HIV-1 cores is readily identified by treating cells with cyclosporine A (CsA), which displaces CypA-DsRed selectively from cores in the cytoplasm, but not from intact viruses trapped in endosomes (**Figure 48A**). Thus, the fraction of long-lived cores that does not complete uncoating within the first 90 min of infection correlates with the intrinsic core stability in living cells (525). We observed a significantly higher fraction of the stable post-fusion INmNG-labeled cores (i.e., cores that lost CypA-DsRed after CsA treatment) (525) for the PF74-resistant variants at 90 min post-infection compared to LAI WT (**Figure 48B**). This result further supports the notion that the PF74 resistance is associated with increased core stability.

To further examine whether the stable cores were intact or partially opened, we utilized an alternative imaging method, which takes advantage of the dependence of viral RNA staining on the opening of the viral capsid (500, 521, 640). Previous work showed that 5-ethynyl uridine (EU) incorporated into HIV-1 RNA during virus production can be stained in cells after virus infection with a decrease in RNA detection over time concurrent with capsid uncoating and reverse transcription (500, 521, 640). The rate of RNA staining is affected by capsid stability, such that viruses with hyperstable capsids have slower RNA staining kinetics and loss of RNA signal compared to WT HIV-1 capsid and viruses with hypostable capsids show faster RNA staining. In

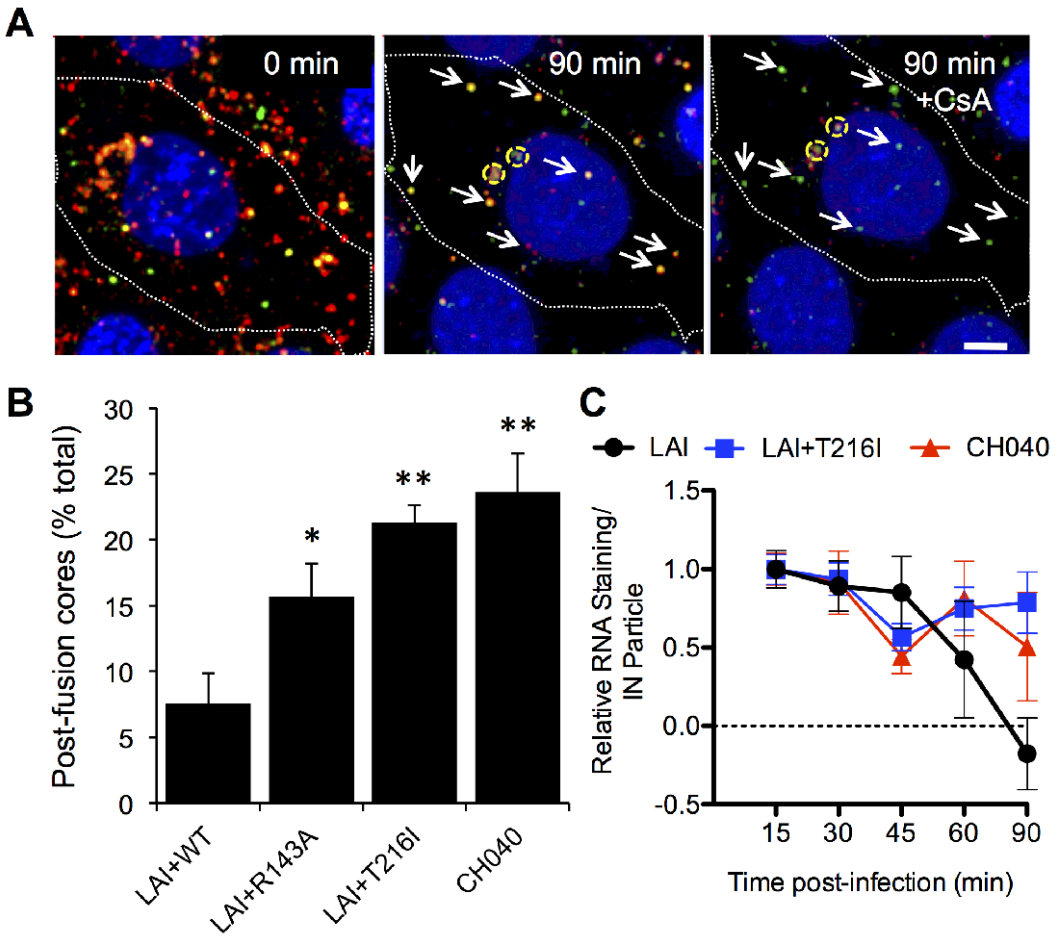

Figure 48. The CH040 capsid and T216I substitution both stabilize cytoplasmic HIV-1 cores. Single virus core stability was studied with two different cell-based imaging assays. The core stability of HIV-1 LAI and CH040 WT viruses or LAI-based CA mutants R143A and T216I was measured in TZM-bl cells (A and B) or in HeLa (C). (A) Post-fusion cores that did not uncoat during the first 90 minutes post-infection were readily identified by the loss of CypA-DsRed (arrows) in response to CsA treatment, whereas endosomal viral complexes retained CypA-DsRed under these conditions (yellow dashed circles). Images are maximum intensity projections of the same cell. Scale bar is 5 μm. (B) A bar chart for the fraction of stable post-fusion HIV-1 cores for different capsid variants. Results represent the average of three experiments. Statistical analysis was performed using student t test. *P < 0.05, **P <0.01. (C) HeLa cells were infected with three HIV-1 variants containing fluorescently tagged integrase and stained for EU (viral RNA) at different time points. Data were compiled from results of three independent experiments and normalized with the dataset for the first time point (15 minutes post infection). Mean values of the normalized data are shown with error bars denoting SEM. Capsid permeabilization kinetics were analyzed by multiple linear regression modeling

in the SAS statistical package to test if the slopes were equivalent. Using the F statistic, the three slopes were not equivalent with P = 0.025. Using the F statistic with the Bonferroni correction for pairwise comparisons, P values less than 0.0167 were considered statistically significant. The P value for CH040 versus LAI+T216I was 0.59. The comparison of LAI WT to LAI T216I or to CH040 yielded P values of 0.011 and 0.038, respectively.

this study, RNA staining of HIV-1 with CH040 capsid was distinct from that of WT HIV-1 (**Figure 48C**). WT LAI virus had a steady decrease in RNA staining after the initial time point, similar to previous results (500, 521, 640). In contrast, higher numbers of RNA-positive particles were observed at 60 and 90 minutes post infection for the CH040 virus than the LAI virus, consistent with delayed capsid permeabilization. The T216I substitution in the LAI capsid phenocopied the CH040 capsid in this capsid permeabilization assay (**Figure 48C**). These results also suggest that the capsid of CH040 is more stable than that of LAI and that this difference is regulated by the T216I substitution.

A.2.4 PF74-resistant variants prevent innate sensing of HIV-1 DNA by cGAS

One potential consequence of stabilized capsids and delayed capsid disassembly in target cells is prevention of viral DNA exposure to cytosolic innate sensors. To test this idea, we used a previously described experimental system based on the monocytic cell line THP-1 in which HIV-1 infection activates cGAS-mediated IFN signaling (526). As reported previously (526), THP-1 infection with GFP-reporter HIV-1 induced type I IFN as well as IP-10, one of the interferon-stimulated genes (ISGs) (**Figure 49A**). This innate immune activation was blocked by nevirapine, a reverse transcriptase inhibitor (**Figure 49A**), but not by raltegravir or dolutegravir, integrase

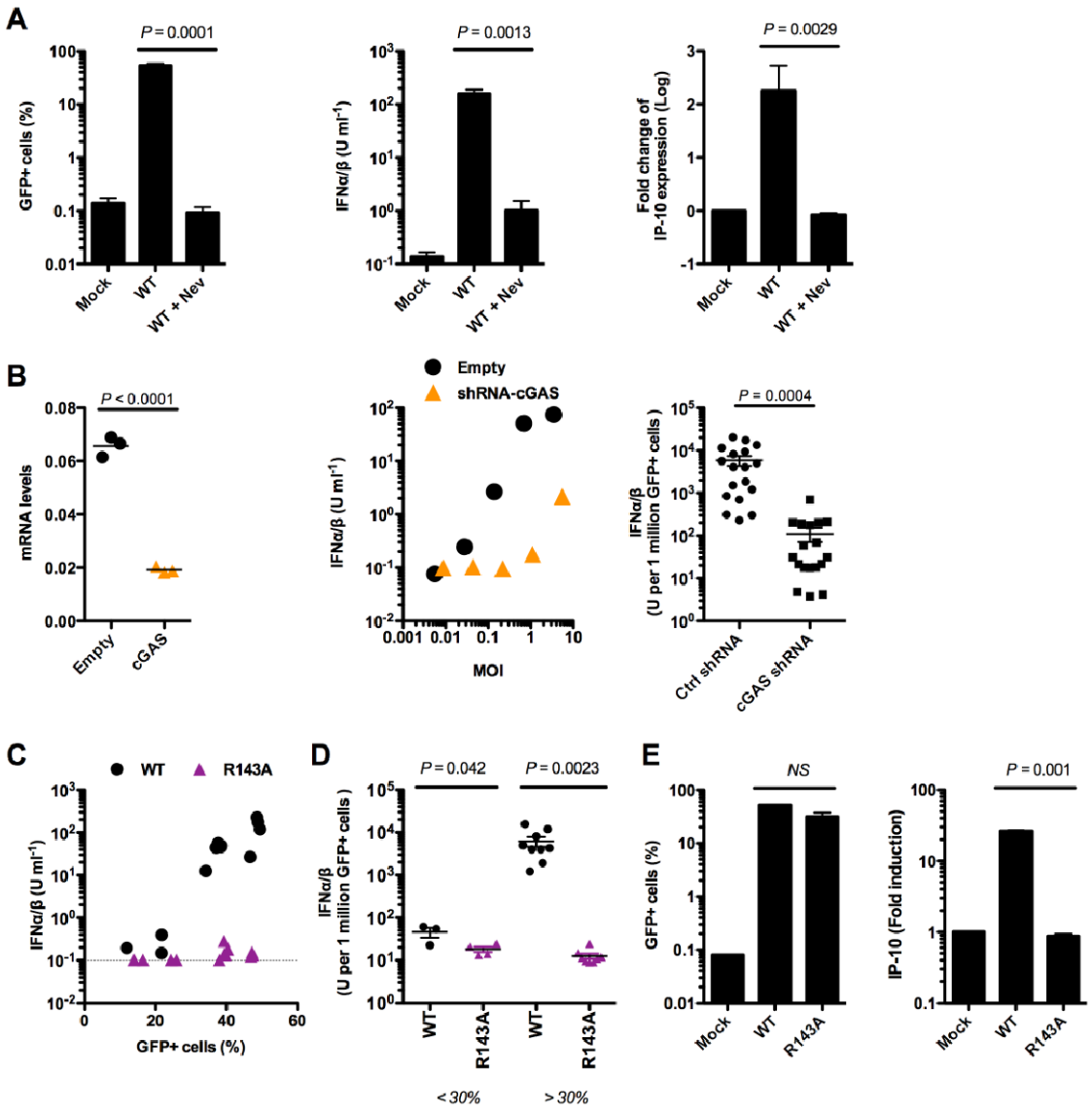

Figure 49. The R143A CA mutation suppresses HIV-induced innate responses in THP-1 cells. (A) THP-1 cells were infected with HIV-1 GFP reporter virus at an MOI of ~1 in the absence or presence of an RT inhibitor, nevirapine, at 5 μM. Virus infection was assessed by counting GFP-positive cells at two days after infection (left panel). A fraction of culture supernatant was used to determine the level of type I IFN using a reporter cell line that expresses luciferase under the ISRE promoter (middle panel). Induction of IP-10 was measured by using qRT-PCR (right panel). The value of mock-infected cells was set as the basal level of IP-10 (right panel). The averages of results from four independent experiments are shown with error bars denoting SEM. (B) Stable gene knockdown by shRNA was validated using qRT-PCR. Expression of the GAPDH gene was quantified in parallel as control to determine the changes of mRNA levels using the 2−ΔΔCT method. Cells stably expressing shRNA directed against cGAS were harvested at three

different occasions for mRNA extraction and qRT-PCR (left panel). Effects of cGAS depletion on IFN production by HIV-1 were determined as described above. In these experiments, increasing amounts of virus input were used to assess the relationship between viral infectivity and ability to stimulate type I IFN production. A representative result is shown from two experiments (middle panel). Results shown in the right panel where IFN production was normalized to the number of GFP-positive cells (i.e. virus-infected cells) were compiled from data generated in four independent experiments. Differences between various conditions were statistically examined using the two-tailed, unpaired t test: *$P < 0.05$, ***$P < 0.0001$. (C) The R143A CA mutant virus was compared to the WT virus in their ability to induce type I IFN in THP-1 cells. THP-1 cells were infected with GFP-reporter virus carrying either the WT capsid or capsid with the R143A mutation. Increasing amounts of virus input were used to achieve viral infectivity ranging between 10 to 60% GFP-positive, virus-infected cells. Results shown were compiled from four independent experiments. The amount of type I IFN was determined by using a bioassay that utilizes a reporter cell line stably encoding the luciferase gene under the promoter of ISRE. (D) Shown is the amount of IFN in culture supernatant normalized by the number of virus-infected cells. Since the WT virus did not induce IFN production at a lower range of virus infection (less than 30% GFP-positive cells), data points were separated into two groups. Each group was analyzed by the two-tailed, unpaired t test. (E) Induction of IP-10 mRNA was quantified using qRT-PCR. Copy numbers of IP-10 were quantified by qRT-PCR and the values were normalized with those obtained in mock-infected cells. Results shown are the averages of two independent experiments with error bars denoting SEM. The data was analyzed with the two-tailed, unpaired t test.

inhibitors (data not shown). Depletion of cGAS significantly reduced the ability of HIV-1 to induce type I IFN upon viral infection (**Figure 49B**).

We next tested the ability of the R143A mutant to activate the cGAS-dependent DNA sensing pathway. In contrast to the WT virus, infection of THP-1 cells with the R143A mutant did not induce a strong type I IFN response (**Figure 49C**). Comparison of data points for infection resulting in more than 20% GFP-positive cells showed a statistically significant 3-log difference in IFN induction between these two viruses when the amount of type I IFN was normalized to the number of virus-infected cells (**Figure 49D**). A very similar result was obtained when levels of interferon gamma-induced protein 10 (IP-10) expression were measured by quantitative reverse transcription PCR (qRT-PCR); compared to mock, a 20-fold increase in IP-10 mRNA induction was observed for the WT virus but there was no increase in IP-10 expression for the R143A mutant virus (**Figure 49E**).

The R143A mutant virus has been reported to be attenuated in infectivity (228, 393). In our hands, we found a 7-to-16 fold decrease in the quantity of virus particles produced by the R143A mutant, as determined by quantification of RT, and concomitant reduced infectivity, although when normalized by virus input, infectivity of the R143A mutant virus was comparable to the WT virus (**Figure 50A**). Thus, to achieve equivalent levels of infection with these two viruses, a larger inoculum size was required for the R143A virus than the WT virus. To rule out the possibility that the difference in the inoculum size inadvertently affected innate immune responses, we utilized an LAI-based chimeric virus carrying CH040 CA, as its virus yield and infectivity were equivalent to those of the parental LAI virus (**Figure 50B**). These observations

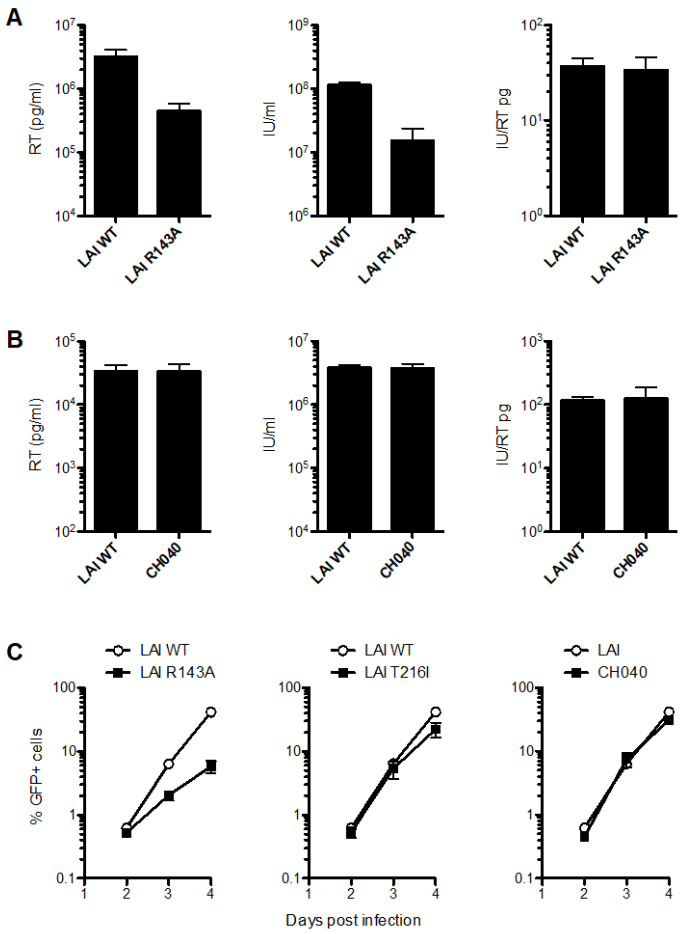

Figure 50. Infectivity and replicative capacity of PF74-resistant viruses. Virion-associated RT amount (left), infectivity (center) and infectivity normalized by the RT amount (right) of the R143A mutant (A) or chimeric virus encoding the CH040 CA (B) were compared to those of the LAI WT virus. Infectious units (IU) were quantified based on the number of virus-infected cells, which were judged by GFP expression. One representative result is shown from two independent experiments of transfection for virus production. Each transfection generated three replicates of virus stock. The mean of triplicate values is shown with error bars denoting standard deviations. (C) Spreading infection was examined by monitoring the number of GFP-expressing cells. Changes in the percentage of GFP-positive cells are plotted for replicates that show a range of 0.3% to 1% of GFP-expressing cells at 2 dpi. At least six replicates are shown with error bars denoting standard errors of the mean.

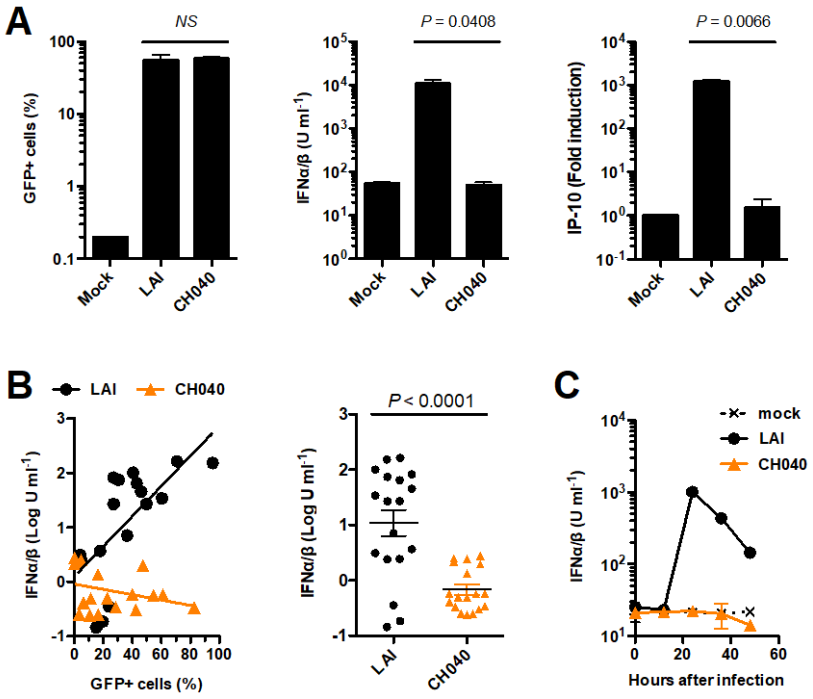

Figure 51. The CH040 capsid attenuates innate immune responses upon HIV-1 infection of THP-1 cells. (A) THP-1 cells were infected with GFP-reporter virus. The number of virus-infected cells was determined by counting GFP-positive cells (left panel). IFN induction by mock-infected or virus-infected cells were examined by transferring culture supernatant onto HEK293-based reporter cells that encode the luciferase gene under the control of the ISRE promoter. A standard curve was generated with known amounts of type I IFN and used for determining the amount of type I IFN for each condition (middle panel). IP-10 induction was quantitated using mRNA extracted from THP-1 cells one day after infection. The number of IP-10 RNA copies in the mock-infected sample was used as the basal level of IP-10 to calculate the magnitude of induction (shown as fold induction). Shown are mean ± SEM; n = 2. Differences between LAI and CH040 were examined by the two-tailed, unpaired t test. (B) A dose-dependent increase in IFN production by LAI but not by CH040. The concentration of IFN in culture supernatant was log10-transformed and plotted against the number of GFP-positive cells (left panel). Linear regression was used to determine correlation between the number of virus-infected cells and IFN production. Results from three independent experiments are shown with each dot representing a single well containing THP-1 cells infected with different amounts of challenging virus. All the results were combined and the difference between two viruses was examined using the two-tailed, unpaired t test (right panel). (C) A time-course experiment for production of type I IFN. THP-1 cells were infected with VSV-G-pseudotyped GFP reporter virus encoding CA from LAI or CH040 using the same amount of virus input. At

indicated time points, culture medium was harvested from virus-infected cells, as well as mock-infected cells (mock), and used for quantification of type I interferon using the same bioassay. One representative result from two independent experiments is shown. The average of triplicate samples is used with error bars denoting standard deviations.

were confirmed in a spreading infection assay (**Figure 50C**). We infected THP-1 cells with GFP-reporter virus that encodes the capsid from the CH040 strain (**Figure 51**). Similar to the observations made with the R143A mutant virus, the capsid of CH040 almost completely eliminated the ability of HIV-1 to induce production of type I IFN and expression of IP-10 in THP-1 cells (**Figure 51A**). This observation was confirmed in a broad range of multiplicities of infection (MOI) (**Figure 51B**). A dose-dependent increase in production of type I IFN (**Figure 51B**) was observed for the LAI strain but not the virus encoding CA from CH040. The differences between these two viruses were statistically significant even when data points for low MOI were not excluded (**Figure 51B**). The observed difference between LAI and CH040 capsids (**Figure 51**) was not due to the delayed type I IFN production by CH040 (**Figure 51C**). The kinetics and extent of viral DNA synthesis by the CH040 virus was indistinguishable from those by the WT LAI virus (data not shown). Finally, a difference in the level of type I IFN production between LAI and CH040 viruses was also observed in primary monocyte-derived macrophages (MDMs) (**Figure 52**).

We showed that amino acids at position 216 in CA govern PF74 sensitivity (**Figure 45**). We next asked whether the same position in CA also regulates innate immune activation. Indeed, this was the case (**Figure 53**). Addition of the T216I substitution eliminated the ability of the WT

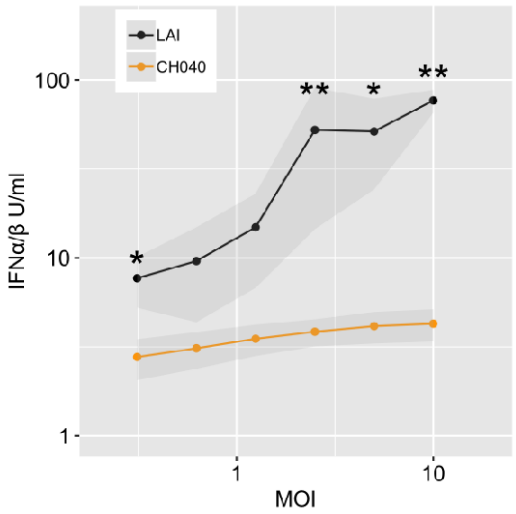

Figure 52. The CH040 capsid reduces the level of type I IFN production from primary macrophages infected with HIV-1. Production of type I IFN by MDMs infected with GFP reporter viruses. MOIs were pre-determined using THP-1 cells. A bioassay was used to quantify the amount of type I IFN in culture medium from MDMs prepared from 2 blood donors. The mean of five independent experiments is shown with gray shades denoting SEM. **P < 0.01; *P < 0.05; Mann-Whitney U test.

LAI virus to induce an appreciated level of type I IFN production whereas the reciprocal substitution (I216T) allowed the chimeric virus carrying the CH040 capsid to efficiently produce type I IFN (**Figure 53**). Thus, the capsid from the CH040 strain was strikingly distinct from the one from the LAI strain in PF74 sensitivity and innate immune recognition of viral DNA while both differences appeared to be regulated by the same amino acid substitution.

The unique ability of the CH040 strain to more effectively prevent cGAS recognition of viral DNA than a lab-adapted strain raised the possibility that this phenotype may be preferentially selected during HIV-1 transmission. Such phenotype would be beneficial for HIV-1, which is susceptible to antiviral activity triggered by type I IFN and executed by a large repertoire of

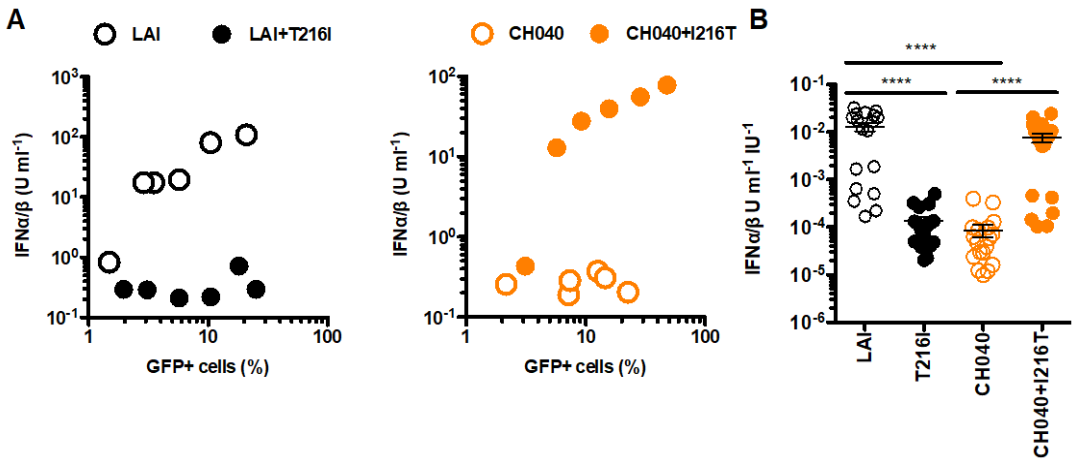

Figure 53. Amino acids at position 216 in CA regulate HIV-induced innate activation of THP-1 cells. (A) THP-1 cells were infected with GFP-encoding reporter virus based on the LAI strain or the chimeric virus carrying CH040 Gag with each strain encoding either a threonine or isoleucine at position 216 in CA. Concentrations of IFN in culture supernatant were measured using a reporter cell line together with known amounts of IFN for generating standard curves. Representative results are shown from three independent experiments. (B) Results were compiled from three experiments. IFN concentrations (units per ml) were normalized to the numbers of virus-infected cells. The mean ± SEM; n = 18 (3 independent experiments with 6 different infectious doses), ****P < 0.00001 (two-tailed, unpaired t test).

ISGs (255, 641, 642). We tested this possibility by studying the ability of a panel of eight additional T/F viruses to induce type I IFN in THP-1 cells. To specifically address the role of CA in our experimental setting, part of the *gag* gene encompassing the entire CA-coding sequence was transferred to an *env*-deficient GFP reporter clone to produce vesicular stomatitis virus (VSV)-G-pseudotyped virus. Infection of THP-1 cells with increasing amounts of virus input showed that chimeric viruses, except for the one containing the capsid from the above described CH040 strain, were able to induce production of type I IFN at a level comparable to the LAI strain (**Figure 54**). Note that none of these strains, except for CH040, carry the T216I substitution. Thus, virus

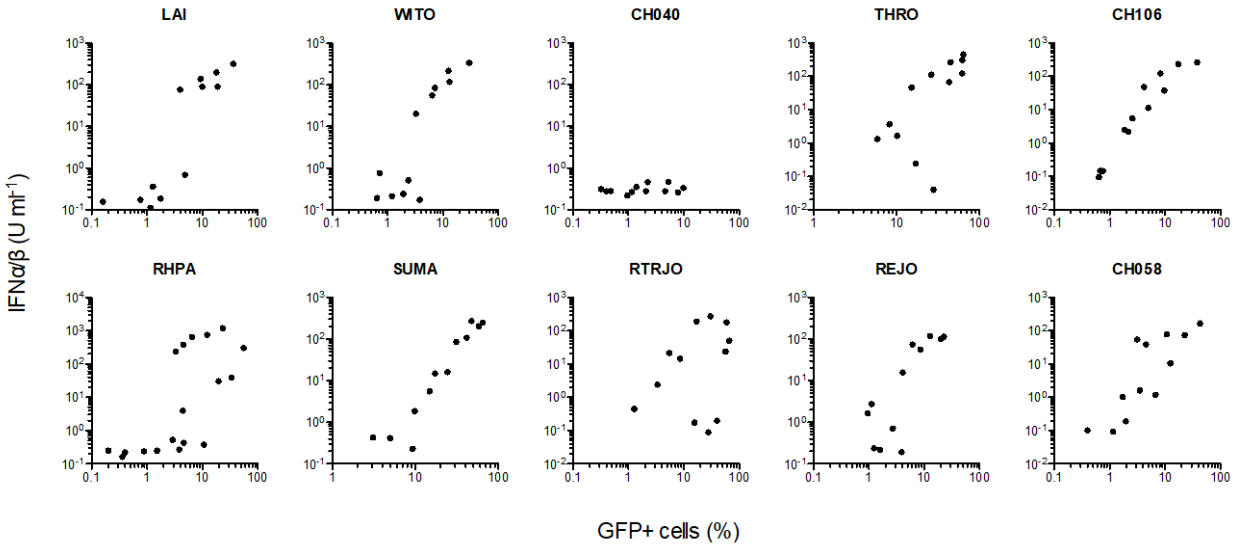

Figure 54. A profile of type I IFN induction of THP-1 cells by HIV-1 reporter virus harboring different capsids from nine T/F strains. Effects of different CA sequences on type I IFN production were examined using a panel of LAI-based chimeric viruses in which part of the Gag-coding sequence, including the entire CA domain, was replaced with those from T/F strains. Activation of type I IFN pathway in THP-1 cells infected with VSVG-pseudotyped viruses was examined as described in the legend to Figure 49. Results obtained in two independent experiments are shown, except for CH040, which was examined three times.

harboring the capsid capable of effectively evading cytosolic DNA sensors in THP-1 cells is rare among the panel of T/F viruses examined in this work.

A.3 Discussion

The present work used both cell-free and cell-based assays to reveal a novel phenotype of the viral capsid. A unique profile of resistance to high doses of PF74 in an infectivity assay was associated with reduced sensitivity to PF74-induced core-destabilization in an *in vitro* assay. The capsid of

PF74-resistant viruses allowed more effective escape from cGAS recognition of viral DNA than those from other strains. Phenotypic variations in PF74 resistance and innate sensing between T/F strains examined in this work were linked to a genetic polymorphism at the trimeric interface between CA hexamers, which mediates key interactions that influences capsid stability. Finally, imaging-based assays revealed that these unique PF74-resistant variants contain stable cores. These observations suggest that capsid stabilization is an underlying mechanism of the new phenotype, which couples capsid stability to HIV-1 DNA sensing.

Three new PF74-resistant viruses identified in this work are two CA mutants (R143A and T216I) and a naturally occurring strain (CH040). Their dose response curves for PF74 were different from those of previously described resistant variants (410, 419, 461, 508, 643), pointing to a novel resistance mechanism. Notably, these new resistant variants counteracted inhibitory effects of PF74 rather specifically at high PF74 concentrations. This is in contrast to drug resistance by blocking capsid binding to the two well-characterized host factors, CPSF6 and CypA, in which PF74 antiviral activity was neutralized at low drug doses (419, 461). These observations suggest that the resistance to high doses of PF74 is mechanistically unique and not caused by differential capsid binding to these cellular proteins. It remains unclear whether any other extrinsic host factors are involved in the unique resistance profile of these drug resistant viruses.

High doses of PF74 have been shown to block reverse transcription in the literature, but their effects on the capsid vary between studies (409, 410, 417-420, 472, 500, 525, 620, 634, 635). PF74 was shown to stabilize or destabilize the capsid, depending on the method used. A possible explanation to reconcile these seemingly conflicting observations was proposed in a recent work

in which high doses of PF74 have two distinct effects – facilitating capsid opening while preventing lattice disassembly (540). It seems reasonable to assume that the newly identified PF74 resistant viruses counteract one or both effects. Given that these resistant viruses contain cores with elevated stability and delay uncoating (**Figures 47 and 48**), it is likely that they counteract the capsid opening activity of PF74.

In a centrifugation-based assay, PF74 displayed core-destabilizing activity (**Figure 42**). This core-destabilizing activity was partially neutralized by new PF74-resistant viruses. The neutralizing effects were modest but statistically significant (**Figures 43, 44, and 46**). This finding appears to contradict with a reported ability of PF74 to prevent capsid disassembly (525, 540, 620, 635). A possible explanation for this disagreement is a dilution effect wherein a host factor(s) that stabilize the capsid are reduced or lost during core isolation, which would lead to capsid destabilization. In this scenario, PF74 triggers initial capsid opening and thereby exacerbates capsid destabilization. We note that the fate-of-capsid assay, another method that found PF74-mediated capsid destabilization, also involves a procedure in which that subviral complexes are diluted. Further studies are needed to confirm this idea.

The critical role played by cGAS in cytosolic DNA sensing has been firmly established (644). This protein appears to be essential for innate recognition of HIV-1 DNA in multiple experimental systems, while other host proteins participate in this sensing pathway (257, 526, 630-632, 645-648). In this work, we asked if a new PF74 resistance phenotype, which appears to be associated with capsid stabilization, influences innate sensing of HIV-1 DNA. To this end, we used monocytic THP-1 cells, which were shown to activate IFN signaling upon HIV-1 infection

through cGAS-dependent recognition of viral DNA (526, 630, 645). Our results showed that genetic changes in CA almost completely eliminated the ability of HIV-1 to induce type I IFN in THP-1 cells. Thus, these viruses are distinct from previously described CA mutants, which displayed elevated levels of innate immune activation in myeloid cells (270, 632, 649, 650). Our observations were made with virus of which infectivity is comparable to that of a widely-used lab-adapted strain and thus argue against the possibility that differences in the inoculum size may inadvertently affect innate responses. Overall, our results support a general model for capsid-mediated regulation of HIV-1 DNA sensing (257, 632, 651) and are in line with the previous work demonstrating a similar role of capsid stability in regulating DNA sensing for murine leukemia virus (652).

HIV-1 uncoating can influence the access to viral DNA by the cytosolic sensor cGAS (257, 632). The precise nature of uncoating remains controversial, but it appears that a certain quantity of CA molecules remains associated with the cytoplasmic RTCs (reviewed in (192, 285, 286)). The simplest scenario is that stable cores disassemble slowly, such that excess CA molecules that remain bound to subviral complexes limit the exposure of viral DNA to cytoplasm DNA sensors. This model accords with the observation that PF74-resistant viruses appear to have stable cores and display delayed kinetics of disassembly in cell-based assays (**Figures 47 and 48**). However, it is also possible that these PF74 variants utilize distinct innate immune evasion mechanisms through different capsid functions.

Phenotypic changes in the sensitivity to antiviral activity of high PF74 doses were perfectly matched to those in type I IFN induction in THP-1 cells. We envision that these two phenotypic

outcomes can be used as indirect indicators for capsid stability. Infection-based approaches are amenable to large-scale studies as primary screening assays. A few caveats inherent to these experimental systems include a lack of the applicability of the PF74-based assay to viruses that bind to PF74 with reduced affinity. Second, normalization in THP-1 cells would be difficult for viruses that impair viral DNA synthesis. Nonetheless, we expect that these new tools will complement with existing assays for capsid stability and disassembly (498, 502, 525, 633, 653, 654).

The CH040 strain was more effective than other strains in the ability to evade cGAS-mediated sensing of viral DNA in the assay system used in this work. This property, which seems beneficial for virus propagation, was rare and found only in one of nine strains, although the number of T/F viruses assessed in this work is limited. One account to explain the rarity of such phenotype is that other evading mechanisms, such as degradation of viral DNA by TREX1 (629, 651) and shielding of viral DNA by cofactor recruitment (257, 632), may be sufficient to prevent HIV-1 DNA sensing in physiologically relevant conditions.

This work uncovered one naturally occurring HIV-1 variant (CH040) that encodes the capsid phenotypically distinct from that of other tested strains. As described above, our results suggest that cores from this variant are more stable than those of others. Interestingly, CH040 strain does not have any obvious defect in infectivity and replicative capacity (522, 642). Therefore, it appears that stable cores do not necessarily impair viral fitness *in vivo*, although this likely depends on the degree of stability. This observation was somewhat unexpected, because the conventional wisdom holds that optimal capsid stability is fine-tuned. However, recent work

showed that certain HIV-1 CA mutants with hyperstable capsid can replicate rather efficiently in T cell lines (410, 639, 643). It should be also noted that among HIV-1 CA mutants that exhibit abnormal capsid stability, the R143A mutant is the only one capable of replicating in primary cells (228).

Among a dozen of T/F viruses examined in this study, only one strain (CH040) had a distinct capsid. Virus with such new capsid phenotype, however, may not be an absolute outlier. The T216I substitution responsible for the capsid phenotype of CH040 is present in 1% of approximately 14,000 HIV-1 group M strains in the Los Alamos HIV-1 databases. Furthermore, amino acids at position 216 in 4% of the predicted CA sequences are not a threonine. Whether amino acid residues other than an isoleucine at position 216 in CA changes the capsid function requires further investigation. It will be also interesting to determine whether the genetic polymorphism at position 216 in CA has any effects on disease parameters, such as CD4+ T cell counts and immune activation levels, and thereby influences HIV-1 pathogenicity.

Together, the present finding adds to a growing body of evidence for phenotypic variations in post-entry steps mediated by the HIV-1 capsid. It has been shown that deviations from the normal course of uncoating by artificial perturbations often do not show strong impacts on viral infectivity (459, 498, 499, 655-657). HIV-1 CA can alter nuclear entry pathways and specific preferences for integration site selection without critically modulating viral replicative capacity (266, 436). These observations suggest that the viral capsid, which is known to be genetically fragile (394), is unexpectedly robust to considerable phenotypic changes during early steps of the viral replication cycle. This may be relevant to therapeutic strategies for capsid-targeting antivirals,

an avenue that has been actively pursued as a next-generation drug, as the evolvability of the viral capsid governs the capacity of HIV-1 to develop drug resistance.

A.4 Materials and Methods

Plasmid DNA

Env-defective reporter virus clones encoding GFP or luciferase in place of the *nef* open reading frame are based on the LAI strain of HIV-1. CA mutants (E45A, R143A and Q219A) have been described previously (268). A BssHII-ApaI fragment containing the entire capsid-encoding segment was PCR amplified using a panel of full-length T/F HIV-1 infectious molecular clones obtained through the NIH AIDS Reagent Program as template and cloned into the LAI-based molecular infectious clone (506). The following molecular clones for T/F viruses were used: RHPA.c/2635, WITO.c/2474, CH040.c/2625, CH058.c/2960, CH077.t/2627, CH106.c/2633, THRO.c/2626, REJO.c2864, RTRJO.c2851 and SUMA.c/2821 (522). Other point mutations were introduced to GFP reporter clones by using standard cloning procedures. Plasmid DNA for HIV-1 Gag-Pol expression (pCRV1-Gag-Pol), Vpr-INmNeonGreen and for expression of the vesicular stomatitis virus G (VSV-G) glycoprotein (pHCMV-G) have been described previously (287, 658, 659). The CypA-DsRed Express2 (CypA-DsRed2) was cloned by replacing the DsRed in the CypA-DsRed plasmid (525) with the brighter and more photostable version DsRed Express2 by molecular cloning using BamHI and NotI sites. Gene depletion vectors were generated based on the plasmid DNA pLKO.1-TRC control (Addgene plasmid #10879) by cloning short hairpin RNA (shRNA)-coding oligonucleotides into the EcoRI and AgeI sites. The targeted sequences, which

were described previously (526), were as follows (only sense strands are listed here): Luciferase: 5'-AACTTACGCTGAGTACTTCGA-3'; cGAS: 5'-GGAAGGAAATGGTTTCCAA-3'.

Cell culture

Adherent cells were cultured in Dulbecco's modified Eagle's medium (DMEM, Corning) supplemented with 10% fetal bovine serum (FBS, Sigma) and 1× penicillin-streptomycin (P/S, Corning). THP-1 and MT4 cell lines were cultured in Roswell Park Memorial Institute (RPMI) 1640 medium (Corning) supplemented with 10% FBS, 1× P/S and 2 mM L-glutamine (Corning). The following reporter cell lines are described previously: TZM-bl (NIH AIDS Reagent Program) and HEK293-ISRE-Luc (gift from Xuguang Li) (660). To generate THP-1 cell lines stably expressing shRNA targeting luciferase or cGAS, THP-1 cells were plated at half million cells per well in 24-well plates and infected with 0.3 ml of 10-fold concentrated virus. Puromycin (Invitrogen) was added at 0.5 μg per ml to the infected cells at two days after infection. Puromycin-resistant cells were expanded for two weeks before using infection and mRNA extraction. Peripheral blood mononuclear cells (PBMCs) were isolated from whole blood by density gradient centrifugation. CD14-positive monocytes were purified from PBMCs using EasySep Human Monocyte Isolation Kit (Stemcell). CD14+ monocytes were differentiated for six days in RPMI 1640 supplemented with 10% FBS, 1× P/S, 2 mM L-glutamine and 100 ng per ml of granulocyte-macrophage colony-stimulating factor (GM-CSF, PeproTech) or macrophage colony-stimulating factor (M-CSF, PeproTech) to generate MDMs.

Viruses

Virus stocks were generated by transient transfection of 293T cells using polyethylenimine (PEI, PolySciences). Virus stocks generated with *env*-deficient infectious clones used for infection assays were pseudotyped with the VSV-G protein by co-transfection with the plasmid pHCMV-G. Virus stocks for the core isolation assay were made without the VSV-G expression vector. Lentivirus vectors encoding shRNA targeting cellular genes were co-transfected with the Gag-Pol expression vector pCRV1-Gag-Pol into five million 293T cells in a 100-mm tissue plate and virus was concentrated with polyethylene glycol (PEG; Sigma). Briefly, 8 ml of filtered supernatant was mixed with 2 ml of 30% (weight/volume) of PEG in 1× phosphate-buffered saline (PBS) and stored at 4 ºC overnight. Virus was pelleted by centrifuging the mixture at 1200× g for at least 45 minutes at 4 ºC and resuspended with 0.8 ml of DMEM with 10% FBS. For generating high-titer virus stocks, several 100 mm plates were seeded with five million 293T cells per plate. Culture supernatant harvested at two days after transfection was filtrated with a Steriflip polyvinylidene difluoride (PVDF) filter unit (0.45 µm, Millipore) and carefully layered onto 5 ml of 20% (weight/volume) sucrose solution made with 1× PBS in a Beckman polyallomer tube (Beckman Coulter) and spun down for two hours at 24,000 rpm and 4 ºC using an SW28 rotor. Virus pellets were resuspended with 3.2 ml of culture medium and aliquots were stored at -80 ºC until use.

Infection and Replication

Adherent cells were plated at 5,000 cells per well in 96-well plates. Infection was enhanced by addition of diethylaminoethyl (DEAE)-dextran (20 µg/ml) and spinocluation (1200× g for 30 minutes). Suspension cells were plated at 30,000 cells per well in 96-well plates. MDMs were plated for infection at 5 × 105 cells per ml in 96-well plates. For infection experiments that

examined the sensitivity of VSV-G-pseudotyped viruses to PF74 (Sigma and Aobious), cells were infected at an MOI of 0.1. To quantify induction of type I IFN, THP-1 cells or MDMs were infected with varying amounts of inoculum. Culture supernatant was harvested at one day after infection for IFN bioassay (see below). The number of GFP-positive cells was counted at two or three days after infection using LSRII flow cytometer (BD Biosciences) or Guava easyCyte (Millipore). Virus-infected TZM-bl cells were lysed with 25 µl of 1× Luciferase Cell Culture Lysis Reagent (Promega) for 5 minutes and one fifth of cell lysates were mixed with 25 µl of the luciferase assay reagent (Promega) before measuring luciferase activity on a luminometer. Nevirapine (NIH AIDS Reagent Program), raltegravir (Aobious), and dolutegravir (Aobious) were used at 50 µM, 10 µM and 10 µM, respectively. In a spreading infection assay, MT-4 cells were used as target cells together with replication-competent GFP reporter viruses. Virus stocks generated with intact provirus clones carrying different CA-encoding sequences were used to infect 20,000 MT-4 cells per well in a 96-well plate with virus inputs that yield approximately 1% of GFP-positive cells at 2 days post infection (dpi). A fraction of virus-infected cells was harvested from 2 to 4 dpi for counting the number of GFP-expressing cells by flow cytometry.

PF74 Binding

The affinity of PF74 for recombinant WT and R143A CA hexamers was determined as described previously (419). Briefly, CA hexamers of the WT virus and R143A mutant (containing a substitution of arginine to alanine at position 143 in CA) were generated by *in vitro* assembly of purified recombinant CA carrying four amino acid substitutions that stabilize the hexamer through disulfide bond formation (661). [^{3}H]-PF74 produced from triiodo-PF74 (410) was used in equilibrium dialysis. Various concentrations (0.10 to 1.0 µM) of [^{3}H]-PF74 in 500 µl solution was

added in duplicate into the buffer chamber and 300 µl of 1.0 µM CA hexameric protein into the sample chamber of the rapid equilibrium dialysis plate (Thermo Fisher Scientific). The plate was rotated at 100 rpm during 24-hour incubation at 37 ºC. ^{3}H in each sample removed from each side of the chamber was quantified by liquid scintillation counting in a TopCount (PerkinElmer) scintillation counter. The [^{3}H]-PF74 concentrations were determined using a reference sample containing a known quantity of [^{3}H]-PF74. Calculation of K_d (dissociation constant) values was performed using a one-site binding model in the GraphPad Prism software (GraphPad software).

Isolation of HIV-1 Cores

Effects of PF74 on HIV-1 cores were assessed using the previously described procedure (228, 410, 633) with several modifications. Virus particles pre-treated with or without 10 µM PF74 at 37 ºC for one hour were subjected to the "spin-thru" method to isolate cores. A sucrose gradient tube consists of a layer of 15% sucrose containing 0.5% Triton X-100 (Sigma), which is placed in between a top barrier fraction of 7.5% sucrose and a linear discontinuous 30-70% sucrose gradient (made with 30, 40, 50, 60 and 70% sucrose). Sucrose solutions were made with the STE buffer (10 mM Tris-HCl pH 7.4, 100 mM NaCl, 1 mM EDTA). Pre-treated virion particles were carefully loaded on the top of the gradient and spun using ultracentrifugation at 100,000× g for 16 to 18 hours at 4 ºC. After the centrifugation, fractions of 700 µl were harvested from the top of the gradient and the pellet was resuspended with 700 µl the STE buffer. The density of fractions was measured by weighing 100 µl of each fraction (except for the pellet fraction) using 1.7 ml microcentrifuge tubes.

RT Activity Assay

RT activity in fractions harvested after ultracentrifugation was quantitated using a SYBR Green I-based product enhanced RT (SG-PERT) assay with several modifications (532). Five µl of each fraction was lysed for 10 minutes at room temperature with the equal amount of 2× lysis buffer (0.25% Triton X-100, 50 mM KCl, 100 mM Tris-HCl pH 7.4, 40% glycerol), which was supplemented with 0.4 units of RiboLock RNase inhibitor (Thermo Fisher Scientific) per µl before use. The lysed materials were diluted 10-fold before used in reverse transcription and quantitative PCR reaction on an Applied Biosystems 7500 fast Real-Time PCR System (Thermo Fisher Scientific). Ten µl of the samples was mixed with equal amounts of 2× reaction buffer. The composition of the 2 × reaction buffer was the following: 5 mM (NH4)2SO4, 20 mM KCl, 20 mM Tris-Cl (pH 8.3), 10mM MgCl2, 0.2 mg/ml bovine serum albumin (BSA, NEB), 1× SYBR Green I Nucleic Acid Gel Stain (Thermo Fisher Scientific), 400 µM dNTP (Bioline), 1 µM forward primer, 1 µM reverse primer, 7 nM MS2 RNA (Sigma), 50 nM ROX Reference Dye (Thermo Fisher Scientific), 40 units per ml of RiboLock RNase inhibitor and 25 units per ml of Hot Diamond Taq DNA Polymerase (Eurogentec).

The following primers were used: MS2fwd: 5'-TCCTGCTCAACTTCCTGTCGAG-3', and MS2rev: 5'-CACAGGTCAAACCTCCTAGGAATG-3'. The real-time PCR condition was as follows: 42 ºC for 20 minutes, 95 ºC for 2 minutes and 40 cycles of 95 ºC for 5 seconds, 60 ºC for 5 seconds, 72 ºC for 15 seconds and 80 ºC for 7 seconds. PCR was run with serially diluted samples of known RT amount, which were used to generate a standard curve for absolute quantification.

p24 CA ELISA

Antigen capture enzyme-linked immunosorbent assay (ELISA) was used to quantify the amount of p24 CA in fractions after the spin-thru procedure using a published protocol with minor modifications (633, 662). Monoclonal anti-HIV-1 p24 antibody (183-h12-5C, NIH AIDS Research and Reference Reagent Program) was used to coat Immulon 2HB 96-well plates (Thermo Fisher Scientific) at 1.3 μg/ml in PBS and 37 ºC overnight. The coated plate was blocked for one hour with 0.25 ml of blocking solution, which consists of 5% milk and 0.5% BSA (Sigma) in PBS. Samples were added to the plates together with serial dilution of a standard sample that contains a predetermined amount of p24 CA. Several dilutions were made from the original fraction so that the values for the p24 amount fell within a linear range of the standard curve. After two hours incubation, hyperimmune human patient serum (HIV immunoglobulin, NIH AIDS Research and Reference Reagent Program) was diluted 1: 20,000 and added before one-hour incubation. Peroxidase conjugated goat anti-human immunoglobulin G (Pierce) was diluted at 20 pg per ml in a PBS-based ELISA sample diluent buffer containing 10% FBS and 0.5% Triton X-100 (Sigma). Plates were washed six times after each process with 0.2% Tween 20 (Sigma) in PBS, except for the washing step before blocking where PBS was used. After the final wash, enzymatic activity of the peroxidase was detected by addition of 3,3',5,5'-tetramethylbenzidine solution using the TMB Microwell Peroxidase Substrate Kit (KPL Inc). Reaction was stopped by adding an equal volume of 0.5 M H2SO4 (EMD Millipore). Optical density at 450 nm was measured on a microplate reader. A standard curve generated with serially diluted virus stocks of known p24 amount was used to interpolate the concentration of samples.

In vitro Imaging Assay for Capsid Stability

In vitro single virus uncoating assay was performed, as described previously (287, 525). Briefly, viruses bearing CA from WT or mutant strains were labeled with INmNeonGreen (INmNG) expressed in producer producer cells. Viruses were bound on a cover glass, and the viral membrane was permeabilized with 100 μg/ml of saponin for 30 seconds to expose the cores. Viral cores were then treated with 0.1 mg/ml of cytosolic extract from 293T cells containing 200 nM of CypA-DsRed for 90 seconds to allow CypA-DsRed binding to cores. After removal of the cytosolic extract, CypA-DsRed bound cores were washed once with PBS to remove any unbound CypA-DsRed and cores co-labeled with INmNG/CypA-DsRed were imaged at room temperature. Images were taken from four fields of view every 30 seconds. CsA (5 μM) was added at 30 min post permeabilization to displace CypA-DsRed from cores that have not completed uncoating. The number of INmNG and CypA-DsRed viral puncta was calculated using the spot detector in the ICY-image analysis platform (http://icy.bioimageanalysis.org/).

Live Cell Imaging of Post-Fusion Cores

A live cell-based assay for capsid uncoating was performed as previously described (287, 525). VSV-G pseudotyped virus particles were co-labeled with INmNeonGreen and CypA-DsRed in 293T producer cells. Virus inoculum containing 10 pg of p24 was allowed to bind to 5×10^5 TZM-bl cells (equivalent to MOI 0.008) by spinoculation at 1500× g, at 12 °C for 30 minutes. Prior to virus binding, cell nuclei were stained for 10 minutes with 2 μg per ml of Hoechst-33342. The cells were washed twice, and virus entry was synchronously initiated on a temperature- and CO2-controlled microscope stage by adding pre-warmed Fluorobrite (Gibco) imaging medium supplemented with 10% FBS. Imaging was performed for a period of 2 hours with 20-seconds

time-lapse acquisition of whole cell-volume. At 90 minutes post infection, CsA (10 μM) was added and imaging was continued. Addition of CsA displaces CypA-DsRed from post-fusion cores that have not yet completed uncoating, without affecting the CypA-DsRed signal from intact viruses residing in endosome. The fraction of post-fusion cores per cell was calculated by dividing the number of cytosolic cores that lost CypA-DsRed upon CsA application at 90 minutes post infection by the total number of CypA-DsRed-positive cores at 0 minutes.

Capsid Permeabilization Assay

HEK293T cells (ATCC) were transfected with 1) pBru3ori-ΔEnv-luc2; 2) pVpr-mRuby3-IN (521); and 3) pCMV-VSV-G plasmids using Lipofectamine 2000 (Thermo Fisher Scientific) in the presence of 5-ethynyl uridine (EU), as previously described (500, 640). After 48 hours, the cell supernatant was collected and filtered through a 0.45 μm polyethersulfone (PES) syringe filter (Millipore). Excess EU was removed and virus was concentrated via Lenti-X Concentrator (Clontech). HeLa cells were synchronously infected with EU-labeled HIV-1 (20 ng of p24 as determined by ELISA; XpressBio). Cells were fixed 15 - 90 minutes post-infection, permeabilized, stained for viral RNA (EU-AF647 Click-iT, Invitrogen) and cell nuclei (Hoechst 33342), and mounted with coverslips. Confocal imaging was performed on a Nikon A1 laser scanning confocal microscope, with 7-9 z-stacks (0.5 μm spacing) taken per sample. RNA punctae and mRuby3-IN labeled particles were enumerated via Imaris software. The average number of RNA puncta in the uninfected negative control samples for each experiment was subtracted from each imaging field. Grubbs' extreme studentized deviate test was used to identify and exclude statistical outliers. The capsid permeabilization kinetics were analyzed by multiple linear regression modeling using the SAS software to test if the slopes were equivalent. Using the F statistic with the Bonferroni

correction for pairwise comparisons, p values less than 0.0167 were considered statistically significant.

IFN Bioassay

We examined the production of type I IFN by using the reporter cell line HEK293-ISRE-Luc (660). This reporter cell line carries IFN-stimulated response element (ISRE) within the promoter region driving the expression of luciferase. One day prior to use, HEK293-ISRE-Luc cells were plated on a 96-well flat bottom plate at 30,000 cells per well with 100 µl of cell suspension. One day after infection of THP-1 cells or MDMs, 50 µl of culture supernatant was harvested and transferred into the 96-well flat bottom plate containing HEK293-ISRE-Luc. In each experiment, the IFN standard curve was generated using a stock solution of recombinant interferon αA/D (Sigma). A working solution of IFN at 10,000 units per ml was used to generate 10-fold serial dilutions. These standard dilutions were added at 10 µl per well in duplicate. The cells were placed in a tissue culture incubator after addition of supernatant samples and IFN standards. At the following day, the cells were lysed with 20 µl of 1× buffer prepared from Luciferase Cell Culture Lysis 5× Reagent (Promega) for five minutes at 37 ºC. Five µl of cells lysates was transferred to an opaque 96-well plate and 25 µl of the luciferase assay reagent (Promega) was added, followed by reading the relative luciferase units in a luminometer.

Quantification of Cellular RNA by Reverse Transcription-PCR (qRT-PCR)

Knockdown efficiency of mRNA encoding cGAS was assessed using qRT-PCR. Total RNA was isolated using the TRIzol reagent (Thermo Fisher Scientific) based on the manufacturer's protocol from cell pellets collected on three different dates. The extracted RNA was used for cDNA

synthesis with random hexamers and a High Capacity cDNA Reverse Transcription Kit (Applied Biosystems). Expression levels of respective genes were determined by a SYBR green-based quantitative PCR using gene-specific primers and normalized to glyceraldehyde-3-phosphate dehydrogenase (GAPDH) mRNA levels using the 2-ΔΔCT method. The primer sequences used were: hcGAS-F: 5'-CCTGCTGTAACACTTCTTAT-3', hcGAS-R; 5'-TTAGTCGTAGTTGCTTCCT-3', GAPDH-F: 5'-GGCTGAGAACGGGAAGCTT-3', GAPDH-R: 5'-AGGGATCTCGCTCCTGGAA-3'.

Expression of C-X-C motif chemokine ligand 10 (CXCL10 also known as IP-10) was assessed by a TaqMan-based real-time PCR. RNA was extracted from virus-infected THP-1 cells at one day after infection by using a NucleoSpin 8 RNA kit (Macherey-Nagel) and used for cDNA synthesis as described above. The cDNA sample was used for real-time PCR with TaqMan universal master mix II (Applied Biosystems). The following primers were used as the forward and reverse primers, respectively: IP10f: 5'-TGAAATTATTCCTGCAAGCCAATT-3', IP10r: 5'-CAGACATCTCTTCTCACCCTTCTTT-3'. The sequence of the TaqMan probe (IP10p) was as follows: 5'-FAM-TGTCCACGTGTTGAGATCATTGCTACAATG-TAMRA-3' (FAM, 6-carboxyfluorescein; TAMRA, 6-carboxytetramethylrhodamine). A standard curve ranging from 9×10^7 to 90 copies per reaction was generated by making 10-fold serial dilutions from the plasmid carrying the amplicon (pGEM-T Easy-huIP10).

Quantitative PCR for Viral DNA

THP-1 cells were infected with virus stocks that were treated with 80 units per ml of Turbo DNase (Thermo Fisher Scientific) at 37 ºC for 1 hour before infection. Virus-infected cells were harvested

at different time points and stored at -80 ºC. Cell pellets were processed for DNA extraction using the NucleoSpin tissue kit (Macherey-Nagel). Concentrations of genomic DNA were measured using the NanoDrop 1000 Spectrophotometer (Thermo Fisher Scientific). Semi-nested qPCR was performed to quantify early and late products of reverse transcription. Amplification of early RT products used ME31 (5'-AGACCAGATTTGAGCCTG-3') and uoLTRr (5'-CCACACTGACTAAAAGGGTCTGA-3') in the first PCR and MH531 5'-TGTGTGCCCGTCTGTTGTGT-3') and uoLTRr in the second PCR. PCR for the late PCR products were performed with MH535 (5'-AACTAGGGAACCCACTGCTTAAG-3') and MH532 (5'-GAGTCCTGCGTCGAGAGAGC-3') in the first reaction and MH531 (5'-TGTGTGCCCGTCTGTTGTGT-3') and MH532 in the second reaction. The second PCR was performed using PowerUp SYBR Green Master Mix (Thermo Fisher Scientific) on the 7500 Fast real-time PCR system (Applied Biosystems). A standard curve was generated using known amounts of template DNA of plasmid DNA pLai3-GFP3 by serially diluting by 10-fold. Results were normalized to the concentration of DNA.

A.5 Acknowledgments

We are grateful to K. Shutt for helping with statistical analysis and to X. Li for sharing the reporter cell line HEK293-ISRE-Luc. The following reagents were obtained through the NIH AIDS Reagent Program, Division of AIDS, NIAID, NIH: Panel of full-length transmitted/founder (T/F) HIV-1 Infectious Molecular Clones (Cat #11919) from Dr. John Kappes, TZM-bl from John C. Kappes, Xiaoyun Wu, and Tranzyme Inc, Nevirapine, HIV-1 p24 monoclonal antibody (183-H12-5C) from Bruce Chesebro and Kathy Wehrly, and HIV Immunoglobulin (HIV-IG) from NABI

and NHLBI. This work was supported by NIH grants R01AI100720 (M.Y.), R01AI114339 (C.A.), R01AI129862 (G.B.M.), P50GM082251 (Z.A.) and T32AI065380 (D.K.F.).

Bibliography

1. **Centers for Disease Control (CDC)**. 1981. Pneumocystis pneumonia -- Los Angeles. MMWR Morb Mortal Wkly Rep **30**:250–252.

2. **Walzer PD**, **Perl DP**, **Krogstad DJ**, **Rawson PG**, **Schultz MG**. 1974. Pneumocystis carinii Pneumonia in the United States: Epidemiologic, Diagnostic, and Clinical Features. AIM **80**:83–93.

3. **Centers for Disease Control (CDC)**. 1981. Kaposi's sarcoma and Pneumocystis pneumonia among homosexual men -- New York City and California. MMWR Morb Mortal Wkly Rep **30**:305–308.

4. **Cesarman E**, **Damania B**, **Krown SE**, **Martin J**, **Bower M**, **Whitby D**. 2019. Kaposi sarcoma. Nat Rev Dis Primers **5**:9.

5. **Gottlieb MS**, **Schroff R**, **Schanker HM**, **Weisman JD**, **Fan PT**, **Wolf RA**, **Saxon A**. 1981. Pneumocystis carinii Pneumonia and Mucosal Candidiasis in Previously Healthy Homosexual Men. N Engl J Med **305**:1425–1431.

6. **Masur H**, **Michelis MA**, **Greene JB**, **Onorato I**, **Vande Stouwe RA**, **Holzman RS**, **Wormser G**, **Brettman L**, **Lange M**, **Murray HW**, **Cunningham-Rundles S**. 1981. An Outbreak of Community-Acquired Pneumocystis carinii Pneumonia. N Engl J Med **305**:1431–1438.

7. **Siegal FP**, **Lopez C**, **Hammer GS**, **Brown AE**, **Kornfeld SJ**, **Gold J**, **Hassett J**, **Hirschman SZ**, **Cunningham-Rundles C**, **Adelsberg BR**, **Parham DM**, **Siegal M**, **Cunningham-Rundles S**, **Armstrong D**. 1981. Severe Acquired Immunodeficiency in Male Homosexuals, Manifested by Chronic Perianal Ulcerative Herpes Simplex Lesions. N Engl J Med **305**:1439–1444.

8. **Centers for Disease Control (CDC)**. 1982. Update on acquired immune deficiency syndrome (AIDS) -- United States. MMWR Morb Mortal Wkly Rep **31**:507–8–513–4.

9. **U.S. Department of Health and Human Services**. 1986. Surgeon General's Report on Acquired Immune Deficiency Syndrome. Office of the Surgeon General, U.S. Public Health Service.

10. **De Cock KM**, **Jaffe HW**, **Curran JW**. 2011. Reflections on 30 years of AIDS. Emerging Infect Dis **17**:1044–1048.

11. **Fauci AS**. 1988. The human immunodeficiency virus: infectivity and mechanisms of pathogenesis. Science **239**:617–622.

12. **World Health Organization**. WHO HIV/AIDS Fact Sheet. https://www.who.int/en/news-room/fact-sheets/detail/hiv-aids. Accessed 16 Apr 2019. WHO Website.

13. **Thompson G**. 2007. American Culture in the 1980s. Edinburgh University Press, Edinburgh.

14. **Rueda S**, **Mitra S**, **Chen S**, **Gogolishvili D**, **Globerman J**, **Chambers L**, **Wilson M**, **Logie CH**, **Shi Q**, **Morassaei S**, **Rourke SB**. 2016. Examining the associations between HIV-related stigma and health outcomes in people living with HIV/AIDS: a series of meta-analyses. BMJ Open **6**:e011453.

15. **Remien RH**, **Mellins CA**. 2007. Long-term psychosocial challenges for people living with HIV: let's not forget the individual in our global response to the pandemic. AIDS **21 Suppl 5**:S55–63.

16. **Mahajan AP**, **Sayles JN**, **Patel VA**, **Remien RH**, **Sawires SR**, **Ortiz DJ**, **Szekeres G**, **Coates TJ**. 2008. Stigma in the HIV/AIDS epidemic: a review of the literature and recommendations for the way forward. AIDS **22 Suppl 2**:S67–79.

17. **World Health Organization**. 1984. Acquired immunodeficiency syndrome -- an assessment of the present situation in the world: Memorandum from a WHO Meeting. Bull World Health Organ **62**:419–432.

18. **Joint United Nations Programme on HIV/AIDS (UNAIDS)**. 25 Years of AIDS. http://www.uncares.org/common/docs/25YearsofAIDS_en.pdf. Accessed 16 Apr 2019. UNAIDS Website.

19. **Piot P**, **Bartos M**, **Ghys PD**, **Walker N**, **Schwartländer B**. 2001. The global impact of HIV/AIDS. Nature **410**:968–973.

20. **Barré-Sinoussi F**, **Chermann JC**, **Rey F**, **Nugeyre MT**, **Chamaret S**, **Gruest J**, **Dauguet C**, **Axler-Blin C**, **Vézinet-Brun F**, **Rouzioux C**, **Rozenbaum W**, **Montagnier L**. 1983. Isolation of a T-lymphotropic retrovirus from a patient at risk for acquired immune deficiency syndrome (AIDS). Science **220**:868–871.

21. **Popovic M**, **Sarngadharan MG**, **Read E**, **Gallo RC**. 1984. Detection, isolation, and continuous production of cytopathic retroviruses (HTLV-III) from patients with AIDS and pre-AIDS. Science **224**:497–500.

22. **Gallo RC**, **Salahuddin SZ**, **Popovic M**, **Shearer GM**, **Kaplan M**, **Haynes BF**, **Palker TJ**, **Redfield R**, **Oleske J**, **Safai B**. 1984. Frequent detection and isolation of cytopathic retroviruses (HTLV-III) from patients with AIDS and at risk for AIDS. Science **224**:500–503.

23. **Schüpbach J**, **Popovic M**, **Gilden RV**, **Gonda MA**, **Sarngadharan MG**, **Gallo RC**. 1984. Serological analysis of a subgroup of human T-lymphotropic retroviruses (HTLV-III) associated with AIDS. Science **224**:503–505.

24. **Sarngadharan MG**, **Popovic M**, **Bruch L**, **Schüpbach J**, **Gallo RC**. 1984. Antibodies reactive with human T-lymphotropic retroviruses (HTLV-III) in the serum of patients with AIDS. Science **224**:506–508.

25. **Arts EJ**, **Hazuda DJ**. 2012. HIV-1 antiretroviral drug therapy. Cold Spring Harb Perspect Med **2**:a007161.

26. **Baeten JM**, **Donnell D**, **Ndase P**, **Mugo NR**, **Campbell JD**, **Wangisi J**, **Tappero JW**, **Bukusi EA**, **Cohen CR**, **Katabira E**, **Ronald A**, **Tumwesigye E**, **Were E**, **Fife KH**, **Kiarie J**, **Farquhar C**, **John-Stewart G**, **Kakia A**, **Odoyo J**, **Mucunguzi A**, **Nakku-Joloba E**, **Twesigye R**, **Ngure K**, **Apaka C**, **Tamooh H**, **Gabona F**, **Mujugira A**, **Panteleeff D**, **Thomas KK**, **Kidoguchi L**, **Krows M**, **Revall J**, **Morrison S**, **Haugen H**, **Emmanuel-Ogier M**, **Ondrejcek L**, **Coombs RW**, **Frenkel L**, **Hendrix C**, **Bumpus NN**, **Bangsberg D**, **Haberer JE**, **Stevens WS**, **Lingappa JR**, **Celum C**, **Partners PrEP Study Team**. 2012. Antiretroviral prophylaxis for HIV prevention in heterosexual men and women. N Engl J Med **367**:399–410.

27. **Deeks SG**, **Lewin SR**, **Havlir DV**. 2013. The end of AIDS: HIV infection as a chronic disease. Lancet **382**:1525–1533.

28. **Pham HT**, **Mesplede T**. 2018. The latest evidence for possible HIV-1 curative strategies. Drugs Context **7**:212522.

29. **Sengupta S**, **Siliciano RF**. 2018. Targeting the Latent Reservoir for HIV-1. Immunity **48**:872–895.

30. **Jacobson JM**, **Khalili K**. 2018. Toward the Cure of HIV-1 Infection: Lessons Learned and Yet to be Learned as New Strategies are Developed. AIDS Rev **20**:220–225.

31. **Joint United Nations Programme on HIV/AIDS (UNAIDS)**. 2018. Miles To Go: Closing Gaps, Breaking Barriers, Righting Injustices. Global AIDS Update. Geneva.

32. **Joint United Nations Programme on HIV/AIDS (UNAIDS)**. Global HIV & AIDS Statistics -- 2018 fact sheet. http://www.unaids.org/en/resources/fact-sheet. Accessed 16 Apr 2019. UNAIDS Website.

33. **Ocfemia MCB**, **Dunville R**, **Zhang T**, **Barrios LC**, **Oster AM**. 2018. HIV Diagnoses Among Persons Aged 13-29 Years - United States, 2010-2014. MMWR Morb Mortal Wkly Rep **67**:212–215.

34. **Centers for Disease Control and Prevention**. 2017. HIV Surveillance Report, 2016; vol. 28. http://www.cdc.gov/hiv/library/reports/hiv-surveillance.html. U.S. Department of Health and Human Services.

35. **GBD 2015 HIV Collaborators**. 2016. Estimates of global, regional, and national incidence, prevalence, and mortality of HIV, 1980-2015: the Global Burden of Disease Study 2015. Lancet HIV **3**:e361–e387.

36. **Shaw GM**, **Hunter E**. 2012. HIV transmission. Cold Spring Harb Perspect Med **2**:a006965.

37. **Hladik F**, **McElrath MJ**. 2008. Setting the stage: host invasion by HIV. Nat Rev Immunol **8**:447–457.

38. **Maartens G**, **Celum C**, **Lewin SR**. 2014. HIV infection: epidemiology, pathogenesis, treatment, and prevention. Lancet **384**:258–271.

39. **Morris M**, **Kretzschmar M**. 1997. Concurrent partnerships and the spread of HIV. AIDS **11**:641–648.

40. **Dulioust E**, **Tachet A**, **De Almeida M**, **Finkielsztejn L**, **Rivalland S**, **Salmon D**, **Sicard D**, **Rouzioux C**, **Jouannet P**. 1998. Detection of HIV-1 in seminal plasma and seminal cells of HIV-1 seropositive men. J Reprod Immunol **41**:27–40.

41. **Goulston C**, **McFarland W**, **Katzenstein D**. 1998. Human immunodeficiency virus type 1 RNA shedding in the female genital tract. Journal of Infectious Diseases **177**:1100–1103.

42. **John GC**, **Kreiss J**. 1996. Mother-to-child transmission of human immunodeficiency virus type 1. Epidemiol Rev **18**:149–157.

43. **Curran JW**, **Lawrence DN**, **Jaffe H**, **Kaplan JE**, **Zyla LD**, **Chamberland M**, **Weinstein R**, **Lui K-J**, **Schonberger LB**, **Spira TJ**, **Alexander WJ**, **Swinger G**, **Ammann A**, **Solomon S**, **Auerbach D**, **Mildvan D**, **Stoneburner R**, **Jason JM**, **Haverkos HW**, **Evatt BL**. 1984. Acquired Immunodeficiency Syndrome (AIDS) Associated with Transfusions. N Engl J Med **310**:69–75.

44. **Fauci AS**, **Folkers GK**, **Lane HC**. 2018. Human Immunodeficiency Virus Disease: AIDS and Related Disorders. *In* Jameson, JL, Fauci, AS, Kasper, DL, Hauser, SL, Longo, DL, Loscalzo, J (eds.), Harrison's Principles of Internal Medicine, 20e. McGraw-Hill Education, New York, NY.

45. **Klatzmann D**, **Barré-Sinoussi F**, **Nugeyre MT**, **Danquet C**, **Vilmer E**, **Griscelli C**, **Brun-Veziret F**, **Rouzioux C**, **Gluckman JC**, **Chermann JC**. 1984. Selective tropism of lymphadenopathy associated virus (LAV) for helper-inducer T lymphocytes. Science **225**:59–63.

46. **Deng H**, **Liu R**, **Ellmeier W**, **Choe S**, **Unutmaz D**, **Burkhart M**, **Di Marzio P**, **Marmon S**, **Sutton RE**, **Hill CM**, **Davis CB**, **Peiper SC**, **Schall TJ**, **Littman DR**, **Landau NR**. 1996. Identification of a major co-receptor for primary isolates of HIV-1. Nature **381**:661–666.

47. **Feng Y**, **Broder CC**, **Kennedy PE**, **Berger EA**. 1996. HIV-1 entry cofactor: functional cDNA cloning of a seven-transmembrane, G protein-coupled receptor. Science **272**:872–877.

48. **van't Wout AB**, **Kootstra NA**, **Mulder-Kampinga GA**, **Albrecht-van Lent N**, **Scherpbier HJ**, **Veenstra J**, **Boer K**, **Coutinho RA**, **Miedema F**, **Schuitemaker H**. 1994. Macrophage-tropic variants initiate human immunodeficiency virus type 1 infection after sexual, parenteral, and vertical transmission. J Clin Invest **94**:2060–2067.

49. **Scarlatti G**, **Tresoldi E**, **Björndal A**, **Fredriksson R**, **Colognesi C**, **Deng HK**, **Malnati MS**, **Plebani A**, **Siccardi AG**, **Littman DR**, **Fenyö EM**, **Lusso P**. 1997. In vivo evolution of HIV-1 co-receptor usage and sensitivity to chemokine-mediated suppression. Nat Med **3**:1259–1265.

50. **van't Wout AB**, **Ran LJ**, **Kuiken CL**, **Kootstra NA**, **Pals ST**, **Schuitemaker H**. 1998. Analysis of the temporal relationship between human immunodeficiency virus type 1 quasispecies in sequential blood samples and various organs obtained at autopsy. J Virol **72**:488–496.

51. **Sattentau QJ**, **Weiss RA**. 1988. The CD4 antigen: physiological ligand and HIV receptor. Cell **52**:631–633.

52. **Clapham PR**, **McKnight A**. 2002. Cell surface receptors, virus entry and tropism of primate lentiviruses. J Gen Virol **83**:1809–1829.

53. **Shen R**, **Richter HE**, **Smith PD**. 2011. Early HIV-1 target cells in human vaginal and ectocervical mucosa. Am J Reprod Immunol **65**:261–267.

54. **Janeway CA**, **Carding S**, **Jones B**, **Murray J**, **Portoles P**, **Rasmussen R**, **Rojo J**, **Saizawa K**, **West J**, **Bottomly K**. 1988. CD4+ T cells: specificity and function. Immunol Rev **101**:39–80.

55. **Luckheeram RV**, **Zhou R**, **Verma AD**, **Xia B**. 2012. $CD4^+$T cells: differentiation and functions. Clin Dev Immunol **2012**:925135.

56. **Batista FD**, **Harwood NE**. 2009. The who, how and where of antigen presentation to B cells. Nat Rev Immunol **9**:15–27.

57. **Douek DC**, **Brenchley JM**, **Betts MR**, **Ambrozak DR**, **Hill BJ**, **Okamoto Y**, **Casazza JP**, **Kuruppu J**, **Kunstman K**, **Wolinsky S**, **Grossman Z**, **Dybul M**, **Oxenius A**, **Price DA**, **Connors M**, **Koup RA**. 2002. HIV preferentially infects HIV-specific CD4+ T cells. Nature **417**:95–98.

58. **Sleasman JW**, **Aleixo LF**, **Morton A**, **Skoda-Smith S**, **Goodenow MM**. 1996. CD4+ memory T cells are the predominant population of HIV-1-infected lymphocytes in neonates and children. AIDS **10**:1477–1484.

59. **McMichael AJ**, **Rowland-Jones SL**. 2001. Cellular immune responses to HIV. Nature **410**:980–987.

60. **Pantaleo G**, **Graziosi C**, **Demarest JF**, **Butini L**, **Montroni M**, **Fox CH**, **Orenstein JM**, **Kotler DP**, **Fauci AS**. 1993. HIV infection is active and progressive in lymphoid tissue during the clinically latent stage of disease. Nature **362**:355–358.

61. **Swanstrom R**, **Coffin J**. 2012. HIV-1 pathogenesis: the virus. Cold Spring Harb Perspect Med **2**:a007443.

62. **Laurent-Crawford AG**, **Krust B**, **Muller S**, **Rivière Y**, **Rey-Cuillé M-A**, **Béchet J-M**, **Montagnier L**, **Hovanessian AG**. 1991. The cytopathic effect of hiv is associated with apoptosis. Virology **185**:829–839.

63. **Doitsh G**, **Galloway NLK**, **Geng X**, **Yang Z**, **Monroe KM**, **Zepeda O**, **Hunt PW**, **Hatano H**, **Sowinski S**, **Muñoz-Arias I**, **Greene WC**. 2014. Cell death by pyroptosis drives CD4 T-cell depletion in HIV-1 infection. Nature **505**:509–514.

64. **Finkel TH**, **Tudor-Williams G**, **Banda NK**, **Cotton MF**, **Curiel T**, **Monks C**, **Baba TW**, **Ruprecht RM**, **Kupfer A**. 1995. Apoptosis occurs predominantly in bystander cells and not in productively infected cells of HIV- and SIV-infected lymph nodes. Nat Med **1**:129–134.

65. **Jekle A**, **Keppler OT**, **De Clercq E**, **Schols D**, **Weinstein M**, **Goldsmith MA**. 2003. In vivo evolution of human immunodeficiency virus type 1 toward increased pathogenicity through CXCR4-mediated killing of uninfected CD4 T cells. J Virol **77**:5846–5854.

66. **Doitsh G**, **Cavrois M**, **Lassen KG**, **Zepeda O**, **Yang Z**, **Santiago ML**, **Hebbeler AM**, **Greene WC**. 2010. Abortive HIV infection mediates CD4 T cell depletion and inflammation in human lymphoid tissue. Cell **143**:789–801.

67. **Doitsh G**, **Greene WC**. 2016. Dissecting How CD4 T Cells Are Lost During HIV Infection. Cell Host Microbe **19**:280–291.

68. **Shearer GM**, **Clerici M**. 1991. Early T-helper cell defects in HIV infection. AIDS **5**:245–253.

69. **Gordon S**, **Taylor PR**. 2005. Monocyte and macrophage heterogeneity. Nat Rev Immunol **5**:953–964.

70. **Ginhoux F**, **Jung S**. 2014. Monocytes and macrophages: developmental pathways and tissue homeostasis. Nat Rev Immunol **14**:392–404.

71. **Haldar M**, **Murphy KM**. 2014. Origin, development, and homeostasis of tissue-resident macrophages. Immunol Rev **262**:25–35.

72. **Aderem A**, **Underhill DM**. 1999. Mechanisms of phagocytosis in macrophages. Annu Rev Immunol **17**:593–623.

73. **Neefjes J**, **Jongsma MLM**, **Paul P**, **Bakke O**. 2011. Towards a systems understanding of MHC class I and MHC class II antigen presentation. Nat Rev Immunol **11**:823–836.

74. **Mantegazza AR**, **Magalhaes JG**, **Amigorena S**, **Marks MS**. 2013. Presentation of phagocytosed antigens by MHC class I and II. Traffic **14**:135–152.

75. **Levy JA**, **Shimabukuro J**, **Mc Hugh T**, **Casavant C**, **Stites D**, **Oshiro L**. 1985. AIDS-associated retroviruses (ARV) can productively infect other cells besides human T helper cells. Virology **147**:441–448.

76. **Ho DD**, **Rota TR**, **Hirsch MS**. 1986. Infection of monocyte/macrophages by human T lymphotropic virus type III. J Clin Invest **77**:1712–1715.

77. **Koenig S**, **Gendelman HE**, **Orenstein JM**, **Dal Canto MC**, **Pezeshkpour GH**, **Yungbluth M**, **Janotta F**, **Aksamit A**, **Martin MA**, **Fauci AS**. 1986. Detection of AIDS virus in macrophages in brain tissue from AIDS patients with encephalopathy. Science **233**:1089–1093.

78. **Gabuzda DH**, **Ho DD**, **la Monte de SM**, **Hirsch MS**, **Rota TR**, **Sobel RA**. 1986. Immunohistochemical identification of HTLV-III antigen in brains of patients with AIDS. Ann Neurol **20**:289–295.

79. **Joseph SB**, **Arrildt KT**, **Sturdevant CB**, **Swanstrom R**. 2015. HIV-1 target cells in the CNS. J Neurovirol **21**:276–289.

80. **Watkins BA**, **Dorn HH**, **Kelly WB**, **Armstrong RC**, **Potts BJ**, **Michaels F**, **Kufta CV**, **Dubois-Dalcq M**. 1990. Specific tropism of HIV-1 for microglial cells in primary human brain cultures. Science **249**:549–553.

81. **Nicholson JK**, **Cross GD**, **Callaway CS**, **McDougal JS**. 1986. In vitro infection of human monocytes with human T lymphotropic virus type III/lymphadenopathy-associated virus (HTLV-III/LAV). J Immunol **137**:323–329.

82. **Salahuddin SZ**, **Rose RM**, **Groopman JE**, **Markham PD**, **Gallo RC**. 1986. Human T lymphotropic virus type III infection of human alveolar macrophages. Blood **68**:281–284.

83. **Carter CA**, **Ehrlich LS**. 2008. Cell biology of HIV-1 infection of macrophages. Annu Rev Microbiol **62**:425–443.

84. **Clayton KL**, **Garcia JV**, **Clements JE**, **Walker BD**. 2017. HIV Infection of Macrophages: Implications for Pathogenesis and Cure. Pathog Immun **2**:179–192.

85. **Salazar-Gonzalez JF**, **Salazar MG**, **Keele BF**, **Learn GH**, **Giorgi EE**, **Li H**, **Decker JM**, **Wang S**, **Baalwa J**, **Kraus MH**, **Parrish NF**, **Shaw KS**, **Guffey MB**, **Bar KJ**, **Davis KL**, **Ochsenbauer-Jambor C**, **Kappes JC**, **Saag MS**, **Cohen MS**, **Mulenga J**, **Derdeyn CA**, **Allen S**, **Hunter E**, **Markowitz M**, **Hraber P**, **Perelson AS**, **Bhattacharya T**, **Haynes BF**, **Korber BT**, **Hahn BH**, **Shaw GM**. 2009. Genetic identity, biological phenotype, and evolutionary pathways of transmitted/founder viruses in acute and early HIV-1 infection. J Exp Med **206**:1273–1289.

86. **Keele BF**, **Derdeyn CA**. 2009. Genetic and antigenic features of the transmitted virus. Curr Opin HIV AIDS **4**:352–357.

87. **DiNapoli SR**, **Ortiz AM**, **Wu F**, **Matsuda K**, **Twigg HL**, **Hirsch VM**, **Knox K**, **Brenchley JM**. 2017. Tissue-resident macrophages can contain replication-competent virus in antiretroviral-naive, SIV-infected Asian macaques. JCI Insight **2**:e91214.

88. **DiNapoli SR**, **Hirsch VM**, **Brenchley JM**. 2016. Macrophages in Progressive Human Immunodeficiency Virus/Simian Immunodeficiency Virus Infections. J Virol **90**:7596–7606.

89. **Arrildt KT**, **LaBranche CC**, **Joseph SB**, **Dukhovlinova EN**, **Graham WD**, **Ping L-H**, **Schnell G**, **Sturdevant CB**, **Kincer LP**, **Mallewa M**, **Heyderman RS**, **Rie AV**, **Cohen MS**, **Spudich S**, **Price RW**, **Montefiori DC**, **Swanstrom R**. 2015. Phenotypic Correlates of HIV-1 Macrophage Tropism. J Virol **89**:11294–11311.

90. **Diamond TL**, **Roshal M**, **Jamburuthugoda VK**, **Reynolds HM**, **Merriam AR**, **Lee KY**, **Balakrishnan M**, **Bambara RA**, **Planelles V**, **Dewhurst S**, **Kim B**. 2004. Macrophage tropism of HIV-1 depends on efficient cellular dNTP utilization by reverse transcriptase. J Biol Chem **279**:51545–51553.

91. **Hrecka K**, **Hao C**, **Gierszewska M**, **Swanson SK**, **Kesik-Brodacka M**, **Srivastava S**, **Florens L**, **Washburn MP**, **Skowronski J**. 2011. Vpx relieves inhibition of HIV-1 infection of macrophages mediated by the SAMHD1 protein. Nature **474**:658–661.

92. **Laguette N**, **Sobhian B**, **Casartelli N**, **Ringeard M**, **Chable-Bessia C**, **Ségéral E**, **Yatim A**, **Emiliani S**, **Schwartz O**, **Benkirane M**. 2011. SAMHD1 is the dendritic- and myeloid-cell-specific HIV-1 restriction factor counteracted by Vpx. Nature **474**:654–657.

93. **Shen R**, **Richter HE**, **Clements RH**, **Novak L**, **Huff K**, **Bimczok D**, **Sankaran-Walters S**, **Dandekar S**, **Clapham PR**, **Smythies LE**, **Smith PD**. 2009. Macrophages in vaginal but not intestinal mucosa are monocyte-like and permissive to human immunodeficiency virus type 1 infection. J Virol **83**:3258–3267.

94. **Koppensteiner H**, **Brack-Werner R**, **Schindler M**. 2012. Macrophages and their relevance in Human Immunodeficiency Virus Type I infection. Retrovirology **9**:82.

95. **Pantaleo G**, **Graziosi C**, **Fauci AS**. 1993. The immunopathogenesis of human immunodeficiency virus infection. N Engl J Med **328**:327–335.

96. **Fiebig EW**, **Wright DJ**, **Rawal BD**, **Garrett PE**, **Schumacher RT**, **Peddada L**, **Heldebrant C**, **Smith R**, **Conrad A**, **Kleinman SH**, **Busch MP**. 2003. Dynamics of HIV viremia and antibody seroconversion in plasma donors: implications for diagnosis and staging of primary HIV infection. AIDS **17**:1871–1879.

97. **Haase AT**. 2010. Targeting early infection to prevent HIV-1 mucosal transmission. Nature **464**:217–223.

98. **Ribeiro RM**, **Qin L**, **Chavez LL**, **Li D**, **Self SG**, **Perelson AS**. 2010. Estimation of the initial viral growth rate and basic reproductive number during acute HIV-1 infection. J Virol **84**:6096–6102.

99. **Tindall B**, **Cooper DA**. 1991. Primary HIV infection: host responses and intervention strategies. AIDS **5**:1–14.

100. **Graziosi C**, **Pantaleo G**, **Butini L**, **Demarest JF**, **Saag MS**, **Shaw GM**, **Fauci AS**. 1993. Kinetics of human immunodeficiency virus type 1 (HIV-1) DNA and RNA synthesis during primary HIV-1 infection. Proc Natl Acad Sci USA **90**:6405–6409.

101. **Lackner AA**, **Lederman MM**, **Rodriguez B**. 2012. HIV pathogenesis: the host. Cold Spring Harb Perspect Med **2**:a007005.

102. **Guadalupe M**, **Reay E**, **Sankaran S**, **Prindiville T**, **Flamm J**, **McNeil A**, **Dandekar S**. 2003. Severe CD4+ T-cell depletion in gut lymphoid tissue during primary human immunodeficiency virus type 1 infection and substantial delay in restoration following highly active antiretroviral therapy. J Virol **77**:11708–11717.

103. **Brenchley JM**, **Schacker TW**, **Ruff LE**, **Price DA**, **Taylor JH**, **Beilman GJ**, **Nguyen PL**, **Khoruts A**, **Larson M**, **Haase AT**, **Douek DC**. 2004. CD4+ T cell depletion during all stages of HIV disease occurs predominantly in the gastrointestinal tract. Journal of Experimental Medicine **200**:749–759.

104. **Mehandru S**, **Poles MA**, **Tenner-Racz K**, **Horowitz A**, **Hurley A**, **Hogan C**, **Boden D**, **Racz P**, **Markowitz M**. 2004. Primary HIV-1 infection is associated with preferential depletion of CD4+ T lymphocytes from effector sites in the gastrointestinal tract. Journal of Experimental Medicine **200**:761–770.

105. **Cohen MS**, **Shaw GM**, **McMichael AJ**, **Haynes BF**. 2011. Acute HIV-1 Infection. N Engl J Med **364**:1943–1954.

106. **Brenchley JM**, **Douek DC**. 2008. The mucosal barrier and immune activation in HIV pathogenesis. Curr Opin HIV AIDS **3**:356–361.

107. **Coffin J**, **Swanstrom R**. 2013. HIV pathogenesis: dynamics and genetics of viral populations and infected cells. Cold Spring Harb Perspect Med **3**:a012526.

108. **Stacey AR**, **Norris PJ**, **Qin L**, **Haygreen EA**, **Taylor E**, **Heitman J**, **Lebedeva M**, **DeCamp A**, **Li D**, **Grove D**, **Self SG**, **Borrow P**. 2009. Induction of a striking systemic cytokine cascade prior to peak viremia in acute human immunodeficiency virus type 1 infection, in contrast to more modest and delayed responses in acute hepatitis B and C virus infections. J Virol **83**:3719–3733.

109. **Alter G**, **Teigen N**, **Ahern R**, **Streeck H**, **Meier A**, **Rosenberg ES**, **Altfeld M**. 2007. Evolution of innate and adaptive effector cell functions during acute HIV-1 infection. Journal of Infectious Diseases **195**:1452–1460.

110. **Naranbhai V**, **Altfeld M**, **Karim SSA**, **Ndung'u T**, **Karim QA**, **Carr WH**. 2013. Changes in Natural Killer cell activation and function during primary HIV-1 Infection. PLoS ONE **8**:e53251.

111. **Fauci AS**, **Desrosiers RC**. 1997. Pathogenesis of HIV and SIV. *In* Coffin, JM, Hughes, SH, Varmus, HE (eds.), Retroviruses. Cold Spring Harbor Laboratory Press, Cold Spring Harbor, NY.

112. **Borrow P**, **Lewicki H**, **Hahn BH**, **Shaw GM**, **Oldstone MB**. 1994. Virus-specific CD8+ cytotoxic T-lymphocyte activity associated with control of viremia in primary human immunodeficiency virus type 1 infection. J Virol **68**:6103–6110.

113. **Koup RA**, **Safrit JT**, **Cao Y**, **Andrews CA**, **McLeod G**, **Borkowsky W**, **Farthing C**, **Ho DD**. 1994. Temporal association of cellular immune responses with the initial control of viremia in primary human immunodeficiency virus type 1 syndrome. J Virol **68**:4650–4655.

114. **Pantaleo G**, **Demarest JF**, **Soudeyns H**, **Graziosi C**, **Denis F**, **Adelsberger JW**, **Borrow P**, **Saag MS**, **Shaw GM**, **Sekaly RP**. 1994. Major expansion of CD8+ T cells with a predominant V beta usage during the primary immune response to HIV. Nature **370**:463–467.

115. **Wilson JD**, **Ogg GS**, **Allen RL**, **Davis C**, **Shaunak S**, **Downie J**, **Dyer W**, **Workman C**, **Sullivan S**, **McMichael AJ**, **Rowland-Jones SL**. 2000. Direct visualization of HIV-1-specific cytotoxic T lymphocytes during primary infection. AIDS **14**:225–233.

116. **Pantaleo G**, **Fauci AS**. 1996. Immunopathogenesis of HIV infection. Annu Rev Microbiol **50**:825–854.

117. **Sierra S**, **Kupfer B**, **Kaiser R**. 2005. Basics of the virology of HIV-1 and its replication. J Clin Virol **34**:233–244.

118. **Tomaras GD**, **Yates NL**, **Liu P**, **Qin L**, **Fouda GG**, **Chavez LL**, **Decamp AC**, **Parks RJ**, **Ashley VC**, **Lucas JT**, **Cohen M**, **Eron J**, **Hicks CB**, **Liao H-X**, **Self SG**, **Landucci G**, **Forthal DN**, **Weinhold KJ**, **Keele BF**, **Hahn BH**, **Greenberg ML**, **Morris L**, **Karim SSA**, **Blattner WA**, **Montefiori DC**, **Shaw GM**, **Perelson AS**, **Haynes BF**. 2008. Initial B-cell responses to transmitted human immunodeficiency virus type 1: virion-binding immunoglobulin M (IgM) and IgG antibodies followed by plasma anti-gp41 antibodies with ineffective control of initial viremia. J Virol **82**:12449–12463.

119. **Moore JP**, **Cao Y**, **Ho DD**, **Koup RA**. 1994. Development of the anti-gp120 antibody response during seroconversion to human immunodeficiency virus type 1. J Virol **68**:5142–5155.

120. **Wei X**, **Decker JM**, **Wang S**, **Hui H**, **Kappes JC**, **Wu X**, **Salazar-Gonzalez JF**, **Salazar MG**, **Kilby JM**, **Saag MS**, **Komarova NL**, **Nowak MA**, **Hahn BH**, **Kwong PD**, **Shaw GM**. 2003. Antibody neutralization and escape by HIV-1. Nature **422**:307–312.

121. **Ogg GS**, **Jin X**, **Bonhoeffer S**, **Dunbar PR**, **Nowak MA**, **Monard S**, **Segal JP**, **Cao Y**, **Rowland-Jones SL**, **Cerundolo V**, **Hurley A**, **Markowitz M**, **Ho DD**, **Nixon DF**, **McMichael AJ**. 1998. Quantitation of HIV-1-specific cytotoxic T lymphocytes and plasma load of viral RNA. Science **279**:2103–2106.

122. **Clark SJ**, **Saag MS**, **Decker WD**, **Campbell-Hill S**, **Roberson JL**, **Veldkamp PJ**, **Kappes JC**, **Hahn BH**, **Shaw GM**. 1991. High Titers of Cytopathic Virus in Plasma of Patients with Symptomatic Primary HIV-1 Infection. N Engl J Med **324**:954–960.

123. **Daar ES**, **Moudgil T**, **Meyer RD**, **Ho DD**. 1991. Transient High Levels of Viremia in Patients with Primary Human Immunodeficiency Virus Type 1 Infection. N Engl J Med **324**:961–964.

124. **Mellors JW**, **Rinaldo CR**, **Gupta P**, **White RM**, **Todd JA**, **Kingsley LA**. 1996. Prognosis in HIV-1 infection predicted by the quantity of virus in plasma. Science **272**:1167–1170.

125. **Goonetilleke N**, **Liu MKP**, **Salazar-Gonzalez JF**, **Ferrari G**, **Giorgi E**, **Ganusov VV**, **Keele BF**, **Learn GH**, **Turnbull EL**, **Salazar MG**, **Weinhold KJ**, **Moore S**, **CHAVI Clinical Core B**, **Letvin N**, **Haynes BF**, **Cohen MS**, **Hraber P**, **Bhattacharya T**, **Borrow P**, **Perelson AS**, **Hahn BH**, **Shaw GM**, **Korber BT**, **McMichael AJ**. 2009. The first T cell response to transmitted/founder virus contributes to the control of acute viremia in HIV-1 infection. J Exp Med **206**:1253–1272.

126. **Alter G**, **Martin MP**, **Teigen N**, **Carr WH**, **Suscovich TJ**, **Schneidewind A**, **Streeck H**, **Waring M**, **Meier A**, **Brander C**, **Lifson JD**, **Allen TM**, **Carrington M**, **Altfeld M**. 2007. Differential natural killer cell-mediated inhibition of HIV-1 replication based on distinct KIR/HLA subtypes. J Exp Med **204**:3027–3036.

127. **Alter G**, **Heckerman D**, **Schneidewind A**, **Fadda L**, **Kadie CM**, **Carlson JM**, **Oniangue-Ndza C**, **Martin M**, **Li B**, **Khakoo SI**, **Carrington M**, **Allen TM**, **Altfeld M**. 2011. HIV-1 adaptation to NK-cell-mediated immune pressure. Nature **476**:96–100.

128. **Carlson JM**, **Le AQ**, **Shahid A**, **Brumme ZL**. 2015. HIV-1 adaptation to HLA: a window into virus-host immune interactions. Trends Microbiol **23**:212–224.

129. **Selik RM**, **Mokotoff ED**, **Branson B**, **Owen SM**, **Whitmore S**, **Hall HI**. 2014. Revised surveillance case definition for HIV infection -- United States, 2014. MMWR Recomm Rep **63**:1–10.

130. **Muñoz A**, **Wang M-C**, **Bass S**, **Taylor JMG**, **Kingsley LA**, **Chmiel JS**, **Polk BF**, **The Multicenter AIDS Cohort Study Group**. 1989. Acquired immunodeficiency syndrome (AIDS)-free time after human immunodeficiency virus type 1 (HIV-1) seroconversion in homosexual men. Am J Epidemiol **130**:530–539.

131. **Lemp GF**, **Payne SF**, **Neal D**, **Temelso T**, **Rutherford GW**. 1990. Survival trends for patients with AIDS. JAMA **263**:402–406.

132. **Crick F**. 1970. Central dogma of molecular biology. Nature **227**:561–563.

133. **Temin HM**, **Mizutani S**. 1970. Viral RNA-dependent DNA Polymerase: RNA-dependent DNA Polymerase in Virions of Rous Sarcoma Virus. Nature **226**:1211–1213.

134. **Baltimore D**. 1970. RNA-dependent DNA polymerase in virions of RNA tumour viruses. Nature **226**:1209–1211.

135. **Temin HM**. 1964. Homology between RNA from Rous Sarcoma Virus and DNA from Rous Sarcoma Virus-infected cells. Proc Natl Acad Sci USA **52**:323–329.

136. **Temin HM**. 1992. Origin and General Nature of Retroviruses, pp. 1–18. *In* Levy, JA (ed.), The Retroviridae. Springer US, Boston, MA.

137. **Temin HM**. 1976. The DNA provirus hypothesis. Science **192**:1075–1080.

138. **Varmus HE**, **Weiss RA**, **Friis RR**, **Levinson W**, **Bishop JM**. 1972. Detection of avian tumor virus-specific nucleotide sequences in avian cell DNAs (reassociation kinetics-RNA tumor viruses-gas antigen-Rous sarcoma virus, chick cells). Proc Natl Acad Sci USA **69**:20–24.

139. **Hughes SH**, **Shank PR**, **Spector DH**, **Kung HJ**, **Bishop JM**, **Varmus HE**, **Vogt PK**, **Breitman ML**. 1978. Proviruses of avian sarcoma virus are terminally redundant, co-extensive with unintegrated linear DNA and integrated at many sites. Cell **15**:1397–1410.

140. **Majors JE**, **Varmus HE**. 1981. Nucleotide sequences at host–proviral junctions for mouse mammary tumour virus. Nature **289**:253–258.

141. **Brown PO**. 1997. Integration. *In* Coffin, JM, Hughes, SH, Varmus, HE (eds.), Retroviruses. Cold Spring Harbor Laboratory Press, Cold Spring Harbor, NY.

142. **Varmus H**. 1988. Retroviruses. Science **240**:1427–1435.

143. **Bishop JM**. 1978. Retroviruses. Annu Rev Biochem **47**:35–88.

144. **International Committee on Taxonomy of Viruses (ICTV)**. Virus Taxonomy: 2018b Release; EC 50, Washington, DC, July 2018; Email ratification February 2019 (MSL #34). https://talk.ictvonline.org/taxonomy/. Accessed 16 Apr 2019. ICTV Website.

145. **Narayan O**, **Clements JE**. 1989. Biology and pathogenesis of lentiviruses. J Gen Virol **70 (Pt 7)**:1617–1639.

146. **Joy JB**, **Liang RH**, **Nguyen T**, **McCloskey RM**, **Poon AFY**. 2015. Origin and Evolution of Human Immunodeficiency Viruses, pp. 587–611. *In* Shapshak, P, Sinnott, JT, Somboonwit, C, Kuhn, JH (eds.), Global Virology I - Identifying and Investigating Viral Diseases. Springer New York, New York, NY.

147. **Thormar H**. 1963. The growth cycle of visna virus in monolayer cultures of sheep cells. Virology **19**:273–278.

148. **Lewis PF**, **Emerman M**. 1994. Passage through mitosis is required for oncoretroviruses but not for the human immunodeficiency virus. J Virol **68**:510–516.

149. **Levy JA**, **Hoffman AD**, **Kramer SM**, **Landis JA**, **Shimabukuro JM**, **Oshiro LS**. 1984. Isolation of lymphocytopathic retroviruses from San Francisco patients with AIDS. Science **225**:840–842.

150. **Brown F**. 1986. Human immunodeficiency virus. Science **232**:1486.

151. **Worobey M**, **Telfer P**, **Souquière S**, **Hunter M**, **Coleman CA**, **Metzger MJ**, **Reed P**, **Makuwa M**, **Hearn G**, **Honarvar S**, **Roques P**, **Apetrei C**, **Kazanji M**, **Marx PA**. 2010. Island biogeography reveals the deep history of SIV. Science **329**:1487.

152. **Gardner MB**. 1996. The history of simian AIDS. J Med Primatol **25**:148–157.

153. **Bibollet-Ruche F**, **Bailes E**, **Gao F**, **Pourrut X**, **Barlow KL**, **Clewley JP**, **Mwenda JM**, **Langat DK**, **Chege GK**, **McClure HM**, **Mpoudi Ngole E**, **Delaporte E**, **Peeters M**, **Shaw GM**, **Sharp PM**, **Hahn BH**. 2004. New simian immunodeficiency virus infecting De Brazza's monkeys (Cercopithecus neglectus): evidence for a cercopithecus monkey virus clade. J Virol **78**:7748–7762.

154. **Peeters M**, **Courgnaud V**, **Abela B**, **Auzel P**, **Pourrut X**, **Bibollet-Ruche F**, **Loul S**, **Liegeois F**, **Butel C**, **Koulagna D**, **Mpoudi Ngole E**, **Shaw GM**, **Hahn BH**, **Delaporte E**. 2002. Risk to human health from a plethora of simian immunodeficiency viruses in primate bushmeat. Emerging Infect Dis **8**:451–457.

155. **Sharp PM**, **Hahn BH**. 2011. Origins of HIV and the AIDS pandemic. Cold Spring Harb Perspect Med **1**:a006841.

156. **Robertson DL**, **Anderson JP**, **Bradac JA**, **Carr JK**, **Foley B**, **Funkhouser RK**, **Gao F**, **Hahn BH**, **Kalish ML**, **Kuiken CL**, **Learn GH**, **Leitner T**, **McCutchan F**, **Osmanov S**, **Peeters M**, **Pieniazek D**, **Salminen M**, **Sharp PM**, **Wolinsky S**, **Korber B**. 1999. HIV-1 Nomenclature Proposal, pp. 492–505. *In* Kuiken, C, Foley, BT, Hahn, BH, Marx, PA, McCutchan, FE, Mellors, J, Mullins, JI, Wolinsky, S, Korber, BT (eds.), Human Retroviruses and AIDS 1999 Compendium. Los Alamos National Laboratory.

157. **Gao F**, **Bailes E**, **Robertson DL**, **Chen Y**, **Rodenburg CM**, **Michael SF**, **Cummins LB**, **Arthur LO**, **Peeters M**, **Shaw GM**, **Sharp PM**, **Hahn BH**. 1999. Origin of HIV-1 in the chimpanzee Pan troglodytes troglodytes. Nature **397**:436–441.

158. **Sharp PM**, **Shaw GM**, **Hahn BH**. 2005. Simian immunodeficiency virus infection of chimpanzees. J Virol **79**:3891–3902.

159. **Worobey M**, **Gemmel M**, **Teuwen DE**, **Haselkorn T**, **Kunstman K**, **Bunce M**, **Muyembe J-J**, **Kabongo J-MM**, **Kalengayi RM**, **Van Marck E**, **Gilbert MTP**, **Wolinsky SM**. 2008. Direct evidence of extensive diversity of HIV-1 in Kinshasa by 1960. Nature **455**:661–664.

160. **Wertheim JO**, **Worobey M**. 2009. Dating the age of the SIV lineages that gave rise to HIV-1 and HIV-2. PLoS Comput Biol **5**:e1000377.

161. **Van Heuverswyn F**, **Li Y**, **Neel C**, **Bailes E**, **Keele BF**, **Liu W**, **Loul S**, **Butel C**, **Liegeois F**, **Bienvenue Y**, **Ngolle EM**, **Sharp PM**, **Shaw GM**, **Delaporte E**, **Hahn BH**, **Peeters M**. 2006. Human immunodeficiency viruses: SIV infection in wild gorillas. Nature **444**:164.

162. **Lemey P**, **Pybus OG**, **Wang B**, **Saksena NK**, **Salemi M**, **Vandamme A-M**. 2003. Tracing the origin and history of the HIV-2 epidemic. Proc Natl Acad Sci USA **100**:6588–6592.

163. **Clavel F**, **Guétard D**, **Brun-Vézinet F**, **Chamaret S**, **Rey MA**, **Santos-Ferreira MO**, **Laurent AG**, **Dauguet C**, **Katlama C**, **Rouzioux C**. 1986. Isolation of a new human retrovirus from West African patients with AIDS. Science **233**:343–346.

164. **Visseaux B**, **Damond F**, **Matheron S**, **Descamps D**, **Charpentier C**. 2016. Hiv-2 molecular epidemiology. Infect Genet Evol **46**:233–240.

165. **Mauclère P**, **Loussert-Ajaka I**, **Damond F**, **Fagot P**, **Souquières S**, **Monny Lobe M**, **Mbopi Keou FX**, **Barré-Sinoussi F**, **Saragosti S**, **Brun-Vézinet F**, **Simon F**. 1997. Serological and virological characterization of HIV-1 group O infection in Cameroon. AIDS **11**:445–453.

166. **Peeters M**, **Gueye A**, **Mboup S**, **Bibollet-Ruche F**, **Ekaza E**, **Mulanga C**, **Ouedrago R**, **Gandji R**, **Mpele P**, **Dibanga G**, **Koumare B**, **Saidou M**, **Esu-Williams E**, **Lombart JP**, **Badombena W**, **Luo N**, **Vanden Haesevelde M**, **Delaporte E**. 1997. Geographical distribution of HIV-1 group O viruses in Africa. AIDS **11**:493–498.

167. **Rodgers MA**, **Vallari AS**, **Harris B**, **Yamaguchi J**, **Holzmayer V**, **Forberg K**, **Berg MG**, **Kenmenge J**, **Ngansop C**, **Awazi B**, **Mbanya D**, **Kaptue L**, **Brennan C**, **Cloherty G**, **Ndembi N**. 2017. Identification of rare HIV-1 Group N, HBV AE, and HTLV-3 strains in rural South Cameroon. Virology **504**:141–151.

168. **Taylor BS**, **Sobieszczyk ME**, **McCutchan FE**, **Hammer SM**. 2008. The challenge of HIV-1 subtype diversity. N Engl J Med **358**:1590–1602.

169. **Désiré N**, **Cerutti L**, **Le Hingrat Q**, **Perrier M**, **Emler S**, **Calvez V**, **Descamps D**, **Marcelin A-G**, **Hué S**, **Visseaux B**. 2018. Characterization update of HIV-1 M subtypes diversity and proposal for subtypes A and D sub-subtypes reclassification. Retrovirology **15**:80.

170. **Vidal N**, **Peeters M**, **Mulanga-Kabeya C**, **Nzilambi N**, **Robertson D**, **Ilunga W**, **Sema H**, **Tshimanga K**, **Bongo B**, **Delaporte E**. 2000. Unprecedented degree of human immunodeficiency virus type 1 (HIV-1) group M genetic diversity in the Democratic Republic of Congo suggests that the HIV-1 pandemic originated in Central Africa. J Virol **74**:10498–10507.

171. 2017. HIV Sequence Compendium 2017. Theoretical Biology and Biophysics Group, Los Alamos National Laboratory.

172. **Ndembi N**, **Iwamoto S**, **Ngansop C**, **Lemey P**, **Abimiku A**, **Mbanya D**, **Kaptue LN**, **Ido E**. 2011. High frequency of HIV-1 dual infections in Cameroon, West Central Africa. J Acquir Immune Defic Syndr **57**:e25–7.

173. **Powell RLR**, **Urbanski MM**, **Burda S**, **Kinge T**, **Nyambi PN**. 2009. High frequency of HIV-1 dual infections among HIV-positive individuals in Cameroon, West Central Africa. J Acquir Immune Defic Syndr **50**:84–92.

174. **Hemelaar J**, **Gouws E**, **Ghys PD**, **Osmanov S**. 2006. Global and regional distribution of HIV-1 genetic subtypes and recombinants in 2004. AIDS **20**:W13–23.

175. **Hemelaar J**. 2012. The origin and diversity of the HIV-1 pandemic. Trends Mol Med **18**:182–192.

176. **Berger EA**, **Doms RW**, **Fenyö EM**, **Korber BT**, **Littman DR**, **Moore JP**, **Sattentau QJ**, **Schuitemaker H**, **Sodroski J**, **Weiss RA**. 1998. A new classification for HIV-1. Nature **391**:240–240.

177. **Kariuki SM**, **Selhorst P**, **Ariën KK**, **Dorfman JR**. 2017. The HIV-1 transmission bottleneck. Retrovirology **14**:22.

178. **Cullen BR**. 2001. Species and Tissue Tropisms of HIV-1: Molecular Basis and Phenotypic Consequences, pp. 1–12. *In* Kuiken, C, Foley, BT, Hahn, BH, Marx, PA, McCutchan, FE, Mellors, J, Sodroski, J, Wolinksy, S, Korber, BT (eds.), HIV Sequence Compendium 2001. Theoretical Biology and Biophysics Group, Los Alamos National Laboratory.

179. **Peden K**, **Emerman M**, **Montagnier L**. 1991. Changes in growth properties on passage in tissue culture of viruses derived from infectious molecular clones of HIV-1LAI, HIV-1MAL, and HIV-1ELI. Virology **185**:661–672.

180. **Adachi A**, **Gendelman HE**, **Koenig S**, **Folks T**, **Willey R**, **Rabson A**, **Martin MA**. 1986. Production of acquired immunodeficiency syndrome-associated retrovirus in human and nonhuman cells transfected with an infectious molecular clone. J Virol **59**:284–291.

181. **Moore JP**, **Cao Y**, **Qing L**, **Sattentau QJ**, **Pyati J**, **Koduri R**, **Robinson J**, **Barbas CF**, **Burton DR**, **Ho DD**. 1995. Primary isolates of human immunodeficiency virus type 1 are relatively resistant to neutralization by monoclonal antibodies to gp120, and their neutralization is not predicted by studies with monomeric gp120. J Virol **69**:101–109.

182. **Platt EJ**, **Kozak SL**, **Kabat D**. 2000. Critical role of enhanced CD4 affinity in laboratory adaptation of human immunodeficiency virus type 1. AIDS Res Hum Retroviruses **16**:871–882.

183. **Kabat D**, **Kozak SL**, **Wehrly K**, **Chesebro B**. 1994. Differences in CD4 dependence for infectivity of laboratory-adapted and primary patient isolates of human immunodeficiency virus type 1. J Virol **68**:2570–2577.

184. **Kwong PD**, **Wyatt R**, **Majeed S**, **Robinson J**, **Sweet RW**, **Sodroski J**, **Hendrickson WA**. 2000. Structures of HIV-1 gp120 envelope glycoproteins from laboratory-adapted and primary isolates. Structure **8**:1329–1339.

185. **Frankel AD**, **Young JA**. 1998. HIV-1: fifteen proteins and an RNA. Annu Rev Biochem **67**:1–25.

186. **Balaji S**, **Sneha P**, **Rama M**, **Shapshak P**. 2015. Global Protein Sequence Variation in HIV-1-B Isolates Derived from Human Blood and Brain, pp. 613–666. *In* Shapshak, P, Sinnott, JT, Somboonwit, C, Kuhn, JH (eds.), Global Virology I - Identifying and Investigating Viral Diseases. Springer New York, New York, NY.

187. **Pawlak EN**, **Dikeakos JD**. 2015. HIV-1 Nef: a master manipulator of the membrane trafficking machinery mediating immune evasion. Biochim Biophys Acta **1850**:733–741.

188. **Marsh M**, **Helenius A**. 2006. Virus entry: open sesame. Cell **124**:729–740.

189. **Kartikeyan S**, **Bharmal RN**, **Tiwari RP**, **Bisen PS**. 2007. HIV and AIDS:. Springer Science & Business Media, Dordrecht.

190. **Brandenberg OF**, **Magnus C**, **Rusert P**, **Regoes RR**, **Trkola A**. 2015. Different infectivity of HIV-1 strains is linked to number of envelope trimers required for entry. PLoS Pathog **11**:e1004595.

191. **Ganser-Pornillos BK**, **Yeager M**, **Pornillos O**. 2012. Assembly and architecture of HIV. Adv Exp Med Biol **726**:441–465.

192. **Campbell EM**, **Hope TJ**. 2015. HIV-1 capsid: the multifaceted key player in HIV-1 infection. Nat Rev Microbiol **13**:471–483.

193. **Kimpton J**, **Emerman M**. 1992. Detection of replication-competent and pseudotyped human immunodeficiency virus with a sensitive cell line on the basis of activation of an integrated beta-galactosidase gene. J Virol **66**:2232–2239.

194. **Piatak M**, **Saag MS**, **Yang LC**, **Clark SJ**, **Kappes JC**, **Luk KC**, **Hahn BH**, **Shaw GM**, **Lifson JD**. 1993. High levels of HIV-1 in plasma during all stages of infection determined by competitive PCR. Science **259**:1749–1754.

195. **Thomas JA**, **Ott DE**, **Gorelick RJ**. 2007. Efficiency of human immunodeficiency virus type 1 postentry infection processes: evidence against disproportionate numbers of defective virions. J Virol **81**:4367–4370.

196. **Arfi V**, **Lienard J**, **Nguyen X-N**, **Berger G**, **Rigal D**, **Darlix J-L**, **Cimarelli A**. 2009. Characterization of the behavior of functional viral genomes during the early steps of human immunodeficiency virus type 1 infection. J Virol **83**:7524–7535.

197. **Sorin M**, **Kalpana GV**. 2006. Dynamics of virus-host interplay in HIV-1 replication. Curr HIV Res **4**:117–130.

198. **Brass AL**, **Dykxhoorn DM**, **Benita Y**, **Yan N**, **Engelman A**, **Xavier RJ**, **Lieberman J**, **Elledge SJ**. 2008. Identification of host proteins required for HIV infection through a functional genomic screen. Science **319**:921–926.

199. **Zhou H**, **Xu M**, **Huang Q**, **Gates AT**, **Zhang XD**, **Castle JC**, **Stec E**, **Ferrer M**, **Strulovici B**, **Hazuda DJ**, **Espeseth AS**. 2008. Genome-scale RNAi screen for host factors required for HIV replication. Cell Host Microbe **4**:495–504.

200. **König R**, **Zhou Y**, **Elleder D**, **Diamond TL**, **Bonamy GMC**, **Irelan JT**, **Chiang C-Y**, **Tu BP**, **De Jesus PD**, **Lilley CE**, **Seidel S**, **Opaluch AM**, **Caldwell JS**, **Weitzman MD**, **Kuhen KL**, **Bandyopadhyay S**, **Ideker T**, **Orth AP**, **Miraglia LJ**, **Bushman FD**, **Young JA**, **Chanda SK**. 2008. Global analysis of host-pathogen interactions that regulate early-stage HIV-1 replication. Cell **135**:49–60.

201. **Bushman FD**, **Malani N**, **Fernandes J**, **D'Orso I**, **Cagney G**, **Diamond TL**, **Zhou H**, **Hazuda DJ**, **Espeseth AS**, **König R**, **Bandyopadhyay S**, **Ideker T**, **Goff SP**, **Krogan NJ**, **Frankel AD**, **Young JAT**, **Chanda SK**. 2009. Host cell factors in HIV replication: meta-analysis of genome-wide studies. PLoS Pathog **5**:e1000437.

202. **Malim MH**, **Bieniasz PD**. 2012. HIV Restriction Factors and Mechanisms of Evasion. Cold Spring Harb Perspect Med **2**:a006940.

203. **Ghimire D**, **Rai M**, **Gaur R**. 2018. Novel host restriction factors implicated in HIV-1 replication. J Gen Virol **99**:435–446.

204. **Merindol N**, **Berthoux L**. 2015. Restriction Factors in HIV-1 Disease Progression. Curr HIV Res **13**:448–461.

205. **Soliman M**, **Srikrishna G**, **Balagopal A**. 2017. Mechanisms of HIV-1 Control. Curr HIV/AIDS Rep **14**:101–109.

206. **Ganser-Pornillos BK**, **Yeager M**, **Sundquist WI**. 2008. The structural biology of HIV assembly. Curr Opin Struct Biol **18**:203–217.

207. **Wilen CB**, **Tilton JC**, **Doms RW**. 2012. HIV: cell binding and entry. Cold Spring Harb Perspect Med **2**:a006866.

208. **Klasse PJ**. 2012. The molecular basis of HIV entry. Cell Microbiol **14**:1183–1192.

209. **Jahn R**, **Lang T**, **Südhof TC**. 2003. Membrane fusion. Cell **112**:519–533.

210. **Wilen CB**, **Tilton JC**, **Doms RW**. 2012. Molecular mechanisms of HIV entry. Adv Exp Med Biol **726**:223–242.

211. **Overbaugh J**, **Morris L**. 2012. The Antibody Response against HIV-1. Cold Spring Harb Perspect Med **2**:a007039.

212. **Li G**, **Piampongsant S**, **Faria NR**, **Voet A**, **Pineda-Peña A-C**, **Khouri R**, **Lemey P**, **Vandamme A-M**, **Theys K**. 2015. An integrated map of HIV genome-wide variation from a population perspective. Retrovirology **12**:18.

213. **Hartley O**, **Klasse PJ**, **Sattentau QJ**, **Moore JP**. 2005. V3: HIV's switch-hitter. AIDS Res Hum Retroviruses **21**:171–189.

214. **Bartz SR**, **Vodicka MA**. 1997. Production of high-titer human immunodeficiency virus type 1 pseudotyped with vesicular stomatitis virus glycoprotein. Methods **12**:337–342.

215. **Dharan A**, **Campbell EM**. 2018. Role of Microtubules and Microtubule-Associated Proteins in HIV-1 Infection. J Virol **92**:e00085–18.

216. **Sabo Y**, **Walsh D**, **Barry DS**, **Tinaztepe S**, **de los Santos K**, **Goff SP**, **Gundersen GG**, **Naghavi MH**. 2013. HIV-1 induces the formation of stable microtubules to enhance early infection. Cell Host Microbe **14**:535–546.

217. **Fernandez J**, **Portilho DM**, **Danckaert A**, **Munier S**, **Becker A**, **Roux P**, **Zambo A**, **Shorte S**, **Jacob Y**, **Vidalain P-O**, **Charneau P**, **Clavel F**, **Arhel NJ**. 2015. Microtubule-associated proteins 1 (MAP1) promote human immunodeficiency virus type I (HIV-1) intracytoplasmic routing to the nucleus. Journal of Biological Chemistry **290**:4631–4646.

218. **Delaney MK**, **Malikov V**, **Chai Q**, **Zhao G**, **Naghavi MH**. 2017. Distinct functions of diaphanous-related formins regulate HIV-1 uncoating and transport. Proc Natl Acad Sci USA **114**:E6932–E6941.

219. **McDonald D**, **Vodicka MA**, **Lucero G**, **Svitkina TM**, **Borisy GG**, **Emerman M**, **Hope TJ**. 2002. Visualization of the intracellular behavior of HIV in living cells. J Cell Biol **159**:441–452.

220. **Dharan A**, **Opp S**, **Abdel-Rahim O**, **Keceli SK**, **Imam S**, **Diaz-Griffero F**, **Campbell EM**. 2017. Bicaudal D2 facilitates the cytoplasmic trafficking and nuclear import of HIV-1 genomes during infection. Proc Natl Acad Sci USA **114**:E10707–E10716.

221. **Malikov V**, **da Silva ES**, **Jovasevic V**, **Bennett G**, **de Souza Aranha Vieira DA**, **Schulte B**, **Diaz-Griffero F**, **Walsh D**, **Naghavi MH**. 2015. HIV-1 capsids bind and exploit the kinesin-1 adaptor FEZ1 for inward movement to the nucleus. Nat Commun **6**:6660.

222. **Lori F**, **di Marzo Veronese F**, **de Vico AL**, **Lusso P**, **Reitz MS**, **Gallo RC**. 1992. Viral DNA carried by human immunodeficiency virus type 1 virions. J Virol **66**:5067–5074.

223. **Trono D**. 1992. Partial reverse transcripts in virions from human immunodeficiency and murine leukemia viruses. J Virol **66**:4893–4900.

224. **Hu W-S**, **Hughes SH**. 2012. HIV-1 reverse transcription. Cold Spring Harb Perspect Med **2**:a006882.

225. **Fassati A**, **Goff SP**. 2001. Characterization of intracellular reverse transcription complexes of human immunodeficiency virus type 1. J Virol **75**:3626–3635.

226. **Nermut MV**, **Fassati A**. 2003. Structural analyses of purified human immunodeficiency virus type 1 intracellular reverse transcription complexes. J Virol **77**:8196–8206.

227. **Iordanskiy S**, **Berro R**, **Altieri M**, **Kashanchi F**, **Bukrinsky M**. 2006. Intracytoplasmic maturation of the human immunodeficiency virus type 1 reverse transcription complexes determines their capacity to integrate into chromatin. Retrovirology **3**:4.

228. **Forshey BM**, **Schwedler von U**, **Sundquist WI**, **Aiken C**. 2002. Formation of a human immunodeficiency virus type 1 core of optimal stability is crucial for viral replication. J Virol **76**:5667–5677.

229. **Dismuke DJ**, **Aiken C**. 2006. Evidence for a functional link between uncoating of the human immunodeficiency virus type 1 core and nuclear import of the viral preintegration complex. J Virol **80**:3712–3720.

230. **Arhel NJ**, **Souquere-Besse S**, **Munier S**, **Souque P**, **Guadagnini S**, **Rutherford S**, **Prévost M-C**, **Allen TD**, **Charneau P**. 2007. HIV-1 DNA Flap formation promotes uncoating of the pre-integration complex at the nuclear pore. EMBO J **26**:3025–3037.

231. **Katz RA**, **Skalka AM**. 1994. The retroviral enzymes. Annu Rev Biochem **63**:133–173.

232. **Panganiban AT**, **Fiore D**. 1988. Ordered interstrand and intrastrand DNA transfer during reverse transcription. Science **241**:1064–1069.

233. **Hu WS**, **Temin HM**. 1990. Retroviral recombination and reverse transcription. Science **250**:1227–1233.

234. **Coffin JM**. 1979. Structure, replication, and recombination of retrovirus genomes: some unifying hypotheses. J Gen Virol **42**:1–26.

235. **Hwang CK**, **Svarovskaia ES**, **Pathak VK**. 2001. Dynamic copy choice: steady state between murine leukemia virus polymerase and polymerase-dependent RNase H activity determines frequency of in vivo template switching. Proc Natl Acad Sci USA **98**:12209–12214.

236. **Le Grice SFJ**. 2012. Human immunodeficiency virus reverse transcriptase: 25 years of research, drug discovery, and promise. Journal of Biological Chemistry **287**:40850–40857.

237. **Lavigne M**, **Roux P**, **Buc H**, **Schaeffer F**. 1997. DNA curvature controls termination of plus strand DNA synthesis at the centre of HIV-1 genome. J Mol Biol **266**:507–524.

238. **Dvorin JD**, **Bell P**, **Maul GG**, **Yamashita M**, **Emerman M**, **Malim MH**. 2002. Reassessment of the roles of integrase and the central DNA flap in human immunodeficiency virus type 1 nuclear import. J Virol **76**:12087–12096.

239. **Ao Z**, **Yao X**, **Cohen ÉA**. 2004. Assessment of the role of the central DNA flap in human immunodeficiency virus type 1 replication by using a single-cycle replication system. J Virol **78**:3170–3177.

240. **Charneau P**, **Mirambeau G**, **Roux P**, **Paulous S**, **Buc H**, **Clavel F**. 1994. HIV-1 reverse transcription. A termination step at the center of the genome. J Mol Biol **241**:651–662.

241. **De Rijck J**, **Debyser Z**. 2006. The central DNA flap of the human immunodeficiency virus type 1 is important for viral replication. Biochem Biophys Res Commun **349**:1100–1110.

242. **Marsden MD**, **Zack JA**. 2007. Human immunodeficiency virus bearing a disrupted central DNA flap is pathogenic in vivo. J Virol **81**:6146–6150.

243. **Roth MJ**, **Schwartzberg PL**, **Goff SP**. 1989. Structure of the termini of DNA intermediates in the integration of retroviral DNA: dependence on IN function and terminal DNA sequence. Cell **58**:47–54.

244. **Ballandras-Colas A**, **Maskell DP**, **Serrao E**, **Locke J**, **Swuec P**, **Jónsson SR**, **Kotecha A**, **Cook NJ**, **Pye VE**, **Taylor IA**, **Andrésdóttir V**, **Engelman AN**, **Costa A**, **Cherepanov P**. 2017. A supramolecular assembly mediates lentiviral DNA integration. Science **355**:93–95.

245. **Passos DO**, **Li M**, **Yang R**, **Rebensburg SV**, **Ghirlando R**, **Jeon Y**, **Shkriabai N**, **Kvaratskhelia M**, **Craigie R**, **Lyumkis D**. 2017. Cryo-EM structures and atomic model of the HIV-1 strand transfer complex intasome. Science **355**:89–92.

246. **Bowerman B**, **Brown PO**, **Bishop JM**, **Varmus HE**. 1989. A nucleoprotein complex mediates the integration of retroviral DNA. Genes Dev **3**:469–478.

247. **Rustagi A**, **Gale M**. 2014. Innate antiviral immune signaling, viral evasion and modulation by HIV-1. J Mol Biol **426**:1161–1177.

248. **Britan-Rosich E**, **Nowarski R**, **Kotler M**. 2011. Multifaceted counter-APOBEC3G mechanisms employed by HIV-1 Vif. J Mol Biol **410**:1065–1076.

249. **Goila-Gaur R**, **Strebel K**. 2008. HIV-1 Vif, APOBEC, and intrinsic immunity. Retrovirology **5**:51.

250. **Khan MA**, **Aberham C**, **Kao S**, **Akari H**, **Gorelick R**, **Bour S**, **Strebel K**. 2001. Human immunodeficiency virus type 1 Vif protein is packaged into the nucleoprotein complex through an interaction with viral genomic RNA. J Virol **75**:7252–7265.

251. **Wang Y**, **Kinlock BL**, **Shao Q**, **Turner TM**, **Liu B**. 2014. HIV-1 Vif inhibits G to A hypermutations catalyzed by virus-encapsidated APOBEC3G to maintain HIV-1 infectivity. Retrovirology **11**:89.

252. **Guyader M**, **Emerman M**, **Montagnier L**, **Peden K**. 1989. VPX mutants of HIV-2 are infectious in established cell lines but display a severe defect in peripheral blood lymphocytes. EMBO J **8**:1169–1175.

253. **Yu XF**, **Yu QC**, **Essex M**, **Lee TH**. 1991. The vpx gene of simian immunodeficiency virus facilitates efficient viral replication in fresh lymphocytes and macrophage. J Virol **65**:5088–5091.

254. **Bonifati S**, **Daly MB**, **St Gelais C**, **Kim SH**, **Hollenbaugh JA**, **Shepard C**, **Kennedy EM**, **Kim D-H**, **Schinazi RF**, **Kim B**, **Wu L**. 2016. SAMHD1 controls cell cycle status, apoptosis and HIV-1 infection in monocytic THP-1 cells. Virology **495**:92–100.

255. **Altfeld M**, **Gale M**. 2015. Innate immunity against HIV-1 infection. Nat Immunol **16**:554–562.

256. **Le Sage V**, **Mouland AJ**, **Valiente-Echeverría F**. 2014. Roles of HIV-1 capsid in viral replication and immune evasion. Virus Res **193**:116–129.

257. **Rasaiyaah J**, **Tan CP**, **Fletcher AJ**, **Price AJ**, **Blondeau C**, **Hilditch L**, **Jacques DA**, **Selwood DL**, **James LC**, **Noursadeghi M**, **Towers GJ**. 2013. HIV-1 evades innate immune recognition through specific cofactor recruitment. Nature **503**:402–405.

258. **Yamashita M**, **Emerman M**. 2006. Retroviral infection of non-dividing cells: old and new perspectives. Virology **344**:88–93.

259. **Ungricht R**, **Kutay U**. 2017. Mechanisms and functions of nuclear envelope remodelling. Nat Rev Mol Cell Biol **18**:229–245.

260. **Bukrinsky MI**, **Sharova N**, **Dempsey MP**, **Stanwick TL**, **Bukrinskaya AG**, **Haggerty S**, **Stevenson M**. 1992. Active nuclear import of human immunodeficiency virus type 1 preintegration complexes. Proc Natl Acad Sci USA **89**:6580–6584.

261. **Bhargava A**, **Lahaye X**, **Manel N**. 2018. Let me in: Control of HIV nuclear entry at the nuclear envelope. Cytokine Growth Factor Rev **40**:59–67.

262. **Terry LJ**, **Wente SR**. 2009. Flexible gates: dynamic topologies and functions for FG nucleoporins in nucleocytoplasmic transport. Eukaryotic Cell **8**:1814–1827.

263. **Sun Y**, **Xian L**, **Xing H**, **Yu J**, **Yang Z**, **Yang T**, **Yang L**, **Ding P**. 2016. Factors influencing the nuclear targeting ability of nuclear localization signals. J Drug Target **24**:927–933.

264. **Levin A**, **Loyter A**, **Bukrinsky M**. 2011. Strategies to inhibit viral protein nuclear import: HIV-1 as a target. Biochim Biophys Acta **1813**:1646–1653.

265. **Yamashita M**, **Emerman M**. 2005. The cell cycle independence of HIV infections is not determined by known karyophilic viral elements. PLoS Pathog **1**:e18.

266. **Lee K**, **Ambrose Z**, **Martin TD**, **Oztop I**, **Mulky A**, **Julias JG**, **Vandegraaff N**, **Baumann JG**, **Wang R**, **Yuen W**, **Takemura T**, **Shelton K**, **Taniuchi I**, **Li Y**, **Sodroski J**, **Littman DR**, **Coffin JM**, **Hughes SH**, **Unutmaz D**, **Engelman A**, **KewalRamani VN**. 2010. Flexible use of nuclear import pathways by HIV-1. Cell Host Microbe **7**:221–233.

267. **Matreyek KA**, **Engelman A**. 2013. Viral and cellular requirements for the nuclear entry of retroviral preintegration nucleoprotein complexes. Viruses **5**:2483–2511.

268. **Yamashita M**, **Perez O**, **Hope TJ**, **Emerman M**. 2007. Evidence for direct involvement of the capsid protein in HIV infection of nondividing cells. PLoS Pathog **3**:1502–1510.

269. **Kane M**, **Rebensburg SV**, **Takata MA**, **Zang TM**, **Yamashita M**, **Kvaratskhelia M**, **Bieniasz PD**. 2018. Nuclear pore heterogeneity influences HIV-1 infection and the antiviral activity of MX2. Elife **7**:4708.

270. **Schaller T**, **Ocwieja KE**, **Rasaiyaah J**, **Price AJ**, **Brady TL**, **Roth SL**, **Hué S**, **Fletcher AJ**, **Lee K**, **KewalRamani VN**, **Noursadeghi M**, **Jenner RG**, **James LC**, **Bushman FD**, **Towers GJ**. 2011. HIV-1 capsid-cyclophilin interactions determine nuclear import pathway, integration targeting and replication efficiency. PLoS Pathog **7**:e1002439.

271. **Di Nunzio F**, **Danckaert A**, **Fricke T**, **Perez P**, **Fernandez J**, **Perret E**, **Roux P**, **Shorte S**, **Charneau P**, **Diaz-Griffero F**, **Arhel NJ**. 2012. Human nucleoporins promote HIV-1 docking at the nuclear pore, nuclear import and integration. PLoS ONE **7**:e46037.

272. **Burdick RC**, **Delviks-Frankenberry KA**, **Chen J**, **Janaka SK**, **Sastri J**, **Hu W-S**, **Pathak VK**. 2017. Dynamics and regulation of nuclear import and nuclear movements of HIV-1 complexes. PLoS Pathog **13**:e1006570.

273. **Matreyek KA**, **Engelman A**. 2011. The requirement for nucleoporin NUP153 during human immunodeficiency virus type 1 infection is determined by the viral capsid. J Virol **85**:7818–7827.

274. **Matreyek KA**, **Yücel SS**, **Li X**, **Engelman A**. 2013. Nucleoporin NUP153 phenylalanine-glycine motifs engage a common binding pocket within the HIV-1 capsid protein to mediate lentiviral infectivity. PLoS Pathog **9**:e1003693.

275. **Buffone C**, **Martinez-Lopez A**, **Fricke T**, **Opp S**, **Severgnini M**, **Cifola I**, **Petiti L**, **Frabetti S**, **Skorupka K**, **Zadrozny KK**, **Ganser-Pornillos BK**, **Pornillos O**, **Di Nunzio F**, **Diaz-Griffero F**. 2018. Nup153 Unlocks the Nuclear Pore Complex for HIV-1 Nuclear Translocation in Nondividing Cells. J Virol **92**:e00648–18.

276. **Kataoka N**, **Bachorik JL**, **Dreyfuss G**. 1999. Transportin-SR, a nuclear import receptor for SR proteins. J Cell Biol **145**:1145–1152.

277. **Lai MC**, **Lin RI**, **Huang SY**, **Tsai CW**, **Tarn WY**. 2000. A human importin-beta family protein, transportin-SR2, interacts with the phosphorylated RS domain of SR proteins. J Biol Chem **275**:7950–7957.

278. **Maertens GN**, **Cook NJ**, **Wang W**, **Hare S**, **Gupta SS**, **Oztop I**, **Lee K**, **Pye VE**, **Cosnefroy O**, **Snijders AP**, **KewalRamani VN**, **Fassati A**, **Engelman A**, **Cherepanov P**. 2014. Structural basis for nuclear import of splicing factors by human Transportin 3. Proc Natl Acad Sci USA **111**:2728–2733.

279. **Jang S**, **Cook NJ**, **Pye VE**, **Bedwell GJ**, **Dudek AM**, **Singh PK**, **Cherepanov P**, **Engelman AN**. 2019. Differential role for phosphorylation in alternative polyadenylation function versus nuclear import of SR-like protein CPSF6. Nucleic Acids Res gkz206.

280. **Christ F**, **Thys W**, **De Rijck J**, **Gijsbers R**, **Albanese A**, **Arosio D**, **Emiliani S**, **Rain J-C**, **Benarous R**, **Cereseto A**, **Debyser Z**. 2008. Transportin-SR2 imports HIV into the nucleus. Curr Biol **18**:1192–1202.

281. **De Iaco A**, **Santoni F**, **Vannier A**, **Guipponi M**, **Antonarakis S**, **Luban J**. 2013. TNPO3 protects HIV-1 replication from CPSF6-mediated capsid stabilization in the host cell cytoplasm. Retrovirology **10**:20.

282. **Fricke T**, **Valle-Casuso JC**, **White TE**, **Brandariz-Nuñez A**, **Bosche WJ**, **Reszka N**, **Gorelick R**, **Diaz-Griffero F**. 2013. The ability of TNPO3-depleted cells to inhibit HIV-1 infection requires CPSF6. Retrovirology **10**:46.

283. **Price AJ**, **Fletcher AJ**, **Schaller T**, **Elliott T**, **Lee K**, **KewalRamani VN**, **Chin JW**, **Towers GJ**, **James LC**. 2012. CPSF6 defines a conserved capsid interface that modulates HIV-1 replication. PLoS Pathog **8**:e1002896.

284. **Hilditch L**, **Towers GJ**. 2014. A model for cofactor use during HIV-1 reverse transcription and nuclear entry. Curr Opin Virol **4**:32–36.

285. **Ambrose Z**, **Aiken C**. 2014. HIV-1 uncoating: connection to nuclear entry and regulation by host proteins. Virology **454-455C**:371–379.

286. **Arhel N**. 2010. Revisiting HIV-1 uncoating. Retrovirology **7**:96.

287. **Francis AC**, **Melikyan GB**. 2018. Single HIV-1 Imaging Reveals Progression of Infection through CA-Dependent Steps of Docking at the Nuclear Pore, Uncoating, and Nuclear Transport. Cell Host Microbe **23**:536–548.e6.

288. **Roa A**, **Hayashi F**, **Yang Y**, **Lienlaf M**, **Zhou J**, **Shi J**, **Watanabe S**, **Kigawa T**, **Yokoyama S**, **Aiken C**, **Diaz-Griffero F**. 2012. RING domain mutations uncouple TRIM5α restriction of HIV-1 from inhibition of reverse transcription and acceleration of uncoating. J Virol **86**:1717–1727.

289. **Engelman A**, **Cherepanov P**. 2008. The lentiviral integrase binding protein LEDGF/p75 and HIV-1 replication. PLoS Pathog **4**:e1000046.

290. **Bushman FD**, **Fujiwara T**, **Craigie R**. 1990. Retroviral DNA integration directed by HIV integration protein in vitro. Science **249**:1555–1558.

291. **Engelman A**, **Mizuuchi K**, **Craigie R**. 1991. HIV-1 DNA integration: mechanism of viral DNA cleavage and DNA strand transfer. Cell **67**:1211–1221.

292. **Bushman FD**, **Craigie R**. 1991. Activities of human immunodeficiency virus (HIV) integration protein in vitro: specific cleavage and integration of HIV DNA. Proc Natl Acad Sci USA **88**:1339–1343.

293. **Farnet CM**, **Haseltine WA**. 1991. Circularization of human immunodeficiency virus type 1 DNA in vitro. J Virol **65**:6942–6952.

294. **Sloan RD**, **Wainberg MA**. 2011. The role of unintegrated DNA in HIV infection. Retrovirology **8**:52.

295. **Lewinski MK**, **Yamashita M**, **Emerman M**, **Ciuffi A**, **Marshall H**, **Crawford G**, **Collins F**, **Shinn P**, **Leipzig J**, **Hannenhalli S**, **Berry CC**, **Ecker JR**, **Bushman FD**. 2006. Retroviral DNA integration: viral and cellular determinants of target-site selection. PLoS Pathog **2**:e60.

296. **Lelek M**, **Casartelli N**, **Pellin D**, **Rizzi E**, **Souque P**, **Severgnini M**, **Di Serio C**, **Fricke T**, **Diaz-Griffero F**, **Zimmer C**, **Charneau P**, **Di Nunzio F**. 2015. Chromatin organization at the nuclear pore favours HIV replication. Nat Commun **6**:6483.

297. **Marini B**, **Kertesz-Farkas A**, **Ali H**, **Lucic B**, **Lisek K**, **Manganaro L**, **Pongor S**, **Luzzati R**, **Recchia A**, **Mavilio F**, **Giacca M**, **Lusic M**. 2015. Nuclear architecture dictates HIV-1 integration site selection. Nature **521**:227–231.

298. **Chin CR**, **Perreira JM**, **Savidis G**, **Portmann JM**, **Aker AM**, **Feeley EM**, **Smith MC**, **Brass AL**. 2015. Direct Visualization of HIV-1 Replication Intermediates Shows that Capsid and CPSF6 Modulate HIV-1 Intra-nuclear Invasion and Integration. Cell Rep **13**:1717–1731.

299. **Achuthan V**, **Perreira JM**, **Sowd GA**, **Puray-Chavez M**, **McDougall WM**, **Paulucci-Holthauzen A**, **Wu X**, **Fadel HJ**, **Poeschla EM**, **Multani AS**, **Hughes SH**, **Sarafianos SG**, **Brass AL**, **Engelman AN**. 2018. Capsid-CPSF6 Interaction Licenses Nuclear HIV-1 Trafficking to Sites of Viral DNA Integration. Cell Host Microbe **24**:392–404.e8.

300. **Rasheedi S**, **Shun M-C**, **Serrao E**, **Sowd GA**, **Qian J**, **Hao C**, **Dasgupta T**, **Engelman AN**, **Skowronski J**. 2016. The Cleavage and Polyadenylation Specificity Factor 6 (CPSF6) Subunit of the Capsid-recruited Pre-messenger RNA Cleavage Factor I (CFIm) Complex Mediates HIV-1 Integration into Genes. Journal of Biological Chemistry **291**:11809–11819.

301. **Sowd GA**, **Serrao E**, **Wang H**, **Wang W**, **Fadel HJ**, **Poeschla EM**, **Engelman AN**. 2016. A critical role for alternative polyadenylation factor CPSF6 in targeting HIV-1 integration to transcriptionally active chromatin. Proc Natl Acad Sci USA **113**:E1054–63.

302. **Ciuffi A**, **Llano M**, **Poeschla E**, **Hoffmann C**, **Leipzig J**, **Shinn P**, **Ecker JR**, **Bushman F**. 2005. A role for LEDGF/p75 in targeting HIV DNA integration. Nat Med **11**:1287–1289.

303. **Marshall HM**, **Ronen K**, **Berry C**, **Llano M**, **Sutherland H**, **Saenz D**, **Bickmore W**, **Poeschla E**, **Bushman FD**. 2007. Role of PSIP1/LEDGF/p75 in lentiviral infectivity and integration targeting. PLoS ONE **2**:e1340.

304. **Vanhamel J**, **Bruggemans A**, **Debyser Z**. 2019. Establishment of latent HIV-1 reservoirs: what do we really know? J Virus Erad **5**:3–9.

305. **Eisele E**, **Siliciano RF**. 2012. Redefining the viral reservoirs that prevent HIV-1 eradication. Immunity **37**:377–388.

306. **Finzi D**, **Hermankova M**, **Pierson T**, **Carruth LM**, **Buck C**, **Chaisson RE**, **Quinn TC**, **Chadwick K**, **Margolick J**, **Brookmeyer R**, **Gallant J**, **Markowitz M**, **Ho DD**, **Richman DD**, **Siliciano RF**. 1997. Identification of a reservoir for HIV-1 in patients on highly active antiretroviral therapy. Science **278**:1295–1300.

307. **Chun TW**, **Stuyver L**, **Mizell SB**, **Ehler LA**, **Mican JA**, **Baseler M**, **Lloyd AL**, **Nowak MA**, **Fauci AS**. 1997. Presence of an inducible HIV-1 latent reservoir during highly active antiretroviral therapy. Proc Natl Acad Sci USA **94**:13193–13197.

308. **Chun TW**, **Carruth L**, **Finzi D**, **Shen X**, **DiGiuseppe JA**, **Taylor H**, **Hermankova M**, **Chadwick K**, **Margolick J**, **Quinn TC**, **Kuo YH**, **Brookmeyer R**, **Zeiger MA**, **Barditch-Crovo P**, **Siliciano RF**. 1997. Quantification of latent tissue reservoirs and total body viral load in HIV-1 infection. Nature **387**:183–188.

309. **Ho Y-C**, **Shan L**, **Hosmane NN**, **Wang J**, **Laskey SB**, **Rosenbloom DIS**, **Lai J**, **Blankson JN**, **Siliciano JD**, **Siliciano RF**. 2013. Replication-competent noninduced proviruses in the latent reservoir increase barrier to HIV-1 cure. Cell **155**:540–551.

310. **Soriano-Sarabia N**, **Bateson RE**, **Dahl NP**, **Crooks AM**, **Kuruc JD**, **Margolis DM**, **Archin NM**. 2014. Quantitation of replication-competent HIV-1 in populations of resting CD4+ T cells. J Virol **88**:14070–14077.

311. **Siliciano RF**, **Greene WC**. 2011. HIV latency. Cold Spring Harb Perspect Med **1**:a007096.

312. **Karn J**, **Stoltzfus CM**. 2012. Transcriptional and posttranscriptional regulation of HIV-1 gene expression. Cold Spring Harb Perspect Med **2**:a006916.

313. **Boireau S**, **Maiuri P**, **Basyuk E**, **la Mata de M**, **Knezevich A**, **Pradet-Balade B**, **Bäcker V**, **Kornblihtt A**, **Marcello A**, **Bertrand E**. 2007. The transcriptional cycle of HIV-1 in real-time and live cells. J Cell Biol **179**:291–304.

314. **Marcello A**, **Zoppé M**, **Giacca M**. 2001. Multiple modes of transcriptional regulation by the HIV-1 Tat transactivator. IUBMB Life **51**:175–181.

315. **Jeang KT**, **Xiao H**, **Rich EA**. 1999. Multifaceted activities of the HIV-1 transactivator of transcription, Tat. J Biol Chem **274**:28837–28840.

316. **Dingwall C**, **Ernberg I**, **Gait MJ**, **Green SM**, **Heaphy S**, **Karn J**, **Lowe AD**, **Singh M**, **Skinner MA**. 1990. HIV-1 tat protein stimulates transcription by binding to a U-rich bulge in the stem of the TAR RNA structure. EMBO J **9**:4145–4153.

317. **Weinberger LS**, **Burnett JC**, **Toettcher JE**, **Arkin AP**, **Schaffer DV**. 2005. Stochastic gene expression in a lentiviral positive-feedback loop: HIV-1 Tat fluctuations drive phenotypic diversity. Cell **122**:169–182.

318. **Purcell DF**, **Martin MA**. 1993. Alternative splicing of human immunodeficiency virus type 1 mRNA modulates viral protein expression, replication, and infectivity. J Virol **67**:6365–6378.

319. **Malim MH**, **Hauber J**, **Le SY**, **Maizel JV**, **Cullen BR**. 1989. The HIV-1 rev trans-activator acts through a structured target sequence to activate nuclear export of unspliced viral mRNA. Nature **338**:254–257.

320. **Hidalgo L**, **Swanson CM**. 2017. Regulation of human immunodeficiency virus type 1 (HIV-1) mRNA translation. Biochem Soc Trans **45**:353–364.

321. **Brierley I**, **Ramos Dos FJ**. 2006. Programmed ribosomal frameshifting in HIV-1 and the SARS-CoV. Virus Res **119**:29–42.

322. **Giese S**, **Marsh M**. 2013. Cellular Trafficking Mechanisms in the Assembly and Release of HIV, pp. 23–53. *In* Freed, EO (ed.), Advances in HIV-1 Assembly and Release. Springer New York, New York, NY.

323. **Dubé M**, **Bego MG**, **Paquay C**, **Cohen ÉA**. 2010. Modulation of HIV-1-host interaction: role of the Vpu accessory protein. Retrovirology **7**:114.

324. **Sundquist WI**, **Krausslich H-G**. 2012. HIV-1 assembly, budding, and maturation. Cold Spring Harb Perspect Med **2**:a006924.

325. **Willey RL**, **Maldarelli F**, **Martin MA**, **Strebel K**. 1992. Human immunodeficiency virus type 1 Vpu protein induces rapid degradation of CD4. J Virol **66**:7193–7200.

326. **Chen J**, **Nikolaitchik OA**, **Dilley KA**, **Hu W-S**. 2013. Packaging of the HIV-1 RNA Genome, pp. 55–73. *In* Freed, EO (ed.), Advances in HIV-1 Assembly and Release. Springer New York, New York, NY.

327. **Lever A**, **Gottlinger H**, **Haseltine W**, **Sodroski J**. 1989. Identification of a sequence required for efficient packaging of human immunodeficiency virus type 1 RNA into virions. J Virol **63**:4085–4087.

328. **Clever JL**, **Miranda D**, **Parslow TG**. 2002. RNA structure and packaging signals in the 5' leader region of the human immunodeficiency virus type 1 genome. J Virol **76**:12381–12387.

329. **Chen J**, **Nikolaitchik O**, **Singh J**, **Wright A**, **Bencsics CE**, **Coffin JM**, **Ni N**, **Lockett S**, **Pathak VK**, **Hu W-S**. 2009. High efficiency of HIV-1 genomic RNA packaging and heterozygote formation revealed by single virion analysis. Proc Natl Acad Sci USA **106**:13535–13540.

330. **Mujeeb A**, **Clever JL**, **Billeci TM**, **James TL**, **Parslow TG**. 1998. Structure of the dimer initiation complex of HIV-1 genomic RNA. Nat Struct Biol **5**:432–436.

331. **Kleiman L**, **Jones CP**, **Musier-Forsyth K**. 2010. Formation of the tRNALys packaging complex in HIV-1. FEBS Lett **584**:359–365.

332. **Guenzel CA**, **Hérate C**, **Benichou S**. 2014. HIV-1 Vpr-a still "enigmatic multitasker". Front Microbiol **5**:127.

333. **Ott DE**. 2008. Cellular proteins detected in HIV-1. Rev Med Virol **18**:159–175.

334. **Dick RA**, **Mallery DL**, **Vogt VM**, **James LC**. 2018. IP6 Regulation of HIV Capsid Assembly, Stability, and Uncoating. Viruses **10**:E640.

335. **de Marco A**, **Krausslich H-G**, **Briggs JAG**. 2013. Structural Biology of HIV Assembly, pp. 1–22. *In* Freed, EO (ed.), Advances in HIV-1 Assembly and Release. Springer New York, New York, NY.

336. **Jouvenet N**, **Simon SM**, **Bieniasz PD**. 2009. Imaging the interaction of HIV-1 genomes and Gag during assembly of individual viral particles. Proc Natl Acad Sci USA **106**:19114–19119.

337. **Carlson L-A**, **Briggs JAG**, **Glass B**, **Riches JD**, **Simon MN**, **Johnson MC**, **Müller B**, **Grünewald K**, **Krausslich H-G**. 2008. Three-dimensional analysis of budding sites and released virus suggests a revised model for HIV-1 morphogenesis. Cell Host Microbe **4**:592–599.

338. **Aiken C**, **Zhang P**. 2013. HIV-1 Maturation, pp. 153–166. *In* Freed, EO (ed.), Advances in HIV-1 Assembly and Release. Springer New York, New York, NY.

339. **Mattei S**, **Schur FK**, **Briggs JA**. 2016. Retrovirus maturation-an extraordinary structural transformation. Curr Opin Virol **18**:27–35.

340. **Murakami T**, **Ablan S**, **Freed EO**, **Tanaka Y**. 2004. Regulation of human immunodeficiency virus type 1 Env-mediated membrane fusion by viral protease activity. J Virol **78**:1026–1031.

341. **Wyma DJ**, **Jiang J**, **Shi J**, **Zhou J**, **Lineberger JE**, **Miller MD**, **Aiken C**. 2004. Coupling of human immunodeficiency virus type 1 fusion to virion maturation: a novel role of the gp41 cytoplasmic tail. J Virol **78**:3429–3435.

342. **Domingo E**, **Holland JJ**. 1997. RNA virus mutations and fitness for survival. Annu Rev Microbiol **51**:151–178.

343. **Abram ME**, **Ferris AL**, **Shao W**, **Alvord WG**, **Hughes SH**. 2010. Nature, position, and frequency of mutations made in a single cycle of HIV-1 replication. J Virol **84**:9864–9878.

344. **Mansky LM**, **Temin HM**. 1995. Lower in vivo mutation rate of human immunodeficiency virus type 1 than that predicted from the fidelity of purified reverse transcriptase. J Virol **69**:5087–5094.

345. **Dimitrov DS**, **Willey RL**, **Sato H**, **Chang LJ**, **Blumenthal R**, **Martin MA**. 1993. Quantitation of human immunodeficiency virus type 1 infection kinetics. J Virol **67**:2182–2190.

346. **Coffin JM**. 1995. HIV population dynamics in vivo: implications for genetic variation, pathogenesis, and therapy. Science **267**:483–489.

347. **Perelson AS**, **Neumann AU**, **Markowitz M**, **Leonard JM**, **Ho DD**. 1996. HIV-1 dynamics in vivo: virion clearance rate, infected cell life-span, and viral generation time. Science **271**:1582–1586.

348. **Keele BF**, **Giorgi EE**, **Salazar-Gonzalez JF**, **Decker JM**, **Pham KT**, **Salazar MG**, **Sun C**, **Grayson T**, **Wang S**, **Li H**, **Wei X**, **Jiang C**, **Kirchherr JL**, **Gao F**, **Anderson JA**, **Ping L-H**, **Swanstrom R**, **Tomaras GD**, **Blattner WA**, **Goepfert PA**, **Kilby JM**, **Saag MS**, **Delwart EL**, **Busch MP**, **Cohen MS**, **Montefiori DC**, **Haynes BF**, **Gaschen B**, **Athreya GS**, **Lee HY**, **Wood N**, **Seoighe C**, **Perelson AS**, **Bhattacharya T**, **Korber BT**, **Hahn BH**, **Shaw GM**. 2008. Identification and characterization of transmitted and early founder virus envelopes in primary HIV-1 infection. Proc Natl Acad Sci USA **105**:7552–7557.

349. **Lauring AS**, **Andino R**. 2010. Quasispecies theory and the behavior of RNA viruses. PLoS Pathog **6**:e1001005.

350. **Biebricher CK**, **Eigen M**. 2006. What is a quasispecies? Curr Top Microbiol Immunol **299**:1–31.

351. **Boutwell CL**, **Rolland MM**, **Herbeck JT**, **Mullins JI**, **Allen TM**. 2010. Viral evolution and escape during acute HIV-1 infection. J Infect Dis **202 Suppl 2**:S309–14.

352. **Troyer RM**, **McNevin J**, **Liu Y**, **Zhang SC**, **Krizan RW**, **Abraha A**, **Tebit DM**, **Zhao H**, **Avila S**, **Lobritz MA**, **McElrath MJ**, **Le Gall S**, **Mullins JI**, **Arts EJ**. 2009. Variable fitness impact of HIV-1 escape mutations to cytotoxic T lymphocyte (CTL) response. PLoS Pathog **5**:e1000365.

353. **Fischl MA**, **Richman DD**, **Grieco MH**, **Gottlieb MS**, **Volberding PA**, **Laskin OL**, **Leedom JM**, **Groopman JE**, **Mildvan D**, **Schooley RT**, **Jackson GG**, **Durack DT**, **King D**, **The AZT Collaborative Working Group**. 1987. The Efficacy of Azidothymidine (AZT) in the Treatment of Patients with AIDS and AIDS-Related Complex. N Engl J Med **317**:185–191.

354. **Teeraananchai S**, **Kerr SJ**, **Amin J**, **Ruxrungtham K**, **Law MG**. 2017. Life expectancy of HIV-positive people after starting combination antiretroviral therapy: a meta-analysis. HIV Med **18**:256–266.

355. **Jean MJ**, **Fiches G**, **Hayashi T**, **Zhu J**. 2019. Current Strategies for Elimination of HIV-1 Latent Reservoirs Using Chemical Compounds Targeting Host and Viral Factors. AIDS Res Hum Retroviruses **35**:1–24.

356. **U.S. Department of Health and Human Services**. FDA-Approved HIV Medicines. https://aidsinfo.nih.gov/understanding-hiv-aids/fact-sheets/21/58/fda-approved-hiv-medicines. Accessed 16 Apr 2019. AIDSinfo Website.

357. **Ramanathan S**, **Mathias AA**, **German P**, **Kearney BP**. 2011. Clinical pharmacokinetic and pharmacodynamic profile of the HIV integrase inhibitor elvitegravir. Clin Pharmacokinet **50**:229–244.

358. **Wei X**, **Ghosh SK**, **Taylor ME**, **Johnson VA**, **Emini EA**, **Deutsch P**, **Lifson JD**, **Bonhoeffer S**, **Nowak MA**, **Hahn BH**. 1995. Viral dynamics in human immunodeficiency virus type 1 infection. Nature **373**:117–122.

359. **Cihlar T**, **Fordyce M**. 2016. Current status and prospects of HIV treatment. Curr Opin Virol **18**:50–56.

360. **Richman DD**. 2001. HIV chemotherapy. Nature **410**:995–1001.

361. **Cheng YC**, **Dutschman GE**, **Bastow KF**, **Sarngadharan MG**, **Ting RY**. 1987. Human immunodeficiency virus reverse transcriptase. General properties and its interactions with nucleoside triphosphate analogs. J Biol Chem **262**:2187–2189.

362. **Balzarini J**, **Herdewijn P**, **De Clercq E**. 1989. Differential patterns of intracellular metabolism of 2',3'-didehydro-2',3'-dideoxythymidine and 3'-azido-2‘,3’-dideoxythymidine, two potent anti-human immunodeficiency virus compounds. J Biol Chem **264**:6127–6133.

363. **Arion D**, **Kaushik N**, **McCormick S**, **Borkow G**, **Parniak MA**. 1998. Phenotypic mechanism of HIV-1 resistance to 3“-azido-3-”deoxythymidine (AZT): increased polymerization processivity and enhanced sensitivity to pyrophosphate of the mutant viral reverse transcriptase. Biochemistry **37**:15908–15917.

364. **Meyer PR**, **Matsuura SE**, **Mian AM**, **So AG**, **Scott WA**. 1999. A mechanism of AZT resistance: an increase in nucleotide-dependent primer unblocking by mutant HIV-1 reverse transcriptase. Mol Cell **4**:35–43.

365. **Boyer PL**, **Sarafianos SG**, **Arnold E**, **Hughes SH**. 2001. Selective excision of AZTMP by drug-resistant human immunodeficiency virus reverse transcriptase. J Virol **75**:4832–4842.

366. **Sluis-Cremer N**, **Temiz NA**, **Bahar I**. 2004. Conformational changes in HIV-1 reverse transcriptase induced by nonnucleoside reverse transcriptase inhibitor binding. Curr HIV Res **2**:323–332.

367. **Kohlstaedt LA**, **Wang J**, **Friedman JM**, **Rice PA**, **Steitz TA**. 1992. Crystal structure at 3.5 A resolution of HIV-1 reverse transcriptase complexed with an inhibitor. Science **256**:1783–1790.

368. **Tantillo C**, **Ding J**, **Jacobo-Molina A**, **Nanni RG**, **Boyer PL**, **Hughes SH**, **Pauwels R**, **Andries K**, **Janssen PA**, **Arnold E**. 1994. Locations of anti-AIDS drug binding sites and resistance mutations in the three-dimensional structure of HIV-1 reverse transcriptase. Implications for mechanisms of drug inhibition and resistance. J Mol Biol **243**:369–387.

369. **Spence RA**, **Kati WM**, **Anderson KS**, **Johnson KA**. 1995. Mechanism of inhibition of HIV-1 reverse transcriptase by nonnucleoside inhibitors. Science **267**:988–993.

370. **Sluis-Cremer N**. 2014. The emerging profile of cross-resistance among the nonnucleoside HIV-1 reverse transcriptase inhibitors. Viruses **6**:2960–2973.

371. **Miller V**. 2001. International perspectives on antiretroviral resistance. Resistance to protease inhibitors. J Acquir Immune Defic Syndr **26 Suppl 1**:S34–50.

372. **Ghosh AK**, **Osswald HL**, **Prato G**. 2016. Recent Progress in the Development of HIV-1 Protease Inhibitors for the Treatment of HIV/AIDS. J Med Chem **59**:5172–5208.

373. **Nijhuis M**, **Deeks S**, **Boucher C**. 2001. Implications of antiretroviral resistance on viral fitness. Curr Opin Infect Dis **14**:23–28.

374. **Doyon L**, **Croteau G**, **Thibeault D**, **Poulin F**, **Pilote L**, **Lamarre D**. 1996. Second locus involved in human immunodeficiency virus type 1 resistance to protease inhibitors. J Virol **70**:3763–3769.

375. **Espeseth AS**, **Felock P**, **Wolfe A**, **Witmer M**, **Grobler J**, **Anthony N**, **Egbertson M**, **Melamed JY**, **Young S**, **Hamill T**, **Cole JL**, **Hazuda DJ**. 2000. HIV-1 integrase inhibitors that compete with the target DNA substrate define a unique strand transfer conformation for integrase. Proc Natl Acad Sci USA **97**:11244–11249.

376. **Hazuda DJ**, **Anthony NJ**, **Gomez RP**, **Jolly SM**, **Wai JS**, **Zhuang L**, **Fisher TE**, **Embrey M**, **Guare JP**, **Egbertson MS**, **Vacca JP**, **Huff JR**, **Felock PJ**, **Witmer MV**, **Stillmock KA**, **Danovich R**, **Grobler J**, **Miller MD**, **Espeseth AS**, **Jin L**, **Chen I-W**, **Lin JH**, **Kassahun K**, **Ellis JD**, **Wong BK**, **Xu W**, **Pearson PG**, **Schleif WA**, **Cortese R**, **Emini E**, **Summa V**, **Holloway MK**, **Young SD**. 2004. A naphthyridine carboxamide provides evidence for discordant resistance between mechanistically identical inhibitors of HIV-1 integrase. Proc Natl Acad Sci USA **101**:11233–11238.

377. **McColl DJ**, **Chen X**. 2010. Strand transfer inhibitors of HIV-1 integrase: bringing IN a new era of antiretroviral therapy. Antiviral Res **85**:101–118.

378. **Smith SJ**, **Zhao XZ**, **Burke TR**, **Hughes SH**. 2018. HIV-1 Integrase Inhibitors That Are Broadly Effective against Drug-Resistant Mutants. Antimicrob Agents Chemother **62**:e01035–18.

379. **Rizza SA**, **Bhatia R**, **Zeuli J**, **Temesgen Z**. 2019. Ibalizumab for the treatment of multidrug-resistant HIV-1 infection. Drugs Today **55**:25.

380. **Dragic T**, **Trkola A**, **Thompson DA**, **Cormier EG**, **Kajumo FA**, **Maxwell E**, **Lin SW**, **Ying W**, **Smith SO**, **Sakmar TP**, **Moore JP**. 2000. A binding pocket for a small molecule inhibitor of HIV-1 entry within the transmembrane helices of CCR5. Proc Natl Acad Sci USA **97**:5639–5644.

381. **Tsamis F**, **Gavrilov S**, **Kajumo F**, **Seibert C**, **Kuhmann S**, **Ketas T**, **Trkola A**, **Palani A**, **Clader JW**, **Tagat JR**, **McCombie S**, **Baroudy B**, **Moore JP**, **Sakmar TP**, **Dragic T**. 2003. Analysis of the mechanism by which the small-molecule CCR5 antagonists SCH-351125 and SCH-350581 inhibit human immunodeficiency virus type 1 entry. J Virol **77**:5201–5208.

382. **Wild C**, **Greenwell T**, **Matthews T**. 1993. A synthetic peptide from HIV-1 gp41 is a potent inhibitor of virus-mediated cell-cell fusion. AIDS Res Hum Retroviruses **9**:1051–1053.

383. **Wild CT**, **Shugars DC**, **Greenwell TK**, **McDanal CB**, **Matthews TJ**. 1994. Peptides corresponding to a predictive alpha-helical domain of human immunodeficiency virus type 1 gp41 are potent inhibitors of virus infection. Proc Natl Acad Sci USA **91**:9770–9774.

384. **Kilby JM**, **Hopkins S**, **Venetta TM**, **DiMassimo B**, **Cloud GA**, **Lee JY**, **Alldredge L**, **Hunter E**, **Lambert D**, **Bolognesi D**, **Matthews T**, **Johnson MR**, **Nowak MA**, **Shaw GM**, **Saag MS**. 1998. Potent suppression of HIV-1 replication in humans by T-20, a peptide inhibitor of gp41-mediated virus entry. Nat Med **4**:1302–1307.

385. **Iyidogan P**, **Anderson KS**. 2014. Current perspectives on HIV-1 antiretroviral drug resistance. Viruses **6**:4095–4139.

386. **Waheed AA**, **Freed EO**. 2012. HIV type 1 Gag as a target for antiviral therapy. AIDS Res Hum Retroviruses **28**:54–75.

387. **Tedbury PR**, **Freed EO**. 2015. HIV-1 gag: an emerging target for antiretroviral therapy. Curr Top Microbiol Immunol **389**:171–201.

388. **Yamashita M**, **Engelman AN**. 2017. Capsid-Dependent Host Factors in HIV-1 Infection. Trends Microbiol **25**:741–755.

389. **James LC**, **Jacques DA**. 2018. The Human Immunodeficiency Virus Capsid Is More Than Just a Genome Package. Annu Rev Virol **5**:209–225.

390. **Cuevas JM**, **Geller R**, **Garijo R**, **López-Aldeguer J**, **Sanjuán R**. 2015. Extremely High Mutation Rate of HIV-1 In Vivo. PLoS Biol **13**:e1002251.

391. **Hu Y**, **Tan PT**, **Tan TW**, **August JT**, **Khan AM**. 2013. Dissecting the dynamics of HIV-1 protein sequence diversity. PLoS ONE **8**:e59994.

392. **Zanini F**, **Puller V**, **Brodin J**, **Albert J**, **Neher RA**. 2017. In vivo mutation rates and the landscape of fitness costs of HIV-1. Virus Evol **3**:vex003.

393. **Schwedler von UK**, **Stray KM**, **Garrus JE**, **Sundquist WI**. 2003. Functional surfaces of the human immunodeficiency virus type 1 capsid protein. J Virol **77**:5439–5450.

394. **Rihn SJ**, **Wilson SJ**, **Loman NJ**, **Alim M**, **Bakker SE**, **Bhella D**, **Gifford RJ**, **Rixon FJ**, **Bieniasz PD**. 2013. Extreme genetic fragility of the HIV-1 capsid. PLoS Pathog **9**:e1003461.

395. **Thenin-Houssier S**, **de Vera IMS**, **Pedro-Rosa L**, **Brady A**, **Richard A**, **Konnick B**, **Opp S**, **Buffone C**, **Fuhrmann J**, **Kota S**, **Billack B**, **Pietka-Ottlik M**, **Tellinghuisen T**, **Choe H**, **Spicer T**, **Scampavia L**, **Diaz-Griffero F**, **Kojetin DJ**, **Valente ST**. 2016. Ebselen, a Small-Molecule Capsid Inhibitor of HIV-1 Replication. Antimicrob Agents Chemother **60**:2195–2208.

396. **Tang C**, **Loeliger E**, **Kinde I**, **Kyere S**, **Mayo K**, **Barklis E**, **Sun Y**, **Huang M**, **Summers MF**. 2003. Antiviral inhibition of the HIV-1 capsid protein. J Mol Biol **327**:1013–1020.

397. **Sticht J**, **Humbert M**, **Findlow S**, **Bodem J**, **Müller B**, **Dietrich U**, **Werner J**, **Krausslich H-G**. 2005. A peptide inhibitor of HIV-1 assembly in vitro. Nat Struct Mol Biol **12**:671–677.

398. **Zhang H**, **Zhao Q**, **Bhattacharya S**, **Waheed AA**, **Tong X**, **Hong A**, **Heck S**, **Curreli F**, **Goger M**, **Cowburn D**, **Freed EO**, **Debnath AK**. 2008. A cell-penetrating helical peptide as a potential HIV-1 inhibitor. J Mol Biol **378**:565–580.

399. **Bhattacharya S**, **Zhang H**, **Debnath AK**, **Cowburn D**. 2008. Solution structure of a hydrocarbon stapled peptide inhibitor in complex with monomeric C-terminal domain of HIV-1 capsid. J Biol Chem **283**:16274–16278.

400. **Jin Y**, **Tan Z**, **He M**, **Tian B**, **Tang S**, **Hewlett I**, **Yang M**. 2010. SAR and molecular mechanism study of novel acylhydrazone compounds targeting HIV-1 CA. Bioorg Med Chem **18**:2135–2140.

401. **Zhang H**, **Curreli F**, **Zhang X**, **Bhattacharya S**, **Waheed AA**, **Cooper A**, **Cowburn D**, **Freed EO**, **Debnath AK**. 2011. Antiviral activity of α-helical stapled peptides designed from the HIV-1 capsid dimerization domain. Retrovirology **8**:28.

402. **Bocanegra R**, **Nevot M**, **Doménech R**, **López I**, **Abián O**, **Rodríguez-Huete A**, **Cavasotto CN**, **Velázquez-Campoy A**, **Gómez J**, **Martinez MA**, **Neira JL**, **Mateu MG**. 2011. Rationally designed interfacial peptides are efficient in vitro inhibitors of HIV-1 capsid assembly with antiviral activity. PLoS ONE **6**:e23877.

403. **Fader LD**, **Bethell R**, **Bonneau P**, **Bös M**, **Bousquet Y**, **Cordingley MG**, **Coulombe R**, **Deroy P**, **Faucher A-M**, **Gagnon A**, **Goudreau N**, **Grand-Maître C**, **Guse I**, **Hucke O**, **Kawai SH**, **Lacoste J-E**, **Landry S**, **Lemke CT**, **Malenfant E**, **Mason S**, **Morin S**, **O'Meara J**, **Simoneau B**, **Titolo S**, **Yoakim C**. 2011. Discovery of a 1,5-dihydrobenzo[b][1,4]diazepine-2,4-dione series of inhibitors of HIV-1 capsid assembly. Bioorg Med Chem Lett **21**:398–404.

404. **Wu G**, **Zalloum WA**, **Meuser ME**, **Jing L**, **Kang D**, **Chen C-H**, **Tian Y**, **Zhang F**, **Cocklin S**, **Lee K-H**, **Liu X**, **Zhan P**. 2018. Discovery of phenylalanine derivatives as potent HIV-1 capsid inhibitors from click chemistry-based compound library. Eur J Med Chem **158**:478–492.

405. **Li F**, **Goila-Gaur R**, **Salzwedel K**, **Kilgore NR**, **Reddick M**, **Matallana C**, **Castillo A**, **Zoumplis D**, **Martin DE**, **Orenstein JM**, **Allaway GP**, **Freed EO**, **Wild CT**. 2003. PA-457: a potent HIV inhibitor that disrupts core condensation by targeting a late step in Gag processing. Proc Natl Acad Sci USA **100**:13555–13560.

406. **Blair WS**, **Cao J**, **Fok-Seang J**, **Griffin P**, **Isaacson J**, **Jackson RL**, **Murray E**, **Patick AK**, **Peng Q**, **Perros M**, **Pickford C**, **Wu H**, **Butler SL**. 2009. New small-molecule inhibitor class targeting human immunodeficiency virus type 1 virion maturation. Antimicrob Agents Chemother **53**:5080–5087.

407. **Lemke CT**, **Titolo S**, **Schwedler von U**, **Goudreau N**, **Mercier J-F**, **Wardrop E**, **Faucher A-M**, **Coulombe R**, **Banik SSR**, **Fader L**, **Gagnon A**, **Kawai SH**, **Rancourt J**, **Tremblay M**, **Yoakim C**, **Simoneau B**, **Archambault J**, **Sundquist WI**, **Mason SW**. 2012. Distinct effects of two HIV-1 capsid assembly inhibitor families that bind the same site within the N-terminal domain of the viral CA protein. J Virol **86**:6643–6655.

408. **Wang W**, **Zhou J**, **Halambage UD**, **Jurado KA**, **Jamin AV**, **Wang Y**, **Engelman AN**, **Aiken C**. 2017. Inhibition of HIV-1 Maturation via Small-Molecule Targeting of the Amino-Terminal Domain in the Viral Capsid Protein. J Virol **91**:e02155–16.

409. **Blair WS**, **Pickford C**, **Irving SL**, **Brown DG**, **Anderson M**, **Bazin R**, **Cao J**, **Ciaramella G**, **Isaacson J**, **Jackson L**, **Hunt R**, **Kjerrstrom A**, **Nieman JA**, **Patick AK**, **Perros M**, **Scott AD**, **Whitby K**, **Wu H**, **Butler SL**. 2010. HIV capsid is a tractable target for small molecule therapeutic intervention. PLoS Pathog **6**:e1001220.

410. **Shi J**, **Zhou J**, **Shah VB**, **Aiken C**, **Whitby K**. 2011. Small-molecule inhibition of human immunodeficiency virus type 1 infection by virus capsid destabilization. J Virol **85**:542–549.

411. **Lamorte L**, **Titolo S**, **Lemke CT**, **Goudreau N**, **Mercier J-F**, **Wardrop E**, **Shah VB**, **Schwedler von UK**, **Langelier C**, **Banik SSR**, **Aiken C**, **Sundquist WI**, **Mason SW**. 2013. Discovery of novel small-molecule HIV-1 replication inhibitors that stabilize capsid complexes. Antimicrob Agents Chemother **57**:4622–4631.

412. **Kortagere S**, **Madani N**, **Mankowski MK**, **Schön A**, **Zentner I**, **Swaminathan G**, **Princiotto A**, **Anthony K**, **Oza A**, **Sierra L-J**, **Passic SR**, **Wang X**, **Jones DM**, **Stavale E**, **Krebs FC**, **Martín-García J**, **Freire E**, **Ptak RG**, **Sodroski J**, **Cocklin S**, **Smith AB**. 2012. Inhibiting early-stage events in HIV-1 replication by small-molecule targeting of the HIV-1 capsid. J Virol **86**:8472–8481.

413. **Xu JP**, **Branson JD**, **Lawrence R**, **Cocklin S**. 2016. Identification of a small molecule HIV-1 inhibitor that targets the capsid hexamer. Bioorg Med Chem Lett **26**:824–828.

414. **Jacques DA**, **McEwan WA**, **Hilditch L**, **Price AJ**, **Towers GJ**, **James LC**. 2016. HIV-1 uses dynamic capsid pores to import nucleotides and fuel encapsidated DNA synthesis. Nature **536**:349–353.

415. **Dochi T**, **Akita A**, **Kishimoto N**, **Takamune N**, **Misumi S**. 2018. Trametinib suppresses HIV-1 replication by interfering with the disassembly of human immunodeficiency virus type 1 capsid core. Biochem Biophys Res Commun **495**:1846–1850.

416. **Vozzolo L**, **Loh B**, **Gane PJ**, **Tribak M**, **Zhou L**, **Anderson I**, **Nyakatura E**, **Jenner RG**, **Selwood D**, **Fassati A**. 2010. Gyrase B inhibitor impairs HIV-1 replication by targeting Hsp90 and the capsid protein. Journal of Biological Chemistry **285**:39314–39328.

417. **Price AJ**, **Jacques DA**, **McEwan WA**, **Fletcher AJ**, **Essig S**, **Chin JW**, **Halambage UD**, **Aiken C**, **James LC**. 2014. Host cofactors and pharmacologic ligands share an essential interface in HIV-1 capsid that is lost upon disassembly. PLoS Pathog **10**:e1004459.

418. **Bhattacharya A**, **Alam SL**, **Fricke T**, **Zadrozny K**, **Sedzicki J**, **Taylor AB**, **Demeler B**, **Pornillos O**, **Ganser-Pornillos BK**, **Diaz-Griffero F**, **Ivanov DN**, **Yeager M**. 2014. Structural basis of HIV-1 capsid recognition by PF74 and CPSF6. Proc Natl Acad Sci USA **111**:18625–18630.

419. **Saito A**, **Ferhadian D**, **Sowd GA**, **Serrao E**, **Shi J**, **Halambage UD**, **Teng S**, **Soto J**, **Siddiqui MA**, **Engelman AN**, **Aiken C**, **Yamashita M**. 2016. Roles of Capsid-Interacting Host Factors in Multimodal Inhibition of HIV-1 by PF74. J Virol **90**:5808–5823.

420. **Fricke T**, **Buffone C**, **Opp S**, **Valle-Casuso J**, **Diaz-Griffero F**. 2014. BI-2 destabilizes HIV-1 cores during infection and Prevents Binding of CPSF6 to the HIV-1 Capsid. Retrovirology **11**:120.

421. **Lingappa JR**, **Reed JC**, **Tanaka M**, **Chutiraka K**, **Robinson BA**. 2014. How HIV-1 Gag assembles in cells: Putting together pieces of the puzzle. Virus Res **193**:89–107.

422. **Briggs JAG**, **Simon MN**, **Gross I**, **Krausslich H-G**, **Fuller SD**, **Vogt VM**, **Johnson MC**. 2004. The stoichiometry of Gag protein in HIV-1. Nat Struct Mol Biol **11**:672–675.

423. **Gross I**, **Hohenberg H**, **Wilk T**, **Wiegers K**, **Grättinger M**, **Müller B**, **Fuller S**, **Krausslich HG**. 2000. A conformational switch controlling HIV-1 morphogenesis. EMBO J **19**:103–113.

424. **Wagner JM**, **Zadrozny KK**, **Chrustowicz J**, **Purdy MD**, **Yeager M**, **Ganser-Pornillos BK**, **Pornillos O**. 2016. Crystal structure of an HIV assembly and maturation switch. Elife **5**:2072.

425. **Dick RA**, **Zadrozny KK**, **Xu C**, **Schur FKM**, **Lyddon TD**, **Ricana CL**, **Wagner JM**, **Perilla JR**, **Ganser-Pornillos BK**, **Johnson MC**, **Pornillos O**, **Vogt VM**. 2018. Inositol phosphates are assembly co-factors for HIV-1. Nature **560**:509–512.

426. **Grime JMA**, **Dama JF**, **Ganser-Pornillos BK**, **Woodward CL**, **Jensen GJ**, **Yeager M**, **Voth GA**. 2016. Coarse-grained simulation reveals key features of HIV-1 capsid self-assembly. Nat Commun **7**:11568.

427. **Mattei S**, **Glass B**, **Hagen WJH**, **Krausslich H-G**, **Briggs JAG**. 2016. The structure and flexibility of conical HIV-1 capsids determined within intact virions. Science **354**:1434–1437.

428. **Ganser BK**, **Li S**, **Klishko VY**, **Finch JT**, **Sundquist WI**. 1999. Assembly and analysis of conical models for the HIV-1 core. Science **283**:80–83.

429. **Li S**, **Hill CP**, **Sundquist WI**, **Finch JT**. 2000. Image reconstructions of helical assemblies of the HIV-1 CA protein. Nature **407**:409–413.

430. **Byeon I-JL**, **Meng X**, **Jung J**, **Zhao G**, **Yang R**, **Ahn J**, **Shi J**, **Concel J**, **Aiken C**, **Zhang P**, **Gronenborn AM**. 2009. Structural convergence between Cryo-EM and NMR reveals intersubunit interactions critical for HIV-1 capsid function. Cell **139**:780–790.

431. **Deshmukh L**, **Schwieters CD**, **Grishaev A**, **Ghirlando R**, **Baber JL**, **Clore GM**. 2013. Structure and dynamics of full-length HIV-1 capsid protein in solution. J Am Chem Soc **135**:16133–16147.

432. **Ganser-Pornillos BK**, **Cheng A**, **Yeager M**. 2007. Structure of full-length HIV-1 CA: a model for the mature capsid lattice. Cell **131**:70–79.

433. **Pornillos O**, **Ganser-Pornillos BK**, **Kelly BN**, **Hua Y**, **Whitby FG**, **Stout CD**, **Sundquist WI**, **Hill CP**, **Yeager M**. 2009. X-ray structures of the hexameric building block of the HIV capsid. Cell **137**:1282–1292.

434. **Ptak RG**, **Fu W**, **Sanders-Beer BE**, **Dickerson JE**, **Pinney JW**, **Robertson DL**, **Rozanov MN**, **Katz KS**, **Maglott DR**, **Pruitt KD**, **Dieffenbach CW**. 2008. Cataloguing the HIV type 1 human protein interaction network. AIDS Res Hum Retroviruses **24**:1497–1502.

435. **Ambrose Z**, **Lee K**, **Ndjomou J**, **Xu H**, **Oztop I**, **Matous J**, **Takemura T**, **Unutmaz D**, **Engelman A**, **Hughes SH**, **KewalRamani VN**. 2012. Human immunodeficiency virus type 1 capsid mutation N74D alters cyclophilin A dependence and impairs macrophage infection. J Virol **86**:4708–4714.

436. **Saito A**, **Henning MS**, **Serrao E**, **Dubose BN**, **Teng S**, **Huang J**, **Li X**, **Saito N**, **Roy SP**, **Siddiqui MA**, **Ahn J**, **Tsuji M**, **Hatziioannou T**, **Engelman AN**, **Yamashita M**. 2016. Capsid-CPSF6 Interaction Is Dispensable for HIV-1 Replication in Primary Cells but Is Selected during Virus Passage In Vivo. J Virol **90**:6918–6935.

437. **Yoo S**, **Myszka DG**, **Yeh C**, **McMurray M**, **Hill CP**, **Sundquist WI**. 1997. Molecular recognition in the HIV-1 capsid/cyclophilin A complex. J Mol Biol **269**:780–795.

438. **Aberham C**, **Weber S**, **Phares W**. 1996. Spontaneous mutations in the human immunodeficiency virus type 1 gag gene that affect viral replication in the presence of cyclosporins. J Virol **70**:3536–3544.

439. **Braaten D**, **Aberham C**, **Franke EK**, **Yin L**, **Phares W**, **Luban J**. 1996. Cyclosporine A-resistant human immunodeficiency virus type 1 mutants demonstrate that Gag encodes the functional target of cyclophilin A. J Virol **70**:5170–5176.

440. **Takemura T**, **Kawamata M**, **Urabe M**, **Murakami T**. 2013. Cyclophilin A-dependent restriction to capsid N121K mutant human immunodeficiency virus type 1 in a broad range of cell lines. J Virol **87**:4086–4090.

441. **Schneidewind A**, **Brockman MA**, **Yang R**, **Adam RI**, **Li B**, **Le Gall S**, **Rinaldo CR**, **Craggs SL**, **Allgaier RL**, **Power KA**, **Kuntzen T**, **Tung C-S**, **LaBute MX**, **Mueller SM**, **Harrer T**, **McMichael AJ**, **Goulder PJR**, **Aiken C**, **Brander C**, **Kelleher AD**, **Allen TM**. 2007. Escape from the dominant HLA-B27-restricted cytotoxic T-lymphocyte response in Gag is associated with a dramatic reduction in human immunodeficiency virus type 1 replication. J Virol **81**:12382–12393.

442. **Carnes SK**, **Zhou J**, **Aiken C**. 2018. HIV-1 Engages a Dynein-Dynactin-BICD2 Complex for Infection and Transport to the Nucleus. J Virol **92**:e00358–18.

443. **Handschumacher RE**, **Harding MW**, **Rice J**, **Drugge RJ**, **Speicher DW**. 1984. Cyclophilin: a specific cytosolic binding protein for cyclosporin A. Science **226**:544–547.

444. **Luban J**, **Bossolt KL**, **Franke EK**, **Kalpana GV**, **Goff SP**. 1993. Human immunodeficiency virus type 1 Gag protein binds to cyclophilins A and B. Cell **73**:1067–1078.

445. **Gamble TR**, **Vajdos FF**, **Yoo S**, **Worthylake DK**, **Houseweart M**, **Sundquist WI**, **Hill CP**. 1996. Crystal structure of human cyclophilin A bound to the amino-terminal domain of HIV-1 capsid. Cell **87**:1285–1294.

446. **Bosco DA**, **Eisenmesser EZ**, **Pochapsky S**, **Sundquist WI**, **Kern D**. 2002. Catalysis of cis/trans isomerization in native HIV-1 capsid by human cyclophilin A. Proc Natl Acad Sci USA **99**:5247–5252.

447. **Liu C**, **Perilla JR**, **Ning J**, **Lu M**, **Hou G**, **Ramalho R**, **Himes BA**, **Zhao G**, **Bedwell GJ**, **Byeon I-J**, **Ahn J**, **Gronenborn AM**, **Prevelige PE**, **Rousso I**, **Aiken C**, **Polenova T**, **Schulten K**, **Zhang P**. 2016. Cyclophilin A stabilizes the HIV-1 capsid through a novel non-canonical binding site. Nat Commun **7**:10714.

448. **Franke EK**, **Yuan HE**, **Luban J**. 1994. Specific incorporation of cyclophilin A into HIV-1 virions. Nature **372**:359–362.

449. **Thali M**, **Bukovsky A**, **Kondo E**, **Rosenwirth B**, **Walsh CT**, **Sodroski J**, **Göttlinger HG**. 1994. Functional association of cyclophilin A with HIV-1 virions. Nature **372**:363–365.

450. **Hatziioannou T**, **Perez-Caballero D**, **Cowan S**, **Bieniasz PD**. 2005. Cyclophilin interactions with incoming human immunodeficiency virus type 1 capsids with opposing effects on infectivity in human cells. J Virol **79**:176–183.

451. **Sokolskaja E**, **Sayah DM**, **Luban J**. 2004. Target cell cyclophilin A modulates human immunodeficiency virus type 1 infectivity. J Virol **78**:12800–12808.

452. **Braaten D**, **Franke EK**, **Luban J**. 1996. Cyclophilin A is required for an early step in the life cycle of human immunodeficiency virus type 1 before the initiation of reverse transcription. J Virol **70**:3551–3560.

453. **Ptak RG**, **Gallay PA**, **Jochmans D**, **Halestrap AP**, **Ruegg UT**, **Pallansch LA**, **Bobardt MD**, **de Béthune M-P**, **Neyts J**, **De Clercq E**, **Dumont J-M**, **Scalfaro P**, **Besseghir K**, **Wenger RM**, **Rosenwirth B**. 2008. Inhibition of human immunodeficiency virus type 1 replication in human cells by Debio-025, a novel cyclophilin binding agent. Antimicrob Agents Chemother **52**:1302–1317.

454. **Gallay PA**, **Bobardt MD**, **Chatterji U**, **Trepanier DJ**, **Ure D**, **Ordonez C**, **Foster R**. 2015. The Novel Cyclophilin Inhibitor CPI-431-32 Concurrently Blocks HCV and HIV-1 Infections via a Similar Mechanism of Action. PLoS ONE **10**:e0134707.

455. **Yang R**, **Aiken C**. 2007. A mutation in alpha helix 3 of CA renders human immunodeficiency virus type 1 cyclosporin A resistant and dependent: rescue by a second-site substitution in a distal region of CA. J Virol **81**:3749–3756.

456. **Li Y**, **Kar AK**, **Sodroski J**. 2009. Target cell type-dependent modulation of human immunodeficiency virus type 1 capsid disassembly by cyclophilin A. J Virol **83**:10951–10962.

457. **Yin L**, **Braaten D**, **Luban J**. 1998. Human immunodeficiency virus type 1 replication is modulated by host cyclophilin A expression levels. J Virol **72**:6430–6436.

458. **Qi M**, **Yang R**, **Aiken C**. 2008. Cyclophilin A-dependent restriction of human immunodeficiency virus type 1 capsid mutants for infection of nondividing cells. J Virol **82**:12001–12008.

459. **De Iaco A**, **Luban J**. 2014. Cyclophilin A promotes HIV-1 reverse transcription but its effect on transduction correlates best with its effect on nuclear entry of viral cDNA. Retrovirology **11**:11.

460. **Braaten D**, **Luban J**. 2001. Cyclophilin A regulates HIV-1 infectivity, as demonstrated by gene targeting in human T cells. EMBO J **20**:1300–1309.

461. **Shah VB**, **Shi J**, **Hout DR**, **Oztop I**, **Krishnan L**, **Ahn J**, **Shotwell MS**, **Engelman A**, **Aiken C**. 2013. The host proteins transportin SR2/TNPO3 and cyclophilin A exert opposing effects on HIV-1 uncoating. J Virol **87**:422–432.

462. **Fricke T**, **Brandariz-Nuñez A**, **Wang X**, **Smith AB**, **Diaz-Griffero F**. 2013. Human cytosolic extracts stabilize the HIV-1 core. J Virol **87**:10587–10597.

463. **Ylinen LMJ**, **Schaller T**, **Price A**, **Fletcher AJ**, **Noursadeghi M**, **James LC**, **Towers GJ**. 2009. Cyclophilin A levels dictate infection efficiency of human immunodeficiency virus type 1 capsid escape mutants A92E and G94D. J Virol **83**:2044–2047.

464. **Yamashita M**, **Emerman M**. 2009. Cellular restriction targeting viral capsids perturbs human immunodeficiency virus type 1 infection of nondividing cells. J Virol **83**:9835–9843.

465. **De Houwer S**, **Demeulemeester J**, **Thys W**, **Taltynov O**, **Zmajkovicova K**, **Christ F**, **Debyser Z**. 2012. Identification of residues in the C-terminal domain of HIV-1 integrase that mediate binding to the transportin-SR2 protein. Journal of Biological Chemistry **287**:34059–34068.

466. **De Iaco A**, **Luban J**. 2011. Inhibition of HIV-1 infection by TNPO3 depletion is determined by capsid and detectable after viral cDNA enters the nucleus. Retrovirology **8**:98.

467. **Krishnan L**, **Matreyek KA**, **Oztop I**, **Lee K**, **Tipper CH**, **Li X**, **Dar MJ**, **KewalRamani VN**, **Engelman A**. 2010. The requirement for cellular transportin 3 (TNPO3 or TRN-SR2) during infection maps to human immunodeficiency virus type 1 capsid and not integrase. J Virol **84**:397–406.

468. **Logue EC**, **Taylor KT**, **Goff PH**, **Landau NR**. 2011. The cargo-binding domain of transportin 3 is required for lentivirus nuclear import. J Virol **85**:12950–12961.

469. **Zhou L**, **Sokolskaja E**, **Jolly C**, **James W**, **Cowley SA**, **Fassati A**. 2011. Transportin 3 promotes a nuclear maturation step required for efficient HIV-1 integration. PLoS Pathog **7**:e1002194.

470. **Valle-Casuso JC**, **Di Nunzio F**, **Yang Y**, **Reszka N**, **Lienlaf M**, **Arhel N**, **Perez P**, **Brass AL**, **Diaz-Griffero F**. 2012. TNPO3 is required for HIV-1 replication after nuclear import but prior to integration and binds the HIV-1 core. J Virol **86**:5931–5936.

471. **Zhao J**, **Hyman L**, **Moore C**. 1999. Formation of mRNA 3' ends in eukaryotes: mechanism, regulation, and interrelationships with other steps in mRNA synthesis. Microbiol Mol Biol Rev **63**:405–445.

472. **Peng K**, **Muranyi W**, **Glass B**, **Laketa V**, **Yant SR**, **Tsai L**, **Cihlar T**, **Müller B**, **Krausslich H-G**. 2014. Quantitative microscopy of functional HIV post-entry complexes reveals association of replication with the viral capsid. Elife **3**:e04114.

473. **Rüegsegger U**, **Blank D**, **Keller W**. 1998. Human pre-mRNA cleavage factor Im is related to spliceosomal SR proteins and can be reconstituted in vitro from recombinant subunits. Mol Cell **1**:243–253.

474. **Ruepp M-D**, **Aringhieri C**, **Vivarelli S**, **Cardinale S**, **Paro S**, **Schümperli D**, **Barabino SML**. 2009. Mammalian pre-mRNA 3' end processing factor CF I m 68 functions in mRNA export. Mol Biol Cell **20**:5211–5223.

475. **Dettwiler S**, **Aringhieri C**, **Cardinale S**, **Keller W**, **Barabino SML**. 2004. Distinct sequence motifs within the 68-kDa subunit of cleavage factor Im mediate RNA binding, protein-protein interactions, and subcellular localization. J Biol Chem **279**:35788–35797.

476. **Henning MS**, **Dubose BN**, **Burse MJ**, **Aiken C**, **Yamashita M**. 2014. In vivo functions of CPSF6 for HIV-1 as revealed by HIV-1 capsid evolution in HLA-B27-positive subjects. PLoS Pathog **10**:e1003868.

477. **Lee K**, **Mulky A**, **Yuen W**, **Martin TD**, **Meyerson NR**, **Choi L**, **Yu H**, **Sawyer SL**, **KewalRamani VN**. 2012. HIV-1 capsid-targeting domain of cleavage and polyadenylation specificity factor 6. J Virol **86**:3851–3860.

478. **Frey S**, **Richter RP**, **Görlich D**. 2006. FG-rich repeats of nuclear pore proteins form a three-dimensional meshwork with hydrogel-like properties. Science **314**:815–817.

479. **Bichel K**, **Price AJ**, **Schaller T**, **Towers GJ**, **Freund SMV**, **James LC**. 2013. HIV-1 capsid undergoes coupled binding and isomerization by the nuclear pore protein NUP358. Retrovirology **10**:81.

480. **Meehan AM**, **Saenz DT**, **Guevera R**, **Morrison JH**, **Peretz M**, **Fadel HJ**, **Hamada M**, **van Deursen J**, **Poeschla EM**. 2014. A cyclophilin homology domain-independent role for Nup358 in HIV-1 infection. PLoS Pathog **10**:e1003969.

481. **Dharan A**, **Talley S**, **Tripathi A**, **Mamede JI**, **Majetschak M**, **Hope TJ**, **Campbell EM**. 2016. KIF5B and Nup358 Cooperatively Mediate the Nuclear Import of HIV-1 during Infection. PLoS Pathog **12**:e1005700.

482. **Di Nunzio F**, **Fricke T**, **Miccio A**, **Valle-Casuso JC**, **Perez P**, **Souque P**, **Rizzi E**, **Severgnini M**, **Mavilio F**, **Charneau P**, **Diaz-Griffero F**. 2013. Nup153 and Nup98 bind the HIV-1 core and contribute to the early steps of HIV-1 replication. Virology **440**:8–18.

483. **Koh Y**, **Wu X**, **Ferris AL**, **Matreyek KA**, **Smith SJ**, **Lee K**, **KewalRamani VN**, **Hughes SH**, **Engelman A**. 2013. Differential effects of human immunodeficiency virus type 1 capsid and cellular factors nucleoporin 153 and LEDGF/p75 on the efficiency and specificity of viral DNA integration. J Virol **87**:648–658.

484. **Craigie R**, **Bushman FD**. 2012. HIV DNA integration. Cold Spring Harb Perspect Med **2**:a006890.

485. **Zhang H**, **Dornadula G**, **Pomerantz RJ**. 1996. Endogenous reverse transcription of human immunodeficiency virus type 1 in physiological microenviroments: an important stage for viral infection of nondividing cells. J Virol **70**:2809–2824.

486. **Jakobsen MR**, **Olagnier D**, **Hiscott J**. 2015. Innate immune sensing of HIV-1 infection. Curr Opin HIV AIDS **10**:96–102.

487. **Solis M**, **Nakhaei P**, **Jalalirad M**, **Lacoste J**, **Douville R**, **Arguello M**, **Zhao T**, **Laughrea M**, **Wainberg MA**, **Hiscott J**. 2011. RIG-I-mediated antiviral signaling is inhibited in HIV-1 infection by a protease-mediated sequestration of RIG-I. J Virol **85**:1224–1236.

488. **Berg RK**, **Melchjorsen J**, **Rintahaka J**, **Diget E**, **Søby S**, **Horan KA**, **Gorelick RJ**, **Matikainen S**, **Larsen CS**, **Østergaard L**, **Paludan SR**, **Mogensen TH**. 2012. Genomic HIV RNA induces innate immune responses through RIG-I-dependent sensing of secondary-structured RNA. PLoS ONE **7**:e29291.

489. **Sauter D**, **Kirchhoff F**. 2016. HIV replication: a game of hide and sense. Curr Opin HIV AIDS **11**:173–181.

490. **Cosnefroy O**, **Murray PJ**, **Bishop KN**. 2016. HIV-1 capsid uncoating initiates after the first strand transfer of reverse transcription. Retrovirology **13**:58.

491. **Rankovic S**, **Varadarajan J**, **Ramalho R**, **Aiken C**, **Rousso I**. 2017. Reverse Transcription Mechanically Initiates HIV-1 Capsid Disassembly. J Virol **91**:e00289–17.

492. **Hulme AE**, **Perez O**, **Hope TJ**. 2011. Complementary assays reveal a relationship between HIV-1 uncoating and reverse transcription. Proc Natl Acad Sci USA **108**:9975–9980.

493. **Yang Y**, **Fricke T**, **Diaz-Griffero F**. 2013. Inhibition of reverse transcriptase activity increases stability of the HIV-1 core. J Virol **87**:683–687.

494. **Farnet CM**, **Haseltine WA**. 1991. Determination of viral proteins present in the human immunodeficiency virus type 1 preintegration complex. J Virol **65**:1910–1915.

495. **Bukrinsky MI**, **Sharova N**, **McDonald TL**, **Pushkarskaya T**, **Tarpley WG**, **Stevenson M**. 1993. Association of integrase, matrix, and reverse transcriptase antigens of human immunodeficiency virus type 1 with viral nucleic acids following acute infection. Proc Natl Acad Sci USA **90**:6125–6129.

496. **Karageorgos L**, **Li P**, **Burrell C**. 1993. Characterization of HIV replication complexes early after cell-to-cell infection. AIDS Res Hum Retroviruses **9**:817–823.

497. **Miller MD**, **Farnet CM**, **Bushman FD**. 1997. Human immunodeficiency virus type 1 preintegration complexes: studies of organization and composition. J Virol **71**:5382–5390.

498. **Lukic Z**, **Dharan A**, **Fricke T**, **Diaz-Griffero F**, **Campbell EM**. 2014. HIV-1 uncoating is facilitated by dynein and kinesin 1. J Virol **88**:13613–13625.

499. **Pawlica P**, **Berthoux L**. 2014. Cytoplasmic dynein promotes HIV-1 uncoating. Viruses **6**:4195–4211.

500. **Xu H**, **Franks T**, **Gibson G**, **Huber K**, **Rahm N**, **De Castillia CS**, **Luban J**, **Aiken C**, **Watkins S**, **Sluis-Cremer N**, **Ambrose Z**. 2013. Evidence for biphasic uncoating during HIV-1 infection from a novel imaging assay. Retrovirology **10**:70.

501. **Mamede JI**, **Cianci GC**, **Anderson MR**, **Hope TJ**. 2017. Early cytoplasmic uncoating is associated with infectivity of HIV-1. Proc Natl Acad Sci USA **114**:E7169–E7178.

502. **Da Silva Santos C**, **Tartour K**, **Cimarelli A**. 2016. A Novel Entry/Uncoating Assay Reveals the Presence of at Least Two Species of Viral Capsids During Synchronized HIV-1 Infection. PLoS Pathog **12**:e1005897.

503. **Fassati A**. 2012. Multiple roles of the capsid protein in the early steps of HIV-1 infection. Virus Res **170**:15–24.

504. **Campbell EM**, **Perez O**, **Anderson JL**, **Hope TJ**. 2008. Visualization of a proteasome-independent intermediate during restriction of HIV-1 by rhesus TRIM5alpha. J Cell Biol **180**:549–561.

505. **Jun S**, **Ke D**, **Debiec K**, **Zhao G**, **Meng X**, **Ambrose Z**, **Gibson GA**, **Watkins SC**, **Zhang P**. 2011. Direct visualization of HIV-1 with correlative live-cell microscopy and cryo-electron tomography. Structure **19**:1573–1581.

506. **Yamashita M**, **Emerman M**. 2004. Capsid is a dominant determinant of retrovirus infectivity in nondividing cells. J Virol **78**:5670–5678.

507. **Song C**, **Aiken C**. 2007. Analysis of human cell heterokaryons demonstrates that target cell restriction of cyclosporine-resistant human immunodeficiency virus type 1 mutants is genetically dominant. J Virol **81**:11946–11956.

508. **Zhou J**, **Price AJ**, **Halambage UD**, **James LC**, **Aiken C**. 2015. HIV-1 Resistance to the Capsid-Targeting Inhibitor PF74 Results in Altered Dependence on Host Factors Required for Virus Nuclear Entry. J Virol **89**:9068–9079.

509. **Liu Z**, **Pan Q**, **Liang Z**, **Qiao W**, **Cen S**, **Liang C**. 2015. The highly polymorphic cyclophilin A-binding loop in HIV-1 capsid modulates viral resistance to MxB. Retrovirology **12**:1.

510. **Donahue DA**, **Amraoui S**, **Di Nunzio F**, **Kieffer C**, **Porrot F**, **Opp S**, **Diaz-Griffero F**, **Casartelli N**, **Schwartz O**. 2016. SUN2 Overexpression Deforms Nuclear Shape and Inhibits HIV. J Virol **90**:4199–4214.

511. **Schaller T**, **Bulli L**, **Pollpeter D**, **Betancor G**, **Kutzner J**, **Apolonia L**, **Herold N**, **Burk R**, **Malim MH**. 2017. Effects of Inner Nuclear Membrane Proteins SUN1/UNC-84A and SUN2/UNC-84B on the Early Steps of HIV-1 Infection. J Virol **91**:e00463–17.

512. **Weinberg JB**, **Matthews TJ**, **Cullen BR**, **Malim MH**. 1991. Productive human immunodeficiency virus type 1 (HIV-1) infection of nonproliferating human monocytes. J Exp Med **174**:1477–1482.

513. **Zaitseva M**, **Blauvelt A**, **Lee S**, **Lapham CK**, **Klaus-Kovtun V**, **Mostowski H**, **Manischewitz J**, **Golding H**. 1997. Expression and function of CCR5 and CXCR4 on human Langerhans cells and macrophages: implications for HIV primary infection. Nat Med **3**:1369–1375.

514. **He J**, **Chen Y**, **Farzan M**, **Choe H**, **Ohagen A**, **Gartner S**, **Busciglio J**, **Yang X**, **Hofmann W**, **Newman W**, **Mackay CR**, **Sodroski J**, **Gabuzda D**. 1997. CCR3 and CCR5 are co-receptors for HIV-1 infection of microglia. Nature **385**:645–649.

515. **Tan J**, **Sattentau QJ**. 2013. The HIV-1-containing macrophage compartment: a perfect cellular niche? Trends Microbiol **21**:405–412.

516. **Antonucci JM**, **St Gelais C**, **Wu L**. 2017. The Dynamic Interplay between HIV-1, SAMHD1, and the Innate Antiviral Response. Front Immunol **8**:1541.

517. **Kumar A**, **Herbein G**. 2014. The macrophage: a therapeutic target in HIV-1 infection. Mol Cell Ther **2**:10.

518. **Gavegnano C**, **Schinazi RF**. 2009. Antiretroviral therapy in macrophages: implication for HIV eradication. Antivir Chem Chemother **20**:63–78.

519. **Montaner LJ**, **Crowe SM**, **Aquaro S**, **Perno C-F**, **Stevenson M**, **Collman RG**. 2006. Advances in macrophage and dendritic cell biology in HIV-1 infection stress key understudied areas in infection, pathogenesis, and analysis of viral reservoirs. J Leukoc Biol **80**:961–964.

520. **Chang SY**, **Bowman BH**, **Weiss JB**, **Garcia RE**, **White TJ**. 1993. The origin of HIV-1 isolate HTLV-IIIB. Nature **363**:466–469.

521. **Ning J**, **Zhong Z**, **Fischer DK**, **Harris G**, **Watkins SC**, **Ambrose Z**, **Zhang P**. 2018. Truncated CPSF6 Forms Higher-Order Complexes That Bind and Disrupt HIV-1 Capsid. J Virol **92**:e00368–18.

522. **Ochsenbauer C**, **Edmonds TG**, **Ding H**, **Keele BF**, **Decker J**, **Salazar MG**, **Salazar-Gonzalez JF**, **Shattock R**, **Haynes BF**, **Shaw GM**, **Hahn BH**, **Kappes JC**. 2012. Generation of transmitted/founder HIV-1 infectious molecular clones and characterization of their replication capacity in CD4 T lymphocytes and monocyte-derived macrophages. J Virol **86**:2715–2728.

523. **Zhao G**, **Perilla JR**, **Yufenyuy EL**, **Meng X**, **Chen B**, **Ning J**, **Ahn J**, **Gronenborn AM**, **Schulten K**, **Aiken C**, **Zhang P**. 2013. Mature HIV-1 capsid structure by cryo-electron microscopy and all-atom molecular dynamics. Nature **497**:643–646.

524. **Gres AT**, **Kirby KA**, **KewalRamani VN**, **Tanner JJ**, **Pornillos O**, **Sarafianos SG**. 2015. STRUCTURAL VIROLOGY. X-ray crystal structures of native HIV-1 capsid protein reveal conformational variability. Science **349**:99–103.

525. **Francis AC**, **Marin M**, **Shi J**, **Aiken C**, **Melikyan GB**. 2016. Time-Resolved Imaging of Single HIV-1 Uncoating In Vitro and in Living Cells. PLoS Pathog **12**:e1005709.

526. **Gao D**, **Wu J**, **Wu Y-T**, **Du F**, **Aroh C**, **Yan N**, **Sun L**, **Chen ZJ**. 2013. Cyclic GMP-AMP synthase is an innate immune sensor of HIV and other retroviruses. Science **341**:903–906.

527. **Maillard PV**, **Zoete V**, **Michielin O**, **Trono D**. 2011. Homology-based identification of capsid determinants that protect HIV1 from human TRIM5α restriction. Journal of Biological Chemistry **286**:8128–8140.

528. **O'Brien WA**, **Koyanagi Y**, **Namazie A**, **Zhao JQ**, **Diagne A**, **Idler K**, **Zack JA**, **Chen IS**. 1990. HIV-1 tropism for mononuclear phagocytes can be determined by regions of gp120 outside the CD4-binding domain. Nature **348**:69–73.

529. **Shioda T**, **Levy JA**, **Cheng-Mayer C**. 1991. Macrophage and T cell-line tropisms of HIV-1 are determined by specific regions of the envelope gp120 gene. Nature **349**:167–169.

530. **Li G**, **Verheyen J**, **Rhee S-Y**, **Voet A**, **Vandamme A-M**, **Theys K**. 2013. Functional conservation of HIV-1 Gag: implications for rational drug design. Retrovirology **10**:126.

531. **Cecilia D**, **KewalRamani VN**, **O'Leary J**, **Volsky B**, **Nyambi P**, **Burda S**, **Xu S**, **Littman DR**, **Zolla-Pazner S**. 1998. Neutralization profiles of primary human immunodeficiency virus type 1 isolates in the context of coreceptor usage. J Virol **72**:6988–6996.

532. **Vermeire J**, **Naessens E**, **Vanderstraeten H**, **Landi A**, **Iannucci V**, **Van Nuffel A**, **Taghon T**, **Pizzato M**, **Verhasselt B**. 2012. Quantification of reverse transcriptase activity by real-time PCR as a fast and accurate method for titration of HIV, lenti- and retroviral vectors. PLoS ONE **7**:e50859.

533. **Julias JG**, **Ferris AL**, **Boyer PL**, **Hughes SH**. 2001. Replication of phenotypically mixed human immunodeficiency virus type 1 virions containing catalytically active and catalytically inactive reverse transcriptase. J Virol **75**:6537–6546.

534. **Di Nunzio F**. 2013. New insights in the role of nucleoporins: a bridge leading to concerted steps from HIV-1 nuclear entry until integration. Virus Res **178**:187–196.

535. **Ganser-Pornillos BK**, **Chandrasekaran V**, **Pornillos O**, **Sodroski JG**, **Sundquist WI**, **Yeager M**. 2011. Hexagonal assembly of a restricting TRIM5alpha protein. Proc Natl Acad Sci USA **108**:534–539.

536. **Stremlau M**, **Perron M**, **Lee M**, **Li Y**, **Song B**, **Javanbakht H**, **Diaz-Griffero F**, **Anderson DJ**, **Sundquist WI**, **Sodroski J**. 2006. Specific recognition and accelerated uncoating of retroviral capsids by the TRIM5alpha restriction factor. Proc Natl Acad Sci USA **103**:5514–5519.

537. **Black LR**, **Aiken C**. 2010. TRIM5alpha disrupts the structure of assembled HIV-1 capsid complexes in vitro. J Virol **84**:6564–6569.

538. **Zhao G**, **Ke D**, **Vu T**, **Ahn J**, **Shah VB**, **Yang R**, **Aiken C**, **Charlton LM**, **Gronenborn AM**, **Zhang P**. 2011. Rhesus TRIM5α disrupts the HIV-1 capsid at the inter-hexamer interfaces. PLoS Pathog **7**:e1002009.

539. **Stremlau M**, **Owens CM**, **Perron MJ**, **Kiessling M**, **Autissier P**, **Sodroski J**. 2004. The cytoplasmic body component TRIM5alpha restricts HIV-1 infection in Old World monkeys. Nature **427**:848–853.

540. **Márquez CL**, **Lau D**, **Walsh J**, **Shah V**, **McGuinness C**, **Wong A**, **Aggarwal A**, **Parker MW**, **Jacques DA**, **Turville S**, **Böcking T**. 2018. Kinetics of HIV-1 capsid uncoating revealed by single-molecule analysis. Elife **7**:e1002762.

541. **Francis AC**, **Melikyan GB**. 2018. Live-Cell Imaging of Early Steps of Single HIV-1 Infection. Viruses **10**:E275.

542. **Zheng Q**, **Lavis LD**. 2017. Development of photostable fluorophores for molecular imaging. Curr Opin Chem Biol **39**:32–38.

543. **Ganim Z**, **Rief M**. 2017. Mechanically switching single-molecule fluorescence of GFP by unfolding and refolding. Proc Natl Acad Sci USA **114**:11052–11056.

544. **Stupak AP**, **Blaudeck T**, **Zenkevich EI**, **Krause S**, **Borczyskowski von C**. 2018. The nature of non-FRET photoluminescence quenching in nanoassemblies from semiconductor quantum dots and dye molecules. Phys Chem Chem Phys **20**:18579–18600.

545. **Perilla JR**, **Schulten K**. 2017. Physical properties of the HIV-1 capsid from all-atom molecular dynamics simulations. Nat Commun **8**:15959.

546. **Kolb HC**, **Finn MG**, **Sharpless KB**. 2001. Click Chemistry: Diverse Chemical Function from a Few Good Reactions. Angew Chem Int Ed Engl **40**:2004–2021.

547. **Bertrand E**, **Chartrand P**, **Schaefer M**, **Shenoy SM**, **Singer RH**, **Long RM**. 1998. Localization of ASH1 mRNA particles in living yeast. Mol Cell **2**:437–445.

548. **Davis JE**, **Strauss JH Jr**, **Sinsheimer RL**. 1961. National Academy of Sciences: Abstracts of Papers Presented at the Autumn Meeting, 29 October, La Jolla, California, 30 October-1 November 1961, Los Angeles. Science **134**:1425–1437.

549. **Strauss JH**, **Sinsheimer RL**. 1963. Purification and properties of bacteriophage MS2 and of its ribonucleic acid. J Mol Biol **7**:43–54.

550. **Min Jou W**, **Haegeman G**, **Ysebaert M**, **Fiers W**. 1972. Nucleotide Sequence of the Gene Coding for the Bacteriophage MS2 Coat Protein. Nature **237**:82–88.

551. **Spahr PF**, **Farber M**, **Gesteland RF**. 1969. Binding Site on R17 RNA for Coat Protein. Nature **222**:455–458.

552. **Bernardi A**, **Spahr PF**. 1972. Nucleotide sequence at the binding site for coat protein on RNA of bacteriophage R17. Proc Natl Acad Sci USA **69**:3033–3037.

553. **Fiers W**, **Contreras R**, **De Wachter R**, **Haegeman G**, **Merregaert J**, **Jou WM**, **Vandenberghe A**. 1971. Recent progress in the sequence determination of bacteriophage MS2 RNA. Biochimie **53**:495–506.

554. **Carey J**, **Cameron V**, **de Haseth PL**, **Uhlenbeck OC**. 1983. Sequence-specific interaction of R17 coat protein with its ribonucleic acid binding site. Biochemistry **22**:2601–2610.

555. **Johansson HE**, **Liljas L**, **Uhlenbeck OC**. 1997. RNA Recognition by the MS2 Phage Coat Protein. Seminars in Virology **8**:176–185.

556. **Fusco D**, **Accornero N**, **Lavoie B**, **Shenoy SM**, **Blanchard JM**, **Singer RH**, **Bertrand E**. 2003. Single mRNA molecules demonstrate probabilistic movement in living mammalian cells. Curr Biol **13**:161–167.

557. **Szent-Gyorgyi C**, **Schmidt BF**, **Schmidt BA**, **Creeger Y**, **Fisher GW**, **Zakel KL**, **Adler S**, **Fitzpatrick JAJ**, **Woolford CA**, **Yan Q**, **Vasilev KV**, **Berget PB**, **Bruchez MP**, **Jarvik JW**, **Waggoner A**. 2008. Fluorogen-activating single-chain antibodies for imaging cell surface proteins. Nat Biotechnol **26**:235–240.

558. **Saunders MJ**, **Szent-Gyorgyi C**, **Fisher GW**, **Jarvik JW**, **Bruchez MP**, **Waggoner AS**. 2012. Fluorogen activating proteins in flow cytometry for the study of surface molecules and receptors. Methods **57**:308–317.

559. **Fitzpatrick JAJ**, **Yan Q**, **Sieber JJ**, **Dyba M**, **Schwarz U**, **Szent-Gyorgyi C**, **Woolford CA**, **Berget PB**, **Waggoner AS**, **Bruchez MP**. 2009. STED nanoscopy in living cells using Fluorogen Activating Proteins. Bioconjug Chem **20**:1843–1847.

560. **Ozhalici-Unal H**, **Pow CL**, **Marks SA**, **Jesper LD**, **Silva GL**, **Shank NI**, **Jones EW**, **Burnette JM**, **Berget PB**, **Armitage BA**. 2008. A rainbow of fluoromodules: a promiscuous scFv protein binds to and activates a diverse set of fluorogenic cyanine dyes. J Am Chem Soc **130**:12620–12621.

561. **Kriz A**, **Schmid K**, **Baumgartner N**, **Ziegler U**, **Berger I**, **Ballmer-Hofer K**, **Berger P**. 2010. A plasmid-based multigene expression system for mammalian cells. Nat Commun **1**:120.

562. **Ott DE**. 2009. Purification of HIV-1 virions by subtilisin digestion or CD45 immunoaffinity depletion for biochemical studies. Methods Mol Biol **485**:15–25.

563. **Halstead JM**, **Lionnet T**, **Wilbertz JH**, **Wippich F**, **Ephrussi A**, **Singer RH**, **Chao JA**. 2015. Translation. An RNA biosensor for imaging the first round of translation from single cells to living animals. Science **347**:1367–1671.

564. **Lim F**, **Peabody DS**. 2002. RNA recognition site of PP7 coat protein. Nucleic Acids Res **30**:4138–4144.

565. **Coulon A**, **Ferguson ML**, **de Turris V**, **Palangat M**, **Chow CC**, **Larson DR**. 2014. Kinetic competition during the transcription cycle results in stochastic RNA processing. Elife **3**:e03939.

566. **Ouellet J**. 2016. RNA Fluorescence with Light-Up Aptamers. Front Chem **4**:29.

567. **Neubacher S**, **Hennig S**. 2019. RNA Structure and Cellular Applications of Fluorescent Light-Up Aptamers. Angew Chem Int Ed Engl **58**:1266–1279.

568. **Paige JS**, **Wu KY**, **Jaffrey SR**. 2011. RNA mimics of green fluorescent protein. Science **333**:642–646.

569. **Dolgosheina EV**, **Jeng SCY**, **Panchapakesan SSS**, **Cojocaru R**, **Chen PSK**, **Wilson PD**, **Hawkins N**, **Wiggins PA**, **Unrau PJ**. 2014. RNA mango aptamer-fluorophore: a bright, high-affinity complex for RNA labeling and tracking. ACS Chem Biol **9**:2412–2420.

570. **Trachman RJ**, **Demeshkina NA**, **Lau MWL**, **Panchapakesan SSS**, **Jeng SCY**, **Unrau PJ**, **Ferré-D'Amaré AR**. 2017. Structural basis for high-affinity fluorophore binding and activation by RNA Mango. Nat Chem Biol **13**:807–813.

571. **Autour A**, **C Y Jeng S**, **D Cawte A**, **Abdolahzadeh A**, **Galli A**, **Panchapakesan SSS**, **Rueda D**, **Ryckelynck M**, **Unrau PJ**. 2018. Fluorogenic RNA Mango aptamers for imaging small non-coding RNAs in mammalian cells. Nat Commun **9**:656.

572. **Hell SW**, **Wichmann J**. 1994. Breaking the diffraction resolution limit by stimulated emission: stimulated-emission-depletion fluorescence microscopy. Opt Lett **19**:780–782.

573. **Klar TA**, **Jakobs S**, **Dyba M**, **Egner A**, **Hell SW**. 2000. Fluorescence microscopy with diffraction resolution barrier broken by stimulated emission. Proc Natl Acad Sci USA **97**:8206–8210.

574. **Blom H**, **Widengren J**. 2017. Stimulated Emission Depletion Microscopy. Chem Rev **117**:7377–7427.

575. **Fletcher TM**, **Soares MA**, **McPhearson S**, **Hui H**, **Wiskerchen M**, **Muesing MA**, **Shaw GM**, **Leavitt AD**, **Boeke JD**, **Hahn BH**. 1997. Complementation of integrase function in HIV-1 virions. EMBO J **16**:5123–5138.

576. **Jowett JB**, **Planelles V**, **Poon B**, **Shah NP**, **Chen ML**, **Chen IS**. 1995. The human immunodeficiency virus type 1 vpr gene arrests infected T cells in the G2 + M phase of the cell cycle. J Virol **69**:6304–6313.

577. **He J**, **Choe S**, **Walker R**, **Di Marzio P**, **Morgan DO**, **Landau NR**. 1995. Human immunodeficiency virus type 1 viral protein R (Vpr) arrests cells in the G2 phase of the cell cycle by inhibiting p34cdc2 activity. J Virol **69**:6705–6711.

578. **Stewart SA**, **Poon B**, **Jowett JB**, **Chen IS**. 1997. Human immunodeficiency virus type 1 Vpr induces apoptosis following cell cycle arrest. J Virol **71**:5579–5592.

579. **Yao XJ**, **Mouland AJ**, **Subbramanian RA**, **Forget J**, **Rougeau N**, **Bergeron D**, **Cohen EA**. 1998. Vpr stimulates viral expression and induces cell killing in human immunodeficiency virus type 1-infected dividing Jurkat T cells. J Virol **72**:4686–4693.

580. **Zhou Y**, **Ratner L**. 2000. Phosphorylation of human immunodeficiency virus type 1 Vpr regulates cell cycle arrest. J Virol **74**:6520–6527.

581. **Barnitz RA**, **Wan F**, **Tripuraneni V**, **Bolton DL**, **Lenardo MJ**. 2010. Protein kinase A phosphorylation activates Vpr-induced cell cycle arrest during human immunodeficiency virus type 1 infection. J Virol **84**:6410–6424.

582. **Bolton DL**, **Lenardo MJ**. 2007. Vpr cytopathicity independent of G2/M cell cycle arrest in human immunodeficiency virus type 1-infected CD4+ T cells. J Virol **81**:8878–8890.

583. **Belzile J-P**, **Duisit G**, **Rougeau N**, **Mercier J**, **Finzi A**, **Cohen ÉA**. 2007. HIV-1 Vpr-mediated G2 arrest involves the DDB1-CUL4AVPRBP E3 ubiquitin ligase. PLoS Pathog **3**:e85.

584. **DeHart JL**, **Zimmerman ES**, **Ardon O**, **Monteiro-Filho CMR**, **Argañaraz ER**, **Planelles V**. 2007. HIV-1 Vpr activates the G2 checkpoint through manipulation of the ubiquitin proteasome system. Virol J **4**:57.

585. **Hrecka K**, **Gierszewska M**, **Srivastava S**, **Kozaczkiewicz L**, **Swanson SK**, **Florens L**, **Washburn MP**, **Skowronski J**. 2007. Lentiviral Vpr usurps Cul4-DDB1[VprBP] E3 ubiquitin ligase to modulate cell cycle. Proc Natl Acad Sci USA **104**:11778–11783.

586. **Schröfelbauer B**, **Hakata Y**, **Landau NR**. 2007. HIV-1 Vpr function is mediated by interaction with the damage-specific DNA-binding protein DDB1. Proc Natl Acad Sci USA **104**:4130–4135.

587. **Belzile J-P**, **Richard J**, **Rougeau N**, **Xiao Y**, **Cohen ÉA**. 2010. HIV-1 Vpr induces the K48-linked polyubiquitination and proteasomal degradation of target cellular proteins to activate ATR and promote G2 arrest. J Virol **84**:3320–3330.

588. **Zhao LJ**, **Mukherjee S**, **Narayan O**. 1994. Biochemical mechanism of HIV-I Vpr function. Specific interaction with a cellular protein. J Biol Chem **269**:15577–15582.

589. **Jacquot G**, **Le Rouzic E**, **Maidou-Peindara P**, **Maizy M**, **Lefrère J-J**, **Daneluzzi V**, **Monteiro-Filho CMR**, **Hong D**, **Planelles V**, **Morand-Joubert L**, **Benichou S**. 2009. Characterization of the molecular determinants of primary HIV-1 Vpr proteins: impact of the Q65R and R77Q substitutions on Vpr functions. PLoS ONE **4**:e7514.

590. **Rogel ME**, **Wu LI**, **Emerman M**. 1995. The human immunodeficiency virus type 1 vpr gene prevents cell proliferation during chronic infection. J Virol **69**:882–888.

591. **Maudet C**, **Bertrand M**, **Le Rouzic E**, **Lahouassa H**, **Ayinde D**, **Nisole S**, **Goujon C**, **Cimarelli A**, **Margottin-Goguet F**, **Transy C**. 2011. Molecular insight into how HIV-1 Vpr protein impairs cell growth through two genetically distinct pathways. Journal of Biological Chemistry **286**:23742–23752.

592. **Bachand F**, **Yao XJ**, **Hrimech M**, **Rougeau N**, **Cohen EA**. 1999. Incorporation of Vpr into human immunodeficiency virus type 1 requires a direct interaction with the p6 domain of the p55 gag precursor. J Biol Chem **274**:9083–9091.

593. **Venkatachari NJ**, **Walker LA**, **Tastan O**, **Le T**, **Dempsey TM**, **Li Y**, **Yanamala N**, **Srinivasan A**, **Klein-Seetharaman J**, **Montelaro RC**, **Ayyavoo V**. 2010. Human immunodeficiency virus type 1 Vpr: oligomerization is an essential feature for its incorporation into virus particles. Virol J **7**:119.

594. **Zhao LJ**, **Wang L**, **Mukherjee S**, **Narayan O**. 1994. Biochemical mechanism of HIV-1 Vpr function. Oligomerization mediated by the N-terminal domain. J Biol Chem **269**:32131–32137.

595. **Shaner NC**, **Lambert GG**, **Chammas A**, **Ni Y**, **Cranfill PJ**, **Baird MA**, **Sell BR**, **Allen JR**, **Day RN**, **Israelsson M**, **Davidson MW**, **Wang J**. 2013. A bright monomeric green fluorescent protein derived from Branchiostoma lanceolatum. Nat Methods **10**:407–409.

596. **Rodrigues MA**, **Gomes DA**, **Leite MF**, **Grant W**, **Zhang L**, **Lam W**, **Cheng Y-C**, **Bennett AM**, **Nathanson MH**. 2007. Nucleoplasmic calcium is required for cell proliferation. J Biol Chem **282**:17061–17068.

597. **Wu X**, **Liu H**, **Xiao H**, **Conway JA**, **Hunter E**, **Kappes JC**. 1997. Functional RT and IN incorporated into HIV-1 particles independently of the Gag/Pol precursor protein. EMBO J **16**:5113–5122.

598. **Xu H**, **Svarovskaia ES**, **Barr R**, **Zhang Y**, **Khan MA**, **Strebel K**, **Pathak VK**. 2004. A single amino acid substitution in human APOBEC3G antiretroviral enzyme confers resistance to HIV-1 virion infectivity factor-induced depletion. Proc Natl Acad Sci USA **101**:5652–5657.

599. **Han Y**, **Ahn J**, **Concel J**, **Byeon I-JL**, **Gronenborn AM**, **Yang J**, **Polenova T**. 2010. Solid-state NMR studies of HIV-1 capsid protein assemblies. J Am Chem Soc **132**:1976–1987.

600. **Zhang H**, **Hou G**, **Lu M**, **Ahn J**, **Byeon I-JL**, **Langmead CJ**, **Perilla JR**, **Hung I**, **Gor'kov PL**, **Gan Z**, **Brey WW**, **Case DA**, **Schulten K**, **Gronenborn AM**, **Polenova T**. 2016. HIV-1 Capsid Function Is Regulated by Dynamics: Quantitative Atomic-Resolution Insights by Integrating Magic-Angle-Spinning NMR, QM/MM, and MD. J Am Chem Soc **138**:14066–14075.

601. **Lu M**, **Hou G**, **Zhang H**, **Suiter CL**, **Ahn J**, **Byeon I-JL**, **Perilla JR**, **Langmead CJ**, **Hung I**, **Gor'kov PL**, **Gan Z**, **Brey W**, **Aiken C**, **Zhang P**, **Schulten K**, **Gronenborn AM**, **Polenova T**. 2015. Dynamic allostery governs cyclophilin A-HIV capsid interplay. Proc Natl Acad Sci USA **112**:14617–14622.

602. **Quinn CM**, **Wang M**, **Fritz MP**, **Runge B**, **Ahn J**, **Xu C**, **Perilla JR**, **Gronenborn AM**, **Polenova T**. 2018. Dynamic regulation of HIV-1 capsid interaction with the restriction factor TRIM5α identified by magic-angle spinning NMR and molecular dynamics simulations. Proc Natl Acad Sci USA **115**:11519–11524.

603. **Wu X**, **Anderson JL**, **Campbell EM**, **Joseph AM**, **Hope TJ**. 2006. Proteasome inhibitors uncouple rhesus TRIM5alpha restriction of HIV-1 reverse transcription and infection. Proc Natl Acad Sci USA **103**:7465–7470.

604. **Hall MP**, **Unch J**, **Binkowski BF**, **Valley MP**, **Butler BL**, **Wood MG**, **Otto P**, **Zimmerman K**, **Vidugiris G**, **Machleidt T**, **Robers MB**, **Benink HA**, **Eggers CT**, **Slater MR**, **Meisenheimer PL**, **Klaubert DH**, **Fan F**, **Encell LP**, **Wood KV**. 2012. Engineered luciferase reporter from a deep sea shrimp utilizing a novel imidazopyrazinone substrate. ACS Chem Biol **7**:1848–1857.

605. **Goldschmidt V**, **Rigourd M**, **Ehresmann C**, **Le Grice SFJ**, **Ehresmann B**, **Marquet R**. 2002. Direct and indirect contributions of RNA secondary structure elements to the initiation of HIV-1 reverse transcription. J Biol Chem **277**:43233–43242.

606. **Watts JM**, **Dang KK**, **Gorelick RJ**, **Leonard CW**, **Bess JW**, **Swanstrom R**, **Burch CL**, **Weeks KM**. 2009. Architecture and secondary structure of an entire HIV-1 RNA genome. Nature **460**:711–716.

607. **Pollom E**, **Dang KK**, **Potter EL**, **Gorelick RJ**, **Burch CL**, **Weeks KM**, **Swanstrom R**. 2013. Comparison of SIV and HIV-1 genomic RNA structures reveals impact of sequence evolution on conserved and non-conserved structural motifs. PLoS Pathog **9**:e1003294.

608. **Sükösd Z**, **Andersen ES**, **Seemann SE**, **Jensen MK**, **Hansen M**, **Gorodkin J**, **Kjems J**. 2015. Full-length RNA structure prediction of the HIV-1 genome reveals a conserved core domain. Nucleic Acids Res **43**:10168–10179.

609. **Jun S**, **Zhao G**, **Ning J**, **Gibson GA**, **Watkins SC**, **Zhang P**. 2013. Correlative microscopy for 3D structural analysis of dynamic interactions. J Vis Exp **76**:e50386.

610. **Hampton CM**, **Strauss JD**, **Ke Z**, **Dillard RS**, **Hammonds JE**, **Alonas E**, **Desai TM**, **Marin M**, **Storms RE**, **Leon F**, **Melikyan GB**, **Santangelo PJ**, **Spearman PW**, **Wright ER**. 2017. Correlated fluorescence microscopy and cryo-electron tomography of virus-infected or transfected mammalian cells. Nat Protoc **12**:150–167.

611. **Freed EO**. 2015. HIV-1 assembly, release and maturation. Nat Rev Microbiol **13**:484–496.

612. **Gaudin R**, **de Alencar BC**, **Arhel N**, **Benaroch P**. 2013. HIV trafficking in host cells: motors wanted! Trends Cell Biol **23**:652–662.

613. **Briggs JAG**, **Krausslich H-G**. 2011. The molecular architecture of HIV. J Mol Biol **410**:491–500.

614. **Perilla JR**, **Gronenborn AM**. 2016. Molecular Architecture of the Retroviral Capsid. Trends Biochem Sci **41**:410–420.

615. **Yufenyuy EL**, **Aiken C**. 2013. The NTD-CTD intersubunit interface plays a critical role in assembly and stabilization of the HIV-1 capsid. Retrovirology **10**:29.

616. **Mallery DL**, **Márquez CL**, **McEwan WA**, **Dickson CF**, **Jacques DA**, **Anandapadamanaban M**, **Bichel K**, **Towers GJ**, **Saiardi A**, **Böcking T**, **James LC**. 2018. IP6 is an HIV pocket factor that prevents capsid collapse and promotes DNA synthesis. Elife **7**:e1002762.

617. **Reicin AS**, **Ohagen A**, **Yin L**, **Hoglund S**, **Goff SP**. 1996. The role of Gag in human immunodeficiency virus type 1 virion morphogenesis and early steps of the viral life cycle. J Virol **70**:8645–8652.

618. **Fitzon T**, **Leschonsky B**, **Bieler K**, **Paulus C**, **Schröder J**, **Wolf H**, **Wagner R**. 2000. Proline residues in the HIV-1 NH2-terminal capsid domain: structure determinants for proper core assembly and subsequent steps of early replication. Virology **268**:294–307.

619. **Tang S**, **Murakami T**, **Agresta BE**, **Campbell S**, **Freed EO**, **Levin JG**. 2001. Human immunodeficiency virus type 1 N-terminal capsid mutants that exhibit aberrant core morphology and are blocked in initiation of reverse transcription in infected cells. J Virol **75**:9357–9366.

620. **Hulme AE**, **Kelley Z**, **Foley D**, **Hope TJ**. 2015. Complementary Assays Reveal a Low Level of CA Associated with Viral Complexes in the Nuclei of HIV-1-Infected Cells. J Virol **89**:5350–5361.

621. **Chen N-Y**, **Zhou L**, **Gane PJ**, **Opp S**, **Ball NJ**, **Nicastro G**, **Zufferey M**, **Buffone C**, **Luban J**, **Selwood D**, **Diaz-Griffero F**, **Taylor I**, **Fassati A**. 2016. HIV-1 capsid is involved in post-nuclear entry steps. Retrovirology **13**:28.

622. **Stultz RD**, **Cenker JJ**, **McDonald D**. 2017. Imaging HIV-1 Genomic DNA from Entry through Productive Infection. J Virol **91**:e00034–17.

623. **Ocwieja KE**, **Brady TL**, **Ronen K**, **Huegel A**, **Roth SL**, **Schaller T**, **James LC**, **Towers GJ**, **Young JAT**, **Chanda SK**, **König R**, **Malani N**, **Berry CC**, **Bushman FD**. 2011. HIV integration targeting: a pathway involving Transportin-3 and the nuclear pore protein RanBP2. PLoS Pathog **7**:e1001313.

624. **Serrao E**, **Engelman AN**. 2016. Sites of retroviral DNA integration: From basic research to clinical applications. Crit Rev Biochem Mol Biol **51**:26–42.

625. **Towers GJ**, **Noursadeghi M**. 2014. Interactions between HIV-1 and the cell-autonomous innate immune system. Cell Host Microbe **16**:10–18.

626. **Lahaye X**, **Manel N**. 2015. Viral and cellular mechanisms of the innate immune sensing of HIV. Curr Opin Virol **11**:55–62.

627. **Sumner RP**, **Thorne LG**, **Fink DL**, **Khan H**, **Milne RS**, **Towers GJ**. 2017. Are Evolution and the Intracellular Innate Immune System Key Determinants in HIV Transmission? Front Immunol **8**:1246.

628. **Tsang J**, **Chain BM**, **Miller RF**, **Webb BLJ**, **Barclay W**, **Towers GJ**, **Katz DR**, **Noursadeghi M**. 2009. HIV-1 infection of macrophages is dependent on evasion of innate immune cellular activation. AIDS **23**:2255–2263.

629. **Yan N**, **Regalado-Magdos AD**, **Stiggelbout B**, **Lee-Kirsch MA**, **Lieberman J**. 2010. The cytosolic exonuclease TREX1 inhibits the innate immune response to human immunodeficiency virus type 1. Nat Immunol **11**:1005–1013.

630. **Yoh SM**, **Schneider M**, **Seifried J**, **Soonthornvacharin S**, **Akleh RE**, **Olivieri KC**, **De Jesus PD**, **Ruan C**, **de Castro E**, **Ruiz PA**, **Germanaud D**, **Portes des V**, **García-Sastre A**, **König R**, **Chanda SK**. 2015. PQBP1 Is a Proximal Sensor of the cGAS-Dependent Innate Response to HIV-1. Cell **161**:1293–1305.

631. **Jønsson KL**, **Laustsen A**, **Krapp C**, **Skipper KA**, **Thavachelvam K**, **Hotter D**, **Egedal JH**, **Kjolby M**, **Mohammadi P**, **Prabakaran T**, **Sørensen LK**, **Sun C**, **Jensen SB**, **Holm CK**, **Lebbink RJ**, **Johannsen M**, **Nyegaard M**, **Mikkelsen JG**, **Kirchhoff F**, **Paludan SR**, **Jakobsen MR**. 2017. IFI16 is required for DNA sensing in human macrophages by promoting production and function of cGAMP. Nat Commun **8**:14391.

632. **Lahaye X**, **Satoh T**, **Gentili M**, **Cerboni S**, **Conrad C**, **Hurbain I**, **Marjou El A**, **Lacabaratz C**, **Lelièvre J-D**, **Manel N**. 2013. The capsids of HIV-1 and HIV-2 determine immune detection of the viral cDNA by the innate sensor cGAS in dendritic cells. Immunity **39**:1132–1142.

633. **Aiken C**. 2009. Cell-free assays for HIV-1 uncoating. Methods Mol Biol **485**:41–53.

634. **Malikov V**, **Naghavi MH**. 2017. Localized Phosphorylation of a Kinesin-1 Adaptor by a Capsid-Associated Kinase Regulates HIV-1 Motility and Uncoating. Cell Rep **20**:2792–2799.

635. **Rankovic S**, **Ramalho R**, **Aiken C**, **Rousso I**. 2018. PF74 Reinforces the HIV-1 Capsid To Impair Reverse Transcription-Induced Uncoating. J Virol **92**:e00845–18.

636. **KewalRamani VN**, **Emerman M**. 1996. Vpx association with mature core structures of HIV-2. Virology **218**:159–168.

637. **Kotov A**, **Zhou J**, **Flicker P**, **Aiken C**. 1999. Association of Nef with the human immunodeficiency virus type 1 core. J Virol **73**:8824–8830.

638. **Fassati A**, **Goff SP**. 1999. Characterization of intracellular reverse transcription complexes of Moloney murine leukemia virus. J Virol **73**:8919–8925.

639. **Yang R**, **Shi J**, **Byeon I-JL**, **Ahn J**, **Sheehan JH**, **Meiler J**, **Gronenborn AM**, **Aiken C**. 2012. Second-site suppressors of HIV-1 capsid mutations: restoration of intracellular activities without correction of intrinsic capsid stability defects. Retrovirology **9**:30.

640. **Fischer DK**, **Saito A**, **Kline C**, **Cohen R**, **Watkins SC**, **Yamashita M**, **Ambrose Z**. 2019. CA Mutation N57A Has Distinct Strain-Specific HIV-1 Capsid Uncoating and Infectivity Phenotypes. J Virol **93**:e00214–19.

641. **Doyle T**, **Goujon C**, **Malim MH**. 2015. HIV-1 and interferons: who's interfering with whom? Nat Rev Microbiol **13**:403–413.

642. **Iyer SS**, **Bibollet-Ruche F**, **Sherrill-Mix S**, **Learn GH**, **Plenderleith L**, **Smith AG**, **Barbian HJ**, **Russell RM**, **Gondim MVP**, **Bahari CY**, **Shaw CM**, **Li Y**, **Decker T**, **Haynes BF**, **Shaw GM**, **Sharp PM**, **Borrow P**, **Hahn BH**. 2017. Resistance to type 1 interferons is a major determinant of HIV-1 transmission fitness. Proc Natl Acad Sci USA **114**:E590–E599.

643. **Shi J**, **Zhou J**, **Halambage UD**, **Shah VB**, **Burse MJ**, **Wu H**, **Blair WS**, **Butler SL**, **Aiken C**. 2015. Compensatory substitutions in the HIV-1 capsid reduce the fitness cost associated with resistance to a capsid-targeting small-molecule inhibitor. J Virol **89**:208–219.

644. **Chen Q**, **Sun L**, **Chen ZJ**. 2016. Regulation and function of the cGAS-STING pathway of cytosolic DNA sensing. Nat Immunol **17**:1142–1149.

645. **Herzner A-M**, **Hagmann CA**, **Goldeck M**, **Wolter S**, **Kübler K**, **Wittmann S**, **Gramberg T**, **Andreeva L**, **Hopfner K-P**, **Mertens C**, **Zillinger T**, **Jin T**, **Xiao TS**, **Bartok E**, **Coch C**, **Ackermann D**, **Hornung V**, **Ludwig J**, **Barchet W**, **Hartmann G**, **Schlee M**. 2015. Sequence-specific activation of the DNA sensor cGAS by Y-form DNA structures as found in primary HIV-1 cDNA. Nat Immunol **16**:1025–1033.

646. **Maelfait J**, **Bridgeman A**, **Benlahrech A**, **Cursi C**, **Rehwinkel J**. 2016. Restriction by SAMHD1 Limits cGAS/STING-Dependent Innate and Adaptive Immune Responses to HIV-1. Cell Rep **16**:1492–1501.

647. **Vermeire J**, **Roesch F**, **Sauter D**, **Rua R**, **Hotter D**, **Van Nuffel A**, **Vanderstraeten H**, **Naessens E**, **Iannucci V**, **Landi A**, **Witkowski W**, **Baeyens A**, **Kirchhoff F**, **Verhasselt B**. 2016. HIV Triggers a cGAS-Dependent, Vpu- and Vpr-Regulated Type I Interferon Response in CD4+ T Cells. Cell Rep **17**:413–424.

648. **Xu S**, **Ducroux A**, **Ponnurangam A**, **Vieyres G**, **Franz S**, **Müsken M**, **Zillinger T**, **Malassa A**, **Ewald E**, **Hornung V**, **Barchet W**, **Häussler S**, **Pietschmann T**, **Goffinet C**. 2016. cGAS-Mediated Innate Immunity Spreads Intercellularly through HIV-1 Env-Induced Membrane Fusion Sites. Cell Host Microbe **20**:443–457.

649. **Wei W**, **Guo H**, **Ma M**, **Markham R**, **Yu X-F**. 2016. Accumulation of MxB/Mx2-resistant HIV-1 Capsid Variants During Expansion of the HIV-1 Epidemic in Human Populations. EBioMedicine **8**:230–236.

650. **Setiawan LC**, **van Dort KA**, **Rits MAN**, **Kootstra NA**. 2016. Mutations in CypA Binding Region of HIV-1 Capsid Affect Capsid Stability and Viral Replication in Primary Macrophages. AIDS Res Hum Retroviruses **32**:390–398.

651. **Kumar S**, **Morrison JH**, **Dingli D**, **Poeschla E**. 2018. HIV-1 Activation of Innate Immunity Depends Strongly on the Intracellular Level of TREX1 and Sensing of Incomplete Reverse Transcription Products. J Virol **92**:75.

652. **Stavrou S**, **Nitta T**, **Kotla S**, **Ha D**, **Nagashima K**, **Rein AR**, **Fan H**, **Ross SR**. 2013. Murine leukemia virus glycosylated Gag blocks apolipoprotein B editing complex 3 and cytosolic sensor access to the reverse transcription complex. Proc Natl Acad Sci USA **110**:9078–9083.

653. **Hulme AE**, **Hope TJ**. 2014. The cyclosporin A washout assay to detect HIV-1 uncoating in infected cells. Methods Mol Biol **1087**:37–46.

654. **Yang Y**, **Luban J**, **Diaz-Griffero F**. 2014. The fate of HIV-1 capsid: a biochemical assay for HIV-1 uncoating. Methods Mol Biol **1087**:29–36.

655. **Guth CA**, **Sodroski J**. 2014. Contribution of PDZD8 to stabilization of the human immunodeficiency virus type 1 capsid. J Virol **88**:4612–4623.

656. **Pawlica P**, **Le Sage V**, **Poccardi N**, **Tremblay MJ**, **Mouland AJ**, **Berthoux L**. 2014. Functional evidence for the involvement of microtubules and dynein motor complexes in TRIM5α-mediated restriction of retroviruses. J Virol **88**:5661–5676.

657. **Zhang S**, **Sodroski J**. 2015. Efficient human immunodeficiency virus (HIV-1) infection of cells lacking PDZD8. Virology **481**:73–78.

658. **Zennou V**, **Bieniasz PD**. 2006. Comparative analysis of the antiretroviral activity of APOBEC3G and APOBEC3F from primates. Virology **349**:31–40.

659. **Yee JK**, **Miyanohara A**, **LaPorte P**, **Bouic K**, **Burns JC**, **Friedmann T**. 1994. A general method for the generation of high-titer, pantropic retroviral vectors: highly efficient infection of primary hepatocytes. Proc Natl Acad Sci USA **91**:9564–9568.

660. **Larocque L**, **Bliu A**, **Xu R**, **Diress A**, **Wang J**, **Lin R**, **He R**, **Girard M**, **Li X**. 2011. Bioactivity determination of native and variant forms of therapeutic interferons. J Biomed Biotechnol **2011**:174615.

661. **Pornillos O**, **Ganser-Pornillos BK**, **Banumathi S**, **Hua Y**, **Yeager M**. 2010. Disulfide bond stabilization of the hexameric capsomer of human immunodeficiency virus. J Mol Biol **401**:985–995.

662. **Wehrly K**, **Chesebro B**. 1997. p24 antigen capture assay for quantification of human immunodeficiency virus using readily available inexpensive reagents. Methods **12**:288–293.